UNIVERSITI TEKNOLOGI MARA

EMBEDDED CLONAL SQUIRREL EVOLUTIONARY PROGRAMMING FOR RESILIENCE IMPROVEMENT IN POWER SYSTEM

FATHIAH BINTI ZAKARIA

PhD

August 2026

UNIVERSITI TEKNOLOGI MARA

EMBEDDED CLONAL SQUIRREL EVOLUTIONARY PROGRAMMING FOR RESILIENCE IMPROVEMENT IN POWER SYSTEM

FATHIAH BINTI ZAKARIA

Thesis submitted in fulfilment
of the requirements for the degree of
Doctor of Philosophy
(Electrical Engineering)

Faculty of Electrical Engineering

August 2026

CONFIRMATION BY PANEL OF EXAMINERS

I certify that a Panel of Examiners has met on 23rd July 2026 to conduct the final examination of Fathiah binti Zakaria on her Doctor of Philosophy thesis entitled "Embedded Clonal Squirrel Evolutionary Programming for Resilience Improvement in Power System" in accordance with Universiti Teknologi MARA Act 1976 (Akta 173). The Panel of Examiners recommends that the student be awarded the relevant degree. The Panel of Examiners was as follows:

Mohamad Fahmi Hussin @ Mohamad, PhD
Associate Professor
Faculty of Electrical Engineering
Universiti Teknologi MARA
(Chairman)

Mohd Abdul Talib Mat Yusoh, PhD
Senior Lecturer
Faculty of Electrical Engineering
Universiti Teknologi MARA
(Internal Examiner)

Nursyarizal Mohd Nor, PhD
Associate Professor
Faculty of Engineering
Universiti Teknologi PETRONAS
(External Examiner)

PROFESSOR DR HJH ZURAEDA IBRAHIM
Dean
Institute of Postgraduate Studies
Universiti Teknologi MARA
Date: 13 August 2026

AUTHOR'S DECLARATION

I declare that the work in this thesis was carried out in accordance with the regulations of Universiti Teknologi MARA. It is original and is the results of my own work, unless otherwise indicated or acknowledged as referenced work. This thesis has not been submitted to any other academic institution or non-academic institution for any degree or qualification.

I, hereby, acknowledge that I have been supplied with the Academic Rules and Regulations for Postgraduate, Universiti Teknologi MARA, regulating the conduct of my study and research.

Name of Student	:	Fathiah binti Zakaria
Student ID. No.	:	2022419872
Programme	:	Doctor of Philosophy (Electrical Engineering) – EEE950
Faculty	:	Electrical Engineering
Thesis Title	:	Embedded Clonal Squirrel Evolutionary Programming for Resilience Improvement in Power System
Signature of Student	:	……..
Date	:	August 2026

ABSTRACT

The increasing demand for reliable electricity supply, coupled with the growing frequency of high-impact low-probability (HILP) events such as hurricanes, natural disasters, and critical equipment failures, has underscored the urgent need for grid hardening and resilience improvement in modern power systems. Severe disruptions are not adequately addressed by conventional reliability measures, as widespread outages and significant degradation in system performance are often caused as a result. This thesis presents the Embedded Clonal Squirrel Evolutionary Programming (ECSEP) for Resilience Improvement in Power Systems. To address these limitations, this study pursues three primary objectives. The first objective is to develop a novel ECSEP algorithm for grid hardening in power systems. The second objective is to formulate a Multi-Objective ECSEP (MOECSEP) for simultaneous loss minimisation and voltage security enhancement in power system planning. The third objective is to develop a Composite Survivability Strategy (CSS) for grid hardening by integrating intelligent distributed generation (DG) installation and load shedding through coordinated optimisation using ECSEP. The proposed ECSEP algorithm is developed by embedding cloning operators and elements of the Squirrel Search Algorithm (SSA) into the Evolutionary Programming (EP) framework, thereby enhancing exploration capability, convergence speed, and solution accuracy. ECSEP is first applied to single-objective optimisation, focusing on minimising transmission losses and improving voltage stability through optimal DG placement and intelligent load shedding under both normal and outage conditions. Subsequently, MOECSEP is formulated using the weighted-sum principle to simultaneously address the conflicting objectives of system loss reduction and voltage stability enhancement. The CSS framework is then developed by combining DG installation and load shedding as a coordinated grid-hardening scheme governed by 22 decision parameters, enabling the simultaneous determination of optimal DG locations, sizes, load shedding locations, and their corresponding power reduction levels. Validation was conducted on the IEEE 30-Bus and IEEE 57-Bus Reliability Test Systems under two hurricane scenarios representing progressively severe disruption conditions. Comparative studies against benchmark algorithms, namely Evolutionary Programming (EP), Clonal Search Optimizer (CSO), and Squirrel Search Algorithm (SSA), consistently demonstrated the superiority of ECSEP, MOECSEP, and CSS across all test cases. The proposed techniques achieved significant reductions in transmission losses, improved voltage stability indices (*FVSI*), and enhanced overall system resilience compared to pre-optimisation baselines and competing methods. In conclusion, the ECSEP-based framework presents a robust, computationally efficient, and practically relevant solution for grid hardening and resilience planning in power systems subjected to HILP events. Future work is recommended to extend the framework to larger network benchmarks such as the IEEE 118-Bus and IEEE 300-Bus systems, incorporate energy storage systems alongside DG and load shedding, and integrate stochastic modelling to account for uncertainties in renewable generation and load profiles. Further extensions to real-time optimisation, cyber-physical resilience, and advanced multi-criteria decision-making approaches are also encouraged to broaden the practical applicability of the developed techniques.

ACKNOWLEDGEMENT

Alhamdulillah, all praise be to Allah, The Most Gracious and The Most Merciful. With His blessings, strength, and guidance, I have been able to complete this PhD journey.

My deepest gratitude goes to my supervisor, Prof. Ir. Dr. Ismail bin Musirin, for his invaluable guidance, patience, and continuous encouragement throughout this research. His wisdom, professionalism, and inspiring mentorship have not only shaped this thesis but also contributed greatly to my personal and academic growth.

I would also like to extend my sincere appreciation to my co-supervisors, Dr. Dalina Johari, Dr. Norziana Aminudin, and Dr. Sharifah Azwa Shaaya, for their constructive feedback, valuable insights, and continuous support that have enriched the quality of this work.

I am deeply grateful to my beloved family for their unconditional love, endless support, encouragement, patience, sacrifices, and prayers throughout this journey. Their constant belief in me gave me the strength and motivation to overcome every challenge and complete this research. This achievement would not have been possible without their love, understanding, and unwavering support.

I would also like to sincerely thank Universiti Teknologi MARA (UiTM) for the funding support and research facilities that made this study possible.

Finally, this thesis is dedicated to my family and loved ones for their constant love and support. May Allah reward all of you abundantly.

TABLE OF CONTENTS

		Page
CONFIRMATION BY PANEL OF EXAMINERS		**ii**
AUTHOR'S DECLARATION		**iii**
ABSTRACT		**iv**
ACKNOWLEDGEMENT		**v**
TABLE OF CONTENTS		**vi**
LIST OF TABLES		**x**
LIST OF FIGURES		**xv**
LIST OF SYMBOLS		**xviii**
LIST OF ABBREVIATIONS		**xxi**
CHAPTER 1 INTRODUCTION		**1**
1.1	Research Background	1
1.2	Problem Statement	3
1.3	Research Objectives	4
1.4	Scope and Limitation of Study	4
1.5	Organization of Thesis	7
CHAPTER 2 LITERATURE REVIEW		**8**
2.1	Introduction	8
2.2	Trends of Power System Resilience	8
	2.2.1 Grid Hardening in Power System Environment	11
	2.2.2 Effect of Disruptive Events to Power System Resilience	12
2.3	Grid Hardening Strategies in Power System	14
	2.3.1 Distributed Generation as a Grid Hardening Strategy	15
	2.3.2 Load Shedding as a Grid Hardening Strategy	16
2.4	Optimisation Techniques in Grid Hardening Schemes	17
	2.4.1 Single-Objective Optimisation Approaches	19
	2.4.2 Multi-Objective Optimisation Approaches	23
	2.4.3 Composite Survivability Strategies	25

2.5 Research Gap 26
2.6 Summary 28

CHAPTER 3 EMBEDDED CLONAL SQUIRREL EVOLUTIONARY PROGRAMMING FOR GRID HARDENING IN POWER SYSTEM 29
3.1 Introduction 29
3.2 Concept of Grid Hardening in Power System 29
3.2.1 Grid Hardening Strategies 30
3.3 Problem Formulations 33
3.3.1 Loss in Power System 34
3.3.2 Voltage Security Index 36
3.3.3 Resilience in Power System 38
3.4 Optimisation Techniques for Grid Hardening 41
3.4.1 Evolutionary Programming (EP) 41
3.4.2 Clonal Search Optimisation (CSO) 43
3.4.3 Squirrel Search Algorithm (SSA) 46
3.4.4 Proposed Embedded Clonal Squirrel Evolutionary Programming (ECSEP) Algorithm 47
3.5 Results and Discussions 51
3.5.1 Test Systems 51
3.5.2 Identification of Line Outage Disturbance 52
3.5.3 Pre-DG Installation Status of the System 57
3.5.4 Distributed Generation Installation for Loss Minimization in Grid Hardening Scheme 59
3.5.5 Distributed Generation Installation for Voltage Security Improvement in Grid Hardening Scheme 67
3.5.6 Load Shedding for Loss Minimization in Grid Hardening Scheme 74
3.5.7 Load Shedding Technique for Voltage Security Improvement in Grid Hardening Scheme 82
3.6 Comparative Studies with Other Techniques 89
3.6.1 Distributed Generation Installation 89
3.6.2 Load Shedding Compensation Scheme 96

3.7 Summary 101

CHAPTER 4 MULTI-OBJECTIVE EMBEDDED CLONAL SQUIRREL EVOLUTIONARY PROGRAMMING ALGORITHM BASED TECHNIQUE FOR RESILIENCE IMPROVEMENT IN POWER SYSTEM 103

4.1 Introduction 103

4.2 Weighted Sum Multi-Objective Optimisation 103

4.3 Research Framework for Resilience Improvement 105

4.3.1 Multi-Objective Evolutionary Programming (MOEP) Algorithm in Power System Resilience Improvement 106

4.3.2 Multi-objective Squirrel Search (MOSS) Algorithm in Power System Resilience Improvement 107

4.3.3 Proposed Multi-Objective Embedded Clonal Squirrel Evolutionary Programming (MOECSEP) in Power System Resilience Improvement 108

4.4 Results and Discussion 111

4.4.1 Distributed Generation (DG) Installation 111

4.4.2 Load shedding Compensation Scheme 134

4.5 Comparative Studies for DG Installation 156

4.5.1 Comparative Studies for DG Installation in IEEE 30-Bus RTS 156

4.5.2 Comparative Studies for DG Installation in IEEE 57-Bus RTS 158

4.6 Comparative Studies for Load Shedding Scheme 160

4.6.1 Comparative Studies for Load Shedding in IEEE 30-Bus RTS 160

4.6.2 Comparative Studies for Load Shedding in IEEE 57-Bus RTS 162

4.7 Summary 163

CHAPTER 5 EMBEDDED CLONAL SQUIRREL EVOLUTIONARY PROGRAMMING (ECSEP)-BASED COMPOSITE STRATEGY FOR ENHANCING POWER SYSTEM SURVIVABILITY 165

5.1 Introduction 165

5.2 Power System Survivability 166

5.3 Algorithm for Power System Survivability 170

5.4 Power System Survivability Strategy Framework 172

5.5 Results and Discussion 175

5.5.1 Composite Survivability Strategy in IEEE 30-Bus RTS 175
5.5.2 Composite Survivability Strategy in IEEE 57-Bus RTS 184
5.6 Summary 192

CHAPTER 6 CONCLUSION AND RECOMMENDATION 194
6.1 Conclusion 194
6.2 Research Contribution 195
6.3 Recommendation for Future Works 197

REFERENCES 199

APPENDICES 221

AUTHOR'S PROFILE 226

LIST OF TABLES

Tables	Title	Page
Table 2.1	Comparison Between Reliability and Resilience in Power Systems	10
Table 3.1	Sustained Winds of Hurricane Category	53
Table 3.2	Bus and Area Allocation for IEEE 30-Bus and IEEE 57-Bus Test Systems	53
Table 3.3	Line Outage Scenarios Based on Wind Categories for the Test Systems	55
Table 3.4	Numerical Results of Pre-Outage (Before Events)	58
Table 3.5	Numerical Results of IEEE 30-Bus RTS (Scenario 1) for Loss Control using 3 DG and 5 DG Units	60
Table 3.6	Numerical Results of IEEE 30-Bus RTS (Scenario 2) for Loss Control using 3 DG and 5 DG Units	63
Table 3.7	Numerical Results of IEEE 57-Bus RTS (Scenario 1) for Loss Control using 3 DG and 5 DG Units	65
Table 3.8	Numerical Results of IEEE 57-Bus RTS (Scenario 2) for Loss Control using 3 DG and 5 DG Units	66
Table 3.9	Numerical Results of IEEE 30-Bus RTS (Scenario 1) for Voltage Security Improvement using 3 DG and 5 DG Units	68
Table 3.10	Numerical Results of IEEE 30-Bus RTS (Scenario 2) for Voltage Security Improvement using 3 DG and 5 DG Units	70
Table 3.11	Numerical Results of IEEE 57-Bus RTS (Scenario 1) for Voltage Security Improvement using 3 DG and 5 DG Units	72
Table 3.12	Numerical Results of IEEE 57-Bus RTS (Scenario 2) for Voltage Security Improvement using 3 DG and 5 DG Units	73
Table 3.13	Numerical Results of IEEE 30-Bus RTS (Scenario 1) for Loss Control using 3-Load Shedding and 4-Load Shedding Technique	76

Table 3.14	Numerical Results of IEEE 30-Bus RTS (Scenario 2) for Loss Control using 3-Load Shedding and 4-Load Shedding Technique	78
Table 3.15	Numerical Results of IEEE 57-Bus RTS (Scenario 1) for Loss Control using 3-Load Shedding and 4-Load Shedding Technique	80
Table 3.16	Numerical Results of IEEE 57-Bus RTS (Scenario 2) for Loss Control using 3-Load Shedding and 4-Load Shedding Technique	81
Table 3.17	Numerical Results of IEEE 30-Bus RTS (Scenario 1) for Voltage Security Improvement using 3-Load Shedding and 4-Load Shedding Technique	83
Table 3.18	Numerical Results of IEEE 30-Bus RTS (Scenario 2) for Voltage Security Improvement using 3-Load Shedding and 4-Load Shedding Technique	85
Table 3.19	Numerical Results of IEEE 57-Bus RTS (Scenario 1) for Voltage Security Improvement using 3-Load Shedding and 4-Load Shedding Technique	87
Table 3.20	Numerical Results of IEEE 57-Bus RTS (Scenario 2) for Voltage Security Improvement using 3-Load Shedding and 4-Load Shedding Technique	88
Table 4.1	Results of MOECSEP Application in DG Installation for Scenario 1 Hurricane Strike for Case 1 in IEEE 30-Bus RTS	113
Table 4.2	Results of MOECSEP Application in DG Installation for Scenario 1 Hurricane Strike for Case 2 in IEEE 30-Bus RTS	114
Table 4.3	Results of MOECSEP Application in DG Installation for Scenario 1 Hurricane Strike for Case 3 in IEEE 30-Bus RTS	116
Table 4.4	Results of MOECSEP Application in DG Installation for Scenario 2 Hurricane Strike for Case 1 in IEEE 30-Bus RTS	118
Table 4.5	Results of MOECSEP Application in DG Installation for Scenario 2 Hurricane Strike for Case 2 in IEEE 30-Bus RTS	119
Table 4.6	Results of MOECSEP Application in DG Installation for Scenario 2 Hurricane Strike for Case 3 in IEEE 30-Bus RTS	121

Table 4.7 Comparative Results of F_{Total} for DG Installation Using MOECSEP in IEEE 30-Bus RTS 122
Table 4.8 Results of MOECSEP Application in DG Installation for Scenario 1 Hurricane Strike for Case 1 in IEEE 57-Bus RTS 124
Table 4.9 Results of MOECSEP Application in DG Installation for Scenario 1 Hurricane Strike for Case 2 in IEEE 57-Bus RTS 125
Table 4.10 Results of MOECSEP Application in DG Installation for Scenario 1 Hurricane Strike for Case 3 in IEEE 57-Bus RTS 127
Table 4.11 Results of MOECSEP Application in DG Installation for Scenario 2 Hurricane Strike for Case 1 in IEEE 57-Bus RTS 129
Table 4.12 Results of MOECSEP Application in DG Installation for Scenario 2 Hurricane Strike for Case 2 in IEEE 57-Bus RTS 130
Table 4.13 Results of MOECSEP Application in DG Installation for Scenario 2 Hurricane Strike for Case 3 in IEEE 57-Bus RTS 131
Table 4.14 Comparative Results of F_{Total} for DG Installation Using MOECSEP in IEEE 57-Bus RTS 133
Table 4.15 Results of MOECSEP Application in Load shedding Scheme for Scenario 1 Hurricane Strike for Case 1 in IEEE 30-Bus RTS 135
Table 4.16 Results of MOECSEP Application in Load shedding Scheme for Scenario 1 Hurricane Strike for Case 2 in IEEE 30-Bus RTS 137
Table 4.17 Results of MOECSEP Application in Load shedding Scheme for Scenario 1 Hurricane Strike for Case 3 in IEEE 30-Bus RTS 138
Table 4.18 Results of MOECSEP Application in Load shedding Scheme for Scenario 2 Hurricane Strike for Case 1 in IEEE 30-Bus RTS 139
Table 4.19 Results of MOECSEP Application in Load shedding Scheme for Scenario 2 Hurricane Strike for Case 2 in IEEE 30-Bus RTS 141
Table 4.20 Results of MOECSEP Application in Load shedding Scheme for Scenario 2 Hurricane Strike for Case 3 in IEEE 30-Bus RTS 142

Table 4.21	Comparative Results of F_{Total} for Load shedding Scheme Using MOECSEP in IEEE 30-Bus RTS	144
Table 4.22	Results of MOECSEP Application in Load Shedding Scheme for Scenario 1 Hurricane Strike for Case 1 in IEEE 57-Bus RTS	146
Table 4.23	Results of MOECSEP Application in Load Shedding Scheme for Scenario 1 Hurricane Strike for Case 2 in IEEE 57-Bus RTS	147
Table 4.24	Results of MOECSEP Application in Load Shedding Scheme for Scenario 1 Hurricane Strike for Case 3 in IEEE 57-Bus RTS	148
Table 4.25	Results of MOECSEP Application in Load Shedding Scheme for Scenario 2 Hurricane Strike for Case 1 in IEEE 57-Bus RTS	150
Table 4.26	Results of MOECSEP Application in Load Shedding Scheme for Scenario 2 Hurricane Strike for Case 2 in IEEE 57-Bus RTS	151
Table 4.27	Results of MOECSEP Application in Load Shedding Scheme for Scenario 2 Hurricane Strike for Case 3 in IEEE 57-Bus RTS	152
Table 4.28	Comparative Results of F_{Total} for Load Shedding Scheme Using MOECSEP in IEEE 57-Bus RTS	155
Table 4.29	Performance Comparison of Multi-Objective Optimisation Algorithms for DG Installation in IEEE 30-Bus RTS for Case 1	157
Table 4.30	Performance Comparison of Multi-Objective Optimisation Algorithms for DG Installation in IEEE 57-Bus RTS for Case 1	158
Table 4.31	Performance Comparison of Multi-Objective Optimization Algorithms for Load Shedding Scheme in IEEE 30-Bus RTS for Case 1	161
Table 4.32	Performance Comparison of Multi-Objective Optimization Algorithms for Load Shedding Scheme in IEEE 57-Bus RTS for Case 1	162

Table 5.1 Configuration of DG Installation and LS Strategies Parameters for Simulation Cases 169
Table 5.2 Performance of DG Installation, Load Shedding, and Composite Survivability Strategy in Terms of Loss Reduction and Resilience Indices (*R1, R2*) for the IEEE 30-Bus RTS at Q_{d26} = 25 MVAr 176
Table 5.3 Performance of DG Installation, Load Shedding, and Composite Survivability Strategy in Terms of Voltage Stability Improvement and Resilience Indices (*R1, R2*) for the IEEE 30-Bus RTS at Bus 26 with Q_d = 25 MVAr 180
Table 5.4 Performance of DG Installation, Load Shedding, and Composite Survivability Strategy in Terms of Loss Reduction and Resilience Indices (*R1, R2*) for the IEEE 57-Bus RTS at Q_{d33} = 15 MVAr 185
Table 5.5 Performance of DG, LS and CSS Strategy on Voltage Stability Improvement and Resilience Indices (*R1, R2*) for the IEEE 57-Bus RTS at Q_{d33} = 15 MVAr 189

LIST OF FIGURES

Figures	Title	Page
Figure 1.1	Research Framework	6
Figure 3.1	Grid Hardening Strategy	30
Figure 3.2	Compensation Process Implementation in Grid Hardening Strategy	31
Figure 3.3	General Intelligent DG Installation Strategy for Grid Hardening	32
Figure 3.4	General Implementation in Intelligent Load Shedding Schemes	33
Figure 3.5	Power Loss Profiles with Pre- and Post-DG Installations under Outage and without Outage	36
Figure 3.6	A General 2-Bus System	36
Figure 3.7	*FVSI* Profiles with Pre- and Post-DG Installations under Outage and without Outage	38
Figure 3.8	Categories of System Resilience Responses	40
Figure 3.9	Flowchart for ECSEP	49
Figure 3.10	Hurricane Impact Zones and Patterns on the IEEE 30-Bus RTS	54
Figure 3.11	Failure Probability of Transmission Tower Versus Wind Speed	56
Figure 3.12	Hurricane Impact Zones and Patterns on the IEEE 57-bus RTS	57
Figure 3.13	Comparison of Loss and *PLR* Results for Loss Minimization in DG Installation in IEEE 30-Bus RTS	90
Figure 3.14	Comparison of Loss and *PLR* Results for Loss Minimization in DG Installation in IEEE 57-Bus RTS	92
Figure 3.15	Comparison of *FVSI* and *PFR* Results for Voltage Security Improvement in DG Installation in IEEE 30-Bus RTS	94
Figure 3.16	Comparison of *FVSI* and *PFR* Results for Voltage Security Improvement in DG Installation in IEEE 57-Bus RTS	95

Figure 3.17	Comparison of Loss and *PLR* Results for Loss Minimization in Load Shedding Scheme in IEEE 30-Bus RTS	97
Figure 3.18	Comparison of Loss and *PLR* Results for Loss Minimization in Load Shedding Scheme in IEEE 57-Bus RTS	98
Figure 3.19	Comparison of *FVSI* and *PFR* Results for Voltage Security Improvement in Load Shedding Scheme in IEEE 30-Bus RTS	99
Figure 3.20	Comparison of *FVSI* and *PFR* Results for Voltage Security Improvement in Load shedding Scheme in IEEE 57-Bus RTS	100
Figure 4.1	The Overall Research Framework for the Multi-Objective Optimisation Implementation	106
Figure 4.2	Flowchart of Multi-Objective Evolutionary Programming (MOEP) for Power System Resilience Improvement	107
Figure 4.3	Flowchart of Multi-Objective Squirrel Search Algorithm (MOSS) for Power System Resilience Improvement	108
Figure 4.4	Flowchart of Multi-Objective Embedded Clonal Squirrel Evolutionary Programming (MOECSEP) for Power System Resilience Improvement	110
Figure 5.1	Conceptual Survivability Curve under Different Compensation Strategies	167
Figure 5.2	Flowchart of the ECSEP-Based Composite Survivability Strategy (CSS) with 5DG and 4LS	172
Figure 5.3	Power System Survivability Strategy Framework: Compensation Techniques and Evaluation Process	174
Figure 5.4	Percentage of Loss Reduction (*PLR*) for DG, LS, and CSS Strategies under Scenario 1 and Scenario 2 in IEEE 30-Bus RTS	178
Figure 5.5	Loss Profile under Different Compensation Strategies in IEEE 30-Bus RTS for Scenario 1	179
Figure 5.6	Loss Profile under Different Compensation Strategies in IEEE 30-Bus RTS for Scenario 2	180
Figure 5.7	Percentage of *FVSI* Reduction (*PFR*) for DG, LS, and CSS Strategies under Scenario 1 and Scenario 2 in IEEE 30-Bus RTS	182

Figure 5.8 *FVSI* Profile under Different Compensation Strategies in IEEE 30-Bus RTS for Scenario 1 183
Figure 5.9 *FVSI* Profile under Different Compensation Strategies in IEEE 30-Bus RTS for Scenario 2 184
Figure 5.10 Percentage Loss Reduction (*PLR*) for DG, LS, and CSS Strategies under Scenario 1 and Scenario 2 in IEEE 57-Bus RTS 186
Figure 5.11 Loss Profile under Different Compensation Strategies in IEEE 57-Bus RTS for Scenario 1 187
Figure 5.12 Loss Profile under Different Compensation Strategies in IEEE 57-Bus RTS for Scenario 2 188
Figure 5.13 Percentage *FVSI* Reduction (*PFR*) for DG, LS and CSS Strategies under Scenario 1 and Scenario 2 in IEEE 57-Bus RTS 190
Figure 5.14 *FVSI* Profile under Different Compensation Strategies in IEEE 57-Bus RTS for Scenario 1 191
Figure 5.15 *FVSI* Profile under Different Compensation Strategies in IEEE 57-Bus RTS for Scenario 2 192

LIST OF SYMBOLS

Symbols

A	The Offset
B	The Minimum Value
E	Evolution Step Current Iteration
$FVSI_{w/o_DG}$	*FVSI* Under Outage Conditions without Compensation
$FVSI_{with_DG}$	*FVSI* Value When Compensation is Implemented
fi	Fitness for the i^{th} Random Number
fmax	Maximum Fitness
j	Number of Control Individuals
$Loss_{w/o_DG}$	Power Loss Under an Outage Condition without Compensation
$Loss_{with_DG}$	Power Loss When Compensation Implemented
n	Number of Control Variables
N	Gaussian Random Variable with Mean and Variance Σ2
PL1	Power Loss Before DG Installation without Outage Event
PL2	Power Loss After DG Installation with Outage Event
PL3	Power Loss Before DG Installation without Outage Event
PL4	Power Loss After DG Installation with Outage Event
P_{loss}	Real Power Loss
P_i & P_j	Active Powers at Bus i and Bus j

Q_i & Q_j	Reactive Powers at Bus i and Bus j
Q_0	Baseline of the System Performance
Q_{min}	Minimum of the System Performance When It Is Affected by an Extreme Event
Q_j	Receiving End Power
r_{ij}	Line Resistance Between Bus i and Bus j
V	Sending End Voltage
V_i & V_j	Voltage Magnitude
X_{ij}	Line Reactance
x	Number Of Rows
x_{n+1}	Updated Parameter
x_n	Current Parameter
x_{random}	Random Squirrel Position
$x_{i+m,j}$	Offspring
$x_{i,j}$	Parent
x_{jmax}	Maximum Random Numbers for Every Variable
x_{jmin}	Minimum Random Numbers for Every Variable
y	Number of Columns
Z_i	Line Impedance
α	Scaling Factor That Regulates the Step Size of the Updates
β	Mutation Scale 0< B <1 (Search Factor)

δ	Parameter That Governs the Balance Between Exploration and Exploitation Within the Algorithm
$\delta_i - \delta_j$	Voltage Angles

LIST OF ABBREVIATIONS

Abbreviations

ANN	Artificial Neural Networks
CSO	Clonal Search Optimizer
CSS	Composite Survivability Strategy
DG	Distributed Generation
ECSEP	Embedded Clonal Squirrel Evolutionary Programming
EP	Evolutionary Programming
FVSI	Fast Voltage Stability Index
HILP	High-impact Low-probability
HSSEPA	Hybrid Squirrel Search Evolutionary Programming Algorithm
MOECSEP	Multi-Objective ECSEP
MOEP	Multi-Objective Evolutionary Programming
MOO	Multi-objective optimisation
MOSS	Multi-Objective Squirrel Search
NHC	National Hurricane Centre
NIAC	National Infrastructure Advisory Council
NOAA	National Oceanic and Atmospheric Administration
PFR	Proportional *FVSI* Reduction
PLR	Proportional Loss Reduction
PV	Photovoltaic

RTS	Reliability Test Systems
SEP	Squirrel Evolutionary Programming
SSA	Squirrel Search Algorithm

CHAPTER 1
INTRODUCTION

1.1 Research Background

The recent advances in power system community considers the importance of power system survivability and sustainability to ensure reliable delivery of electricity to the consumers. Ensuring the sustainability of power systems is crucial for modern societies, as daily life and economic activities depend on a safe and efficient electricity supply that serves as the backbone of the society [1]. However, the rising frequency and severity of power outages caused by natural disasters and other disruptive events have highlighted the vulnerability of existing grids. Extreme weather events such as hurricanes, floods, wildfires, and earthquakes have repeatedly demonstrated their capacity to cause large-scale blackouts, with significant social and economic consequences. For instance, Hurricane Katrina left more than 2.6 million customers without power across Louisiana, Mississippi, and Alabama [2-3], Hurricane Sandy caused outages affecting over 8.5 million customers in 21 U.S. states, while Hurricane Maria devastated Puerto Rico's grid, resulting in a complete island-wide blackout for 3.4 million people [4]. These events underscore how fragile infrastructures, particularly transmission lines, substations, and overhead lines, can collapse under high-impact low-probability events, prolonging recovery and restoration efforts [5].

Resilience emphasizes the ability of power systems to anticipate, absorb, adapt, and recover from such events [6-7]. Reports from the U.S. Department of Energy and the National Infrastructure Advisory Council (NIAC) have highlighted that resilience must be prioritized to prepare for the growing risks associated with climate change, cyber-attacks, and aging infrastructure [8]. The economic stakes are high: in the United States alone, weather-related damages cost an estimated USD 25-70 billion annually, and these costs are projected to rise further [9]. Thus, developing robust strategies to strengthen resilience has become a pressing need for the power system community worldwide.

A range of remedial and preventive strategies have been proposed under the umbrella of grid hardening. Physical hardening measures include reinforcing transmission lines, undergrounding power lines, and installing storm-resistant poles

[10], while operational approaches focus on distributed generation (DG), microgrids, intelligent load shedding, and advanced monitoring systems [11]. These measures collectively aim to reduce vulnerability, enhance adaptability, and accelerate recovery following disruptive events. However, the effectiveness of such measures depends critically on optimal planning, sizing and coordination. Non-optimal placement or sizing of compensating devices such as DG units or load shedding schemes can lead to over- or under-compensation, ultimately reducing their contribution to resilience improvement [12]. Similarly, the unpredictable nature of disruptive events adds further uncertainty, making resilience planning a complex optimisation challenge [13-14]. Thus, a reliable optimisation technique is crucial to ensure any efforts to alleviate this phenomenon is worth.

To address these challenges, this study introduces a novel optimisation technique called Embedded Clonal Squirrel Evolutionary Programming (ECSEP), designed for grid hardening in power systems. The algorithm integrates cloning mechanisms and the exploratory characteristics of the Squirrel Search Algorithm within the evolutionary programming algorithm to enhance its optimisation capability, with performance benchmarked against established methods such as SSA, CSO, and EP. The study further extends this approach into a Multi-Objective ECSEP (MOECSEP) using the weighted-sum method to address loss minimization and voltage stability enhancement simultaneously. Comprehensive comparative analyses were also carried out to evaluate the performance of MOECSEP against established techniques, namely Multi-Objective Evolutionary Programming (MOEP) and Multi-Objective Squirrel Search (MOSS), to validate its effectiveness. In addition, a Composite Survivability Strategy (CSS) is developed by combining DG installation with intelligent load shedding, providing a coordinated solution for resilience improvement under stressed and contingency conditions. The proposed methods are validated on the IEEE 30-Bus and IEEE 57-Bus Reliability Test Systems (RTS) using MATLAB simulations. The results highlight the potential of the proposed techniques as practical tools for advancing resilient and sustainable power system planning.

1.2 Problem Statement

Problem Statement 1: Inadequacy of existing optimization approaches for grid hardening.

Conventional grid hardening strategies rely on single-objective optimization methods that are insufficient for addressing the multi-dimensional nature of power system resilience. These approaches fail to simultaneously handle competing goals such as loss minimization and voltage stability, while also lacking the computational efficiency needed to manage the uncertainty introduced by disruptive events. The consequence is suboptimal decision-making in resilience planning, leaving power systems vulnerable to cascading failures and prolonged outages.

Problem Statement 2: Limitations in achieving balanced, multi-dimensional resilience solutions.

The inherently multi-dimensional nature of power system resilience encompassing simultaneous goals such as minimizing power losses and maintaining voltage security cannot be adequately addressed by conventional single-objective formulations. Forcing a single-objective lens onto these problems results in solutions that optimize one dimension at the expense of others, leading to unbalanced and impractical outcomes in power system planning.

Problem Statement 3: Non-optimal allocation of compensation devices and the unpredictability of their performance

Grid hardening initiatives depend on the coordinated deployment of compensation strategies such as distributed generation (DG) placement and load shedding schemes. However, non-optimal sizing and allocation of these devices compounded by the dynamic and uncertain nature of their performance under varying load conditions and fault scenarios reduces their effectiveness and compromises system resilience. Without a structured and intelligent strategy to guide their deployment, power systems remain susceptible to over- or under-compensation, resulting in degraded operational efficiency and inadequate resilience during disruptive events.

1.3 Research Objectives

The objectives of this research are as follows:

1. To develop a novel Embedded Clonal Squirrel Evolutionary Programming (ECSEP) for Grid Hardening in Power Systems.
2. To formulate a Multi-Objective Embedded Clonal Squirrel Evolutionary Programming (MOECSEP) for loss and voltage security study in power system planning.
3. To develop a Composite Survivability Strategy (CSS) for grid hardening using ECSEP, integrating intelligent DG installation and load shedding to enhance power system resilience.

1.4 Scope and Limitation of Study

The scope and limitation of the study is designated to ensure that this study works within the stipulated breadth and depth in accordance with the formulated. To accomplish the research objectives, the following scopes of the study were defined:

i. A new optimisation technique is derived termed the Embedded Clonal Squirrel Evolutionary Programming (ECSEP) framework by embedding cloning mechanisms into the Squirrel Evolutionary Programming (SEP) paradigm for grid hardening applications.
ii. The proposed ECSEP is utilised for intelligent distributed generation installation and intelligent load shedding initiatives in voltage stability enhancement and loss minimisation in power system.
iii. Comparative studies for the proposed ECSEP with respect to the independent Evolutionary Programming (EP), Clonal Search Algorithm (CSO) and Squirrel Search Algorithm (SSA) as the benchmarked techniques are conducted.
iv. Two reliability test systems (RTS) namely the IEEE 30-Bus and IEEE 57-Bus RTS are utilized as the test specimens for the purpose of validation process in this study.
v. Hurricane-induced line outages are specified under two separated scenarios, namely Scenario 1 and Scenario 2. Each scenario will involve the line outage

contingencies of several transmission lines in both IEEE 30-Bus RTS and IEEE 57-Bus RTS.

vi. A new weighted sum based multi-objective optimisation technique is developed termed Multi-Objective ECSEP (MOECSEP) which integrated the Power loss and Voltage stability equations as one equivalent fitness equation, termed $F_{total} = w_1{}^{*}Loss + w_2{}^{*}FVSI$.

vii. The weighted sum coefficients are varied based on Case 1: $w_1 = 0.1$ and $w_2 = 0.9$, Case 2: $w_1 = 0.5$ and $w_2 = 0.5$ and Case 3: $w_1 = 0.9$ and $w_2 = 0.1$.

viii. Comparative studies for the proposed MOECSEP with respect to the independent Multi-Objective Evolutionary Programming (MOEP), Multi-Objective Squirrel Search Algorithm (MOSS) as the benchmarked techniques are also conducted.

ix. A Composite Survivability Strategy (CSS) is proposed integrating Optimal Distributed Generation (DG) installation, and Intelligent load shedding mechanisms, to enhance system survivability under stressed and contingency conditions.

x. Simulation scenarios are designated to include the Base case condition, Contingency case (line outage), and Stressed case (increased reactive loading at selected weak buses).

Figure 1.1 depicts the overall research framework, clarifying the linkage between the stated research objectives and the defined scope of work. The framework of this study is organized into three main phases, each corresponding to the research objectives. Phase I involves the development of a new optimisation algorithm, termed Embedded Clonal Squirrel Evolutionary Programming (ECSEP), for grid hardening applications. In this phase, the ECSEP technique is applied to determine the optimal location and sizing of Distributed Generation (DG) units and to design effective load shedding schemes under a single-objective formulation. The two main objective functions considered are loss minimization and voltage stability improvement. The performance of ECSEP is benchmarked against conventional methods, including Evolutionary Programming (EP), Clonal Search Optimizer (CSO), and Squirrel Search Algorithm (SSA), on IEEE 30-Bus and IEEE 57-Bus Reliability Test Systems (RTS).

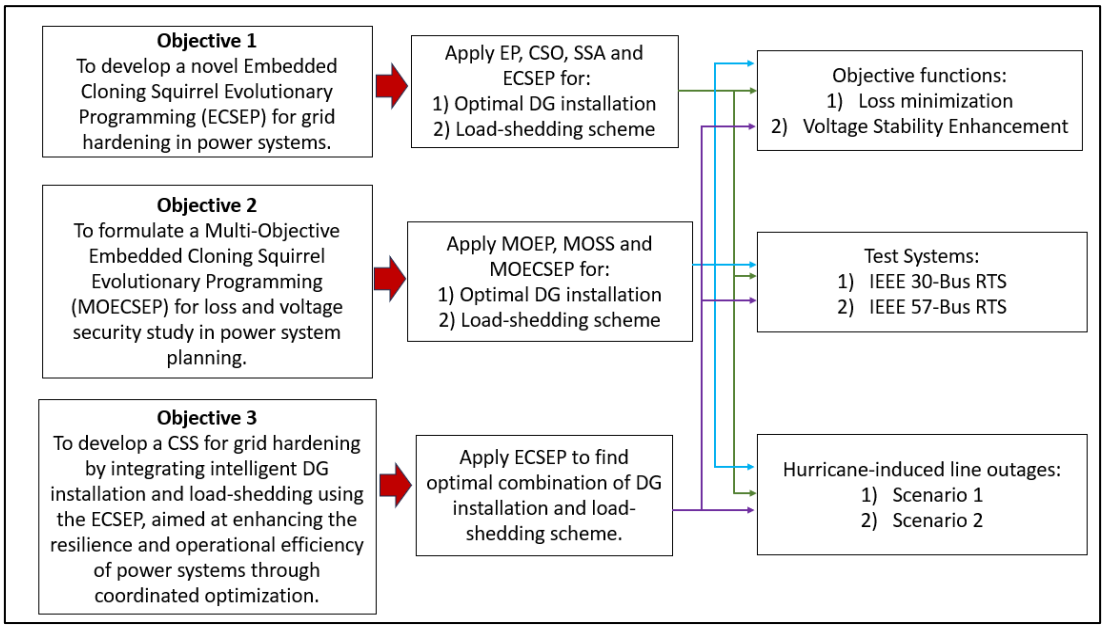


Figure 1.1 Research Framework

Phase II extends the algorithm into a multi-objective framework, known as MOECSEP (Multi-Objective ECSEP). Using the weighted-sum principle, MOECSEP is employed to optimize conflicting objectives simultaneously, particularly minimizing transmission loss and enhancing voltage stability. The performance of MOECSEP is validated by comparing it with other multi-objective techniques such as Multi-Objective Evolutionary Programming (MOEP) and Multi-Objective Squirrel Search (MOSS). This phase demonstrates the ability of the proposed algorithm to achieve balanced trade-offs between technical and operational objectives in power system planning.

Phase III focuses on the development of a Composite Survivability Strategy (CSS) for grid hardening. In this phase, ECSEP is used to integrate intelligent DG installation with load shedding into a coordinated optimisation framework. By combining these two strategies, CSS enhances both resilience and operational efficiency under normal and contingency conditions, including hurricane-induced line outages. The results confirm that CSS consistently outperforms standalone strategies by delivering higher resilience, lower power losses, and improved voltage stability.

This three-phase framework ensures a systematic progression, starting from the development of a novel single-objective optimisation technique, advancing to multi-objective optimisation, and finally applying a composite strategy for comprehensive resilience improvement in modern power systems.

1.5 Organization of Thesis

This thesis consists of six chapters, beginning with preliminary studies on grid hardening and power system resilience. Chapter One introduces the research background, highlighting the importance of resilience enhancement in modern power systems and the motivation for this study. The formulated problem statements are discussed, followed by the objectives and scope of the research. Finally, the organization of the thesis is outlined to provide an overview of the work.

Chapter Two presents the literature review relevant to this research. This chapter discusses the concept of power system resilience and grid hardening, along with the effects of disruptive events on system performance. It also reviews compensation schemes such as DG installation and load shedding, and surveys single-objective, multi-objective, and hybrid optimisation techniques applied in power system planning.

Chapter Three focuses on the development of the proposed ECSEP technique. The optimisation framework is enhanced by integrating cloning operators with elements of the squirrel search algorithm, thereby improving exploration capability and solution accuracy. Its effectiveness for single-objective optimisation is demonstrated through applications on the IEEE 30-Bus and IEEE 57-Bus Reliability Test Systems, focusing on transmission loss minimization and voltage stability improvement. Comparative studies with benchmark techniques are also presented.

Chapter Four describes the formulation of the Multi-Objective ECSEP (MOECSEP) technique using the weighted-sum approach. This chapter emphasizes the simultaneous minimization of power system loss and enhancement of voltage stability. The results are analysed and compared with existing multi-objective optimisation methods to demonstrate the advantages of the proposed technique.

Chapter Five introduces the CSS, which integrates intelligent DG installation with load shedding under the ECSEP framework. This chapter demonstrates how coordinated compensation strategies improve grid resilience under stressed and contingency conditions. Detailed simulations on IEEE test systems are presented, along with comparative performance analysis between standalone and composite approaches.

Chapter Six presents the overall findings, linking results across the single-objective, multi-objective, and composite strategy studies, and highlights the implications of the proposed techniques for power system planning and operation. It closes the thesis by summarizing key contributions and future research directions.

CHAPTER 2
LITERATURE REVIEW

2.1 Introduction

This chapter presents a comprehensive literature review on power system resilience, grid hardening schemes, and optimisation techniques. It begins with an overview of resilience trends in modern power systems, emphasizing the grid hardening environment and examining the impacts of disruptive events on overall system resilience [15]. The discussion then turns to widely implemented grid hardening measures, with particular attention to DG installation and load shedding schemes, both of which are commonly adopted to enhance system robustness.

In addition, this chapter reviews the optimisation approaches applied in grid hardening schemes. Both single-objective and multi-objective optimisation methods are examined, along with composite survivability strategies that combine multiple compensation techniques. The findings from previous studies are outlined to identify existing achievements, limitations, and gaps in the literature, which provide the foundation for the present research.

2.2 Trends of Power System Resilience

In electrical power systems, resilience has become a critical attribute to ensure secure and reliable operation under increasingly uncertain and extreme conditions. Modern grids are increasingly exposed to high-impact, low-probability events such as hurricanes, floods, wildfires, cyber-attacks, and large-scale equipment failures [15-20]. The concept of power system resilience is relatively recent, with its first appearance in technical literature traced back to Amin, who emphasized the need for infrastructures capable of adapting to evolving challenges in the electric grid [21]. Since then, resilience has gained growing attention within the power systems community [22-25]. For instance, the UK Energy Research Centre defined power system resilience as “the capacity of an energy system to tolerate disturbance and to continue to deliver affordable energy services to consumers [26]. A resilient energy system can speedily recover from shocks and provide alternative means of satisfying energy service needs

in the event of changed external circumstances".

Building on these foundations, resilience research has evolved from conceptual definitions to the development of resilience metrics, fragility models, and probabilistic risk-based frameworks [16], [25], [27-33]. Studies have also proposed resilience indices for distribution systems focusing on critical loads [34-35] and new quantitative models to measure resilience as a function of time [28], [36]. In particular, fragility modelling and probabilistic assessment methods have been applied to evaluate the impact of extreme weather, especially hurricanes, on transmission systems and to design adaptation strategies [16-17], [19], [20], [37]. More recently, the literature has emphasized integrating resilience considerations into planning and operation by linking metrics with decision-making tools, enabling power systems to prepare, withstand, and adapt under multiple hazard scenarios [38-43].

The increasing frequency and intensity of extreme weather events such as hurricanes, floods, wildfires, and heatwaves have exposed the limitations of conventional reliability-based planning and highlighted the need for systems that can not only prevent failures but also adapt and recover rapidly once disruptions occur [18-19], [44-45]. Unlike reliability, which primarily focuses on the frequency and duration of outages under normal operating conditions, resilience emphasizes the system ability to anticipate, withstand, adapt, and recover from extreme and unexpected events [15], [41]. A key distinction lies in the difference between reliability and resilience. Reliability is typically quantified using indices such as SAIDI (System Average Interruption Duration Index) and SAIFI (System Average Interruption Frequency Index) [38], [46], whereas resilience extends beyond routine disturbances by incorporating the capacity of the system to respond and adapt under severe and uncertain disruptions. In this sense, reliability is a necessary but insufficient attribute of modern power systems, whereas resilience provides a broader and more dynamic framework for ensuring long-term survivability [47- 49]. This paradigm shift marks a transition from maintaining routine operational security toward preparing for and responding effectively to rare but catastrophic events [43].

To further clarify this difference, Table 2.1 summarizes the key differences between reliability and resilience in terms of scope, event focus, measurement, and objectives. As shown in the table, reliability provides a measure of performance under normal and routine operating conditions, while resilience extends this perspective to encompass extreme, high-impact disturbances. This comparison highlights why

reliability alone is inadequate in modern power system planning and why resilience has become a necessary complement to ensure survivability under uncertain and evolving threats [50-54].

Table 2.1
Comparison Between Reliability and Resilience in Power Systems

Aspect	Reliability	Resilience
Definition	Ability of a power system to deliver electricity consistently under normal operating conditions.	Ability of a power system to anticipate, absorb, adapt, and recover from extreme or unexpected events.
Event Focus	Routine disturbances and component failures (e.g., line faults, equipment outages).	High-impact, low-probability disturbances (e.g., hurricanes, floods, cyber-attacks).
Key Metrics	SAIDI (System Average Interruption Duration Index), SAIFI (System Average Interruption Frequency Index), ENS (Energy Not Supplied).	Resilience curve, recovery time, load restoration indices, resilience indices
Time Horizon	Short-term operational reliability and continuity of service.	Full cycle: before, during, and after disruptions (anticipate, withstand, adapt, recover).
Objective	Minimize service interruptions and maintain acceptable performance under normal conditions.	Ensure system survivability and rapid recovery under extreme and unforeseen disturbances.
Nature	Static and probability-based, focused on predictable events.	Dynamic and adaptive, focused on uncertain and evolving threats.

More recent studies have also pointed toward several emerging trends in resilience research. These include the integration of cyber-physical resilience frameworks that account for both digital and physical vulnerabilities [39-40], [44] the growing role of distributed generation, microgrids, and energy storage in providing localized support during disruptions [41-42], [55-56] and the application of advanced optimisation, artificial intelligence, and computational intelligence to guide resilience-based planning and operations [43], [57-58]. Furthermore, multi-infrastructure interdependencies, such as the coupling between power, gas, water, and communication networks, are increasingly recognized as critical to resilience assessments [50], [59]. Additional work has also highlighted temporal-spatial disaster models that integrate distributed generation and line hardening as practical measures for resilience improvement, bridging both planning and operational perspectives [60]. These emerging trends highlight the necessity of moving beyond traditional reliability measures toward dynamic, adaptive, and optimisation-driven strategies. In this context,

the adoption of advanced multi-objective optimisation techniques such as those explored in this thesis offers a promising pathway for strengthening power system resilience against diverse and evolving threats.

2.2.1 Grid Hardening in Power System Environment

Grid hardening encompasses a range of measures designed to strengthen both the physical and operational elements of power systems to withstand, adapt to, and recover from disruptive events [15], [61]. On the physical side, strategies such as reinforcing towers, installing storm-resistant poles, undergrounding lines, and adding redundant substations reduce vulnerability to hurricanes, floods, and wildfires [17], [46], [54], [62-66]. More advanced approaches extend to integrated energy infrastructures, where optimal hardening in combined power and natural gas systems can mitigate earthquake impacts, while switching strategies in transmission networks help reduce cascading failures [67-69]. In addition to physical reinforcements, operational and technological measures such as distributed generation, renewable resources, and microgrids help maintain local electricity supply when disruptions occur [18].

Intelligent load shedding strategies further enhance survivability by prioritizing critical loads and disconnecting non-essential demand during emergencies [63], [70], while advanced monitoring, predictive outage estimation, and self-healing grid mechanisms enable rapid fault detection and recovery [18], [71] supported by cyber-physical resilience frameworks that address digital vulnerabilities [44], [72]. Intelligent load shedding strategies enhance survivability by prioritizing critical loads and disconnecting non-essential demand during emergencies, as discussed by Afzal et al. and Lyu et al. [25], [34]. Advanced monitoring, predictive outage estimation, and self-healing grid mechanisms further enable rapid fault detection and recovery, as highlighted by [51] and Pilatásig et al. [69]. These measures are also supported by cyber-physical resilience frameworks that address digital vulnerabilities, as emphasized by Wang et al. and Afzal et al. [36-56]. Overall, grid hardening strengthens infrastructure, supports local supply, and enables faster recovery, making it essential for improving power system resilience.

Recent studies emphasize that grid hardening is most effective when implemented as part of an integrated resilience framework, combining physical

reinforcement, DG, intelligent load management, and advanced control with optimisation-based planning tools [38]. Computational intelligence and decision-analysis models now guide investment prioritization, balancing resilience improvement with economic feasibility [68-69], [72]. In this context, grid hardening remains one of the most widely adopted resilience strategies, providing a robust foundation for system survivability under threats. Having discussed grid hardening as a proactive strategy, the next subsection examines the disruptive events that necessitate such measures and explains the corresponding impacts on overall system resilience.

Based on the review, it is discovered that power system resilience has evolved from a conceptual notion to a central framework for ensuring secure and sustainable grid operation under extreme conditions. Early studies focused on defining resilience and differentiating it from reliability, while recent research emphasizes the integration of quantitative metrics, fragility analysis, and probabilistic approaches to assess system robustness. The increasing frequency of disruptive events such as hurricanes and floods has driven the adoption of grid hardening strategies, distributed generation, and cyber-physical control mechanisms. Furthermore, the incorporation of artificial intelligence, optimisation techniques, and multi-infrastructure interdependencies reflects a shift toward proactive and adaptive resilience planning. Overall, resilience research has matured into a multidisciplinary field that combines physical reinforcements, operational intelligence, and computational optimisation to anticipate, withstand, and recover from catastrophic disturbance, ensuring long-term survivability and reliability of modern power systems.

2.2.2 Effect of Disruptive Events to Power System Resilience

Disruptive events are commonly defined as high-impact, low-probability disturbances that significantly damage the normal operation of power systems. These events include natural hazards such as hurricanes, typhoons, earthquakes, floods, and wildfires, as well as man-made disturbances such as cyber-attacks and equipment failures. In contrast to routine faults, extreme events are characterised by extensive impacts, inherent unpredictability, and cascading consequences affecting multiple components of the power grid. According to the National Hurricane Centre [73], hurricanes are classified under the Saffir-Simpson scale based on wind speed and expected damage, ranging from minor roof damage at Category 1 to catastrophic

infrastructure destruction at Category 5.

Historically, hurricanes have been among the most destructive events for power system resilience. For example, the U.S. Department of Energy [2] reported that Hurricane Katrina caused catastrophic damage to the Gulf Coast, leaving more than 2.6 million customers without electricity across Louisiana, Mississippi, and Alabama. Campbell [3] noted that Hurricane Sandy led to a blackout affecting over 8.5 million customers in 21 states, highlighting the vulnerability of dense urban grids and coastal substations to storm surges and flooding. Similarly, FEMA [4] documented how Hurricane Maria devastated Puerto Rico's transmission and distribution infrastructure, resulting in an island-wide blackout for 3.4 million people and marking one of the longest power outages in U.S. history. Panteli and Mancarella [64] emphasized that these historical cases demonstrate how hurricanes not only damage physical assets such as towers, poles, and substations but also overwhelm restoration capacity, prolonging the societal and economic impacts of power outages. Disruptive events, particularly hurricanes, have repeatedly shown their capacity to devastate power systems by causing large-scale blackouts, severe infrastructure damage, and prolonged recovery challenges.

The most immediate effect of such events is the physical damage to grid infrastructure. Yang and Li [74] showed that typhoon disasters can trigger large-scale transmission failures, where the collapse of a small set of critical lines quickly propagates into system-wide disconnections. Bhusal et al. [75] highlighted that hurricanes often cause structural failures in overhead lines and towers, which are among the most vulnerable assets in the network. These failures not only interrupt bulk power delivery but also delay restoration efforts, especially when repair crews face unsafe conditions or limited access to damaged areas.

Beyond physical destruction, disruptive events induce severe operational instabilities in the grid. Puhan et al. [76] demonstrated that extreme contingencies significantly degrade voltage stability margins, increasing the likelihood of blackouts if corrective measures are not applied rapidly. Xu et al. [77] highlighted that renewable energy systems, due to their variable and unpredictable output, can increase the risk of instability under sudden disturbances, making emergency operations more difficult. Overall, disruptive events threaten power system resilience in two ways: by directly damaging critical infrastructure and by causing operational instabilities that spread through the system. Historical blackouts caused by hurricanes illustrate the severe and lasting consequences of such events, emphasising the urgent need for resilience-

oriented planning and grid hardening strategies. Disruptive events compromise power system resilience by causing both direct infrastructure damage and severe operational instabilities, leading to widespread blackouts and underscoring the importance of resilience-focused grid hardening. Based on the review, it is discovered that power system resilience has evolved from a conceptual notion to a central framework for ensuring secure and sustainable grid operation under extreme conditions. Early studies focused on defining resilience and differentiating it from reliability, while recent research emphasizes the integration of quantitative metrics, fragility analysis, and probabilistic approaches to assess system robustness. The increasing frequency of disruptive events such as hurricanes and floods has driven the adoption of grid hardening strategies, distributed generation, and cyber-physical control mechanisms. Furthermore, the incorporation of artificial intelligence, optimization techniques, and multi-infrastructure interdependencies reflects a shift toward proactive and adaptive resilience planning. Overall, resilience research has matured into a multidisciplinary field that combines physical reinforcements, operational intelligence, and computational optimization to anticipate, withstand, and recover from catastrophic disturbances ensuring long-term survivability and reliability of modern power systems.

2.3 Grid Hardening Strategies in Power System

Grid hardening schemes are proactive strategies designed to strengthen the ability of power systems to withstand, adapt to, and recover from disruptive events. Unlike post-event restoration, which deals with repairing damage, grid hardening focuses on preventive measures that minimize vulnerabilities and reduce the impact of high-impact, low-probability events. These measures combine physical reinforcements with operational strategies to ensure that power systems remain stable and secure under stress.

In line with the focus of this research, two grid hardening schemes are emphasized: DG installation and load shedding schemes. DG introduces localized energy resources that enhance supply security and reduce dependence on centralized generation, while load shedding provides an essential operational mechanism to maintain stability during contingencies by prioritizing critical demand. The following subsections discuss these two schemes in detail, highlighting their roles in grid hardening and their contributions to enhancing overall power system resilience.

2.3.1 Distributed Generation as a Grid Hardening Strategy

Distributed Generation (DG) has emerged as a cornerstone of grid hardening strategies, offering localized and flexible energy sources that enhance the resilience of modern power systems [78-80]. By decentralizing power production, DG reduces dependency on vulnerable transmission networks and provides backup supply during disruptions. Technologies such as solar photovoltaics, wind turbines, biomass, fuel cells, and small hydro plants enable systems to operate independently or in coordination with the main grid, thereby ensuring continuity of service during high-impact, low-probability events [81-82].

One of the most significant resilience benefits of DG is its ability to support microgrids, which can isolate from the central grid and supply critical loads during outages. Xu et al. [83] and Gao et al. [84] demonstrated that DG-enabled microgrids play a vital role in critical load restoration under extreme conditions. Similarly, Liu et al. [85] emphasized that microgrids powered by DG can sustain vital services during hurricanes, floods, and other large-scale disasters, while Jiménez-Estévez et al. [86] highlighted their importance in supporting isolated communities. Bajwa et al. [87] provided a comprehensive review showing that microgrids integrated with DG significantly strengthen resilience by enhancing local autonomy and system survivability.

Beyond islanding and black start capabilities, DG also contributes to resilience by improving system restoration. Pham et al. [88] noted that the widespread integration of DG introduces new challenges in restoration strategies, requiring innovative coordination mechanisms. More recently, Bajwa et al. [89] introduced resilience-oriented restoration models that incorporate DG into service restoration while accounting for interdependent critical loads. Similarly, Hamidieh and Ghassemi [90] reviewed the evolving role of DG-based microgrids in resilience strategies, emphasizing their growing relevance in system recovery.

DG deployment also supports multi-microgrid networks, which can share resources and improve resilience at scale. Mishra et al. [91] proposed a framework combining multi-microgrids with mobile energy storage, while Baghbanzadeh et al. [92] demonstrated that distributed generation significantly improves the resilience of interconnected microgrid distribution networks. Zhang et al. [93] further advanced this perspective by developing stochastic models for mobile emergency generator planning,

enhancing flexibility in disaster-prone areas.

Furthermore, DG integration has been studied in relation to extreme weather and natural disasters. Yang and Li [74] proposed a hybrid data-model approach to evaluate resilience under typhoon impacts, while Xu et al. [77] reviewed resilience enhancement strategies in renewable integrated systems exposed to events, stressing the importance of DG as a stabilizing resource. Paliwal et al. [81] and Rezaee Jordehi [82] highlighted that careful planning of DG placement and sizing is essential to avoid over or under compensation, which may otherwise compromise system stability.

DG has evolved from being a supplemental power source to becoming a strategic tool for resilience. It supports localized autonomy through microgrids, enhances restoration processes, improves redundancy, and reduces vulnerability to large-scale outages. While challenges remain regarding variability, coordination, and restoration, the extensive body of research demonstrates that DG, particularly when integrated with microgrids and supported by innovative restoration frameworks, is indispensable for grid hardening and resilience improvement.

2.3.2 Load Shedding as a Grid Hardening Strategy

Load shedding is one of the most common methods used to keep power systems stable during emergency conditions. It works by reducing the demand on the system when generation cannot meet the required load. Early studies, such as Mostafa and Amah [94], showed that steady-state load shedding can prevent widespread blackouts when the system faces serious supply problems. Over time, load shedding has moved from being a last-resort action to an important grid hardening strategy, helping protect critical services and reduce the risk of cascading failures [95-99].

Load shedding is also widely applied in resilience studies. Yu et al. [100] used it in evaluating integrated energy system resilience, while Abrar et al. [101] introduced an adaptive approach for renewable-integrated systems. Liu et al. [102] presented a preplanned shedding strategy to protect microgrids during unplanned islanding, and Kabir et al. [103] proposed a dynamic-adaptive method to strengthen frequency resilience. These studies show that load shedding is not only a basic emergency action but also an important resilience tool, with adaptive and planned strategies making it more effective in renewable-based systems and microgrids.

Other researchers have expanded the role of load shedding beyond traditional use. Amraee and Saberi [104] combined transmission switching with load shedding to enable controlled islanding. Ouyang et al. [105] designed an emergency frequency control approach that coordinates shedding with generator-tripping and switching. Abbasizadeh and Azad-Farsani [106] addressed cyber risks by developing cyber-constrained load shedding strategies for modern smart grids. Recent studies show that load shedding is evolving from a traditional emergency tool into advanced strategies, including controlled islanding, coordinated frequency control, and even cyber-secure applications in smart grids.

Overall, these studies show how load shedding has progressed from simple, fixed-rule approaches to more advanced, adaptive, and cyber-aware strategies. It continues to play a vital role in grid hardening, allowing power systems to withstand and recover from both routine disturbances and high-impact, low-probability events. Load shedding has moved from basic fixed methods to advanced adaptive and cyber-aware strategies, and it remains an important way to strengthen grids against everyday faults and extreme events. The review discovers that grid hardening strategies, notably DG and load shedding, are essential for improving power system resilience. DG enhances supply reliability and supports microgrid operation during disturbances, while load shedding ensures system stability through adaptive and cyber-aware control. Together, these strategies strengthen grid survivability and speed up recovery from high-impact events.

2.4 Optimisation Techniques in Grid Hardening Schemes

Optimisation techniques are essential in ensuring the effective design and implementation of grid hardening strategies [107]. While reinforcement of infrastructure and operational measures, such as DG installation and load shedding, significantly enhances system resilience, the resulting impact depends heavily on optimal planning and coordination. Non-optimal solutions may lead to overcompensation or under compensation, excessive costs, and limited resilience improvement. Therefore, optimisation offers a systematic approach to balance resilience objectives with operational and economic constraints [108-109]. Classical optimisation methods such as linear programming (LP), nonlinear programming (NLP), and mixed-integer programming (MIP) have long been applied in power system planning. These methods are effective when system conditions are well-defined and the

problem structure remains relatively simple, for example in determining optimal load shedding schedules, unit commitment, and resource allocation in conventional grids. However, their reliance on convexity and deterministic assumptions makes them less suitable for modern power systems characterized by uncertainty, high variability, and nonlinear behaviour [109] .

To address these challenges, metaheuristic algorithms have gained significant attention. Techniques such as Genetic Algorithms (GA), Particle Swarm Optimisation (PSO), Differential Evolution (DE), Ant Colony Optimisation (ACO), and Evolutionary Programming (EP) have been successfully applied in DG placement, load shedding coordination, and resilience-oriented planning. More advanced approaches have also been proposed, such as the Water Cycle Algorithm for distribution network reconfiguration [110], hybrid fuzzy–metaheuristic frameworks for DG sizing and placement [111], Krill Herd Algorithm [112], Quasi-Oppositional Swine Influenza Model Optimisation [113], and Cuckoo Search Algorithm for simultaneous DG and capacitor placement [114]. Hybrid metaheuristics continue to show strong potential [115-121]. Muhamad Hapiz et al. [122] introduced a hybrid swarm evolutionary programming method for optimizing photovoltaic-based DG placement, while Kansal et al. [123] presented a hybrid approach for multi-type DG in distribution networks. Similarly, El-Fergany [124] applied a backtracking search optimisation algorithm for optimal DG allocation, and Salimon et al. [114] used Cuckoo Search for simultaneous DG and capacitor sizing. These examples highlight how metaheuristic and hybrid methods can overcome the limitations of classical optimisation by addressing nonlinearities and uncertainties inherent in modern power systems [125-126].

More recently, research has focused on multi-objective optimisation techniques, which allow simultaneous consideration of goals such as minimizing power losses while improving voltage stability and resilience. Approaches based on weighted-sum methods, Pareto-front analysis, and evolutionary multi-objective frameworks are now widely adopted in grid hardening studies [111], [122]. These methods enable planners to evaluate trade-offs among technical reliability, economic feasibility, and resilience enhancement, leading to balanced and practical solutions. As modern power systems evolve with higher levels of renewable integration, microgrids, and smart technologies, optimisation techniques have become essential. Beyond supporting resilient infrastructure planning, these optimisation techniques facilitate adaptive system operation under high-impact, low-probability events. Ultimately, optimisation provides

the foundation for transforming grid hardening measures into coordinated and intelligent strategies that enhance long-term power system survivability.

2.4.1 Single-Objective Optimisation Approaches

Single-objective optimisation has long been a foundation in power system operation and planning. It is based on minimizing or maximizing a single fitness function such as power loss minimization, voltage profile improvement, or load shedding reduction while adhering to network constraints like power balance, voltage stability, and transmission limits. This framework has been particularly valuable in grid hardening studies, where the goal is often to improve system resilience under base-case or contingency conditions. Classical mathematical methods such as linear programming (LP), nonlinear programming (NLP), and mixed-integer programming (MIP) were initially applied in power system planning problems. While effective in well-structured formulations, these methods face challenges when dealing with nonlinear, large-scale, and uncertain grid hardening problems, making them less suitable for modern resilience planning.

2.4.1.1 Evolutionary Programming

Evolutionary Programming (EP), introduced by Fogel as one of the earliest evolutionary algorithms, is inspired by the principles of biological evolution where candidate solutions evolve through mutation and selection over successive generations [127]. Unlike traditional mathematical methods, EP does not require convexity or differentiability in the objective function, making it suitable for solving nonlinear, stochastic, and large-scale optimisation problems. Over the years, EP has been widely applied across engineering, energy, and computing domains, establishing itself as a versatile optimisation tool [128-132].

In the power systems field, EP has been extensively used for planning and operational studies. Mashudi et al. [133] applied EP for generation expansion planning, integrating renewable resources such as photovoltaic (PV) and wind systems into long-term system planning. Similarly, Ibrahim et al. [134] developed an Integrated Immune Chaotic Evolutionary Programming (IICEP) technique to optimize the integration of Battery Energy Storage Systems (BESS) into transmission networks, demonstrating

improvements in system stability and efficiency. Kamalrolzaman et al. [135] proposed a hybrid Grasshopper Algorithm EP method to allocate distributed energy resources effectively, highlighting the potential of hybrid EP approaches for resource optimisation in modern grids.

Beyond power systems, EP has been successfully applied in broader energy and computing applications. Dahlan et al. [136] combined EP with Artificial Neural Networks (ANN) to create a hybrid model for evaluating energy efficiency policies, particularly in measurement and verification baselines. This hybridization illustrates the adaptability of EP in addressing energy policy and sustainability challenges. In addition, Gore et al. [137] employed EP for dynamic resource management and energy optimisation in cloud computing, showing its capability to handle real-time, large-scale, and resource-constrained environments.

EP has also been extended into non-energy fields, demonstrating its flexibility. Tian et al. [138] applied EP for deep feature and model selection in visual data classification, improving computational efficiency and classification accuracy. Dolganov [139] used EP in biomedical engineering to estimate blood pressure indirectly through heart rate variability parameters, demonstrating EP's applicability to health monitoring and medical data processing.

The versatility of EP across domains ranging from generation expansion, storage integration, and distributed resource allocation in power systems, to hybrid energy efficiency modeling, cloud computing optimisation, visual data classification and biomedical applications highlights its robustness and adaptability. Researchers have further enhanced EP by embedding chaotic maps, immune-based operators, and hybridization with other metaheuristics, thereby improving convergence speed and solution quality.

In summary, EP remains a powerful and flexible optimisation approach with applications far beyond traditional power system studies. Its adaptability to hybridization and multi-domain problems ensures its continuing relevance in addressing the complex challenges of modern power, energy, computing, and biomedical systems.

2.4.1.2 Clonal Search Optimizer

The Clonal Search Optimizer (CSO) is an immune-inspired optimisation algorithm based on the clonal selection principle, where high-affinity antibodies proliferate through cloning and mutation while low-affinity antibodies are eliminated. This process provides an effective balance between exploration and exploitation, making CSO widely applicable to nonlinear and multi-objective problems [140]. Recent improvements have focused on enhancing CSO convergence and robustness. Zhang et al. [141] proposed an improved intelligent clonal optimizer with adaptive parameter strategies, which refined solution accuracy while accelerating convergence. Sahargahi et al. [142] introduced an intelligent chaotic clonal optimizer, combining chaos theory with the clonal process to avoid premature convergence and improve diversity in the search space. These advancements demonstrate how CSO can be extended to tackle high-dimensional problems more effectively.

CSO has also been applied to multi-objective optimisation. Lian [143] developed an adaptive multi-objective immune algorithm using clonal principles for reactive power optimisation, showing its effectiveness in balancing competing objectives such as voltage stability and power loss minimization. Similar concepts were applied by Lima et al. [144], who utilized artificial immune mechanisms with clonal search for disturbance detection in distribution systems, highlighting CSO adaptability beyond pure optimisation tasks. In the field of power distribution and system reconfiguration, Oliveira et al. [145] applied artificial immune systems inspired by clonal selection to minimize energy losses in electrical networks, achieving more efficient network operation. Bayar et al. [146] provided a broader review of fault detection and diagnosis using immune-based algorithms, emphasizing CSO potential in system monitoring, fault recovery, and anomaly detection. Hatata et al. [147] further employed immune-inspired optimisation, including clonal search, for sizing hybrid solar, wind and battery systems, ensuring reliability and cost efficiency in renewable integration.

Applications have also extended to dispatch and planning problems. Souza et al. [148] applied clonal search principles in distribution system reconfiguration with variable demand, showing improved adaptability under changing operating conditions. Basu [149-150] employed artificial immune and clonal search approaches for hydrothermal power dispatch and combined heat and power dispatch, respectively. These studies confirmed that CSO based algorithms can efficiently handle non-linear

cost functions, multi-variable constraints, and the competing objectives often encountered in real-world energy systems.

Overall, the CSO have been successfully applied to a wide range of problems, from reactive power optimisation and system reconfiguration to renewable energy planning, fault detection, and economic dispatch [144], [151-152]. Its flexibility, scalability, and immune inspired learning ability make it a strong candidate for solving complex engineering problems, particularly in modern power systems facing uncertainty, variability, and the demand for resilience.

2.4.1.3 Squirrel Search Algorithm

The Squirrel Search Algorithm (SSA), introduced by Jain et al. [153], is a nature-inspired metaheuristic optimisation algorithm modelled on the dynamic foraging behaviour of flying squirrels. In SSA, candidate solutions imitate squirrels gliding between trees in search of acorns, balancing exploration and exploitation. Its adaptability and simplicity have made SSA a promising tool for solving complex optimisation problems in both power system engineering and other fields. Early studies applied SSA to multi-objective optimisation and real-world scheduling problems. Zhu et al. [154] demonstrated its capability for solving multi-objective assignment problems in surgical case scheduling, showing that SSA can efficiently manage trade-offs between competing objectives. Dhaini and Mansour [155] employed SSA for portfolio optimisation, highlighting its robustness in financial decision-making under uncertainty. Sakthivel et al. [156] extended SSA to address combined economic and emission dispatch (CEED) problems in power systems, showing that multi-objective SSA can simultaneously minimize fuel cost and emissions.

SSA has also been widely applied in power system optimisation. Basu [157] utilized SSA for multi-region combined heat and power (CHP) dispatch incorporating renewable resources, confirming its efficiency in managing multiple fuel sources and renewable variability. Sakthivel and Sathya [158] proposed a fuzzified SSA for single- and multi-area multi-fuel dispatch problems, reporting improved convergence and solution quality compared to conventional techniques. Wekesa et al. [159] further developed a hybrid differential SSA to optimize reactive power dispatch, demonstrating significant improvements in voltage stability enhancement. To expand its capabilities, various improved and hybrid SSA versions have been proposed. Yuan et al. [160]

introduced an improved SSA with adaptive strategies to enhance convergence speed and solution accuracy. Artuğer [161] applied SSA to design a nonlinear component generator, showcasing its potential in VLSI design and electronics. Javed et al. [162] presented a flying squirrel-based optimisation algorithm to improve hybrid photovoltaic–thermoelectric systems, reporting higher efficiency in renewable-thermal energy integration.

In the context of resilience and distributed generation, Muhamad Syukor et al. [158] proposed the Hybrid Squirrel Search Evolutionary Programming Algorithm (HSSEPA), applying SSA to distributed generation installation for voltage stability improvement. Their results demonstrated the advantage of combining SSA exploration strength with evolutionary programming convergence capabilities. Recent literature has continued to explore SSA in multi-objective and hybridized forms. For instance, Sakthivel et al. [158] emphasized its effectiveness in balancing cost and environmental objectives, while new studies such as Wekesa et al. [159] integrated SSA with other metaheuristics to enhance stability under stressed power system conditions. These advancements show SSA flexibility as a baseline algorithm adaptable to different optimisation frameworks.

SSA has evolved from a novel bio inspired optimizer into a versatile tool applied across multiple domains, including power dispatch, renewable integration, reactive power optimisation, financial modelling, scheduling, and electronics design. Continuous modifications, hybridization, and domain-specific applications highlight its potential as an effective metaheuristic for solving nonlinear, large scale, and multi-objective problems in modern complex systems.

2.4.2 Multi-Objective Optimisation Approaches

Multi-objective optimisation (MOO), also referred to as multi-criteria optimisation, involves solving problems with two or more conflicting objectives simultaneously [163-164]. Unlike single-objective optimisation, which seeks to minimize or maximize a single fitness function, MOO focuses on obtaining a set of trade-off solutions that balance multiple criteria such as cost, loss, emissions, and voltage stability. In power system applications, this is particularly relevant since grid hardening strategies often require addressing technical, economic, and environmental goals at the same time.

A commonly used method for solving MOO problems is the weighted-sum technique, which aggregates multiple objectives into a single scalar fitness function by assigning weight coefficients to each objective. The total fitness value is obtained by multiplying each objective function with its corresponding weight and summing the results. This approach is straightforward, computationally efficient, and widely adopted in power system planning. For example, Selim et al. [165] applied weighted-sum formulations in DG placement problems using improved Harris Hawks Optimisation, while Zeinalzadeh et al. [166] utilized a multi-objective PSO framework for simultaneous DG and capacitor allocation under load uncertainty. Similarly, H. P. C et al. [167] demonstrated the use of whale optimisation in addressing the trade-off between technical performance and economic feasibility.

Several studies have emphasized the versatility of weighted-sum approaches when applied to DG integration and loss minimization problems. Mansor et al. [168] introduced a multi-objective immune-commensal evolutionary programming method that simultaneously reduced total production cost and transmission loss, while Paliwal et al. [81] explored operational optimisation of integrated urban energy networks using similar principles. Kansal et al. [169] and El-Fergany [124] also showed that weighted-sum formulations remain practical for solving multi-DG allocation problems in distribution systems.

Apart from weighted-sum, other MOO techniques have been employed in resilience-oriented studies. The Pareto front approach identifies a set of non-dominated solutions, providing decision-makers with multiple trade-offs rather than a single solution. This method was highlighted in studies such as Bajwa et al. [87], who applied Pareto-based chaotic mutation immune evolutionary programming for PV integration, and Yehia et al. [111], who proposed hybrid fuzzy metaheuristic approaches for DG sizing and placement. The ε-constraint method and goal programming have also been used in power system optimisation to transform multiple objectives into constraints or assign target values to performance indicators. Meanwhile, lexicographic ordering has been adopted where objectives are ranked by importance, solving them sequentially.

In more recent work, advanced metaheuristic techniques have been extended to multi-objective formulations. For instance, ChithraDevi et al. [112] applied a krill herd algorithm for multi-objective DG placement. Hybrid swarm-based methods, such as those demonstrated by Muhamad Hapiz et al. [122], further highlight the flexibility of metaheuristics in balancing multiple resilience objectives. More recently, Zhu et al.

[154] explored the application of squirrel search algorithms to multi-objective optimisation, further demonstrating the adaptability of newer bio-inspired techniques. MOO improves decision-making by showing a wider range of possible solutions, allowing stakeholders to choose options that best match resilience, cost, and reliability goals. It also makes planning and operations stronger by considering different performance factors together.

2.4.3 Composite Survivability Strategies

Composite Survivability Strategies (CSS) in power systems combine two or more complementary techniques to strengthen resilience, reduce losses, and ensure reliable supply under disruptive conditions. Unlike single-method approaches, CSS leverages the advantages of multiple solutions, thereby addressing both technical and operational challenges in modern grids.

Leghari et al. [170] introduced a framework that integrates distributed generation (DG) with capacitor units to support both grid-connected and islanded operations. This composite approach improves voltage stability and minimizes power loss, enabling networks to function effectively under different operational modes. Similarly, Shen et al. [171] highlighted the role of energy storage in microgrids by presenting an optimisation method that considers multi-energy coupling and demand response. Their study showed that combining energy storage with demand-side strategies significantly enhances flexibility and operational reliability.

Beyond energy storage and DG, composite approaches have been applied in load management. Parsadust et al. [172] developed a dual-objective model combining telecommunication switch optimisation with DG integration, enabling efficient load management while ensuring reliable supply. Mishra et al. [91] further expanded this perspective by proposing multi-microgrid coordination combined with mobile energy storage to quantify and improve resilience in active distribution systems. Their study confirmed that interlinked microgrids with mobile resources provide higher adaptability during extreme events compared to isolated solutions.

At the system reliability level, Zhou et al. [68] addressed mixed cascading failures in dependent network systems by optimizing reliability improvement and resilience simultaneously. Their work emphasized that composite modelling is crucial for capturing the interdependence between failures and recovery strategies. Likewise,

Wang et al. [173] explored a coordination optimisation method that integrates load shedding with distribution network reconfiguration. The results showed that this combination significantly improves service continuity and accelerates restoration during emergencies. Amraee and Saberi [104] presented a composite method of controlled islanding that combines transmission switching with load shedding. This integrated approach helps to contain cascading failures while maintaining supply to critical loads. At a broader level, Ismail et al. [174] conducted a comparative analysis of loss control techniques in transmission systems and demonstrated that composite compensation schemes consistently outperform individual measures.

These studies collectively illustrate that composite survivability strategies represent a key advancement in resilience planning. By integrating multiple techniques such as DG, capacitor placement, energy storage, demand response, mobile resources, and controlled islanding, CSS enables power systems to withstand high-impact low-probability events more effectively. The literature consistently shows that the combined benefits of these methods surpass their individual contributions, positioning CSS as a foundation for future resilient and adaptive power systems.

From the review, it is discovered that optimisation techniques play a crucial role in enhancing grid hardening strategies by ensuring efficient planning, coordination, and operation under uncertain and nonlinear conditions. Classical optimisation methods, though foundational, are limited in handling complex modern grid problems. Metaheuristic and hybrid algorithms such as EP, CSO, and SSA provide robust solutions for nonlinear and multi-objective problems. Moreover, multi-objective frameworks and composite survivability strategies enable simultaneous optimisation of resilience, cost, and reliability. Collectively, these optimisation approaches form the basis for developing intelligent, adaptive, and resilient power systems capable of withstanding high-impact, low-probability disturbances.

2.5 Research Gap

1. Conceptual and Methodological Gaps in Grid Resilience Studies

- Most existing works focus on resilience evaluation and qualitative frameworks but lack quantitative, optimization-based resilience enhancement models.
- Resilience is often treated as a post-event or restoration issue, whereas proactive grid hardening optimization remains underexplored.

- Studies tend to analyse resilience indicators (e.g., SAIDI, SAIFI, recovery time) rather than optimizing grid configurations or compensation parameters to strengthen system survivability.
- There is limited integration between resilience quantification and optimization, particularly using modern metaheuristic or hybrid algorithms.

2. Limitations in Grid Hardening Strategies (DG and Load Shedding)
    - Existing grid hardening schemes mainly study DG installation or load shedding individually, with fewer studies addressing their coordinated optimization under resilience objectives.
    - DG placement and sizing studies often emphasize voltage stability or loss minimization, but not explicitly resilience metrics such as survivability or system restoration speed.
    - Load shedding schemes are primarily reactive; adaptive or predictive load shedding optimization for resilience enhancement is still limited.
    - Few studies integrate operational schemes (e.g., DG, capacitor, and load shedding) into a unified optimization model targeting resilience improvement.

3. Optimization Technique Gaps
    - Classical optimization approaches (LP, NLP, MIP) struggle with nonlinearity, uncertainty, and scalability, making them less effective for real-world resilience planning.
    - While numerous metaheuristics (GA, PSO, DE, ACO, etc.) have been tested, comparative studies show inconsistencies in convergence reliability and solution diversity.
    - Evolutionary Programming (EP), though recognized for robustness, has been underutilized for resilience-based multi-objective grid hardening problems.
    - Hybrid and bio-inspired algorithms such as Clonal Search Optimizer (CSO) and Squirrel Search Algorithm (SSA) have shown potential individually, but their embedded or hybridized applications for grid resilience remain unexplored.
    - Multi-objective frameworks are increasingly adopted but most focus on cost-loss trade-offs, not on resilience-oriented objectives such as voltage stability margin *(V_{min})* or Fast Voltage Stability Index *(FVSI)*.

4. Emerging Gaps in Composite Survivability Strategies (CSS)

- Current composite strategies (DG + capacitor, DG + storage, etc.) focus primarily on loss and voltage improvement, with limited consideration of resilience metrics.
- Few studies model cascading failures or interdependent system effects within composite optimization frameworks.
- There remains a lack of adaptive or intelligent CSS optimization using evolutionary hybrid models that can respond dynamically to high-impact, low-probability (HILP) events.

2.6 Summary

This chapter has reviewed the literature relevant to power system resilience and grid hardening. The review highlighted that resilience has become a critical focus in modern power systems due to the increasing frequency of high-impact, low-probability disruptive events such as hurricanes, floods, and cyber-attacks. Various grid hardening schemes were discussed, with emphasis on distributed generation and load shedding as two key strategies that enhance survivability by decentralizing supply and stabilizing the grid under stressed conditions. The role of optimisation techniques was also explored, ranging from classical single-objective methods to advanced multi-objective and hybrid approaches, which have been widely applied in DG placement, load shedding coordination, and resilience-based planning. More recent studies demonstrated the growing importance of composite survivability strategies, where DG, load shedding, microgrids, and storage are integrated to provide holistic resilience improvement. From the literature review, it is evident that optimisation-driven approaches are essential in grid hardening, ensuring that strategies are not only technically effective but also coordinated, adaptive, and efficient in addressing modern resilience challenges. From the literature review, it is evident that optimisation-driven approaches are essential in grid hardening, ensuring that strategies are not only technically effective but also coordinated, adaptive, and efficient in addressing modern resilience challenges. However, existing studies lack a unified hybrid optimisation framework that simultaneously maximizes voltage stability and enhances resilience under stressed system conditions this gap forms the basis of the present research work.

CHAPTER 3
EMBEDDED CLONAL SQUIRREL EVOLUTIONARY PROGRAMMING FOR GRID HARDENING IN POWER SYSTEM

3.1 Introduction

Grid hardening is an important current issue in power system operation and planning. The resilience of power systems and critical infrastructure can be greatly enhanced through grid hardening against multiple threats. A weak grid can lead to disastrous effects, including vast blackouts, severe economic losses, and failure of many essential systems. There are weaknesses in grid systems such as aged infrastructure, insufficient redundancy, and insufficient protection against cyber-attacks that may worsen the impacts of all types of disruptions, including natural disasters and cyber-attacks[64].

This chapter presents a new optimisation approach called Embedded Clonal Squirrel Evolutionary Programming (ECSEP) for hardening of the grid. This technique is proposed based on integration of three optimisation techniques which are Clonal Search Optimizer (CSO), Squirrel Search Algorithm (SSA) and Evolutionary Programming (EP). ECSEP is formulated to compute the best placement of DG and appropriate load shedding in the transmission system during disruptive events to improve network robustness. ECSEP aims at reducing power system total losses and enhancing voltage security margin in transmission power systems. Each problem formulation is solved independently in two separate components. The effectiveness of the ECSEP technique is evaluated by applying it to two reliability test systems, namely the IEEE 30-Bus RTS and the 57-Bus RTS systems. The performance of ECSEP is evaluated in that it compares the optimisation results with those acquired by individual CSO, SSA, and EP techniques.

3.2 Concept of Grid Hardening in Power System

Grid hardening theory concerns of making the electrical grid more secure, resilient, and robust to withstand a wide range of threats so that it can continue supplying power under tough conditions. It is particularly vital in the background of

increasing threats like climate change, cyber-attacks, and outdated infrastructure as illustrated in Figure 3.1. Among the significant challenges in grid are cyber threats, high demand growth, aging infrastructure and extreme weather. These challenges require grid hardening action which will lead to increasing resilience, preventing outages and enhancing reliability. Among the important initiatives which could be implemented are smart grid technology, upgraded equipment, cybersecurity measures, renewable energy integration, load shedding process and DG installation. Grid hardening refers to physical and nonphysical improvement to the electricity infrastructure, with a goal of reducing sensitivity to catastrophic outages and increased overall resilience [24], [76], [108], [175-176]. Physical hardening refers to the installation of new infrastructure and reorganization of the current topology of the network. Nonphysical hardening, however, refers to altering patterns of consumption, generation, and power transfer.

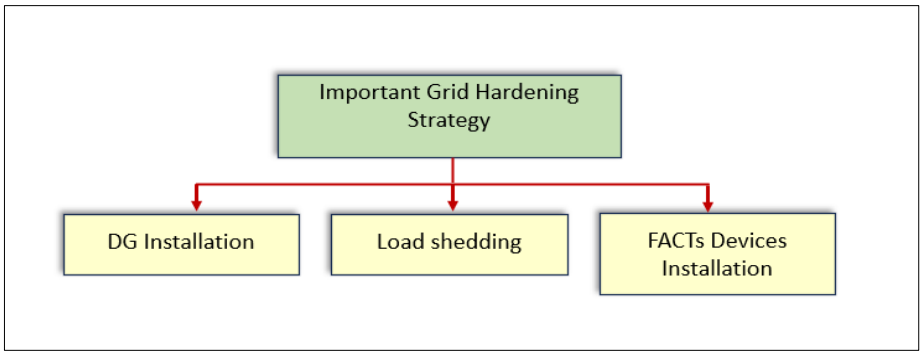


Figure 3.1 Grid Hardening Strategy

3.2.1 Grid Hardening Strategies

Two important grid hardening strategies are DG installation and load shedding as the compensation scheme shown in the Figure 3.2. Implementation of DG installation concerns on the identification of optimal location and sizing of DG, in particular DG Type-1 where only real power is injected into the grid. On the other hand, load shedding compensation scheme deals with the optimal locations of loads to be shed, along with the identification of real and reactive power to be shed from the system. Figure 3.2 presents the strategy of implementing grid hardening through compensation techniques. In this study, two important power models i.e. IEEE 30-Bus RTS and IEEE-57-Bus RTS are chosen to realise the effectiveness of grid hardening strategies.

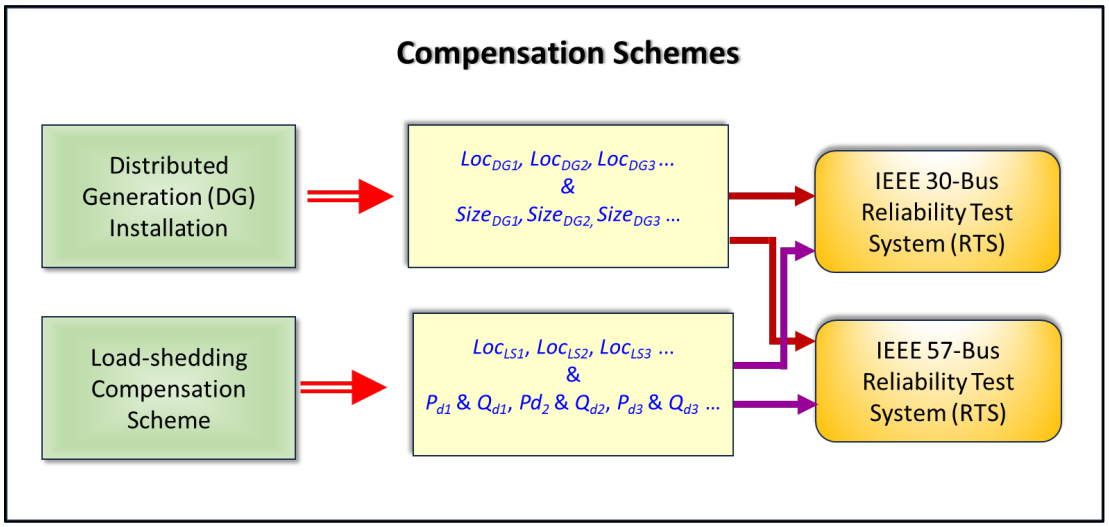


Figure 3.2 Compensation Process Implementation in Grid Hardening Strategy

3.2.1.1 Intelligent Distributed Generation Installation

DG is the process of generating electricity at the point of use in order to reduce the dependency on the centralized power system supply [177]. The DG systems are usually powered by small scale technologies such as solar photovoltaic panels, wind turbines and micro-hydro power stations. Distributed generation has many advantages to the power systems which include; reduced energy losses during transmission, improved grid reliability through local power generation, increased energy independence and increased use of renewable energy resources [178-184]. The above-mentioned types of sources can be classified depending with their terminal capabilities in power delivery into four categories: Type I only provides real power, Type II only provides reactive power, both real and reactive power is provided by Type III and real power is provided by Type IV but it consumes reactive power [185]. In this study, DG Type-I installed in the strategy to harden the grid condition. Figure 3.3 illustrates the setup of general Intelligent DG Installation Strategy for grid hardening initiative. Real implementation for this strategy concerns on both reliability test systems (RTS) depending on the desired breadth and depth which will be reported in the Results and Discussion section.

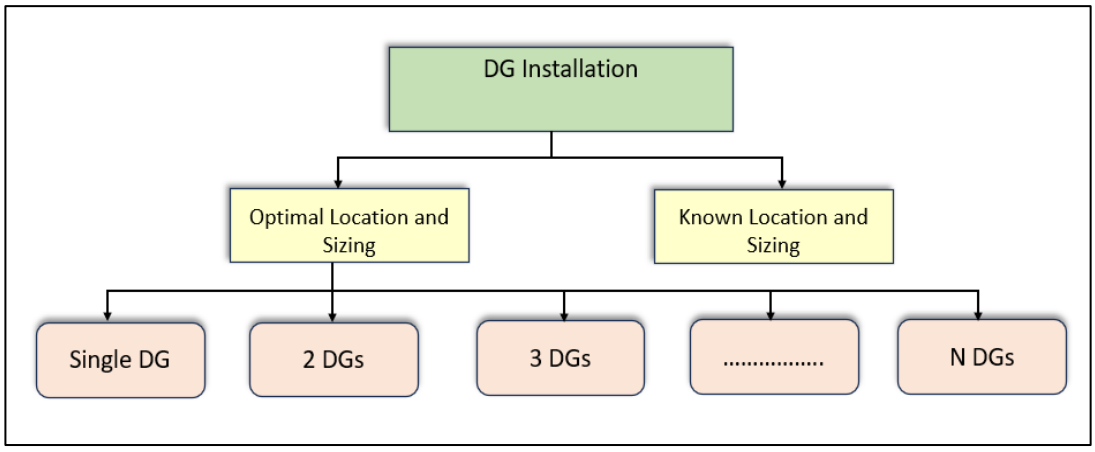


Figure 3.3 General Intelligent DG Installation Strategy for Grid Hardening

Figure 3.3 shows that DG installation can be divided into two main approaches: optimal location and sizing, and known location and sizing. In the optimal approach, the placement and size of DG units are determined using optimisation methods, allowing better system performance such as reduced losses and improved voltage stability. In contrast, the known location and sizing approach is based on practical constraints, where DG units are fixed in advance. While this method is easier to implement, it does not always give the best technical results.

The figure also shows that DG installation can involve different number of units, from a single DG to multiple DGs, depending on the system needs. However, without proper optimisation process, increasing the number of DGs does not necessarily lead to better performance.

3.2.1.2 Intelligent Load Shedding Scheme

In order to ensure that there is a balance between the supply of electricity and demand at all times, power systems employ a critical mechanism known as load shedding during periods of extreme stress or shortages. It helps the operators to avoid system wide failures like blackouts that may result from overloads or insufficient generation capacity by temporarily and strategically reducing the load on the grid. In enhancing the power system resilience, load shedding is used as a crucial tool to support the stability of the grid and to enable it to operate during adverse conditions including natural disasters, equipment failures or unexpected spikes in demand [186]. Power system resilience indicates the strength of grid which refers to the ability of the power

system to absorb and recover from such disruptions and load shedding plays a pivotal role in this process by reducing the risk of cascading failures and enabling the system to recover more quickly. Intelligent load shedding schemes are shown in Figure 3.4 that depicts the optimal bus locations as well as the known locations and optimal sizing of real power (P_d) and reactive power (Q_d) to be curtailed.

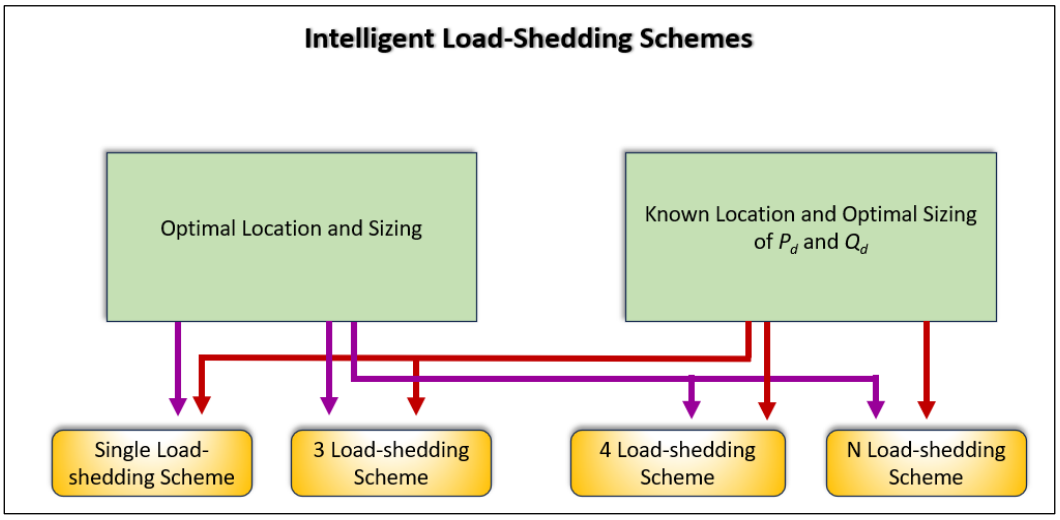


Figure 3.4 General Implementation in Intelligent Load Shedding Schemes

Figure 3.4 illustrates the general setup for an intelligent load shedding scheme. It is configured in two approaches, namely (i) the optimal location and sizing, and (ii) known location and optimal sizing. In the optimal location and sizing, the control variables will involve locations and sizing to be optimised in the load shedding scheme. On the other hand, in the known locations, the sizing of load to be shed will be conducted on the pre-determined locations. Load shedding can be implemented considering single load shedding, 2-load shedding, or N-load shedding. Real implementation on both reliability test systems will be presented in the Results and Discussion section.

3.3 Problem Formulations

Problem formulations required to be solved by the intelligent DG installation and load shedding scheme concentrates on the loss minimisation and voltage stability improvement which led to the grid hardening. Grid hardening will then be quantified in the form of power system resilience improvement. However, it is crucial to analyse the

optimal location for the integration of DG and load shedding. Incorrect location or level of integration of DG and load shedding may lead to either over or under compensation, thus leading to poor system performance and in some cases, exacerbate the problems on the power system. Thus, optimisation techniques are the pre-requisite to determine the appropriate size and location of DG and load shedding. As a result, the efficiency of electrical power transmission can be greatly enhanced especially in regards to power losses and voltage stability.

This chapter applies optimisation methods to find the best locations and capacities of DG and load shedding points to meet the optimisation problems. The research is based on two main objective functions: minimizing power losses and optimizing the voltage security index. Details of power system losses and voltage security index will be explained in detail in the following subchapters.

3.3.1 Loss in Power System

Due to wide area and long transmission line, power systems may have high power losses. These losses, which are commonly known as thermal losses, depend on the line resistance and the currents passing through them [118]. Power losses are computed in this research via load flow analysis, with the objective function of loss minimisation, taking into consideration power loss equation as the fitness equation, Equation (3.1);

$$O.F = Minimize \sum_{j=1}^{n} P_{loss} \tag{3.1}$$

where n represents the number of buses in the system, the power loss P_{loss} for each i line can be determined using (3.2), (3.3) and (3.4) [187];

$$P_{loss} = \sum_{i=1}^{n} \sum_{j=1}^{n} [a_{ij}(P_i P_j + Q_i Q_j) + \beta_{ij}(Q_i P_j + P_i Q_j)] \tag{3.2}$$

$$a_{ij} = \frac{r_{ij}}{V_i V_j} \cos(\delta_i \, \delta_j) \tag{3.3}$$

$$\beta = \frac{r_{ij}}{V_i V_j} \sin(\delta_i - \delta_j) \tag{3.4}$$

where:

r_{ij} : line resistance between bus i and bus j
V_i & V_j : voltage magnitude
$\delta_i - \delta_j$: voltage angles
P_i & P_j : active powers at bus i and bus j
Q_i & Q_j : reactive powers at bus i and bus j

Loss can also be quantified as a percentage to enable comparison. A metric namely, Proportional Loss Reduction (*PLR*) quantifies the percentage by which power losses are reduced when compensation techniques was taking place in the system as opposed to losses that occur during an outage scenario with no compensation. *PLR* is given as in equation (3.5):

$$PLR = \frac{Loss_{w/o_DG} - Loss_{with_DG}}{Loss_{w/o_DG}} \times 100 \quad (3.5)$$

$Loss_{w/o_DG}$ represents the power loss in the system under an outage condition without compensation action and $Loss_{with_DG}$ denotes the power loss in the system when compensation is implemented. This phenomenon is illustrated in Figure 3.5.

In general, $Loss_{with_DG}$ is lower than the $Loss_{w/o_DG}$, where the DG installation acts as the grid hardening strategy in power system. The loss values can be calculated during outage or without outage. With the line outage event, the power loss is higher than that in the non-outage event. These phenomena can be mathematically represented by:

$$P = 0 \quad ; \quad t < T_1$$
$$; \quad t < T_2$$
$$P_{L1} > P_{L2} \quad ; T_1 < t < T_2$$
$$P_{L3} > P_{L4} \quad ; \ T_1 < t < T_2$$

where

P_{L1}: Power loss before DG installation without outage event.

P_{L2}: Power loss after DG installation without outage event.

P_{L3}: Power loss before DG installation with outage event.

P_{L4}: Power loss after DG installation with outage event.

At t = T_2, P_{L4} can either be smaller or larger than P_{L2}; $PL_4 < P_{L2}$ *or* $P_{L2} > P_{L4}$. A higher *PLR* percentage indicates a more effective reduction in losses due to DG installation and load shedding compensation, contributing to overall system resilience.

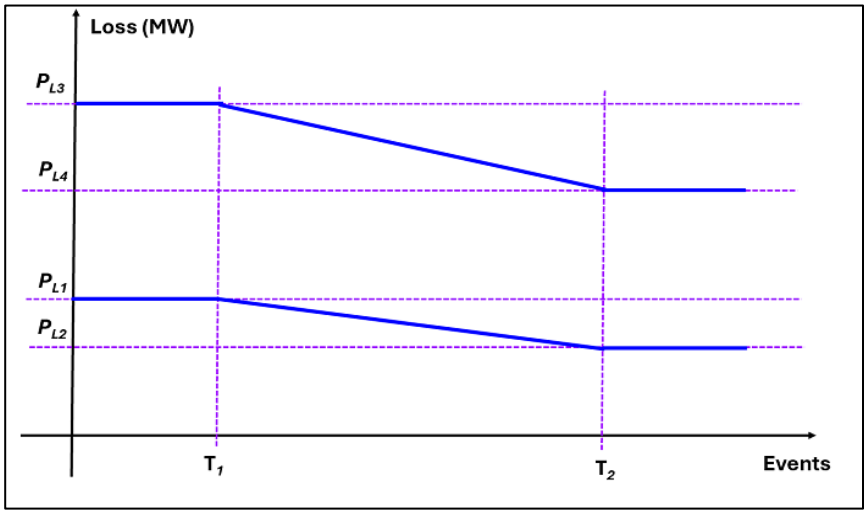


Figure 3.5 Power Loss Profiles with Pre- and Post-DG Installations under Outage and without Outage

3.3.2 Voltage Security Index

In this study, Fast Voltage Stability Index (*FVSI*), a pre-established voltage stability indicator, has been used to assess voltage stability extensively. For the system to be secure, the *FVSI* value must be less than 1. If the *FVSI* value of any line is greater than 1, it means voltage instability condition is experienced by a particular line, which may finally lead to total voltage collapse. Nevertheless, a maximum *FVSI* value termed $FVSI_{max}$ is already indicative to quantify the whole system stability. *FVSI* is derived as a line index for the 2-bus power system model in Figure 3.6 by considering current flow from bus 1 (sending bus) to bus 2 (receiving bus).

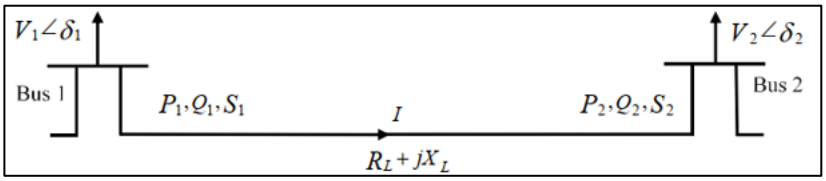


Figure 3.6 A General 2-Bus System

The voltage at Bus 1 is represented as $V_1\angle\delta_1$, while the voltage at Bus 2 is represented as $V_2\angle\delta_2$. The mathematical formulation of the *FVSI* is based on finding the expression for current flow in the transmission line given by the general equation of:

$$FVSI_{ij} = \frac{4Z_{ij}^2 Q_j}{V_i^2 X_{ij}} \tag{3.6}$$

where:

Z_i : line impedance
X_{ij} : line reactance
Q_j : receiving end reactive power
V : sending end voltage

For the purpose of comparison, it is practical to express *FVSI* in percentage form through the introduction of a metric entitled Proportional *FVSI* Reduction (*PFR*). The *PFR* formula determines the percentage reduction in *FVSI* when the compensation technique is applied to the system compared to the *FVSI* occurring during an outage scenario with no compensation. The mathematical representation of this relationship follow:

$$PFR = \frac{FVSI_{w/o_DG} - FVSI_{withDG}}{FVSI_{w/o_DG}} \times 100 \tag{3.7}$$

$FVSI_{w/o_DG}$ refers to the voltage stability index of the system during outage conditions without DG compensation whereas, $FVSI_{with_DG}$ denotes the voltage stability index after DG compensation is applied under the same outage conditions. This phenomenon is illustrated in Figure 3.7. In general, $FVSI_{with_DG}$ is lower than the $FVSI_{w/o_DG}$, where the DG installation acts as the grid hardening strategy in power system. It means that the DG installation will help reducing the *FVSI* value of the system. The loss values can also be calculated during outage or without outage. With the line outage event, the power loss is higher than that in the non-outage event.

This phenomenon can be mathematically represented by:

$$\begin{aligned} FVSI = 0 \quad &; \ t < T_1 \\ &; \ t < T_2 \\ FVSI_{L1} > FVSI_{L2} \quad &; \ T_1 < t < T_2 \\ FVSI_{L3} > FVSI_{L4} \quad &; \ T_1 < t < T_2 \end{aligned}$$

Where:

$FVSI_{L1}$: *FVSI* before DG installation without outage event.

$FVSI_{L2}$: *FVSI* after DG installation without outage event.

$FVSI_{L3}$: *FVSI* before DG installation with outage event.

$FVSI_{L4}$: *FVSI* after DG installation with outage event.

At t = T_2, $FVSI_{L4}$ can either be smaller or larger than $FVSI_{L2}$; $FVSI_{L4} < FVSI_{L2}$ or $FVSI_{L2} > FVSI_{L4}$.

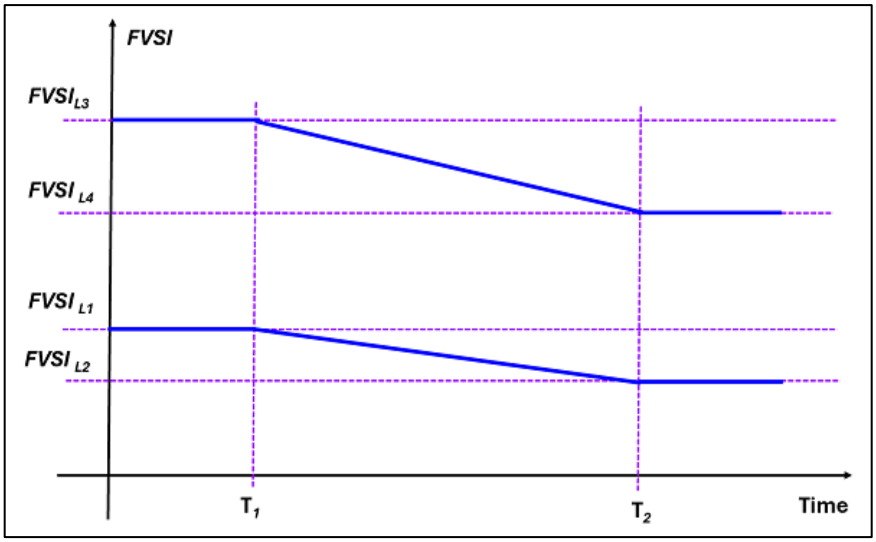


Figure 3.7 *FVSI* Profiles with Pre- and Post-DG Installations under Outage and without Outage

3.3.3 Resilience in Power System

Power grids use quantitative resilience indices to quantify their capability to endure and restore service after natural disaster events. The resilience index provides a holistic view of system performance by evaluating grid capacity for stable voltage regulation and reduced power losses during stress conditions combined with adaptability to changing parameters influencing both power loss and voltage stability [30]. In general, resilience can be defined as the ability of a system to withstand, adapt to, respond to, and recover from unexpected and disruptive events. It involves approaches to ensure the stability and effectiveness of the power system during and after an event such as natural disasters, equipment failures, cyber-attacks or any other unexpected incident. The power system resilience can be categorised into regions

namely the disturbance state, post-disturbance state, and restorative state as shown in Figure 3.8. The figure presents four cases which are used to explain the ideal resilience, degradation, partial degradation and total degradation with no recovery.

- Case 1 (Ideal resilience): The system does not experience any degradation in this situation and actually withstands the disruptive event. This is the ideal case and the system's resilience makes it possible for the system to stay in a stable operational state during external stress.
- Case 2 (Degradation without restoration): The system experiences degradation and does not recover from it. This could be the case, for instance, where crucial lines to some buses are broken and without the help of compensation action, the service cannot be restored. The time window for this case is between t_1 to t_2 which shows degradation and there is no restoration after t_2.
- Case 3 (Partial degradation with limited recovery): The system experiences a degradation followed by partial recovery to operate at a level which is higher than that during the disturbance. The time period for the degradation is observed from t_1 to t_2 and remains constant at this state from t_2 and t_3. The restoration state is observed from t_3 to t_4. This restoration is steady for $t > t_4$.
- Case 4 (Total degradation with no recovery): The system is completely blacked out and fails to come back on after the disturbance. The system cannot even regain functionality after a severe event. The time period for degradation is in between t_1 and t_2 and it remains as constant state for t greater than t_2.

In this study, resilience in power systems is evaluated through a methodological framework designed to assess and enhance the capacity of grid to withstand and recover from disruptions. The methodology centres on the integration of compensation actions and the use of resilience metrics quantitatively measure the system's performance under stress conditions. The goal is to improve the system's ability to absorb disturbances, adapt to varying operational conditions, and ensure a swift recovery to pre-disturbance states.

A resilience index in power system is a quantitative measure of the capability of a power grid to absorb, resist, and recover from various disturbances, for instance, natural disasters. This index gives a general view of the system strength by taking into

consideration the grid ability to sustain stable voltage levels and optimal power losses during stress and the grid resilience to variations that may impact both power loss and voltage stability. The resilience of a power system to a particular extreme event is primarily seen through the changes in system performance that occur after the event has occurred [140].

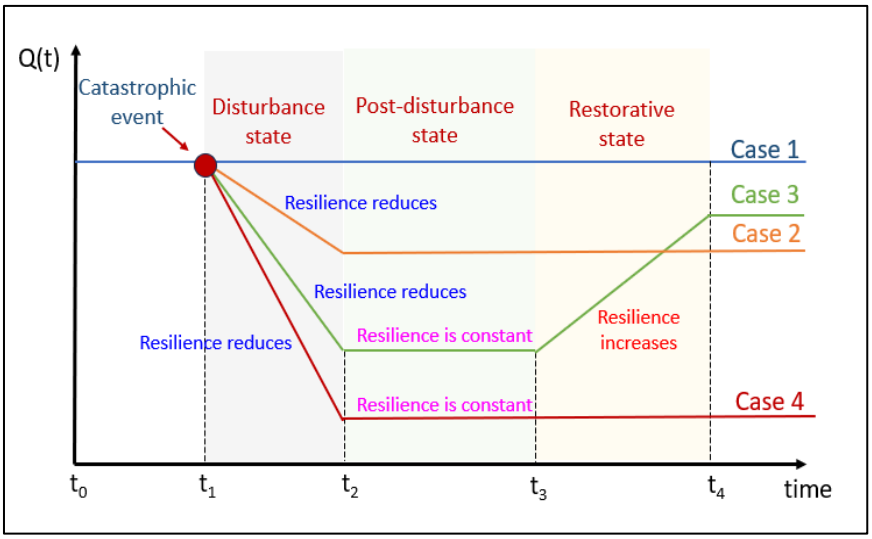


Figure 3.8 Categories of System Resilience Responses

The resilience of the system concerning the extreme event can be quantified as the inverse of the performance of system loss [55]. The mathematical representation for power system resilience can be represented by (3.8):

$$Resilience = \frac{1}{Loss} \tag{3.8}$$

Performance loss can be quantified by measuring its largest deviation from the normal level (3.9);

$$Loss = \frac{Q_0 - Q_{min}}{Q_{min}} \tag{3.9}$$

In this case, Q_0 is the baseline of the system performance, and Q_{min} is the minimum of the system performance when it is affected by an extreme event. The resilience of a power system in a given extreme event is evident in the changes in system performance as the event progresses. Performance can be defined in terms of generation, operational security and power quality. Therefore, the degree of resilience

can be quantified in a scale that is ranging from 0 to infinity. In this case, an infinite resilience value is taken to mean perfect resilience, that is, the system does not experience any drop in performance during the extreme event. On the other hand, a resilience value of 0 means that there is no resilience, and the system does not even survive the impact of the extreme event or collapses immediately after.

3.4 Optimisation Techniques for Grid Hardening

Optimisation techniques are the pre-requisite in grid hardening strategy, since its absence will lead to non-optimal solution that may cause to unsolved problem. This study applies EP, CSO, and SSA as the benchmarked techniques as the effort to highlight a newly proposed optimisation technique to solve for optimisation problems in the context of natural disaster outages. New optimisation technique called Embedded Clonal Squirrel Evolutionary Programming (ECSEP) has also been introduced and implemented in this study.

3.4.1 Evolutionary Programming (EP)

EP has been used in research and technological applications for many years. Based on the Darwinian model of evolution, EP is based on the principle of natural selection, where individuals compete in an environment of limited resources, and only the fittest survive. The main advantage of EP is its conceptual simplicity: it is a structured process. The EP algorithm was developed from seven key operations: initial population generation, fitness evaluation, mutation, combination, selection, generating a new generation, and checking for convergence [188]. Each of these operations is described in detail below.

(i) Initialization

In EP, the initialization process is used to randomly generate individuals for all the control variables in accordance with the objective function. A uniform distribution number generator is used for this purpose to ensure that the random numbers satisfy the pre-determined equality or inequality constraints. To maintain feasibility, constraints must be imposed to ensure that the generated random numbers meet the criteria of the objective function. In general, x can be mathematically represented by:

$$x = rand\ (x, y) * A + B \tag{3.10}$$

$$x_j^i = \left[x_j^1\ x_j^2\ x_j^3 \ldots \ldots x_j^n \right] \tag{3.11}$$

where:
x: Number of rows
y: Number of columns
A: The offset
B: The minimum value

where n = number of control variables and j is the number of control of individuals. This will determine how the sizing of the initial population. If we wish to generate 3 control variables within 20 individuals, the sizing of this matrix will be 20 rows by 3 columns. For example, if we plan to install 3 random capacitor banks with 3 random locations, that means the sizing of the matrix during initialization is 20 rows by 6 columns. 3 control variables denote 3 DG sizing and 3 control variables for random locations.

(ii) Fitness Computation

Fitness refers to the equation, function, or subroutine that needs to be optimised. It can range from a simple mathematical equation to a complex subroutine. The general representation of the fitness equation and objective function is as follows:

$$Fitness\ Equation = f(x_1\ , x_2, x_3\ \ldots . x_n) \tag{3.12}$$

$$Objective\ Function = min(F)\ or\ max(F) \tag{3.13}$$

In this study, the fitness equations are the power loss equation or voltage security index. The power loss equation has been explained in equation (3.2). The other fitness equation is *FVSI* as discussed in equation (3.6).

(iii) Mutation

Mutation process is conducted to breed offsprings or children. The Gaussian mutation operator is applied to the parent random numbers, $x_{i,j}$ to generate offspring (mutated

parent), $x_{i+m,j}$, using a standard deviation σ. The mutation process follows the equation below:

$$x_{i+m,j} = x_{i,j} + N\left(0, \sigma_{i,j}^2\right) \tag{3.14}$$

$$\sigma_{i,j}^2 = \beta\,(x_{jmax} - x_{jmin})\left(\frac{f_i}{f_{max}}\right) \tag{3.15}$$

where

$x_{i+m,j}$	:	Offspring
$x_{i,j}$	:	Parent
N	:	Gaussian random variable with mean and variance σ^2
β	:	Mutation scale $0< \beta <1$ (Search Factor)
$x_{jmax:}$	:	Maximum random numbers for every variable
x_{jmin}	:	Minimum random numbers for every variable
f_i	:	Fitness for the i^{th} random number
f_{max}	:	Maximum fitness

(iv) Combination

The combination operator merges the parent and offspring populations while retaining their respective fitness values. This combination process allows arrange both populations top and down. This process doubles the rows within the same control variables. If the number of individuals is 20 during initialization process, this process makes the number of individuals is 40.

(v) Selection

The selection process is performed on the combined population of parents and offspring to determine the candidates for the next generation as recommended by Ismail et al. in [189]. The population is then sorted in descending order based on fitness values.

(vi) Convergence Test

The convergence test is conducted to verify that the difference between the maximum and minimum fitness values of the objective function is ≤ 0.001, serving as the stopping criterion. The process terminates once this condition is satisfied.

3.4.2 Clonal Search Optimisation (CSO)

The CSO technique, inspired by the biological immune system, has been widely applied in computational models to solve complex real-world problems. By

incorporating clonal selection, immune network theory, vaccination and other adaptive mechanisms, the optimisation approach is able to improve both the quality and efficiency of solutions. Immune optimisation algorithms typically work with a population of individuals known as antibodies to meet specific objectives or comply with problem constraints. According to the clonal selection principle, all antibodies are cloned or duplicated in order to increase population size. The cloned individuals then go through a maturation process, hypermutation, through which diversity is introduced and the solution space is effectively explored. After that, their fitness is determined and the high affinity ones are chosen to proceed to the next stage of evolution. The chosen individuals become a new population of the same number as the original and this is to ensure that there is a continuous process of improvement. This process of cloning, mutation and selection is done iteratively until the algorithm converges to an optimal solution, which shows the robustness and adaptability of the clonal search optimisation technique in complex problem solving.

The CSO algorithm first sets a population of size n as the potential solutions for the optimisation problem. The number of control variables m and the cloning scalar k are also specified. A stopping criterion is set based on either a predefined number of iterations or a convergence condition to determine when the optimisation process should terminate. The search space is randomly populated to create the initial population matrix X. The algorithm then performs a constraint violation test to check if the generated candidates fulfil the given problem constraints. If a candidate violates any constraints, it is repeated until it becomes a valid solution. This ensures that only the feasible solutions are used for the optimisation process. After the valid population is obtained, the cloning process starts. The population is duplicated k times so that each solution in the population is cloned to maintain diversity and keep promising candidate solutions in the algorithm, k times.

The algorithm moves ahead with fitness evaluation after mutation value for every mutated solution. The selection process goes ahead to rank all candidate solutions based on their fitness values where it keeps the best n individuals for the next iteration. This makes it possible for the optimisation process to favour high performing solutions while at the same time discarding fewer effective ones. The algorithm goes on to iterate until the convergence criteria are reached. When the halting condition is fulfilled, the optimisation process stops and the optimal solution $X*$ is declared as the final output. If the algorithm has not yet converged, it repeats the cloning, mutation, fitness evaluation,

and selection processes for the next iteration. The Pseudocode for CSO algorithm is as follows:

Algorithm: Clonal Search Optimisation (CSO)

Set the initial population size n, number of control variables m and cloning scalar k.
Determine the termination criteria based on convergence or a maximum number of iterations.
Create an initial population matrix X of size $n \times m$ with randomly generated numbers.
Perform a **constraint** violation test for each candidate in X:
    If candidate violates constraints, regenerate until a valid solution is obtained.
Check pool filling condition:
While the solution pool is not full, repeat steps 8-14
    Cloning process:
    - Duplicate each solution k times to create a cloned population.
    Mutation process:
    - Apply mutation to each cloned individual to introduce diversity.
Evaluate fitness:
- Compute the objective function value for each mutated solution.
Selection process:
- Rank all candidate solutions based on fitness values
- Retain the best n individuals for the next iteration.
Check **convergence** criteria:
    If termination condition is met, exit the loop.
Return the best solution $X*$.
End Procedure

The CSO algorithm achieves exploration-exploitation balance through its cloning and mutation processes. The cloning phase maintains solution diversity and mutation continue to improve results through small incremental changes. Through the selection step, only the best solutions are moved ahead which results in incremental improvement across successive iterations. Due to this approach CSO proves to be a robust and efficient optimisation technique which is suitable for solving complex real-world problems.

3.4.3 Squirrel Search Algorithm (SSA)

SSA is a recent nature inspired optimisation approach. This algorithm replicates the efficient foraging behaviour of flying squirrels between food sources. The mathematical representation of SSA was formulated based on a thorough analysis of the foraging tactics used by squirrels during their natural feeding activities. The algorithm has been thoroughly validated, analysed and compared with other traditional nature inspired optimisation techniques.

The SSA starts with the creation of a population of n squirrels where each squirrel is positioned randomly within the specified search area. The fitness of all squirrels is calculated and the best solution is determined. An iteration counter E is set to 1 to monitor the optimisation process. The algorithm runs in a loop until a termination condition is fulfilled which could be a fixed number of iterations E_{max} or when a target fitness level is attained.

In each iteration, a squirrel from the population is randomly picked and denoted as $X_{selected}$. The variables of the selected squirrel are determined and then reassigned to new positions within the solution space. The position update is done using the SSA equation. This equation helps in the dynamic repositioning of the squirrel using its current status and another location drawn from the search space. The exponential decay term $e^{-\delta * E}$ regulates the exploration-exploitation trade-off so that at the beginning of the iterations, the algorithm focuses more on exploration and then shifts to exploitation as the iterations continue. The fitness of the new squirrel is then calculated right after the position of the squirrel has been updated. If the new position leads to a higher fitness score, then the old squirrel is replaced by the new one. Thus, all the squirrels in the population are taken through this process. The best solution is updated at every stage of the optimisation process. Then, the iteration counter E is incremented by 1, and the procedure is continued until the termination condition is fulfilled.

The SSA effectively balances random selection and guided movement to explore the search space efficiently. By dynamically adjusting the position of the squirrels, the algorithm enhances its ability to locate optimal solutions. The SSA has the ability to explore the entire search space using the combination of the principles of random selection and directed movement of the squirrels. The algorithm improves its solution finding capability through the moving of the squirrels' centre of mass over time. The convergence property implies that the optimisation stops when the optimal solution

is found, which makes SSA a powerful approach to solve difficult optimisation problems. The following is the pseudocode of the SSA algorithm:

Algorithm: Squirrel Search Algorithm (SSA)

Initialize a population of $\boldsymbol{n}$ squirrels with random positions $\boldsymbol{X_n}$ within the search space.
Evaluate fitness for each squirrel and determine the best solution.
Set iteration counter $\boldsymbol{E = 1}$.
While stopping criteria **not met** (e.g., $\boldsymbol{E \leq E_{max}}$)
    Select a random squirrel $\boldsymbol{X_{selected}}$ from the population.
    Identify all variables within the selected squirrel as a random location.
    Update position using SSA equation:
    $x_{n+1} = x_n + \alpha * e^{-\delta * E} * (x_{random} - x_n)$
Evaluate fitness of the updated squirrel.
Replace old squirrel with new one if the fitness improves.
Repeat steps 5–9 for all squirrels in the population.
Update the best solution found so far.
Increment iteration counter $\boldsymbol{E = E + 1}$.
Return the optimal solution $\boldsymbol{X*}$.
End Procedure

3.4.4 Proposed Embedded Clonal Squirrel Evolutionary Programming (ECSEP) Algorithm

Embedded Clonal Squirrel Evolutionary Programming (ECSEP) is a hybrid configuration that combines the SSA, CSO, and EP optimisation algorithms. The proposed ECSEP technique incorporates CSO and SSA elements into the main EP algorithm, creating a hybrid approach that overcomes the limitations of traditional EP and SSA techniques, which often face issues with local optima entrapment. As shown in Figure 3.9, ECSEP design enhances optimisation performance by effectively mitigating these challenges. The following procedures are implemented in this study to identify the optimal location and capacity for the DG.

Step 1 Perform Normal Load Flow Analysis.

The first step involves running a normal load flow analysis to assess the pre-outage condition of the system. At this stage, no outages occur, allowing for a baseline study of the operational state of the system under standard conditions.

Step 2 Perform Load Flow Under Outage Condition.

The next step is to conduct a load flow analysis under outage conditions. This post-outage analysis enables observation of the effects on system performance, providing insights into how the system responds to disruptions.

Step 3 Generate Initial Population

The ECSEP technique starts by creating an initial population, represented as $X_{i,j}$ where i indicates the population size and j corresponds to the dimension of the control variables. Based on recommendations for EP in optimisation problems, a population size of $i = 20$ is commonly suggested [190].

This study adheres to the recommended guideline by setting the population size to 20 to ensure effective performance. The initial population is structured as follows:

$$\mathrm{X_{i,\,j}} = \begin{bmatrix} X_{1,1} & X_{1,2} & \cdots & X_{1,j} \\ X_{2,1} & X_{2,2} & \cdots & X_{2,j} \\ \vdots & \vdots & \vdots & \vdots \\ X_{i,1} & X_{n,2} & \cdots & X_{i,j} \end{bmatrix} \tag{3.16}$$

Random parameters are generated for active power injections at random load buses. This emulates the DG Type I installation. These generated parameters must meet specified conditions before being stored in a predesigned pool. All generated individuals are then integrated into the system data, followed by the computation of the fitness value, specifically the *FVSI* or loss value depending on the objective function of the study. For loss minimization as the objective function, loss values are the concerned fitness. In this setup, each of the 20 individuals inserted into the system produces a corresponding *FVSI* calculation, resulting in 20 fitness values. These values must be lower than the *FVSI* obtained from the standard load flow calculation, where EP and DG units were not yet integrated into the system.

Step 4 Cloning Process

In the cloning process, the individuals in the initial population pool, referred to as the parent, will be cloned by a factor. In this work, the cloning factor is set to 10. It was suggested by Musirin et. al in [190]. By cloning process, the population size is now 10 times higher, becoming 200 rows.

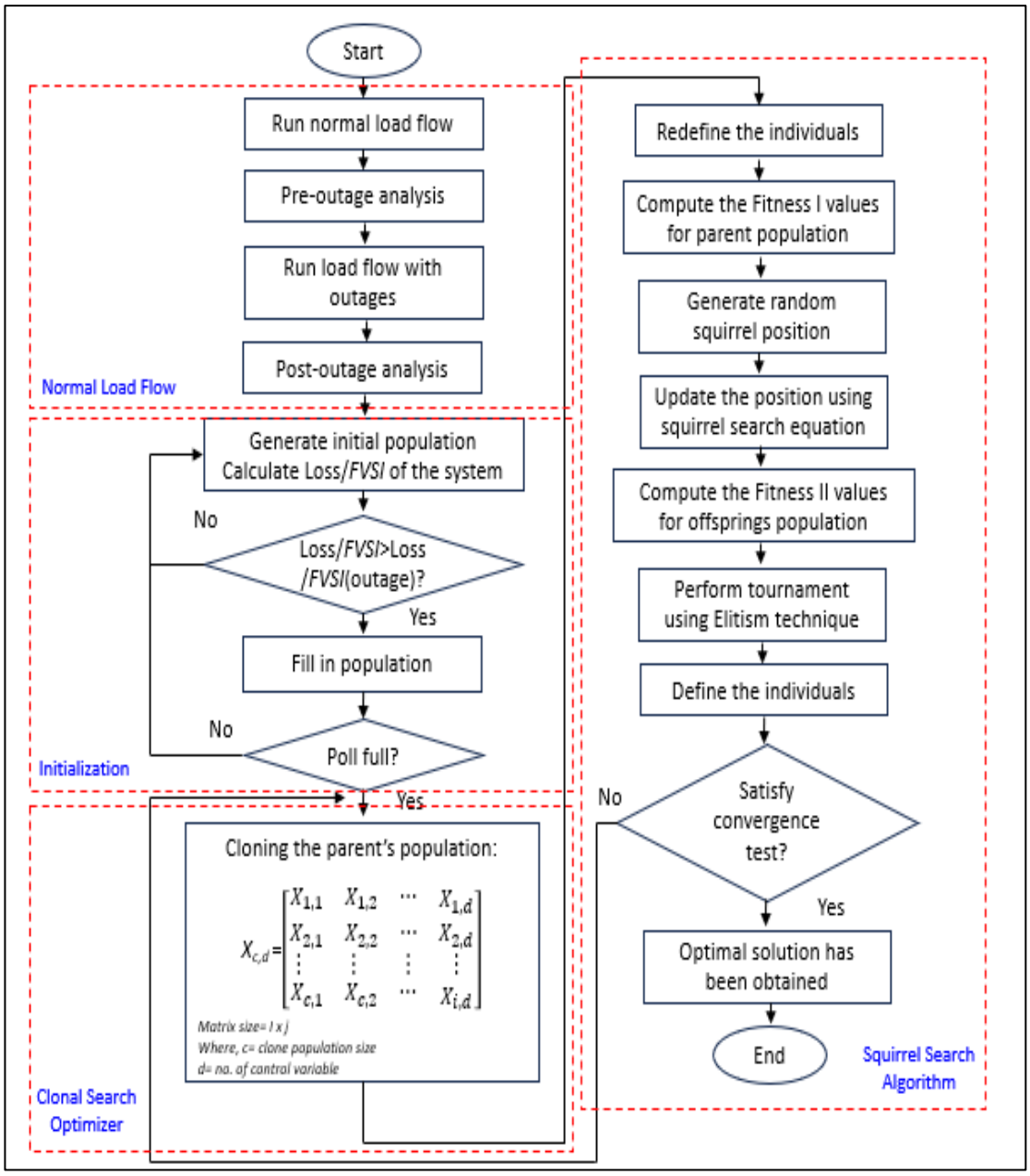


Figure 3.9 Flowchart for ECSEP

Step 5 Fitness I Calculation.

At this point, the Fitness I calculation uses the parent group of randomly generated individuals. During the initial iteration, the fitness values obtained here should match those from the initialization phase, as the same set of random variables are applied. Real power injection occurs at the designated bus, followed by a load flow analysis. Additionally, the *FVSI*, or loss is evaluated. All calculated fitness values are then stored in the 'Fitness I' matrix or array for further reference.

Step 6 Update Position Using SSA Equation.

This phase begins by randomly selecting one individual, or "squirrel," from the group of 20 to determine a new position. All variables within this individual are considered to be a random location after a squirrel is chosen. The position of the squirrel is updated using the SSA equation based on this selected individual and the corresponding variables. This step is crucial to the proposed method as it helps in the exploration of the search space in the hope of getting a better solution. It is another way of navigating the search space to get the best result as each squirrel's position is updated based on the location of the current squirrel and that of other squirrels selected at random. This phase is a vital part of the proposed method that enables the search of the solution space. Thus, the method attempts to find other possible solutions in the search space by updating the position of each squirrel based on its current location and the influence of other squirrels chosen at random.

$$x_{n+1} = x_n + \alpha * e^{-\delta * E} * (x_{random} - x_n) \tag{3.17}$$

where

x_{n+1}	:	Updated parameter
x_n	:	Current parameter
x_{random}	:	Random squirrel position
α	:	Scaling factor that regulates the step size of the updates
δ	:	Parameter that governs the balance between exploration and exploitation within the algorithm
E	:	Evolution step current iteration

Step 7 Fitness II Calculation

In this stage, Fitness II calculation is performed to determine the second fitness metric, known as Fitness II. This process utilizes the offspring generated through the SSA mutation scheme, distinct from the parent individuals used in Fitness I. The array size for storing Fitness II values is identical to that of Fitness I, ensuring consistency in storage while incorporating the unique qualities of the offspring in the fitness evaluation.

Step 8 Combination and Selection

Combination and Selection are two sequential processes involving Fitness I and Fitness II populations. The first step is to merge the parent and offspring populations, incorporating their respective fitness values. This merging doubles the total number of individuals, forming a combined population. Following this, the combined Fitness I and

Fitness II population undergo a tournament process to identify the fittest individuals. In this study, an elitism technique is applied, where individuals are sorted based on fitness values. The sorting order ascending or descending depends on the objective function. For minimization objectives, individuals are ranked in ascending order of fitness values, favouring those with the lowest scores. Conversely, for maximization objectives, the ranking is done in descending order, prioritizing higher fitness values. This approach ensures the preservation of top-performing individuals according to the optimisation goals.

Step 9 Convergence Test

The Convergence Test determines when the optimisation process should stop by evaluating the specified stopping criterion. This criterion is defined as the difference between the maximum and minimum fitness values of the offspring population, set to be less than 0.0001. If this condition is met, the function executes a return statement, terminating the optimisation as it indicates convergence has been achieved. If the condition is not satisfied, the process reverts to Fitness I calculation, bringing the fittest individuals forward to continue the optimisation through the next iteration.

3.5 Results and Discussions

This section presents the results and discussion. It also presents the test systems used in this study, identifies line outages during disturbances. The discussion begins with the outcomes of DG installation for loss minimization within the grid hardening scheme, conducted on the IEEE 30-Bus RTS and IEEE 57-Bus RTS. Following this, the results of DG installation aimed at improving voltage security in the grid hardening scheme are presented. This section also discusses the results of load shedding compensation strategies set up to reduce losses and improve voltage support for grid hardening schemes. A comparison has also been made between the proposed ECSEP and benchmark techniques: SSA, CSO, and EP have been conducted.

3.5.1 Test Systems

The performance of the proposed ECSEP technique, along with its component techniques, is tested using two IEEE-standard transmission system networks: the IEEE 30-Bus Reliability Test System (RTS) and the IEEE 57-Bus RTS for validation

purposes. The IEEE 30-Bus RTS system has five generators at Bus 2, Bus 5, Bus 8, Bus 11 and Bus 13 and it has only 41 interconnecting lines. There are 24 load buses, with a total real power demand of 283.4 MW and a reactive power demand of 126.2 MVAr. The system's total real generation power is 301 MW, and the total reactive generation power is 125 MVAr. This can be referred to Appendix 1. The IEEE 57-Bus System is a widely recognized test system used in power systems. It comprises 57 buses, 7 generators, 17 transformers, and 80 transmission lines. The system has a total real power demand of 1250.8 MW and a reactive power demand of 336.4 MVAr as detailed out in Appendix 2. Typically, Bus 1 serves as the slack bus, while the generator buses include Buses 2, 3, 6, 8, 9, and 12. The remaining buses are primarily load buses with industrial, commercial, and residential loads.

3.5.2 Identification of Line Outage Disturbance

A power system must be resilient against various unpredictable events, including floods, tsunamis, hurricanes, earthquakes, vandalism, and cyberattacks. In this study, hurricanes of different categories are chosen as the primary disruptive events, focusing on transmission line fragility under varying wind speeds. Simulations of sustained wind speeds for different hurricane categories are conducted according to the Saffir-Simpson Hurricane Wind Scale, provided by the National Hurricane Centre (NHC), a branch of the National Oceanic and Atmospheric Administration (NOAA) of the U.S. government as reported in [73] . Table 3.1 categorizes hurricanes based on sustained wind speeds, outlining five distinct categories according to their intensity and potential for damage. Category 1 hurricanes, with wind speeds between 74-95 mph (119-153 km/h), represent the lowest level of impact, while Category 2 hurricanes, with wind speeds of 96-110 mph (154-177 km/h), indicate a moderate increase in destructive potential. Category 3, characterized by winds of 111-129 mph (178-208 km/h), is the threshold for major hurricanes, signalling significant damage potential. Category 4 hurricanes, with wind speeds ranging from 130-156 mph (209-251 km/h), can cause severe structural damage. Finally, Category 5 hurricanes, the most intense, exhibit sustained winds of 157 mph (252 km/h) or higher, posing catastrophic risks to infrastructure and public safety. This classification, based on the Saffir-Simpson Hurricane Wind Scale, provides essential information for assessing hurricane impact and planning resilience measures. For this study, only Category 1 and Category 2

hurricanes are considered. The purpose to choose only two scenarios due to the fact that Category 1 and Category 2 hurricanes occur more frequently than higher-category hurricanes, making them more practical and relevant focus for this research.

Table 3.1
Sustained Winds of Hurricane Category

Hurricane Category	Wind Speed
Category 1	74-95 mph / 119-153 km/h
Category 2	96-110 mph / 154-177 km/h
Category 3	111-129 mph / 178-208 km/h
Category 4	130-156 mph / 209-251 km/h
Category 5	157 mph or higher / 252 km/h or higher

Figure 3.10 and Figure 3.12 provide the visual representations of hurricane patterns and the regions impacted within the test systems. Figure 3.10 shows the hurricane impact zones and patterns for the IEEE 30-Bus RTS, while Figure 3.12 illustrates the corresponding zones for the IEEE 57-Bus RTS. Since real-world transmission systems span multiple geographic regions, the IEEE 30-Bus RTS and IEEE 57-Bus RTS are divided into two distinct regions, which are visually depicted in both figures and summarized in Table 3.2. The test systems are distributed into regions based on number of buses as suggested by [89].

Table 3.2
Bus and Area Allocation for IEEE 30-Bus and IEEE 57-Bus Test Systems

	Area	Bus
IEEE 30-Bus RTS	1	1, 2, 3, 4, 5, 6, 7, 8, 9, 11, 12, 13, 16, 28
	2	10, 14, 15, 17, 18, 19, 20, 21, 22, 23, 24, 25, 26, 27, 29, 30
IEEE 57-Bus RTS	1	1, 2, 3, 4, 5, 6, 7, 8, 10, 12, 13, 14, 15, 16, 17, 18, 19, 20, 38, 44, 45, 46, 47, 48, 49, 50, 51
	2	9, 11, 21, 22, 23, 24, 25, 26, 27, 28, 29, 30, 31, 32, 33, 34, 35, 36, 37, 39, 40, 41, 42, 43, 52, 53, 54, 55, 56, 57

Table 3.2 outlines the area and bus allocations for the IEEE 30-Bus and IEEE 57-Bus RTS, illustrating how buses are distributed across distinct operational areas within each network. This structure allows for sectionalized monitoring and testing within the systems, enabling distinct regions to be managed or analysed independently. This area allocation of buses is crucial for conducting resilience studies, and

optimisation efforts, as it allows for targeted interventions and detailed evaluation of specific sections within each test system. In actual transmission systems, transmission lines play a critical role, and their failure likelihood under various hazards is evaluated using fragility functions and curves. The probabilities of line failure, derived from fragility functions based on different wind speeds, are thoroughly discussed and visualized in [191-193]. Using this information, the failure probabilities of transmission lines in the test system for this study are computed. Table 3.2 presents line outage scenarios for the IEEE 30-Bus and IEEE 57-Bus RTS, based on wind categories and their respective failure probabilities. The Table 3.3 categorizes the line outages by different wind scenarios, highlighting the influence of wind speed on grid stability. Each scenario associates specific wind categories with the affected areas, failure probabilities, and the bus numbers impacted by potential outages.

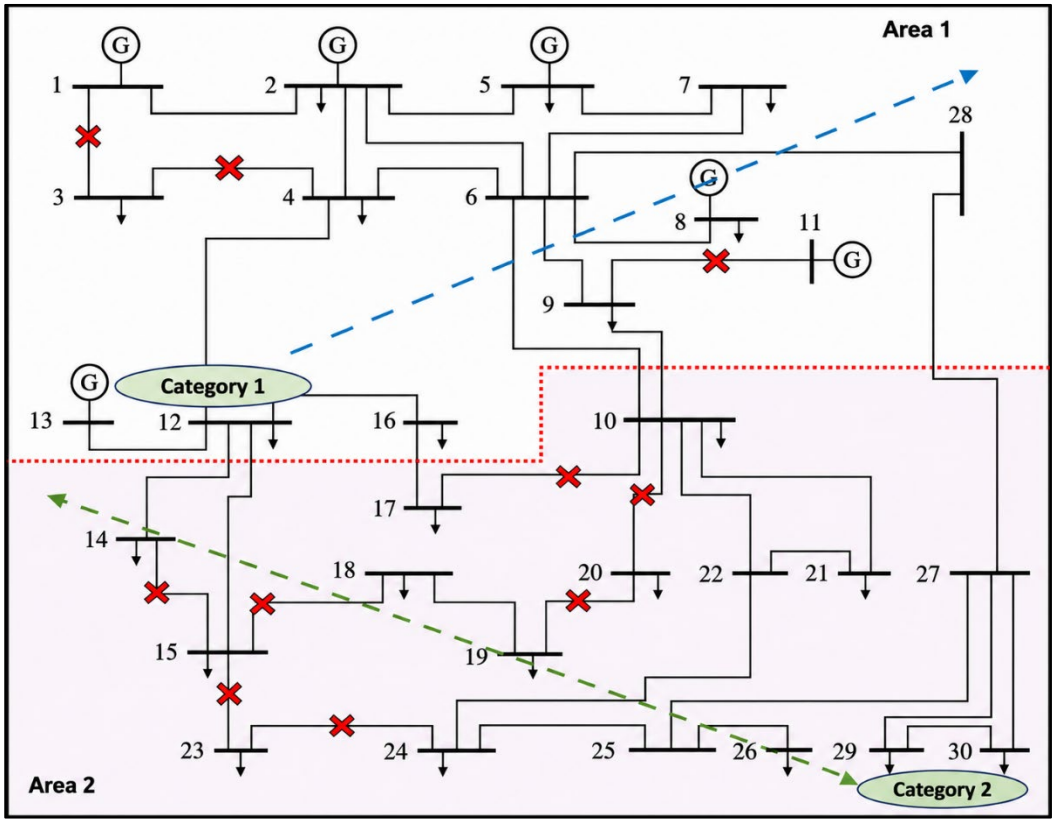


Figure 3.10 Hurricane Impact Zones and Patterns on the IEEE 30-Bus RTS

In Scenario 1 for the IEEE 30-Bus RTS, wind speeds of 74-95 mph (Category 1) impact Area 1, with a failure probability of 0.24, affecting transmission lines (1-3), (3-4) and (9-11) where each pair denotes the from-to bus connection. In Scenario 2,

Category 2 winds (96-110 mph) affect Area 2, increasing the failure probability to 0.35, impacting lines (14-15), (15-18), (19-20), (10-20), (10-17), (15-23) and (23-24).

For instance, in the IEEE 57-Bus RTS, a probability of failure of 0.17 is observed in Area 2 for transmission lines (9-11), (22-23), (23-24), (35-36), (37-39) and (41-42) for Category 1 winds (Scenario 1) with wind speeds of 74-95 mph. In Category 2 winds (Scenario 2), with speeds of 96-110 mph, transmission lines (1-2), (2-3), (3-4), (4-5), (4-6), (6-7), (6-8), (13-14), (1-16), (1-17), (4-18), (12-17), (15-45) and (46-47) are affected by a higher failure probability of 0.36 in Area 1. This Table 3.3 is crucial for evaluating the robustness of the IEEE 30-Bus and IEEE 57-Bus systems in the presence of various wind conditions to support outage simulation, failure probability analysis and grid hardening planning. The wind speed based outage scenario categorization helps in implementing specific countermeasures to improve system stability during extreme weather events.

Table 3.3
Line Outage Scenarios Based on Wind Categories for the Test Systems

	Scenarios	Wind Categories	Affected Area	Failure Probability	Outage Lines
IEEE 30-Bus RTS	1	1 (74-95 mph)	1	0.24	(1-3), (3-4), (9-11)
	2	2 (96-110 mph)	2	0.35	(14-15), (15-18), (19-20), (10-20), (10-17), (15-23), (23-24)
IEEE 57-Bus RTS	1	1 (74-95 mph)	2	0.17	(9-11), (22-23), (23-24), (35-36), (37-39), (41-42)
	2	2 (96-110 mph)	1	0.36	(1-2), (2-3), (3-4), (4-5), (4-6), (6-7), (6-8), (13-14), (1-16), (1-17), (4-18), (12-17), (15-45), (46-47)

With the help of this information, the failure probabilities of transmission lines for the test system in this study are estimated. The failure probability of the IEEE 30-Bus RTS in relation to various hurricane categories is shown in Table 3.3 The failure probability is calculated by comparing the wind speeds of different hurricane categories with their corresponding fragility curves.

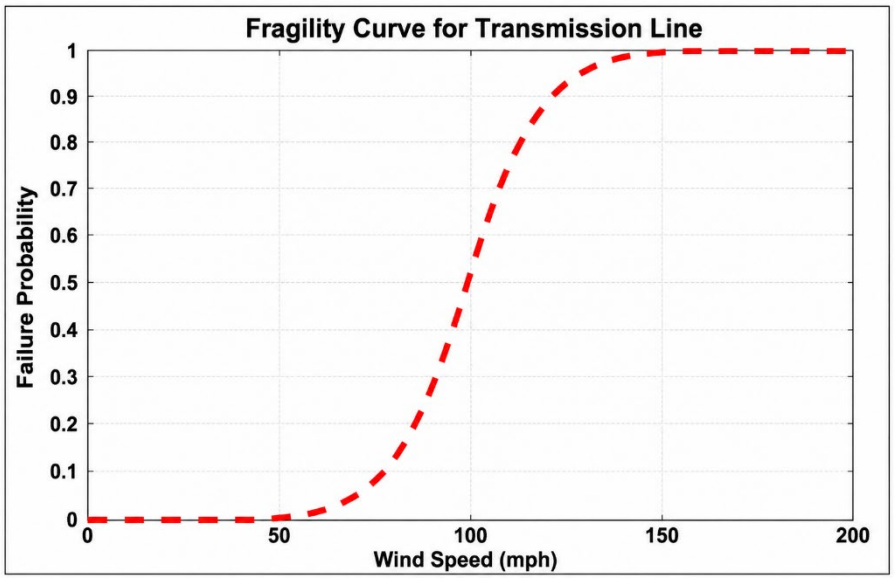


Figure 3.11 Failure Probability of Transmission Tower Versus Wind Speed

Figure 3.11 shows the fragility curve of a transmission line, illustrating the increase in failure probability with respect to wind speed. The curve indicates low failure probability under normal conditions and a rapid increase beyond a critical wind speed, approaching certain failure under extreme conditions. This relationship is used to model line vulnerability in the resilience analysis. In this study, Category 1 (74–95 mph) and Category 2 (96–110 mph) hurricanes were considered to estimate the failure probability of transmission poles and to assess the vulnerability of the power system network. As can be seen from the Table 3.3, a Category 1 hurricane leads to 24 % failure probability of transmission lines which results in 3-line outage probability in the IEEE 30-Bus RTS. As an example, Figure 3.12 presents the division of the IEEE 57-bus RTS into two areas, in which two different wind speeds are assumed for each region during Category 1 and Category 2 hurricane conditions, respectively. The detailed information about the two divisions of the system, including the affected buses and their probabilities of failure, is shown in Table 3.3. For example, a Category 1 hurricane in the IEEE 57-Bus RTS leads to 17 % probability of transmission line failure, which results in 6-line outages. These results clearly show how extreme weather conditions affect power system physical infrastructure and therefore how important it is to have resilience actions that can help to reduce the failure risk.

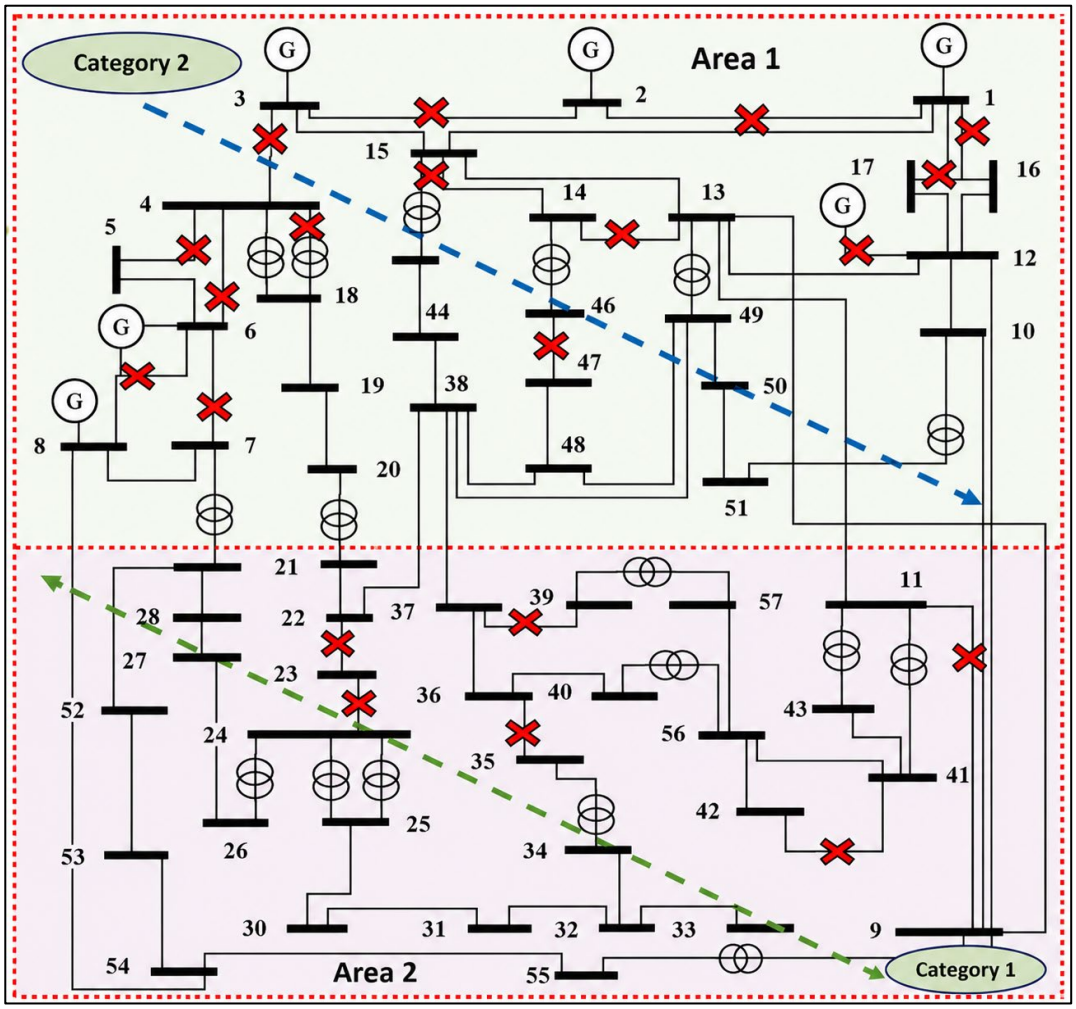


Figure 3.12 Hurricane Impact Zones and Patterns on the IEEE 57-bus RTS

3.5.3 Pre-DG Installation Status of the System

The ECSEP optimisation technique was proposed for the purpose of reducing system losses and improving voltage stability with the help of DG installation and load shedding techniques. ECSEP was employed to determine the location and size of DG unit to reduce loss and to improve the voltage stability index of the system. Besides, the location and size of the load shedding technique have been optimised with the help of ECSEP. Two scenarios with different disruptive events were simulated in this research: Scenario 1 and Scenario 2. The simulations were performed on IEEE 30-Bus RTS and IEEE 57-Bus RTS systems.

In the pre compensation techniques application scenario, the total power losses and *FVSI* values were calculated for both the IEEE 30-Bus and IEEE 57-Bus RTS systems without compensation techniques. In order to gain more insight into the

performance of the system, the loading conditions were changed and the impact of reactive power loading changes on the system stability and performance was investigated. This analysis was used as a baseline to compare the improvements achieved by compensation techniques, to gain understanding of how the system behaves under different loading conditions, and to reveal the potential for improving power loss and voltage stability with compensation techniques.

The numerical results during pre-outage are given in Table 3.4 for the IEEE 30-Bus and IEEE 57- RTS systems under different reactive power demands (Q_d) at specific buses. The values, $Loss_{Set}$ and $FVSI_{\text{Set}}$ are the baseline of power loss and voltage stability condition of the system before any disruptive events or outages. $Loss_{Set}$ is defined as the power losses calculated in the system for different reactive power demands, whereas the $FVSI_{\text{Set}}$ is the stability condition before any events in the system.

The IEEE 30-Bus RTS experiences with reactive load variations at Buses 26, 29, and 30 worth 10 MVAr, 20 MVAr and 25 MVAr which influence both $Loss_{Set}$ and $FVSI_{\text{Set}}$ values. For instance, at Bus 26, with the increase in Q_d from 10 MVAr to 25 MVAr, $Loss_{Set}$ increases from 18.23 MW to 22.27 MW and $FVSI_{\text{Set}}$ increases from 0.2248 to 0.6529 indicating that voltage stability is reduced at higher reactive loads. In addition, for the IEEE 57-Bus RTS, Buses 31, 32, and 33 are subjected to Q_d values of 5 MVAr, 10 MVAr, and 15 MVAr.

Table 3.4
Numerical Results of Pre-Outage (Before Events)

IEEE 30-Bus RTS									
Bus	**26**			**29**			**30**		
Q_d	**10**	**20**	**25**	**10**	**20**	**25**	**10**	**20**	**25**
$Loss_{Set}$	18.23	20.25	22.27	18.12	19.39	20.53	18.11	19.55	20.93
$FVSI_{Set}$	0.2248	0.4919	0.6529	0.2111	0.3573	0.4646	0.2114	0.4073	0.5349
IEEE 57-Bus RTS									
Bus	**31**			**32**			**33**		
Q_d	**5**	**10**	**15**	**5**	**10**	**15**	**5**	**10**	**15**
$Loss_{Set}$	28.46	29.22	30.57	28.67	29.42	30.66	28.56	29.30	30.55
$FVSI_{Set}$	0.4028	0.3977	0.4339	0.4005	0.3948	0.4973	0.4016	0.3960	0.4613

* Notes: Unit for Q_d = MVAr, Loss = MW and $FVSI$ = p.u.

The results indicate that increasing Q_d is associated with higher $Loss_{Set}$ and $FVSI_{\text{Set}}$ values, which indicate higher vulnerability to voltage instability as the reactive power demand increases. For instance, at Bus 32, $FVSI_{\text{Set}}$ increases from 0.4005 to 0.4973 when Q_d increases from 5 MVAr to 15 MVAr which highlights the effect of higher demand on system stability condition.

This Table 3.4 allows for an essential baseline to be set for the assessment of system resilience, giving an understanding of power loss and voltage stability during standard conditions prior to any outage events. These pre-event values are vital to understanding system behaviour and for comparing the response of the system to stress and the development of mitigation strategies to enhance grid stability and resilience. Further results for $Loss_{Set}$ and $FVSI_{Set}$ under several reactive power load variation at other load buses for both systems can be referred to the same table.

3.5.4 Distributed Generation Installation for Loss Minimization in Grid Hardening Scheme

This section presents and discusses the results obtained through the implementation of the proposed ECSEP technique for determining the optimal location and size of DG for loss minimization in the grid hardening scheme. The effectiveness of the technique is evaluated through the implementation on two test systems, namely the IEEE 30-Bus RTS and IEEE 57-Bus RTS. The results in the form of total system losses, resilience index values, and optimal DG sizing and location are presented for each test system in the following sections.

3.5.4.1 IEEE 30-Bus RTS

This study simulates two scenarios of disruptive events occurring in the IEEE 30-Bus RTS. Following these events, the proposed ECSEP technique was used to determine the optimal locations for DG installation within the system. With both 3 DG and 5 DG units, simulations were performed to evaluate how the number of DG installations affects system loss reduction following line outages. The results aimed to assess how different DG configurations can reduce losses and enhance system resilience after disruptions.

A. Scenario 1

Table 3.5 presents the numerical results for loss control in the IEEE 30-Bus RTS under Scenario 1, focusing on the impact of installing DG units across varying reactive power demands Q_d at buses 26, 29, and 30. The Table 3.5 compares two DG

configurations: one with 3 DG units and the other with 5 DG units. It provides critical insights into power losses, resilience indices, and the optimal placement and sizing of DG units necessary to enhance stability and reduce losses under a post-outage scenario. In the 3 DG units installation scheme, power losses $Loss_{3DG}$ and resilience indices RI_{Pre} before DG installation and RI_{Post} after installation are recorded across different Q_d levels (10 MVAr, 20 MVAr, and 25 MVAr.

Table 3.5
Numerical Results of IEEE 30-Bus RTS (Scenario 1) for Loss Control using 3 DG and 5 DG Units

3 DG Units Installation									
Bus	**26**			**29**			**30**		
Q_d	**10**	**20**	**25**	**10**	**20**	**25**	**10**	**20**	**25**
$Loss_{Set}$	18.23	20.25	22.27	18.12	19.39	20.53	18.11	19.55	20.93
$Loss_{Out}$	60.89	66.45	70.49	60.76	65.03	67.24	60.71	65.26	67.98
$Loss_{3DG}$	18.33	20.37	22.36	18.31	19.59	20.80	18.30	19.79	21.26
RI_{Pre}	0.427	0.438	0.462	0.425	0.425	0.439	0.425	0.428	0.445
RI_{Post}	0.431	0.442	0.464	0.431	0.431	0.448	0.432	0.435	0.455
Loc_{3DG1}	21	21	23	18	7	21	6	9	14
Loc_{3DG2}	6	7	5	7	5	5	23	11	5
Loc_{3DG3}	7	6	7	5	22	6	6	14	9
$Size_{3DG1}$	46.57	40.62	30.97	22.28	34.37	43.01	43.11	42.34	36.39
$Size_{3DG2}$	33.09	48.11	26.98	35.31	34.97	26.53	56.60	35.80	48.71
$Size_{3DG3}$	44.77	30.16	45.38	27.12	45.08	39.28	36.86	43.53	35.15
5 DG Units Installation									
Bus	**26**			**29**			**30**		
Q_d	**10**	**20**	**25**	**10**	**20**	**25**	**10**	**20**	**25**
$Loss_{Set}$	18.23	20.25	22.27	18.12	19.39	20.53	18.11	19.55	20.93
$Loss_{Out}$	60.89	66.45	70.49	60.76	65.03	67.24	60.71	65.26	67.98
$Loss_{5DG}$	18.32	20.35	22.33	18.29	19.56	20.77	18.29	19.76	21.25
RI_{Pre}	0.427	0.438	0.462	0.425	0.425	0.439	0.425	0.428	0.445
RI_{Post}	0.430	0.442	0.464	0.431	0.430	0.447	0.431	0.434	0.455
Loc_{5DG1}	11	11	5	7	14	3	11	11	8
Loc_{5DG2}	3	12	25	6	7	8	3	15	7
Loc_{5DG3}	8	17	15	11	6	23	8	8	11
Loc_{5DG4}	5	5	27	8	23	5	23	22	12
Loc_{5DG5}	7	7	7	23	5	7	5	3	15
$Size_{5DG1}$	32.88	20.25	31.84	48.47	45.16	31.78	49.50	43.50	23.45
$Size_{5DG2}$	23.89	20.93	20.54	19.86	30.54	47.63	11.89	42.58	20.09
$Size_{5DG3}$	41.76	37.23	18.08	40.04	34.68	38.12	22.15	38.29	32.93
$Size_{5DG4}$	45.89	37.07	30.94	31.46	23.83	14.32	38.07	26.10	38.20
$Size_{5DG5}$	39.07	43.39	41.62	29.29	26.64	44.24	23.01	5.45	26.39

* Notes: Unit for Q_d = MVAr, Loss = MW and Size = MW

At Bus 26 with a reactive demand (Q_d) of 10 MVAr, the recorded power loss prior to the disruptive event ($Loss_{Set}$) was 18.23 MW. However, following the event and subsequent outage, this loss escalated sharply to 60.89 MW ($Loss_{Out}$). With 3 units of DG installation, optimally positioned using the ECSEP optimisation technique, the power loss was reduced to 18.33 MW, as shown in Table 3.5. This is indeed a significant

losses reduction worth 69.90 %. Furthermore, the resilience index improved from 0.427 (RI_{Pre}) to 0.431 (RI_{Post}), highlighting enhanced system resilience achieved through the integration of DG. The improvement of resilience index is not that high, but it is already indicative to demonstrate the grid hardening phenomenon. Table 3.5 further provides the details of optimal DG locations, noted as Loc_{3DG1}, Loc_{3DG2} and Loc_{3DG3} along with their respective capacities: $Size_{3DG1,}$ $Size_{3DG2}$ and $Size_{3DG3}$ for 3 DG units installation scheme. For instance, Q_{d26} = 10 MVAr, the DG units are optimally placed at Buses 21, 6, and 7 with capacities of 46.57 MW, 33.09 MW, and 44.77 MW, respectively.

The 5 DG units installation scheme provides a more granular distribution of DG resources, generally resulting in reduced losses and enhanced resilience indices compared to the 3 DG configuration. For example, at Q_{d26} = 10 MVAr, $Loss_{5DG}$ is 18.32 MW, which is lower than the 18.33 MW observed in the 3 DG installation. The resilience index also improves from 0.427 (RI_{Pre}) to 0.430 (RI_{Post}).

In this scheme, optimal DG locations include five positions: Loc_{5DG1} through Loc_{5DG5}, with their corresponding sizes $Size_{5DG1}$ through $Size_{5DG5}$ specified to minimize power losses. For instance, at Bus 26 with Q_d = 10 MVAr, the DG units are placed at locations 11, 3, 8, 5 and 7 with respective capacities of 32.88 MW, 23.89 MW, 41.76 MW, 45.89 MW, and 39.07 MW, respectively. The optimal placement of DG units using the ECSEP optimisation technique significantly improved system resilience, as indicated by an increase in the resilience index, while maintaining low power losses through strategic sizing and placement. Table 3.5 has tabulated the results involving the pre-outage without DG installation and post-outage before and after DG installation. In general, when line outage occurs, the loss in power system is abruptly increased. With DG installation power loss is significantly reduced implying grid hardening in power system. Detail results involving other load variations can be referred to the same table.

B. Scenario 2

In Scenario 2, the ECSEP optimisation technique was applied to the IEEE 30-Bus RTS to control transmission losses during disruptive events through DG installation. In this scenario, different line outages are experienced in this system. Both 3 DG and 5 DG unit configurations were utilized in this process. Table 3.6 presents the numerical results for loss control in the IEEE 30-Bus RTS (Scenario 2) using 3 DG units and 5 DG units for hardening the power system grid. The tested buses and reactive

power loading variations in Scenario 2 are the same as those in Scenario 1. With the reactive load at Bus 30 (Q_d) set to 25 MVAr, the installation of 3 DG units via the ECSEP technique led to a substantial decrease in system losses. Referring to Table 3.6, for Scenario 2 at Bus 29 with a reactive demand (Q_d) of 20 MVAr, the recorded power loss prior to the disruptive event ($Loss_{Set}$) was 19.39 MW. Following the outage, this loss increased to 22.87 MW ($Loss_{Out}$). However, with the application of ECSEP, to optimize the sizing and locations for DG installation the power loss is reduced to 19.41 MW ($Loss_{3DG}$). This trend is accompanied by an improved resilience index from 5.571 (RI_{Pre}) to 5.622 (RI_{Post}), indicating enhanced resiliency leading to grid hardening of the system. The DG units are optimally positioned at locations Loc_{3DG1}, Loc_{3DG2}, Loc_{3DG3} with corresponding sizes $Size_{3DG1}$, $Size_{3DG2}$, $Size_{3DG3}$. For instance, at Q_{d29} = 20 MVAr, DG units are optimally placed at Buses 15, 6 and 18 with their corresponding sizes of 38.69 MW, 33.43 MW, and 48.85 MW, respectively.

Meanwhile, the 5 DG units installation scheme in Scenario 2 offers a more distributed DG setup, which generally yields better outcomes in terms of loss reduction and resilience improvement compared to the 3 DG configuration. For instance, with 5 DG installation scheme, at Bus 29 with Q_d = 20 MVAr, $Loss_{5DG}$ is reduced to 19.40 MW. The resilience index improves from 5.571 to 5.596. Optimal DG placement in this scheme includes five locations Loc_{5DG1} through Loc_{5DG5}, with sizes tailored to reduce power losses. At this loading condition, the DG units are positioned at locations 8, 13, 28, 6, and 11 with sizes of 20.43 MW, 44.10 MW, 44.73 MW, 34.57 MW, and 13.87 MW respectively, providing enhanced resilience of the system.

On the overall, the results in Table 3.6 illustrate the advantages of DG installations in IEEE 30-Bus RTS for reducing power losses and enhancing the grid resilience, as evidenced by lower $Loss_{3DG}$ and $Loss_{5DG}$ along with improved RI_{Post} values in both DG installation schemes. The 5 DG units installation scheme tends to yield better outcomes, with lower power losses and it is supported by the increment of resilience index which also implies grid hardening has been achieved. These findings underscore the importance of carefully optimizing DG size and location to improve power system resilience, especially under varying load conditions in post-outage scenarios. This analysis will form an understanding for assessing the resilience and effectiveness of DG integrated systems in maintaining strong grid in a high demand critical power network.

Table 3.6
Numerical Results of IEEE 30-Bus RTS (Scenario 2) for Loss Control using 3 DG and 5 DG Units

3 DG Units Installation									
Bus	**26**			**29**			**30**		
Q_d	**10**	**20**	**25**	**10**	**20**	**25**	**10**	**20**	**25**
$Loss_{Set}$	18.23	20.25	22.27	18.12	19.39	20.53	18.11	19.55	20.93
$Loss_{Out}$	20.41	25.03	29.92	19.78	22.87	24.82	20.27	23.59	28.33
$Loss_{3DG}$	18.29	21.12	22.39	18.80	19.41	22.11	18.35	19.62	21.19
RI_{Pre}	8.381	4.236	2.910	10.894	5.571	4.782	8.379	4.833	2.826
RI_{Post}	8.634	5.405	2.972	19.124	5.622	8.160	9.578	4.939	2.965
Loc_{3DG1}	15	5	5	8	15	12	5	15	24
Loc_{3DG2}	5	4	7	5	6	5	6	5	18
Loc_{3DG3}	6	17	10	15	18	22	10	4	6
$Size_{3DG1}$	29.67	34.16	32.32	31.57	38.69	17.76	19.74	28.98	31.66
$Size_{3DG2}$	47.72	28.63	41.47	40.50	33.43	44.64	26.44	43.53	29.13
$Size_{3DG3}$	38.28	40.61	6.45	13.40	48.85	20.28	35.14	45.09	31.57
5 DG Units Installation									
Bus	**26**			**29**			**30**		
Q_d	**10**	**20**	**25**	**10**	**20**	**25**	**10**	**20**	**25**
$Loss_{Set}$	18.23	20.25	22.27	18.12	19.39	20.53	18.11	19.55	20.93
$Loss_{Out}$	20.41	25.03	29.92	19.78	22.87	24.82	20.27	23.59	28.33
$Loss_{5DG}$	18.27	20.99	22.27	18.63	19.40	22.00	18.20	19.60	21.04
RI_{Pre}	8.381	4.236	2.910	10.894	5.571	4.782	8.379	4.833	2.826
RI_{Post}	8.537	5.189	2.913	16.246	5.596	7.774	8.769	4.900	2.883
Loc_{5DG1}	5	5	15	5	8	15	13	4	5
Loc_{5DG2}	8	19	22	9	13	4	18	5	11
Loc_{5DG3}	13	13	24	23	28	21	5	18	7
Loc_{5DG4}	28	6	15	10	6	5	17	6	12
Loc_{5DG5}	19	29	5	18	11	7	21	22	15
$Size_{5DG1}$	37.64	20.08	28.70	32.58	20.43	18.04	43.39	22.17	44.37
$Size_{5DG2}$	40.38	17.48	20.32	42.69	44.10	39.86	30.87	48.92	44.41
$Size_{5DG3}$	22.45	19.69	10.65	27.20	44.73	37.17	38.94	19.36	49.34
$Size_{5DG4}$	23.01	33.75	12.33	46.90	34.57	32.48	33.08	44.39	39.34
$Size_{5DG5}$	19.08	23.08	36.77	11.75	13.87	48.97	14.80	18.97	32.29

* Notes: Unit for Q_d = MVAr, Loss = MW and Size = MW

3.5.4.2 IEEE 57-Bus RTS

Implementation of the proposed ECSEP optimisation technique on a larger test model, i.e. IEEE 57-Bus RTS is aimed to see the robustness and feasibility of the proposed technique in addressing loss reduction and power system resilience improvement in the effort of grid hardening of the system. Buses 31, 32, and 33 were found to be the weak buses in this system [189]. To investigate the effect of Q_d on system performance, reactive load (Q_d) was adjusted at 5 MVAr, 10 MVAr, and 15 MVAr. Furthermore, two disruptive events were modelled on the IEEE 57-Bus RTS.

After these events, the proposed ECSEP technique was employed to identify the best locations to add DG into the system. The effect of the number of DG installations on the reduction of system losses due to line outages was investigated through simulations with both 3 and 5 DG units installation schemes.

A. Scenario 1

The results for loss minimization involving IEEE 57-Bus RTS for Scenario 1 in the effort of grid hardening is also conducted in this study. The results are tabulated in Table 3.7 with the impact of installing 3 DG and 5 DG units. The Table 3.7 is divided into two main sections: the upper section presents the results for 3 DG unit installation, and the lower section shows the results for 5 DG unit installation. In both cases, results are provided for three Buses (31, 32, and 33) with varying reactive loads (Q_d) set to 5 MVAr, 10 MVAr, and 15 MVAr, providing insights into system performance under outage scenario.Table 3.7 shows the impacts on post-DG power losses, ($Loss_{3DG}$ and $Loss_{5DG}$) and resilience indices before (RI_{Pre}) and after (RI_{Post}) DG placement, as well as the optimal locations and sizes of DG units.

In Table 3.7, the 3 DG units installation scheme demonstrates varying results in terms of power losses and resilience across the system. At Q_{d33} = 15 MVAr, the power loss before the event ($Loss_{Set}$) was recorded at 30.55 MW. Following a hurricane-induced outage, the power loss increased to 38.00 MW ($Loss_{Out}$). With the compensation effort as a meant to grid hardening, the installation of 3 DG units, optimised using ECSEP, reduced the power loss to 32.22 MW ($Loss_{3DG}$). This grid hardening initiative has improved the resilience index from RI_{Pre} = 4.101 to RI_{Post} = 5.574, indicating enhanced system resilience. The DG units were optimally positioned at locations Loc_{3DG1}, Loc_{3DG2}, and Loc_{3DG3}, at Buses 35, 53, and 49, with the corresponding sizes of 98.69 MW, 12.50 MW, and 26.94 MW.

With the 5 DG unit installation as the grid hardening effort, the results demonstrate enhanced performance in reducing power losses. At Q_{d33} = 15 MVAr, the power loss decreases to 30.57 MW, compared to 32.22 MW in the 3 DG unit installation. The resilience index improves from 4.101 to 4.112 following DG installation. The five DG units are optimally distributed across the optimal locations at Buses 50, 35, 14, 17, and 27, with respective sizes of 36.77 MW, 40.04 MW, 87.09 MW, 31.14 MW, and 13.70 MW, effectively reducing losses and enhancing power

system resilience implying grid hardening. This demonstrates the advantage of installing more DG units to achieve better loss reduction along with the increment in resilience index.

Table 3.7
Numerical Results of IEEE 57-Bus RTS (Scenario 1) for Loss Control using 3 DG and 5 DG Units

3 DG Units Installation									
Bus		**31**			**32**			**33**	
Q_d	**5**	**10**	**15**	**5**	**10**	**15**	**5**	**10**	**15**
$Loss_{Set}$	28.46	29.22	30.57	28.67	29.42	30.66	28.56	29.30	30.55
$Loss_{Out}$	32.85	34.41	42.75	33.25	34.84	39.15	33.03	34.51	38.00
$Loss_{3DG}$	28.67	30.87	30.98	29.22	30.87	31.84	29.96	31.07	32.22
RI_{Pre}	6.488	5.627	2.508	6.250	5.437	3.613	6.382	5.618	4.101
RI_{Post}	6.858	8.716	2.632	7.233	7.788	4.358	9.760	9.030	5.574
Loc_{3DG1}	51	43	13	12	35	35	12	12	35
Loc_{3DG2}	36	38	51	29	53	53	29	29	53
Loc_{3DG3}	13	50	36	49	49	49	49	49	49
$Size_{3DG1}$	61.91	77.66	97.79	72.58	69.60	51.80	87.76	58.90	98.69
$Size_{3DG2}$	45.70	55.56	33.07	88.32	64.29	81.44	81.12	32.73	12.50
$Size_{3DG3}$	47.90	49.51	37.39	44.22	82.96	60.55	89.73	88.53	26.94
5 DG Units Installation									
Bus		**31**			**32**			**33**	
Q_d	**5**	**10**	**15**	**5**	**10**	**15**	**5**	**10**	**15**
$Loss_{Set}$	28.46	29.22	30.57	28.67	29.42	30.66	28.56	29.30	30.55
$Loss_{Out}$	32.85	34.41	42.75	33.25	34.84	39.15	33.03	34.51	38.00
$Loss_{5DG}$	28.55	29.30	30.78	28.70	29.51	30.82	28.63	29.32	30.57
RI_{Pre}	6.488	5.627	2.508	6.250	5.437	3.613	6.382	5.618	4.101
RI_{Post}	6.646	5.729	2.571	6.295	5.541	3.702	6.509	5.648	4.112
Loc_{5DG1}	13	27	12	40	16	49	20	47	50
Loc_{5DG2}	51	11	18	15	40	43	31	20	35
Loc_{5DG3}	40	46	52	20	37	35	14	12	14
Loc_{5DG4}	46	38	38	13	12	47	38	53	17
Loc_{5DG5}	28	12	15	47	13	18	16	49	27
$Size_{5DG1}$	73.77	45.40	80.18	35.80	84.33	42.48	7.50	66.87	36.77
$Size_{5DG2}$	39.53	20.40	97.19	83.42	35.97	38.40	27.12	16.98	40.04
$Size_{5DG3}$	30.41	72.04	18.17	18.59	19.76	19.12	94.25	86.83	87.09
$Size_{5DG4}$	24.09	74.78	77.21	31.48	58.25	85.71	33.03	17.66	31.14
$Size_{5DG5}$	48.07	73.29	59.17	69.24	49.46	86.61	53.07	71.58	13.70

* Notes: Unit for Q_d = MVAr, Loss = MW and Size = MW

In summary, Table 3.7 clearly demonstrates that both 3 and 5 DG units effectively reduce system losses and enhance resilience. However, the installation of 5 DG units leads to superior performance, as evidenced by the lower post-installation losses and higher resilience indices, particularly in the scenario with a 15 MVAr reactive load at Bus 33, highlighted in the shaded column.

B. Scenario 2

Table 3.8 illustrates the results for DG installation as an effort in grid hardening of Scenario 2, showcasing the response of the system under varying reactive power loading. The power losses with respect to reactive power increment at each bus, display a consistent decreasing trend after implementing 3 DG units installation as an effort for grid hardening.

Table 3.8
Numerical Results of IEEE 57-Bus RTS (Scenario 2) for Loss Control using 3 DG and 5 DG Units

3 DG Units Installation									
Bus	**31**			**32**			**33**		
Q_d	**5**	**10**	**15**	**5**	**10**	**15**	**5**	**10**	**15**
$Loss_{Set}$	28.46	29.22	30.57	28.67	29.42	30.66	28.56	29.30	30.55
$Loss_{Out}$	47.34	49.47	54.69	47.77	49.81	55.06	47.52	49.56	53.90
$Loss_{3DG}$	30.70	32.10	33.47	30.17	31.65	34.51	31.27	32.15	33.65
RI_{Pre}	1.508	1.443	1.267	1.501	1.443	1.257	1.506	1.446	1.308
RI_{Post}	1.845	1.848	1.577	1.714	1.742	1.679	1.923	1.846	1.661
Loc_{3DG1}	18	6	6	50	10	51	44	48	18
Loc_{3DG2}	31	24	38	6	5	44	5	6	17
Loc_{3DG3}	10	10	13	48	22	5	12	13	23
$Size_{3DG1}$	60.20	82.67	73.90	72.24	58.29	54.71	70.42	81.89	51.40
$Size_{3DG2}$	26.30	50.16	76.67	89.26	69.19	71.54	91.98	87.94	70.34
$Size_{3DG3}$	65.41	77.92	94.09	81.81	60.95	66.44	66.97	14.95	69.61
5 DG Units Installation									
Bus	**31**			**32**			**33**		
Q_d	**5**	**10**	**15**	**5**	**10**	**15**	**5**	**10**	**15**
$Loss_{Set}$	28.46	29.22	30.57	28.67	29.42	30.66	28.56	29.30	30.55
$Loss_{Out}$	47.34	49.47	54.69	47.77	49.81	55.06	47.52	49.56	53.90
$Loss_{5DG}$	28.87	30.22	31.65	29.19	29.63	32.59	29.02	29.34	31.98
RI_{Pre}	1.508	1.443	1.267	1.501	1.443	1.257	1.506	1.446	1.308
RI_{Post}	1.563	1.570	1.374	1.571	1.468	1.450	1.568	1.451	1.458
Loc_{5DG1}	39	18	13	38	51	48	12	49	38
Loc_{5DG2}	45	53	14	3	18	50	48	12	5
Loc_{5DG3}	49	51	38	18	49	13	18	18	49
Loc_{5DG4}	50	34	27	12	35	32	49	23	16
Loc_{5DG5}	18	13	5	14	12	18	15	9	46
$Size_{5DG1}$	47.41	38.14	68.71	83.74	72.57	26.65	61.47	15.36	83.18
$Size_{5DG2}$	91.60	10.21	69.23	47.19	55.72	41.40	45.56	77.80	34.55
$Size_{5DG3}$	74.32	59.70	75.38	61.87	27.76	78.72	65.24	48.83	43.86
$Size_{5DG4}$	38.87	18.69	36.74	42.12	29.37	15.52	83.05	51.76	34.95
$Size_{5DG5}$	40.81	58.27	62.18	37.06	93.49	51.33	82.45	23.63	85.88

* Notes: Unit for Q_d = MVAr, Loss = MW and Size = MW

For example, at Bus 31, with Q_d values of 5 MVAr, 10 MVAr, and 15 MVAr, the power losses during the outage at all the reactive power load variations are 47.34 MW, 49.47 MW, and 54.69 MW, respectively. After the installation of 3 DG units,

these losses are reduced to 30.70 MW, 32.10 MW, and 33.47 MW, respectively. With the installation of 5 DG units, the losses are brought down to 28.87 MW, 30.22 MW, and 31.65 MW, respectively. As shown in Table 3.8, the impact of DG installation on loss reduction during outages is clearly significant. The 5 DG installation scheme is found to be very effective in reducing losses across the different load conditions thus underscoring the role of DG in enhancing system resilience which implies grid hardening is achieved. This points to the need for proper DG placement for better performance in contemporary power systems.

3.5.5 Distributed Generation Installation for Voltage Security Improvement in Grid Hardening Scheme

This section presents the results of applying the proposed ECSEP technique to determine the optimal DG locations and capacities to enhance voltage security within the grid hardening framework indicated by the reduction in *FVSI* value. The studies were conducted on IEEE 30-Bus RTS and IEEE 57-Bus RTS systems. The subsequent sections will detail out the analysis of the results, including *FVSI* values, resilience index values for indicating voltage security and the optimal DG placement and sizing for each system.

3.5.5.1 IEEE 30-Bus RTS

Voltage stability improvement was conducted using the DG installation schemes involving 3 DGs and 5 DGs installation schemes in IEEE 30-Bus RTS. Similar hurricane scenarios are considered for this initiative as one of the strategies in grid hardening indicated by the improvement in the resilience index resulted from the voltage stability improvement.

A. Scenario 1

The results show that DG units have an important impact on improving the voltage stability of power systems through the decrease of *FVSI* value of the system. Small *FVSI* values mean that the voltage stability is improved which is very vital in order to ensure safe and stable operation of a transmission network. Table 3.9 presents

the detailed results of voltage security improvements in IEEE 30-Bus RTS under Scenario 1 involving 3 DGs and 5 DGs installation. The key parameters include the *FVSI* values during post-DG installation, $FVSI_{DG}$, resilience indices before (RI_{Pre}) and after DG installation (RI_{Post}), and the optimal locations and sizes of the DG units.

Table 3.9
Numerical Results of IEEE 30-Bus RTS (Scenario 1) for Voltage Security Improvement using 3 DG and 5 DG Units

3 DG Units Installation									
Bus	**26**			**29**			**30**		
Q_d	**10**	**20**	**25**	**10**	**20**	**25**	**10**	**20**	**25**
$FVSI_{Set}$	0.2248	0.4919	0.6529	0.2111	0.3573	0.4646	0.2114	0.4073	0.5349
$FVSI_{Out}$	0.2968	0.5673	0.7707	0.2953	0.4072	0.5370	0.2939	0.4635	0.6188
$FVSI_{3DG}$	0.2541	0.5320	0.6781	0.2410	0.3902	0.4721	0.2591	0.4333	0.5514
RI_{Pre}	3.122	6.524	5.542	2.507	7.160	6.417	2.562	7.247	6.375
RI_{Post}	5.967	15.116	7.350	4.458	22.813	7.274	7.326	13.952	8.154
Loc_{3DG1}	17	8	17	9	5	4	23	5	7
Loc_{3DG2}	26	10	26	27	11	24	3	16	4
Loc_{3DG3}	5	26	19	7	29	29	24	4	10
$Size_{3DG1}$	34.79	32.30	8.86	23.49	23.96	7.85	44.71	22.67	36.13
$Size_{3DG2}$	40.73	21.90	25.38	39.54	22.29	3.01	34.82	18.88	49.65
$Size_{3DG3}$	24.58	42.55	35.56	45.73	47.48	47.74	0.19	25.14	35.04
5 DG Units Installation									
Bus	**26**			**29**			**30**		
Q_d	**10**	**20**	**25**	**10**	**20**	**25**	**10**	**20**	**25**
$FVSI_{Set}$	0.2248	0.4919	0.6529	0.2111	0.3573	0.4646	0.2114	0.4073	0.5349
$FVSI_{Out}$	0.2968	0.5673	0.7707	0.2953	0.4072	0.5370	0.2939	0.4635	0.6188
$FVSI_{5DG}$	0.2411	0.4932	0.6540	0.2123	0.3591	0.4661	0.2322	0.4080	0.5361
RI_{Pre}	3.122	6.524	5.542	2.507	7.160	6.417	2.562	7.247	6.375
RI_{Post}	4.338	6.646	5.615	2.562	7.466	6.586	3.710	7.382	6.473
Loc_{5DG1}	29	25	26	9	9	3	16	16	30
Loc_{5DG2}	19	6	23	8	4	10	18	7	7
Loc_{5DG3}	5	17	7	5	3	29	4	19	21
Loc_{5DG4}	17	6	4	29	27	7	8	3	4
Loc_{5DG5}	26	27	8	10	23	5	20	24	10
$Size_{5DG1}$	8.75	31.68	21.47	33.40	24.95	21.33	21.12	21.78	12.69
$Size_{5DG2}$	41.05	43.45	35.15	16.83	24.18	33.31	8.42	17.29	28.86
$Size_{5DG3}$	39.85	20.58	26.16	26.26	45.26	23.73	28.85	1.87	30.58
$Size_{5DG4}$	44.12	28.28	35.68	47.03	32.25	39.77	25.82	43.15	22.53
$Size_{5DG5}$	46.85	27.23	15.94	40.62	44.84	20.58	43.23	41.19	31.16

*Notes: Unit for Q_d = MVAr, *FVSI* = p.u. and Size = MW

It involves different reactive power demand levels Q_d at Buses 26, 29, and 30. The 3 DG units installation scheme shows moderate improvements in *FVSI* values, which indicate enhanced voltage stability improvement. At Q_{d26} = 10 MVAr, the initial *FVSI* value ($FVSI_{Set}$) is 0.2248. Following a hurricane and the resulting outages, the *FVSI* value increases to 0.2968 ($FVSI_{Out}$). Using ECSEP to determine the optimal locations and sizes for DG units, the *FVSI* is reduced to 0.2541 ($FVSI_{3DG}$). Additionally,

the resilience index (RI_{Post}) improves significantly from 3.122 to 5.967, reflecting enhanced system resiliency leading to hardened grid of the system. The DG units are optimally placed at Buses 17, 26, and 5, with corresponding sizes of 34.79 MW, 40.73 MW, and 24.58 MW, as specified by Loc_{3DG1}, Loc_{3DG2}, Loc_{3DG3}, and their respective sizes.

The 5 DG unit installation scheme offers a more distributed arrangement, leading to further reductions in *FVSI* values indicating improved voltage stability. For instance, at Bus 26 with Q_d = 10 MVAr, the *FVSI* value ($FVSI_{5DG}$) decreases to 0.2411, reflecting better stability compared to the 3 DG scheme. Additionally, the RI_{Post} value improves to 4.338, indicating enhanced overall system resilience or hardened grid. The DG units are strategically positioned at five locations, designated as Loc_{5DG1} through Loc_{5DG5}, with optimal sizes to maximize voltage stability. These units are located at Buses 29, 19, 5, 17, and 26, with respective capacities of 8.75 MW, 41.05 MW, 39.85 MW, 44.12 MW, and 46.85 MW.

B. Scenario 2

Similar to Scenario 1, Table 3.10 presents the numerical results of IEEE 30-Bus RTS in Scenario 2 for voltage security improvement using 3 DG and 5 DG installation schemes. It provides a quantitative assessment of voltage security improvements in the IEEE 30-Bus RTS under Scenario 2, examining the efficacy of 3 and 5 DG units for maintaining stability across different reactive power demands Q_d at Buses 26, 29, and 30. In the 3 DG units installation scheme, at Q_{d29} = 25 MVAr, the *FVSI* value after DG installation, $FVSI_{3DG}$ is 0.4620 which is lower than the *FVSI* value before DG installation $FVSI_{out}$ at 0.5880. This implies voltage stability improvement in the system. The resilience index after DG installation RI_{Post} also shows considerable enhancement. At Q_{d29} = 25 MVAr, RI_{Post} reaches a substantial value of 177.69, indicating a strengthened resilience due to DG integration. The DG units in this scheme are allocated to strategic locations Loc_{3DG1}, Loc_{3DG2} *and* Loc_{3DG3}, with sizes optimised to maintain system stability. The DG units are placed at Buses 12, 19, and 29, with sizes 34.60 MW, 20.16 MW, and 25.58 MW, respectively, supporting voltage security at higher reactive loads.

Table 3.10
Numerical Results of IEEE 30-Bus RTS (Scenario 2) for Voltage Security Improvement using 3 DG and 5 DG Units

3 DG Units Installation									
Bus	**26**			**29**			**30**		
Q_d	**10**	**20**	**25**	**10**	**20**	**25**	**10**	**20**	**25**
$FVSI_{Set}$	0.2248	0.4919	0.6529	0.2111	0.3573	0.4646	0.2114	0.4073	0.5349
$FVSI_{Out}$	0.2470	0.6904	1.0000	0.2193	0.4201	0.5880	0.2190	0.4657	0.6805
$FVSI_{3DG}$	0.1779	0.1642	0.1826	0.1775	0.3512	0.4620	0.1947	0.4012	0.4825
RI_{Pre}	2.57	0.31	0.18	4.25	5.10	3.67	8.01	6.22	2.44
RI_{Post}	3.79	0.50	0.39	5.28	57.57	177.69	11.66	65.77	9.21
Loc_{3DG1}	13	26	24	17	10	12	4	13	12
Loc_{3DG2}	26	7	12	6	24	19	12	21	16
Loc_{3DG3}	10	23	4	16	26	29	27	6	30
$Size_{3DG1}$	44.14	20.13	49.57	37.09	11.81	34.60	30.85	17.54	36.28
$Size_{3DG2}$	27.07	36.88	12.53	22.12	21.09	20.16	40.19	27.14	23.23
$Size_{3DG3}$	38.61	42.43	27.66	30.39	45.78	25.58	31.03	39.33	46.38
5 DG Units Installation									
Bus	**26**			**29**			**30**		
Q_d	**10**	**20**	**25**	**10**	**20**	**25**	**10**	**20**	**25**
$FVSI_{Set}$	0.2248	0.4919	0.6529	0.2111	0.3573	0.4646	0.2114	0.4073	0.5349
$FVSI_{Out}$	0.2470	0.6904	1.0000	0.2193	0.4201	0.5880	0.2190	0.4657	0.6805
$FVSI_{5DG}$	0.1401	0.1610	0.1785	0.1738	0.2312	0.4069	0.1917	0.2136	0.4521
RI_{Pre}	1.31	0.30	0.18	3.82	1.22	2.25	7.02	0.85	1.98
RI_{Post}	1.65	0.49	0.38	4.66	1.83	7.05	9.73	1.10	5.46
Loc_{5DG1}	26	4	4	20	26	17	14	27	3
Loc_{5DG2}	10	7	7	5	3	26	6	3	30
Loc_{5DG3}	20	9	5	29	16	19	21	14	21
Loc_{5DG4}	17	10	10	8	7	7	8	23	10
Loc_{5DG5}	14	26	20	21	21	8	6	9	12
$Size_{5DG1}$	44.32	49.84	28.06	39.92	23.60	48.62	44.33	23.57	40.53
$Size_{5DG2}$	5.98	33.36	48.34	43.21	36.81	29.71	29.60	21.43	30.58
$Size_{5DG3}$	26.43	28.72	49.57	12.50	39.39	28.64	39.28	29.12	34.54
$Size_{5DG4}$	31.89	37.12	33.61	11.67	21.68	35.16	28.59	24.48	21.55
$Size_{5DG5}$	37.92	41.01	23.91	36.53	39.57	44.80	25.51	31.63	29.44

*Notes: Unit for Q_d = MVAr, $FVSI$ = p.u. and Size = MW

For 5 DG units installation scheme, at Q_{d29} = 25 MVAr, $FVSI_{5DG}$ value is 0.4069, reflecting a voltage stability improvement due to the distributed DG installation. The RI_{Post} is also markedly improved across the system. At Q_{d29} = 25 MVAr, RI_{Post} is 7.05, demonstrating the significant impact of additional DG units on system resilience. DG placements in this scheme are spread across five optimal locations $Loc5_{DG1}$ through Loc_{5DG5} with optimal sizing to maximize voltage security. At this loading condition, 5 DG units need to be positioned at Buses 17, 26, 19, 7, and 8, with sizes 48.62 MW, 29.71 MW, 28.64 MW, 35.16 MW, and 44.80 MW, contributing effectively to the

ability of the system to withstand higher reactive loads.

3.5.5.2 IEEE 57-Bus RTS

Voltage stability improvement was also conducted using the DG installation schemes involving 3 DGs and 5 DGs installation schemes in IEEE 57-Bus RTS. Similar hurricane scenarios are considered for this initiative as one of the strategies in grid hardening indicated by the improvement in the resilience index resulted from the voltage stability improvement.

A. Scenario 1

In this section, the focus shifts to the IEEE 57-Bus RTS, where Table 3.11 presents the results for IEEE 57-Bus RTS under Scenario 1, examining the effectiveness of 3 and 5 DG unit installations in enhancing voltage security. The primary objective here is minimizing the *FVSI* value when reactive load variations are subjected to Buses 31, 32, and 33. Both schemes, the 3 DG units installation and the 5 DG units installation is evaluated in terms of *FVSI* reduction, resilience index improvements RI_{Pre} and RI_{Post} and optimised DG placements and sizes. In the 3 DG units installation scheme, *FVSI* values remain relatively stable across varying Q_d levels, with a slight increase at higher reactive demands. For example, at Q_{d32} = 15 MVAr, $FVSI_{3DG}$ reaches 0.4973 from its original value of 0.767, reflecting a consistent pattern of voltage stability. The post-DG resilience index RI_{Post} shows a substantial improvement, increasing to 1.858 from the pre-DG value RI_{Pre} of 1.844, highlighting enhanced system resiliency.

DG units in this scheme are optimally located at Loc_{3DG1}, Loc_{3DG2} *and* Loc_{3DG3} with optimal sizing to ensure voltage stability is improved. For instance, Q_{d32} = 15 MVAr, DG units are positioned at Buses 38, 52, and 35 with sizes 46.75 MW, 80.67 MW, and 36.52 MW, respectively, demonstrating strategic deployment to achieve *FVSI* reduction from 0.7670 to 0.4986. In contrast, the 5 DG units installation scheme shows enhanced performance, with consistently slightly lower *FVSI* values supported with resilience index improvements. For example, at Q_{d32} = 15 MVAr, the $FVSI_{5DG}$ value is 0.4979 compared to $FVSI_{Out}$ 0.7670. The resilience index is improved from 1.844 to 1.850. DG units are placed at Buses 35, 20, 27, 49, and 10, with corresponding sizes 59.46 MW, 27.79 MW, 52.53 MW, 24.20 MW and 76.85 MW respectively,

contributing to the overall system stability under this load condition.

Table 3.11
Numerical Results of IEEE 57-Bus RTS (Scenario 1) for Voltage Security Improvement using 3 DG and 5 DG Units

3 DG Units Installation									
Bus		**31**			**32**			**33**	
Q_d	**5**	**10**	**15**	**5**	**10**	**15**	**5**	**10**	**15**
$FVSI_{Set}$	0.4028	0.3977	0.4339	0.4005	0.3948	0.4973	0.4016	0.3960	0.4613
$FVSI_{Out}$	0.4395	0.4355	1.000	0.4372	0.4318	0.7670	0.4382	0.4331	0.6679
$FVSI_{3DG}$	0.4035	0.4060	0.5080	0.4120	0.4111	0.4986	0.4035	0.4070	0.4704
RI_{Pre}	10.975	10.521	0.269	10.913	10.670	1.844	10.973	10.674	2.233
RI_{Post}	11.208	13.763	0.331	16.349	19.860	1.858	11.628	15.594	2.382
Loc_1	36	32	40	40	38	38	43	34	38
Loc_{3DG1}	35	36	27	16	50	52	49	50	52
Loc_{3DG2}	33	33	26	35	34	35	50	40	35
Loc_{3DG3}	76.64	19.49	49.94	67.45	13.88	46.75	53.59	20.16	46.65
$Size_{3DG1}$	23.61	10.39	58.61	57.50	92.72	80.67	79.65	57.04	80.76
$Size_{3DG2}$	31.11	95.37	22.00	32.96	27.81	36.52	69.38	76.22	36.78
5 DG Units Installation									
Bus		**31**			**32**			**33**	
Q_d	**5**	**10**	**15**	**5**	**10**	**15**	**5**	**10**	**15**
$FVSI_{Set}$	0.4028	0.3977	0.4339	0.4005	0.3948	0.4973	0.4016	0.3960	0.4613
$FVSI_{Out}$	0.4395	0.4355	1.000	0.4372	0.4318	0.7670	0.4382	0.4331	0.6679
$FVSI_{5DG}$	0.4034	0.4021	0.4817	0.4022	0.4003	0.4979	0.4021	0.4056	0.4631
RI_{Pre}	10.975	10.521	0.269	10.913	10.670	1.844	10.973	10.674	2.233
RI_{Post}	11.175	12.039	0.308	11.491	12.708	1.850	11.139	14.749	2.261
Loc_{5DG1}	49	16	24	6	17	35	29	19	26
Loc_{5DG2}	57	33	31	36	6	20	20	18	37
Loc_{5DG3}	12	10	21	29	40	27	15	35	35
Loc_{5DG4}	38	34	39	28	38	49	36	31	49
Loc_{5DG5}	54	38	10	49	11	10	25	10	14
$Size_{5DG1}$	97.57	51.19	16.20	89.65	17.89	59.46	91.46	63.72	30.72
$Size_{5DG2}$	10.79	23.12	31.32	73.87	10.46	27.79	43.07	81.50	64.64
$Size_{5DG3}$	17.89	73.58	29.15	29.75	68.75	52.53	87.62	66.13	25.15
$Size_{5DG4}$	74.66	55.02	7.47	64.72	58.41	24.20	75.38	33.49	49.72
$Size_{5DG5}$	4.95	40.63	23.18	74.02	80.06	76.85	45.37	95.92	53.84

*Notes: Unit for Q_d = MVAr, $FVSI$ = p.u. and Size = MW

B. Scenario 2

Table 3.12 provides an in-depth analysis of the IEEE 57-Bus RTS under Scenario 2. In the 3 DG units installation scheme, the results indicate modest stability improvements with variations in $FVSI$ values at different Q_d levels. At Q_{d31} = 15 MVAr, the $FVSI$ value in the 3 DG units installation scheme $FVSI_{3DG}$ is reduced to 0.4598, compared to a pre-DG value of $FVSI_{Out}$ of 1.000, indicating a significant improvement in voltage stability.

Table 3.12
Numerical Results of IEEE 57-Bus RTS (Scenario 2) for Voltage Security Improvement using 3 DG and 5 DG Units

3 DG Units Installation									
Bus	**31**			**32**			**33**		
Q_d	**5**	**10**	**15**	**5**	**10**	**15**	**5**	**10**	**15**
$FVSI_{Set}$	0.4028	0.3977	0.4339	0.4005	0.3948	0.4973	0.4016	0.3960	0.4613
$FVSI_{Out}$	0.4521	0.4518	1.0000	0.4520	0.4516	0.7846	0.4520	0.4518	0.7086
$FVSI_{3DG}$	0.4254	0.4199	0.4598	0.4245	0.4054	0.4821	0.4175	0.4178	0.4700
RI_{Pre}	8.170	7.351	0.708	7.777	6.951	1.731	3.722	7.097	1.865
RI_{Post}	15.933	13.163	0.784	15.436	8.775	1.594	4.538	12.288	1.970
Loc_{3DG1}	47	47	24	47	47	47	47	47	14
Loc_{3DG2}	31	36	51	32	52	19	31	6	32
Loc_{3DG3}	40	19	32	42	10	52	6	31	53
$Size_{3DG1}$	69.65	85.83	31.91	79.31	9.51	98.88	71.86	94.28	34.95
$Size_{3DG2}$	57.79	99.76	13.09	91.54	98.44	19.40	93.99	27.43	34.35
$Size_{3DG3}$	94.89	21.50	24.85	43.25	73.81	4.84	41.31	93.37	59.38
5 DG Units Installation									
Bus	**31**			**32**			**33**		
Q_d	**5**	**10**	**15**	**5**	**10**	**15**	**5**	**10**	**15**
$FVSI_{Set}$	0.4028	0.3977	0.4339	0.4005	0.3948	0.4973	0.4016	0.3960	0.4613
$FVSI_{Out}$	0.4521	0.4518	1.0000	0.4520	0.4516	0.7846	0.4520	0.4518	0.7086
$FVSI_{5DG}$	0.4251	0.4196	0.4526	0.4242	0.4012	0.5001	0.4137	0.4095	0.4635
RI_{Pre}	8.170	7.351	0.708	7.777	6.951	1.731	7.968	7.097	1.865
RI_{Post}	15.744	13.031	0.762	15.259	7.960	1.758	10.802	9.681	1.891
Loc_{5DG1}	14	47	43	2	29	16	47	47	20
Loc_{5DG2}	33	15	11	15	47	18	5	29	12
Loc_{5DG3}	30	16	31	14	10	20	22	5	34
Loc_{5DG4}	18	18	50	47	50	23	52	9	48
Loc_{5DG5}	70	10	30	10	40	32	35	7	44
$Size_{5DG1}$	70.21	78.38	39.37	67.68	46.32	81.57	59.06	94.90	34.08
$Size_{5DG2}$	58.31	75.34	56.54	38.60	85.44	49.78	59.66	11.80	52.86
$Size_{5DG3}$	47.85	86.21	19.43	76.96	86.13	25.79	83.23	82.63	66.85
$Size_{5DG4}$	37.32	90.98	20.32	52.29	61.96	43.95	57.76	78.49	34.09
$Size_{5DG5}$	87.68	87.43	14.61	92.76	22.90	24.66	32.86	62.84	26.70

*Notes: Unit for Q_d = MVAr, $FVSI$ = p.u. and Size = MW

The resilience index RI_{Post} also shows substantial enhancement, increasing from 0.708 to 0.784. In this scheme, DG units are optimally positioned at locations Loc_{3DG1}, Loc_{3DG2} and Loc_{3DG3}, with each unit sized to effectively support voltage stability. Specifically, the DG units are located at Buses 24, 51, and 32, with capacities of 31.91 MW, 13.09 MW, and 24.85 MW, respectively, ensuring a targeted deployment that effectively addresses voltage stability challenges.

With 5 DG unit installation it demonstrates a notable improvement in voltage security, with consistently lower $FVSI$ values. At Q_{d31} = 15 MVAr, the $FVSI_{5DG}$

decreases to 0.4526 from a pre-DG value of $FVSI_{Out}$ 1.000. Additionally, the post-DG resilience index RI_{Post} shows a significant enhancement, rising from 0.708 to 0.762. The DG units are strategically positioned at locations 43, 11, 31, 50, and 30, with respective capacities of 39.37 MW, 56.54 MW, 19.43 MW, 20.32 MW, and 14.61 MW. This targeted placement strengthens voltage security across various load conditions, ensuring stability under higher reactive power demands. Results for other loading conditions at other load buses can be witnessed from the same table.

Table 3.12 reveals how DG placement and scheme affects voltage stability in the IEEE 57-Bus RTS under Scenario 2. The 5 DG units installation scheme provides more favourable results, with lower *FVSI* values and higher resilience indices in most of the demand levels, which highlights the importance of a distributed DG layout for voltage security and resilience in complex networks. The findings of this analysis are significant in understanding how DG deployment strategies help to enhance the stability of power systems during variable load conditions. It is also worth to state that the grid hardening initiative has been successfully achieved in this study indicated by the improvement of resilience index under hurricanes.

3.5.6 Load Shedding for Loss Minimization in Grid Hardening Scheme

Load shedding process is another initiative for grid hardening strategy. In this study, the optimal locations and amount of load to be shed were determined using the ECSEP technique. The proposed method was applied to both the IEEE 30-Bus RTS and IEEE 57-Bus RTS to assess its effectiveness in strengthening the grid against disruptive events by minimizing system losses. By identifying strategic locations for load shedding, the ECSEP method puts measure to support the most affected parts of the grid to prevent system collapse. Disruptive event scenarios were modelled using two hurricanes' conditions namely Scenario 1 and Scenario 2 on the test systems and two load shedding schemes: a 3-bus load shedding and a 4-bus load shedding scheme were implemented to address this issue. The impact of load shedding application on the systems was analysed and will be discussed in detail in the following subchapter.

3.5.6.1 IEEE 30-Bus RTS

Loss minimization was also conducted using the load shedding schemes involving 3-load shedding 4-load shedding schemes in IEEE 30-Bus RTS. Similar hurricane scenarios are considered for this initiative as one of the strategies in grid hardening indicated by the improvement in the resilience index resulted from the loss minimization improvement.

A. Scenario 1

The results of loss minimization using load shedding scheme of IEEE 30-Bus RTS for Scenario 1 is tabulated in Table 3.13. Table 3.13 is divided into two sections: the upper section presents the 3-load shedding scheme, and the lower section focuses on the 4-load shedding scheme. The discussion covers key parameters related to the load shedding scheme, including transmission loss and resilience index.

The loss is analysed for before ($Loss_{Out}$) and after ($Loss_{3LS,}$ $Loss_{4LS}$) implementing the load shedding scheme. Additionally, the resilience index is evaluated in terms of its pre-load shedding (RI_{Pre}) and post-load shedding (RI_{Post}) values. The load shedding scheme involves optimal identifications of locations to experience load shedding denoted by (Loc_{3LS1} - Loc_{3LS3}) and (Loc_{4LS1} – Loc_{4LS4}). It also determines the amount of real power (P_{d3LS1} - P_{d3LS3}, P_{d4LS1} - P_{d4LS4}) and reactive power (Q_{d3LS1} - Q_{d3LS3}, Q_{d4LS1} -Q_{d4LS4}) to be shed on the optimal locations for optimal system performance and resilience improvement. This will achieve grid hardening as the final aim.

Reactive power load was varied involving Buses 26, 29 and 30. The analysis of the load shedding scheme for Bus 30 with a reactive power demand (Q_d) of 25 MVAr highlights significant improvements in system performance, particularly in terms of transmission losses and resilience index. Before implementing the load shedding scheme, the transmission loss ($Loss_{Out}$) is 67.98 MW. However, after applying the 3-bus load shedding scheme, the loss is significantly reduced to 23.27 MW ($Loss_{3LS}$). This notable decrease in power losses indicates the effectiveness of the load shedding scheme in reducing excessive transmission losses. The resilience index before load shedding (RI_{Pre}) is 0.445. After the load shedding scheme is applied, the resilience index improves to 0.520 (RI_{Post}). This increase demonstrates an enhancement in system resilience,

Table 3.13
Numerical Results of IEEE 30-Bus RTS (Scenario 1) for Loss Control using 3-Load Shedding and 4-Load Shedding Technique

3-Load Shedding									
Bus	**26**			**29**			**30**		
Q_d	**10**	**20**	**25**	**10**	**20**	**25**	**10**	**20**	**25**
$Loss_{Set}$	18.23	20.25	22.27	18.12	19.39	20.53	18.11	19.55	20.93
$Loss_{Out}$	60.88	66.45	70.49	60.76	65.02	67.24	60.71	65.26	67.98
$Loss_{3LS}$	23.22	22.65	23.99	23.22	20.35	23.90	23.32	23.98	23.27
RI_{Pre}	0.437	0.438	0.462	0.425	0.425	0.439	0.425	0.428	0.445
RI_{Post}	0.616	0.517	0.516	0.618	0.456	0.551	0.624	0.581	0.520
Loc_{3LS1}	8	21	21	10	5	9	10	8	15
Loc_{3LS2}	5	5	5	8	9	5	13	5	7
Loc_{3LS3}	6	13	13	7	12	13	5	21	6
P_{d3LS1}	65.75	74.44	107.10	31.97	112.40	59.57	70.28	46.98	37.51
P_{d3LS2}	150.54	167.95	75.69	61.78	139.98	140.67	44.10	133.32	51.34
P_{d3LS3}	57.48	29.35	48.95	73.51	63.58	39.55	150.83	51.21	50.49
Q_{d3LS1}	98.60	34.71	26.10	41.47	139.84	75.43	157.97	64.35	15.83
Q_{d3LS2}	27.42	119.45	13.25	99.12	26.89	90.27	157.97	64.35	15.83
$Q_{d\ 3LS3}$	46.36	181.46	43.97	73.51	63.58	39.55	83.89	41.94	111.52
4-Load Shedding									
Bus	**26**			**29**			**30**		
Q_d	**10**	**20**	**25**	**10**	**20**	**25**	**10**	**20**	**25**
$Loss_{Set}$	18.23	20.25	22.27	18.12	19.39	20.53	18.11	19.55	20.93
$Loss_{Out}$	60.88	66.45	70.49	60.76	65.02	67.24	60.71	65.26	67.98
$Loss_{4LS}$	21.54	21.02	22.99	20.98	22.12	21.22	21.03	21.30	21.87
RI_{Pre}	0.427	0.438	0.462	0.425	0.425	0.439	0.425	0.428	0.445
RI_{Post}	0.548	0.463	0.484	0.528	0.516	0.461	0.530	0.485	0.474
Loc_{4LS1}	17	17	23	8	18	12	7	5	11
Loc_{4LS2}	5	12	11	9	7	11	17	25	18
Loc_{4LS3}	9	5	4	13	6	22	9	7	20
Loc_{4LS4}	12	21	5	24	9	5	11	6	5
P_{d4LS1}	25.11	31.66	40.11	42.42	26.40	18.20	61.65	68.32	98.88
P_{d4LS2}	12.56	27.48	44.44	187.17	72.36	64.41	74.85	60.60	30.75
P_{d4LS3}	114.42	105.20	110.00	25.52	80.39	88.27	94.44	83.46	31.08
P_{d4LS4}	46.83	57.56	96.80	2.58	37.88	100.91	44.27	126.65	118.62
Q_{d4LS1}	62.47	58.11	94.35	154.76	35.02	103.95	8.59	21.23	90.49
Q_{d4LS2}	38.90	40.20	147.98	42.80	34.11	136.71	23.24	23.95	52.29
$Q_{d\ 4LS3}$	133.36	61.92	75.22	84.57	104.48	42.90	135.46	25.32	37.21
Q_{d4LS4}	78.87	58.37	121.08	35.91	8.27	87.48	37.62	146.41	79.53

* Notes: Unit for Q_d = MVAr, P_d = MW, Loss = MW and Size = MW

resulted from the load shedding implementation. The load shedding scheme strategically selects the buses for load shedding, optimised by ECSEP. In this case, the identified optimal locations for load shedding are Bus 15 (Loc_{3LS1}), Bus 7 (Loc_{3LS2}), and Bus 6 (Loc_{3LS3}). These buses play a crucial role in maintaining system balance when

load shedding is applied involving reactive load variations at Bus 30. The corresponding power to be shed includes 37.51 MW (P_{d3LS1}), 51.34 MW (P_{d3LS2}), and 50.49 MW (P_{d3LS3}) for real power, along with 15.83 MVAr (Q_{d3LS1}), 15.83 MVAr (Q_{d3LS2}), and 111.52 MVAr (Q_{d3LS3}) for reactive power.

In comparison, the 4 load shedding schemes for the same reactive load variation at Bus 30 with a reactive load of 25 MVAr shows similar results. The $Loss_{Pre}$ remained the same at 67.98 MW, while the $Loss_{4LS}$ slightly decreased to 21.87 MW, which is significantly better than the 3 load shedding schemes. The resilience index (RI_{Pre}) before load shedding was 0.445, which has been increased to 0.474 (RI_{Post}) after the load shedding. The optimal load shedding locations in this case identified by ECSEP are Bus 11, Bus 18, Bus 20, and Bus 5, with corresponding real power shedding values of 98.88 MW, 30.75 MW, 31.08 MW, and 118.62 MW. The reactive power to be shed are 90.49 MVAr, 52.29 MVAr, 37.21 MVAr, and 79.53 MVAr, respectively at all the optimal locations. In summary, both the 3-load shedding and 4 load shedding schemes effectively reduce system losses and improve resilience of the system. The 4-load shedding scheme achieves slightly better results in terms of loss minimization.

B. Scenario 2

The study was further extended to Scenario 2 for implementation in IEEE 30-Bus RTS. Table 3.14 presents the results of loss minimization using both 3 load shedding and 4 load shedding schemes in the effort of grid hardening. At Q_{d26} = 25 MVAR, 3-load shedding scheme managed to reduce the loss from 29.92 MW to 24.52 MW. The loss value before the hurricane is experienced was 22.27 MW as tabulated in the Table 3.14. Apparently, hurricane has increased loss in the system. This load shedding scheme has caused the increment in resilience index from 2.910 to 4.542, implying the grid has been hardened. To achieve this improvement, ECSEP identified Bus 5, Bus 6, and Bus 27 as the optimal location to undergo load shedding which require 97.01 MW, 153.54 MW, and 29.89 MW, respectively and 123.45 MVAr, 33.32 MVAr, and 149.05 MVAr to be shed at these buses as indicated in the Table 3.14.

The implementation of 4 load shedding scheme, at the same loading condition for Bus 26 i.e. Q_{d26} = 25 MVAr, the system losses are further reduced from 29.92 MW to 23.00 MW. The resilience index is also improved from 2.910 to 3.325. To achieve this improvement, the optimal loads to be shed are 56.20 MW and 94.92 MVAr at Bus

5, 128.20 MW and 124.94 MVAr at Bus 11, 50.80 MW and 68.80 MVAr at Bus 27, and 60.33 MW and 28.23 MVAr at Bus 14, respectively. These results highlight the effectiveness of the 4-load shedding scheme in further minimizing system losses compared to the 3-load shedding scheme.

Table 3.14
Numerical Results of IEEE 30-Bus RTS (Scenario 2) for Loss Control using 3-Load Shedding and 4-Load Shedding Technique

3-Load Shedding									
Bus	**26**			**29**			**30**		
Q_d	**10**	**20**	**25**	**10**	**20**	**25**	**10**	**20**	**25**
$Loss_{Set}$	18.23	20.25	22.27	18.12	19.39	20.53	18.11	19.55	20.93
$Loss_{Out}$	20.40	25.03	29.92	19.78	22.87	24.82	20.27	23.59	28.33
$Loss_{3LS}$	19.87	23.87	24.52	19.33	20.55	22.85	19.21	22.32	23.69
RI_{Pre}	8.381	4.236	2.910	10.894	5.571	4.782	8.379	4.833	2.826
RI_{Post}	37.391	20.600	4.542	42.567	8.864	11.620	18.190	17.529	5.100
Loc_{3LS1}	5	12	5	10	10	9	5	5	6
Loc_{3LS2}	10	7	6	5	11	5	22	8	27
Loc_{3LS3}	8	27	27	9	28	27	9	12	10
P_{d3LS1}	44.20	29.90	97.01	38.10	65.57	57.65	41.70	121.64	195.85
P_{d3LS2}	162.71	114.91	153.54	128.91	102.87	111.53	32.96	42.50	33.30
P_{d3LS3}	57.54	87.83	29.89	151.94	32.53	53.67	115.16	36.28	11.47
Q_{d3LS1}	168.64	54.32	123.45	113.12	98.10	177.99	47.58	156.93	4.61
Q_{d3LS2}	135.88	23.99	33.32	102.37	35.49	58.45	44.87	77.05	58.27
$Q_{d\,3LS3}$	57.13	45.49	149.05	26.65	45.01	118.38	26.28	84.39	196.12
4-Load Shedding									
Bus	**26**			**29**			**30**		
Q_d	**10**	**20**	**25**	**10**	**20**	**25**	**10**	**20**	**25**
$Loss_{Set}$	18.23	20.25	22.27	18.12	19.39	20.53	18.11	19.55	20.93
$Loss_{Out}$	20.40	25.03	29.92	19.78	22.87	24.82	20.27	23.59	28.33
$Loss_{4LS}$	18.98	21.29	23.00	18.01	19.98	20.92	18.93	20.17	21.22
RI_{Pre}	8.381	4.236	2.910	10.894	5.571	4.782	8.379	4.833	2.826
RI_{Post}	13.340	5.692	3.325	10.196	6.931	5.363	14.125	5.887	2.981
Loc_{4LS1}	10	24	5	9	27	7	10	22	12
Loc_{4LS2}	5	5	11	12	9	5	5	11	10
Loc_{4LS3}	6	12	27	10	13	10	7	17	13
Loc_{4LS4}	14	17	14	14	5	17	13	12	11
P_{d4LS1}	74.54	10.98	56.20	90.73	32.20	68.50	29.55	18.00	29.53
P_{d4LS2}	105.66	45.45	128.20	10.25	64.60	34.15	127.80	141.58	48.49
P_{d4LS3}	31.33	93.13	50.80	11.36	33.44	131.30	65.85	25.10	103.49
P_{d4LS4}	44.62	47.98	60.33	43.60	70.09	19.37	19.75	115.21	25.48
Q_{d4LS1}	64.69	54.82	94.92	140.51	94.36	23.41	99.54	25.58	92.92
Q_{d4LS2}	81.44	109.48	124.94	49.10	40.59	58.94	121.54	48.18	140.42
Q_{d4LS3}	75.45	171.61	68.80	126.67	25.22	19.43	55.71	38.54	31.48
Q_{d4LS4}	42.26	59.49	28.23	10.38	180.44	41.99	165.26	160.92	37.64

* Notes: Unit for Q_d = MVAr, P_d = MW, Loss = MW and Size = MW

The identification of optimal locations and sizing plays a critical role in ensuring that load shedding scheme is worth under disruptive events. This approach is essential for grid hardening, particularly under high-stress scenarios involving Scenario 2 of the IEEE 30-Bus RTS.

3.5.6.2 IEEE 57-Bus RTS

Loss minimization was also conducted using the load shedding schemes involving 3-load shedding 4-load shedding schemes in IEEE 57-Bus RTS. Similar hurricane scenarios are considered for this initiative as one of the strategies in grid hardening indicated by the improvement in the resilience index resulted from the loss minimization improvement.

A. Scenario 1

The load shedding scheme for loss minimization in the grid hardening strategy is further implemented in IEEE 57-Bus RTS. The results are presented in Table 3.15. As in previous analyses, two scenarios of disruptive events are considered, featuring 3-load shedding and 4-load shedding. In Scenario 1, both load shedding schemes show a decreasing trend in losses. In 3-load shedding scheme, at Q_{d32} = 10 MVAr, the losses are reduced from 34.84 MW to 31.85 MW, with the resilience index increased from 5.437 to 10.676 implying grid hardening. The optimal locations for load shedding are Bus 41, Bus 15, and Bus 10. The corresponding real and reactive power to be shed are: 71.85 MW and 61.57 MVAr for Bus 41, 163.75 MW and 31.14 MVAr for Bus 15, and 79.52 MW and 20.04 MVAr for Bus 10. With 4-load shedding implementation, the losses are further reduced to 30.37 MW, with the *RI* increasing from 5.437 to 6.793. The optimal locations and sizes for real and reactive power shedding 138.02 MW and 55.37 MVAr at Bus 15, 57.74 MW and 42.71 MVAr at Bus 13, 140.28 MW and 110.40 MVAr at Bus 12 and 76.62 MW and 152.79 MVAr at Bus 17. The results from the 4-load shedding scheme indicate a better loss reduction compared to the 3-load shedding scheme.

Table 3.15
Numerical Results of IEEE 57-Bus RTS (Scenario 1) for Loss Control using 3-Load Shedding and 4-Load Shedding Technique

3-Load Shedding									
Bus	**31**			**32**			**33**		
Q_d	**5**	**10**	**15**	**5**	**10**	**15**	**5**	**10**	**15**
$Loss_{Set}$	28.46	29.22	30.57	28.67	29.42	30.66	28.56	29.30	30.55
$Loss_{Out}$	32.85	34.41	42.75	33.25	34.84	39.15	33.03	34.51	38.00
$Loss_{3LS}$	29.49	31.23	32.22	30.00	31.85	32.54	31.25	32.51	32.61
RI_{Pre}	6.488	5.627	2.508	6.250	5.437	3.613	6.382	5.618	4.101
RI_{Post}	8.762	9.816	3.057	9.213	10.676	4.926	17.587	16.271	6.059
Loc_{3LS1}	15	51	36	43	41	49	49	12	36
Loc_{3LS2}	43	30	10	38	15	36	13	45	14
Loc_{3LS3}	12	46	45	12	10	4	16	10	16
P_{d3LS1}	131.27	90.99	40.49	58.71	71.85	86.77	115.53	130.59	32.16
P_{d3LS2}	63.09	22.86	75.38	31.70	163.75	23.07	65.69	120.46	140.43
P_{d3LS3}	158.87	114.94	182.14	133.42	79.52	105.13	103.74	68.31	135.13
Q_{d3LS1}	105.82	37.52	46.30	54.21	61.57	38.59	48.32	51.30	47.62
Q_{d3LS2}	64.79	21.19	39.90	28.91	31.14	47.05	39.35	77.67	70.06
$Q_{d\ 3LS3}$	64.83	23.77	53.46	149.68	20.04	15.35	71.96	17.64	76.39
4-Load Shedding									
Bus	**31**			**32**			**33**		
Q_d	**5**	**10**	**15**	**5**	**10**	**15**	**5**	**10**	**15**
$Loss_{Set}$	28.46	29.22	30.57	28.67	29.42	30.66	28.56	29.30	30.55
$Loss_{Out}$	32.85	34.41	42.75	33.25	34.84	39.15	33.03	34.51	38.00
$Loss_{4LS}$	28.83	30.32	31.99	29.14	30.37	31.74	29.68	30.52	31.25
RI_{Pre}	6.488	5.627	2.508	6.250	5.437	3.613	6.382	5.618	4.101
RI_{Post}	7.175	7.405	2.973	7.075	6.793	4.286	8.861	7.653	4.635
Loc_{4LS1}	17	25	14	16	15	13	18	15	12
Loc_{4LS2}	18	15	16	18	13	16	16	18	13
Loc_{4LS3}	16	13	12	13	12	12	15	12	15
Loc_{4LS4}	13	18	15	17	17	18	12	14	14
P_{d4LS1}	13.21	26.49	47.26	65.74	138.02	100.68	58.89	115.70	138.03
P_{d4LS2}	127.65	75.53	89.75	111.41	57.74	86.09	55.57	44.09	117.55
P_{d4LS3}	128.45	173.65	106.60	109.52	140.28	102.46	85.01	114.66	68.41
P_{d4LS4}	172.18	73.61	113.29	118.31	76.62	113.22	94.61	101.96	21.05
Q_{d4LS1}	83.75	53.38	58.49	62.01	55.37	115.01	91.93	47.84	92.39
Q_{d4LS2}	23.93	121.51	82.46	93.89	42.71	105.68	97.27	104.59	52.93
Q_{d4LS3}	51.18	86.24	142.10	55.21	110.40	94.56	100.75	109.10	27.52
Q_{d4LS4}	92.28	12.56	73.67	63.47	152.79	85.88	100.55	89.36	21.14

* Notes: Unit for Q_d = MVAr, P_d = MW, Loss = MW and Size = MW

B. Scenario 2

Similar study was conducted to IEEE 57-Bus RTS with hurricane event under Scenario 2. The results are tabulated in Table 3.16. In this scenario, at Q_{d31} = 15 MVAr with a 3-load shedding scheme, the total system loss before the outage was recorded at

30.57 MW, as indicated in the Table 3.16. The 3-load shedding scheme effectively reduces the system losses from 54.69 MW to 32.56 MW, achieving a reduction of 40.46%. The *RI* improves from 1.267 to 1.471 implying the grid has been hardened.

Table 3.16
Numerical Results of IEEE 57-Bus RTS (Scenario 2) for Loss Control using 3-Load Shedding and 4-Load Shedding Technique

3-Load Shedding									
Bus		**31**			**32**			**33**	
Q_d	**5**	**10**	**15**	**5**	**10**	**15**	**5**	**10**	**15**
$Loss_{Set}$	28.46	29.22	30.57	28.67	29.42	30.66	28.56	29.30	30.55
$Loss_{Out}$	47.34	49.47	54.69	47.77	49.81	55.06	47.52	49.56	53.90
$Loss_{3LS}$	29.87	31.85	32.56	30.25	31.25	31.03	32.51	32.51	32.25
RI_{Pre}	1.508	1.443	1.267	1.501	1.443	1.257	1.506	1.446	1.308
RI_{Post}	1.709	1.808	1.471	1.727	1.684	1.291	2.165	1.907	1.489
Loc_{3LS1}	12	50	55	28	15	18	55	10	23
Loc_{3LS2}	38	32	38	22	44	15	17	35	13
Loc_{3LS3}	45	18	10	51	29	38	23	29	6
P_{d3LS1}	182.49	39.20	36.89	26.83	153.82	65.06	86.59	67.11	112.64
P_{d3LS2}	145.80	27.42	114.21	113.51	63.38	29.62	156.01	57.69	135.32
P_{d3LS3}	95.60	82.32	89.90	88.12	51.74	72.52	58.36	48.60	72.97
Q_{d3LS1}	118.86	69.05	87.52	52.41	42.13	33.06	65.84	36.24	32.79
Q_{d3LS2}	31.25	27.85	1173.97	115.91	95.84	184.40	30.68	27.53	75.10
$Q_{d\ 3LS3}$	78.30	41.97	33.59	82.61	33.78	81.10	99.65	64.85	104.48
4-Load Shedding									
Bus		**31**			**32**			**33**	
Q_d	**5**	**10**	**15**	**5**	**10**	**15**	**5**	**10**	**15**
$Loss_{Set}$	28.46	29.22	30.57	28.67	29.42	30.66	28.56	29.30	30.55
$Loss_{Out}$	47.34	49.47	54.69	47.77	49.81	55.06	47.52	49.56	53.90
$Loss_{4LS}$	28.60	30.89	31.28	29.32	30.97	30.99	29.33	30.42	31.00
RI_{Pre}	1.508	1.443	1.267	1.501	1.443	1.257	1.506	1.446	1.308
RI_{Post}	1.526	1.663	1.336	1.590	1.644	1.288	1.612	1.590	1.354
Loc_{4LS1}	45	35	48	12	18	17	13	18	16
Loc_{4LS2}	31	24	11	46	13	1	40	5	36
Loc_{4LS3}	30	49	15	33	15	38	25	13	5
Loc_{4LS4}	14	46	10	17	25	45	33	22	13
P_{d4LS1}	122.55	35.86	43.51	15.91	0.24	83.43	35.16	83.47	42.29
P_{d4LS2}	21.71	1.59	2.92	27.09	42.39	42.24	90.60	42.29	80.71
P_{d4LS3}	81.74	132.14	127.62	163.39	113.78	80.67	53.59	80.71	21.76
P_{d4LS4}	21.71	162.74	103.31	171.94	104.84	21.71	81.78	21.76	72.39
Q_{d4LS1}	7.19	23.03	49.53	19.71	139.65	72.35	90.92	72.39	19.33
Q_{d4LS2}	81.73	15.26	38.90	121.45	12.91	19.31	190.86	19.33	40.75
Q_{d4LS3}	21.71	115.92	18.18	106.79	22.60	40.73	191.77	40.75	77.40
Q_{d4LS4}	7.21	119.75	73.15	114.03	66.74	77.34	96.44	77.40	1.59

* Notes: Unit for Q_d = MVAr, P_d = MW, Loss = MW and Size = MW

To achieve these results, the load shedding needs to be experienced at Bus 55 (36.89 MW and 87.52 MVAr), Bus 38 (114.21 MW and 173.97 MVAr), and Bus 10 (89.90 MW and 33.59 MVAr). In comparison, the 4-load shedding scheme further reduces the system losses from 54.69 MW to 31.28 MW, resulting in 42.81% reduction. The *RI* also improves from 1.267 to 1.336. The optimal locations to undergo load-

shedding are Bus 48 (43.51 MW and 49.53 MVAr), Bus 11 (2.92 MW and 38.90 MVAr), Bus 15 (127.62 MW and 18.18 MVAr), and Bus 10 (103.31 MW and 73.15 MVAr). These results demonstrate the effectiveness of both load shedding schemes in reducing system losses and enhancing resilience, with the 4-load shedding scheme providing slightly better performance in terms of loss reduction. However, both schemes managed to harden the grid of the system.

3.5.7 Load Shedding Technique for Voltage Security Improvement in Grid Hardening Scheme

Another strategy for grid hardening can be addressed through the voltage security improvement initiative. In this study, ECSEP is also utilised to enhance the voltage security in a system. This is monitored through the *FVSI* value reduction, which serves as a critical indicator of voltage stability within the grid. Voltage security is essential for ensuring grid resilience, especially during disruptive events where maintaining voltage security of a system can prevent the system from experiencing collapse.

Using the same procedure as for the loss minimisation problem, the newly proposed ECSEP technique was also applied to both IEEE 30-Bus RTS and IEEE 57-Bus RTS to evaluate its performance in improving voltage stability through load shedding scheme. Thus, minimising *FVSI* values through strategic load shedding scheme may lead to the improvement of the grid strength.

3.5.7.1 IEEE 30-Bus RTS

The IEEE 30-Bus RTS was the first test model in addressing the grid hardening process through intelligent load shedding scheme under the hurricane conditions represented in two scenarios.

A. Scenario 1

In the IEEE 30-Bus RTS, two scenarios were simulated to assess the impact of load shedding on improving voltage stability following a line outage caused by a hurricane.

Table 3.17
Numerical Results of IEEE 30-Bus RTS (Scenario 1) for Voltage Security Improvement using 3-Load Shedding and 4-Load Shedding Technique

3-Load Shedding									
Bus	**26**			**29**			**30**		
Q_d	**10**	**20**	**25**	**10**	**20**	**25**	**10**	**20**	**25**
$FVSI_{Set}$	0.2248	0.4919	0.6529	0.2111	0.3573	0.4646	0.2114	0.4073	0.5349
$FVSI_{Out}$	0.2968	0.5673	0.7707	0.2953	0.4072	0.5370	0.2939	0.4635	0.6188
$FVSI_{3LS}$	0.2691	0.5444	0.7242	0.2521	0.3832	0.5101	0.2534	0.4320	0.6043
RI_{Pre}	3.122	6.524	5.542	2.507	7.160	6.417	2.562	7.247	6.375
RI_{Post}	9.793	22.937	15.328	5.836	15.967	19.112	6.203	13.761	41.095
Loc_{3LS1}	28	24	28	21	22	23	28	9	7
Loc_{3LS2}	8	23	26	10	27	27	6	30	23
Loc_{3LS3}	26	26	8	29	9	11	26	27	6
P_{d3LS1}	14.27	129.07	167.59	181.76	109.77	72.09	100.27	192.69	9.49
P_{d3LS2}	40.29	99.51	33.42	124.65	176.01	73.06	183.01	152.74	132.36
P_{d3LS3}	62.28	27.66	129.68	43.84	194.08	117.92	63.12	169.84	24.95
Q_{d3LS1}	31.71	68.10	156.42	29.47	109.51	34.50	51.20	87.17	189.81
Q_{d3LS2}	42.46	22.04	25.89	66.16	77.58	71.42	94.09	37.76	96.81
$Q_{d\ 3LS3}$	16.33	15.01	17.51	5.27	35.75	68.31	2.11	184.30	124.18
4-Load Shedding									
Bus	**26**			**29**			**30**		
Q_d	**10**	**20**	**25**	**10**	**20**	**25**	**10**	**20**	**25**
$FVSI_{Set}$	0.2248	0.4919	0.6529	0.2111	0.3573	0.4646	0.2114	0.4073	0.5349
$FVSI_{Out}$	0.2968	0.5673	0.7707	0.2953	0.4072	0.5370	0.2939	0.4635	0.6188
$FVSI_{4LS}$	0.2432	0.5091	0.7044	0.2292	0.3671	0.4733	0.2254	0.4141	0.5921
RI_{Pre}	3.122	6.524	5.542	2.507	7.160	6.417	2.562	7.247	6.375
RI_{Post}	4.537	8.681	10.469	3.434	9.180	7.404	3.291	8.326	22.176
Loc_{4LS1}	9	9	21	6	6	21	20	5	6
Loc_{4LS2}	6	8	6	25	9	4	6	6	19
Loc_{4LS3}	16	6	16	15	24	14	9	11	27
Loc_{4LS4}	14	15	26	6	4	6	12	13	9
P_{d4LS1}	94.19	18.88	151.99	97.63	147.72	137.33	24.28	62.15	80.54
P_{d4LS2}	81.86	187.40	157.72	40.26	52.94	133.29	162.17	18.86	169.84
P_{d4LS3}	151.95	149.19	86.75	117.37	90.57	28.43	142.27	6.41	163.89
P_{d4LS4}	35.11	130.61	64.19	105.97	186.52	12.98	77.91	159.72	158.68
Q_{d4LS1}	32.31	87.86	59.63	18.62	132.01	71.26	6.69	33.40	74.85
Q_{d4LS2}	147.31	155.39	97.02	15.99	76.72	46.24	192.62	124.05	1.91
Q_{d4LS3}	60.98	185.57	7.68	29.51	91.41	23.38	34.85	174.38	95.94
Q_{d4LS4}	24.20	119.34	37.60	35.29	117.39	194.15	4.49	17.61	127.80

* Notes: Unit for Q_d = MVAr, P_d = MW, Loss = MW and Size = MW

The application of load shedding in these scenarios aims to enhance the voltage security under disruptive conditions. The results for grid hardening of Scenario 1 in this system are presented in Table 3.17. The overall results of the 3 and 4-load shedding schemes show a decreasing trend in *FVSI* values while the *RI* values increase. The pre-outage event demonstrates low *FVSI* value denoted by $FVSI_{Set}$. The occurrence of hurricane indicated by outage of the lines has led to the increment of *FVSI* values, denoted by $FVSI_{Out}$. The implementation of load shedding schemes has reduced the *FVSI* values in the system. For example, the implementation of 3-load shedding at Q_{d26} = 25 MVAr, results in a reduction of *FVSI* from 0.7707 to 0.7242, representing a 6.03% reduction. Meanwhile, the *RI* increases from 5.542 to 15.328 implying a successful grid hardening. ECSEP identified Buses 28, 26 and 8 as the optimal location for 3-load shedding scheme. The corresponding real and reactive power to be shed at these buses are 167.59 MW and 156.42 MVAr at Bus 28, 33.42 MW and 25.89 MVAr at Bus 26, and 129.68 MW and 17.51 MVAr at Bus 8.

With 4-load shedding scheme, the *FVSI* reduces from 0.7707 to 0.7044 while *RI* increase from 5.542 to 10.469 indicating a successful grid hardening. To achieve this, 151.99 MW and 59.63 MVAr need to be shed at Bus 21, 157.72 MW and 97.02 MVAr need to be shed at Bus 6, 86.75 MW and 97.02 MVAr need to be shed at Bus 16 and 64.19 MW and 37.60 MVAr need to be shed at Bus 26. These findings reinforce the effectiveness of multi load shedding in improving voltage security and enhancing the system's resilience.

B. Scenario 2

Table 3.18 shows the numerical results of IEEE 30-Bus RTS (Scenario 2) for voltage security improvement using 3 and 4-load shedding schemes. In general, the results for *FVSI* denoted by $FVSI_{Set}$ before the hurricane occurrence are lower as compared to those *FVSI* value after this event. With load shedding scheme the *FVSI* values are reduced implying voltage security improvement. In this scenario at Q_{d26} = 20 MVAr, the *FVSI* decreases from 0.6904 to 0.5212 with 3-load shedding scheme while its value is reduced to 0.5041 for the 4-load shedding scheme. *RI* increases from 2.478 to 3.066 with 3-load shedding scheme and 2.696 with 4-load shedding scheme. Both schemes demonstrate significant grid hardening have been achieved. For the 3-load-shedding scheme, the optimal locations are Bus 4, Bus 25, and Bus 27.

Table 3.18
Numerical Results of IEEE 30-Bus RTS (Scenario 2) for Voltage Security Improvement using 3-Load Shedding and 4-Load Shedding Technique

3-Load Shedding									
Bus	**26**			**29**			**30**		
Q_d	**10**	**20**	**25**	**10**	**20**	**25**	**10**	**20**	**25**
$FVSI_{Set}$	0.2248	0.4919	0.6529	0.2111	0.3573	0.4646	0.2114	0.4073	0.5349
$FVSI_{Out}$	0.2470	0.6904	1.0000	0.2193	0.4201	0.5880	0.2190	0.4657	0.6805
$FVSI_{3LS}$	0.2401	0.5212	0.7374	0.2181	0.3812	0.5012	0.2170	0.4280	0.5601
RI_{Pre}	10.126	2.478	1.881	25.744	5.689	3.765	27.816	6.974	3.674
RI_{Post}	33.789	3.066	2.795	218.300	9.799	5.782	114.263	11.485	4.633
Loc_{3LS1}	8	4	6	10	12	4	10	28	22
Loc_{3LS2}	26	25	25	20	14	9	28	20	19
Loc_{3LS3}	4	27	10	6	7	6	24	10	25
P_{d3LS1}	105.53	60.39	133.58	2.22	38.16	144.75	81.42	192.59	166.88
P_{d3LS2}	37.43	154.82	149.96	163.30	61.15	59.40	70.16	120.73	131.94
P_{d3LS3}	66.54	19.82	195.71	125.81	126.60	10.12	170.14	105.20	146.04
Q_{d3LS1}	64.80	31.37	174.09	58.38	38.77	95.56	160.02	29.42	128.54
Q_{d3LS2}	17.09	40.85	75.72	21.63	6.25	91.43	35.70	33.32	69.86
$Q_{d\ 3LS3}$	84.06	75.96	85.14	69.57	73.63	104.00	48.13	58.35	106.93
4-Load Shedding									
Bus	**26**			**29**			**30**		
Q_d	**10**	**20**	**25**	**10**	**20**	**25**	**10**	**20**	**25**
$FVSI_{Set}$	0.2248	0.4919	0.6529	0.2111	0.3573	0.4646	0.2114	0.4073	0.5349
$FVSI_{Out}$	0.2470	0.6904	1.0000	0.2193	0.4201	0.5880	0.2190	0.4657	0.6805
$FVSI_{4LS}$	0.2321	0.5041	0.6591	0.2152	0.3603	0.4763	0.2134	0.4111	0.5440
RI_{Pre}	10.126	2.478	1.881	25.744	5.689	3.765	27.816	6.974	3.674
RI_{Post}	15.577	2.696	1.937	55.231	6.002	4.264	35.500	7.498	3.978
Loc_{4LS1}	12	6	3	14	6	4	16	10	7
Loc_{4LS2}	6	4	24	18	7	3	6	4	9
Loc_{4LS3}	17	9	12	4	4	9	27	19	6
Loc_{4LS4}	4	7	7	12	9	7	10	6	14
P_{d4LS1}	150.38	147.90	157.54	67.34	137.32	153.35	79.41	145.46	136.50
P_{d4LS2}	118.03	17.16	173.43	164.66	79.33	78.17	183.67	143.93	143.57
P_{d4LS3}	54.62	111.58	89.45	147.69	117.48	42.22	100.10	67.38	143.95
P_{d4LS4}	141.83	91.36	24.91	82.51	144.90	129.35	137.99	52.60	156.91
Q_{d4LS1}	20.05	125.75	79.93	98.76	49.27	175.29	7.94	50.54	31.05
Q_{d4LS2}	106.98	33.10	23.25	8.16	13.04	11.17	111.86	87.75	79.81
Q_{d4LS3}	2.36	165.64	62.16	156.95	146.91	109.39	21.32	12.02	199.43
Q_{d4LS4}	157.43	69.24	64.72	98.76	49.27	175.29	7.94	50.54	31.05

* Notes: Unit for Q_d = MVAr, P_d = MW, Loss = MW and Size = MW

The real and reactive power to be shed are 60.39 MW, 154.82 MW, and 19.82 MW for real power, and 31.37 MVAr, 40.85 MVAr, and 75.96 MVAr for reactive power as indicated in the Table 3.18. For 4-load shedding scheme, the optimal locations identified by ECSEP are Bus 6, Bus 4, Bus 9, and Bus 7. The real power to be shed at

these buses are 147.90 MW, 17.16 MW, 111.58 MW, and 91.36 MW, while the reactive power to be shed are 125.75 MVAr, 33.10 MVAr, 165.64 MVAr, and 69.24 MVAr, respectively. Results for other load other variations in both schemes can be referred to the same table.

3.5.7.2 IEEE 57-Bus RTS

Similar study was also conducted to the two similar hurricane conditions denoted by Scenario 1 and Scenario 2 in the effort to realise the effectiveness of ECSEP in addressing the grid hardening strategy of IEEE 57-Bus RTS.

A. Scenario 1

Hurricane condition denoted in Scenario 1 for the IEEE 57-Bus RTS, involving line outage in the system was tabulated in Table 3.19. The results of Scenario 1 are shown in Table 3.19. In Scenario 1, with the implementation of ECSEP optimisation technique, *FVSI* was successfully reduced using both the 3-load shedding and 4-load shedding scheme. These schemes proved effective in enhancing voltage stability under disruptive conditions. For instance, when Q_{d33} = 15 MVAr, the *FVSI* value decreased from 0.6679 to 0.4823. Consequently, the resilience index increased from 2.233 to 2.595 implying a successful grid hardening has been achieved. The ECSEP algorithm identified Bus 7, Bus 33, and Bus 53 as the optimal locations for load shedding, with real power to be shed worth 160.90 MW, 34.05 MW, and 106.02 MW, and while the reactive power to be shed at those buses are of 195.44 MVAr, 9.74 MVAr, and 33.46 MVAr, respectively as tabulated in the Table 3.19. Additionally, with 4-load shedding scheme, the optimal locations are buses, Bus 24, Bus 16, Bus 14, and Bus 10. The corresponding real power to be shed at these buses are 124.25 MW, 177.35 MW, 127.01 MW, and 125.84 MW, while the reactive power shed are 43.11 MVAr, 112.76 MVAr, 85.41 MVAr, and 120.72 MVAr, respectively. In this load shedding scheme, the *FVSI* value decreased from 0.6679 to 0.4741, and the resilience index increased from 2.233 to 2.436. These findings demonstrate the effectiveness of ECSEP in optimizing bus selection and significantly improving voltage stability and system resilience.

Table 3.19
Numerical Results of IEEE 57-Bus RTS (Scenario 1) for Voltage Security Improvement using 3-Load Shedding and 4-Load Shedding Technique

3-Load Shedding									
Bus	**31**			**32**			**33**		
Q_d	**5**	**10**	**15**	**5**	**10**	**15**	**5**	**10**	**15**
$FVSI_{Set}$	0.4028	0.3977	0.4339	0.4005	0.3948	0.4973	0.4016	0.3960	0.4613
$FVSI_{Out}$	0.4395	0.4355	1.000	0.4372	0.4318	0.7670	0.4382	0.4331	0.6679
$FVSI_{3LS}$	0.4151	0.4130	0.4452	0.4241	0.4131	0.5413	0.4252	0.4223	0.4823
RI_{Pre}	10.975	10.521	0.766	10.913	10.670	1.844	10.973	10.674	2.233
RI_{Post}	14.314	20.348	1.341	26.497	25.329	2.123	21.472	30.846	2.595
Loc_{3LS1}	28	7	7	14	14	14	34	24	7
Loc_{3LS2}	8	34	37	31	31	37	36	28	33
Loc_{3LS3}	14	3	54	8	8	28	29	35	53
P_{d3LS1}	72.94	149.25	70.42	148.34	133.28	186.36	187.82	104.78	160.90
P_{d3LS2}	88.16	182.31	39.62	120.02	49.45	148.46	125.17	117.24	34.05
P_{d3LS3}	28.36	121.97	87.63	177.73	168.80	23.66	104.60	154.74	106.02
Q_{d3LS1}	27.80	20.02	134.32	126.93	105.77	130.09	34.13	9.27	195.44
Q_{d3LS2}	186.71	42.33	108.93	51.81	104.46	20.46	56.87	140.11	9.74
$Q_{d\ 3LS3}$	155.77	171.50	111.09	184.34	146.05	14.13	86.58	28.59	33.46
4-Load Shedding									
Bus	**31**			**32**			**33**		
Q_d	**5**	**10**	**15**	**5**	**10**	**15**	**5**	**10**	**15**
$FVSI_{Set}$	0.4028	0.3977	0.4339	0.4005	0.3948	0.4973	0.4016	0.3960	0.4613
$FVSI_{Out}$	0.4395	0.4355	1.000	0.4372	0.4318	0.7670	0.4382	0.4331	0.6679
$FVSI_{4LS}$	0.4093	0.4031	0.4431	0.4114	0.4012	0.5071	0.4042	0.4023	0.4741
RI_{Pre}	10.975	10.521	0.766	10.913	10.670	1.844	10.973	10.674	2.233
RI_{Post}	13.553	12.483	0.796	15.815	13.065	1.955	11.738	12.706	2.436
Loc_{4LS1}	27	20	11	17	16	24	10	15	24
Loc_{4LS2}	8	14	14	14	14	13	16	14	16
Loc_{4LS3}	37	15	24	15	11	14	23	16	14
Loc_{4LS4}	34	25	16	11	20	25	14	11	10
P_{d4LS1}	18.86	0.68	73.81	61.60	23.41	105.09	163.08	95.32	124.25
P_{d4LS2}	158.64	84.28	150.49	79.30	142.42	51.40	122.48	188.99	177.35
P_{d4LS3}	193.12	153.01	33.34	111.94	65.53	78.87	25.56	67.31	127.01
P_{d4LS4}	140.26	66.47	167.51	152.19	38.83	43.40	193.29	80.82	125.84
Q_{d4LS1}	135.21	1.92	65.22	53.01	83.42	66.97	37.66	76.69	43.11
Q_{d4LS2}	164.49	176.71	131.39	163.56	154.25	135.76	102.08	67.77	112.76
Q_{d4LS3}	23.78	179.49	13.09	124.13	41.94	120.07	8.23	116.54	85.41
Q_{d4LS4}	87.39	16.13	127.81	160.80	63.56	24.82	108.44	99.65	120.72

* Notes: Unit for Q_d = MVAr, P_d = MW, Loss = MW and Size = MW

B. Scenario 2

The results for load shedding scheme in voltage security improvement strategy under Scenario 2 of the IEEE 57-Bus RTS are tabulated in Table 3.20. This study also

focuses on both 3-load shedding and 4-load shedding schemes to improve voltage stability following disruptive events impacting the system.

Table 3.20
Numerical Results of IEEE 57-Bus RTS (Scenario 2) for Voltage Security Improvement using 3-Load Shedding and 4-Load Shedding Technique

3-Load Shedding									
Bus	**31**			**32**			**33**		
Q_d	**5**	**10**	**15**	**5**	**10**	**15**	**5**	**10**	**15**
$FVSI_{Set}$	0.4028	0.3977	0.4339	0.4005	0.3948	0.4973	0.4016	0.3960	0.4613
$FVSI_{Out}$	0.4521	0.4518	1.0000	0.4520	0.4516	0.7846	0.4520	0.4518	0.7086
$FVSI_{3LS}$	0.4151	0.4132	0.4451	0.4243	0.4131	0.5411	0.4252	0.4223	0.5711
RI_{Pre}	8.170	7.351	0.766	7.777	6.951	1.731	7.968	7.097	1.865
RI_{Post}	11.319	10.496	0.803	14.860	10.609	2.224	15.803	14.010	4.157
Loc_{3LS1}	28	9	7	8	4	6	27	9	12
Loc_{3LS2}	6	30	23	26	25	25	4	30	17
Loc_{3LS3}	26	27	6	4	27	10	22	27	25
P_{d3LS1}	100.27	192.69	9.49	105.53	60.39	133.58	93.17	192.69	85.60
P_{d3LS2}	183.01	152.74	132.36	37.43	154.82	149.96	169.94	152.74	71.41
P_{d3LS3}	63.12	169.84	24.95	66.54	19.82	195.71	86.62	169.84	154.39
Q_{d3LS1}	51.20	87.17	189.81	64.80	31.37	174.09	22.08	87.17	36.11
Q_{d3LS2}	94.09	37.76	96.81	17.09	40.85	75.72	98.83	37.76	61.79
$Q_{d\ 3LS3}$	2.11	184.30	124.18	84.06	75.96	85.14	21.09	184.30	32.16
4-Load Shedding									
Bus	**31**			**32**			**33**		
Q_d	**5**	**10**	**15**	**5**	**10**	**15**	**5**	**10**	**15**
$FVSI_{Set}$	0.4028	0.3977	0.4339	0.4005	0.3948	0.4973	0.4016	0.3960	0.4613
$FVSI_{Out}$	0.4521	0.4518	1.0000	0.4520	0.4516	0.7846	0.4520	0.4518	0.7086
$FVSI_{4LS}$	0.4101	0.4082	0.4401	0.4120	0.4091	0.5151	0.4181	0.4093	0.4822
RI_{Pre}	8.170	7.351	0.766	7.777	6.951	1.731	7.968	7.097	1.865
RI_{Post}	9.688	9.199	0.785	10.414	9.478	1.907	12.216	9.531	2.128
Loc_{4LS1}	27	15	38	38	21	4	23	17	28
Loc_{4LS2}	35	36	31	31	12	7	27	15	26
Loc_{4LS3}	28	31	34	34	28	19	28	19	16
Loc_{4LS4}	34	29	26	26	19	21	3	28	4
P_{d4LS1}	1.48	167.15	86.72	191.05	72.36	158.90	167.77	122.79	130.73
P_{d4LS2}	174.92	24.66	6.53	193.45	107.85	139.19	117.47	51.28	83.15
P_{d4LS3}	172.28	194.61	185.79	195.66	90.96	150.55	185.21	7.93	140.19
P_{d4LS4}	39.59	5.83	21.10	189.75	80.29	133.86	77.93	124.14	182.03
Q_{d4LS1}	138.16	16.02	53.20	32.49	48.04	126.64	46.53	68.70	152.39
Q_{d4LS2}	98.99	98.80	96.32	11.26	16.57	11.23	16.53	4.83	52.44
Q_{d4LS3}	51.45	153.80	158.47	121.89	84.27	119.59	92.77	34.28	9.45
Q_{d4LS4}	103.81	186.71	51.43	109.20	94.43	45.35	38.98	122.14	147.17

* Notes: Unit for Q_d = MVAr, P_d = MW, Loss = MW and Size = MW

For instance, with 3-load shedding scheme, the *FVSI* value decreased from 0.7846 to 0.5411, while the resilience index increased significantly from 1.731 to 2.224.

The amount of load to be shed are 133.58 MW and 174.09 MVAr at Bus 6, 149.96 MW and 75.72 MVAr at Bus 25, and 195.71 MW and 85.14 MVAr) at Bus 10. When the 4-load shedding scheme is implemented, the *FVSI* is further reduced to 0.5151 while resilience index saw an increase from 1.731 to 1.907. The identified optimal locations are Bus 4, Bus 7, Bus 19, and Bus 21 with the corresponding real and reactive power to be shed 158.90 MW, 139.19 MW, 150.55 MW, and 133.86 MW for real power, and 126.64 MVAr, 11.23 MVAr, 119.59 MVAr, and 45.35 MVAr for reactive power. The results clearly demonstrate the effectiveness of load shedding for voltage security improvement.

The increase in resilience index indicates an enhanced ability of the grid to withstand further disruptive events. Remarkably, the 4-load shedding scheme achieved a greater improvement in both voltage stability and system resilience compared to the 3-load shedding scheme. These findings highlight the potential of the ECSEP technique in optimizing grid hardening strategies through optimal locations and sizing in the system.

3.6 Comparative Studies with Other Techniques

Comparative studies were carried out to evaluate the performance of ECSEP with respect to SSA, CSO, and EP as the benchmarked techniques. The comparison focused on minimizing transmission losses and enhancing the voltage security, using DG installation and load shedding compensation techniques as the grid hardening strategies. The results in these sections will focus exclusively on the 5 DG unit installation and the 4-load shedding scheme, as these approaches have been found to yield better outcomes compared to the 3 DG unit installation and the 3-load shedding scheme.

3.6.1 Distributed Generation Installation

The comparative studies result for both test models under both scenarios (i.e. Scenario 1 and Scenario 2) consider both the loss minimization and voltage security improvement as the objective function using all the optimization techniques, i.e. SSA, CSO, EP and ECSEP for pre- and post-outage events resulted from the hurricane occurrences.

3.6.1.1 Loss Minimization

A. IEEE 30-Bus RTS

Figure 3.13 illustrates the results of comparative studies of the overall system loss (Loss) and Proportional Loss Reduction (*PLR*) across different optimisation techniques applied to the IEEE 30-Bus RTS involving Scenario 1 and Scenario 2. This analysis focuses on three Buses (26, 29, and 30) under varying reactive power demand levels Q_d = 10, 20, and 25 MVAr and evaluates the impact of each method on minimizing power loss and enhancing *PLR*.

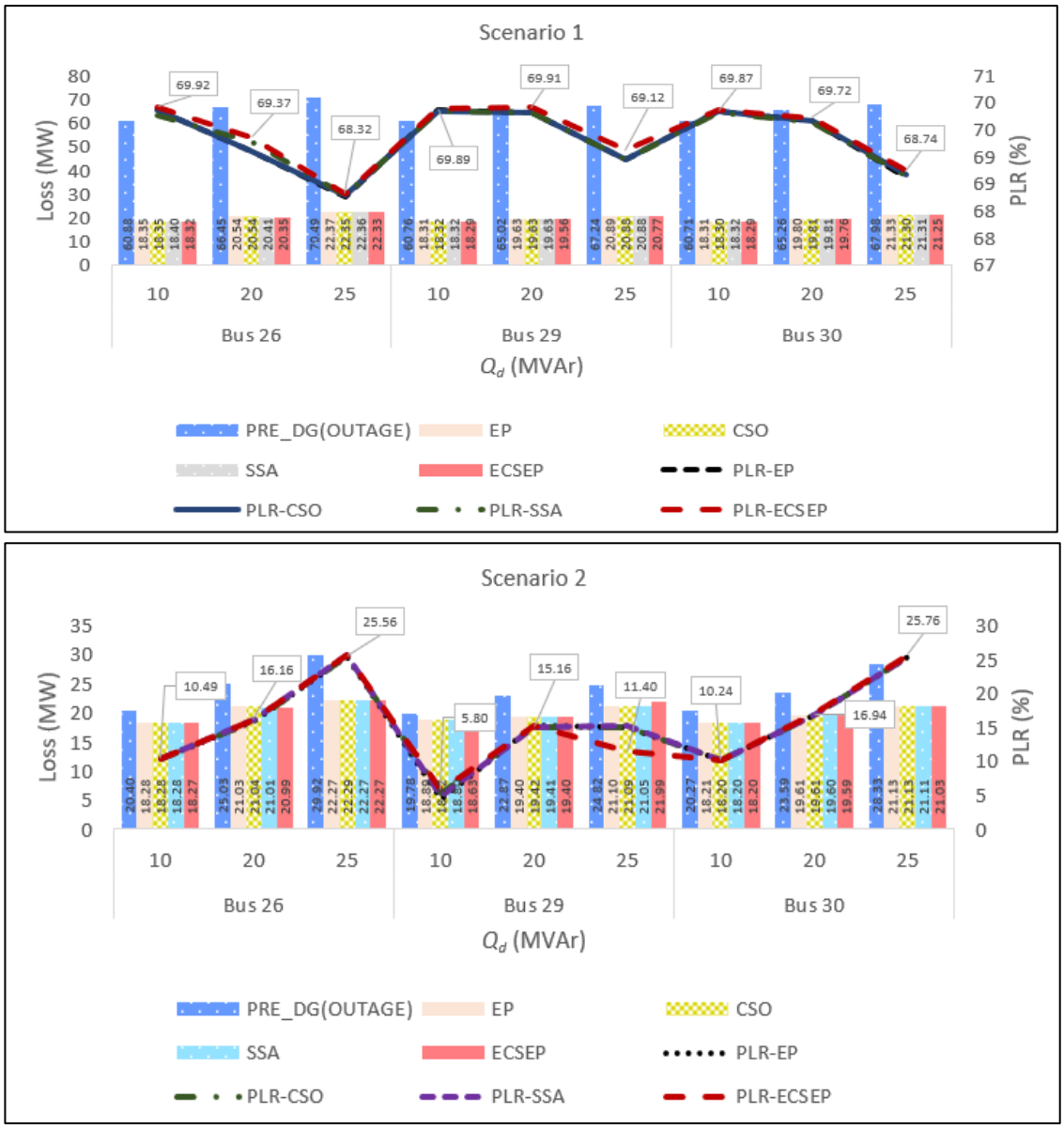


Figure 3.13 Comparison of Loss and *PLR* Results for Loss Minimization in DG Installation in IEEE 30-Bus RTS

The bar charts present the Loss in MW for each method, while the lines denote *PLR* percentages. The plot presents six conditions: PRE-DG (Outage), EP, CSO, SSA, and the proposed ECSEP, with pre-DG representing the baseline without DG installation.

The y-axis on the left displays the results for Loss (MW), while the right y-axis shows the *PLR* (%) values. For each demand level, all optimisation techniques yield lower losses compared to the pre-DG baseline. ECSEP consistently achieves the lowest power loss values, showcasing its effectiveness in minimizing losses values compared to EP, CSO, and SSA. In terms of *PLR*, represented by dotted and dashed lines, ECSEP also demonstrates higher *PLR* percentages, particularly at higher Q_d values.

In Scenario 1, at Q_{d26} = 10 MVAr, the ECSEP method demonstrates a substantial improvement in loss reduction and *PLR*. ECSEP specifically achieves a power loss of 18.32 MW which is a significant reduction from the pre-DG scenario of 60.88 MW. The ECSEP performs better than traditional methods such as EP, SSA, and CSO, achieving a transmission loss of 18.32 MW compared to 18.35 MW for EP, 18.40 MW for SSA, and 18.35 MW for CSO. Furthermore, ECSEP produces the highest *PLR* value of 69.92% which means that it is more effective in reducing losses at this demand. In Scenario 2, at Bus 26 with Q_d = 10 MVAr, ECSEP method reduces the power loss significantly and produces a high *PLR*. Specifically, ECSEP results in a power loss of 18.27 MW while from the pre-DG (Outage) condition the loss is 20.40 MW. In comparison, other methods such as EP, CSO, and SSA show losses of 18.28 MW or all higher than ECSEP. Regarding *PLR*, ECSEP has the highest reduction percentage and the *PLR* is 10.49% thus highlighting ECSEP's superiority in minimizing losses as well as improving system robustness at this demand level.

B. IEEE 57-Bus RTS

Figure 3.14 illustrates the comparative results of Loss and PLR optimised using different optimisation techniques applied to the IEEE 57-Bus RTS in Scenario 1 and Scenario 2. In the IEEE 57-Bus RTS, the ECSEP method consistently demonstrates the lowest power loss across all participating buses, highlighting its superior performance in minimizing losses. For instance, for Scenario 1 at Q_{d31} = 10 MVAr, ECSEP achieves a loss reduction to 29.30 MW compared to 34.41 MW in the pre-DG condition,

representing a significant improvement. Similarly, at Q_{d33} = 15 MVAr, ECSEP reduces the loss to 30.56 MW, the lowest among the methods being evaluated.

The ECSEP method in the IEEE 57-Bus RTS produces the lowest power loss across all reactive load variations which indicates its effectiveness in loss minimization.

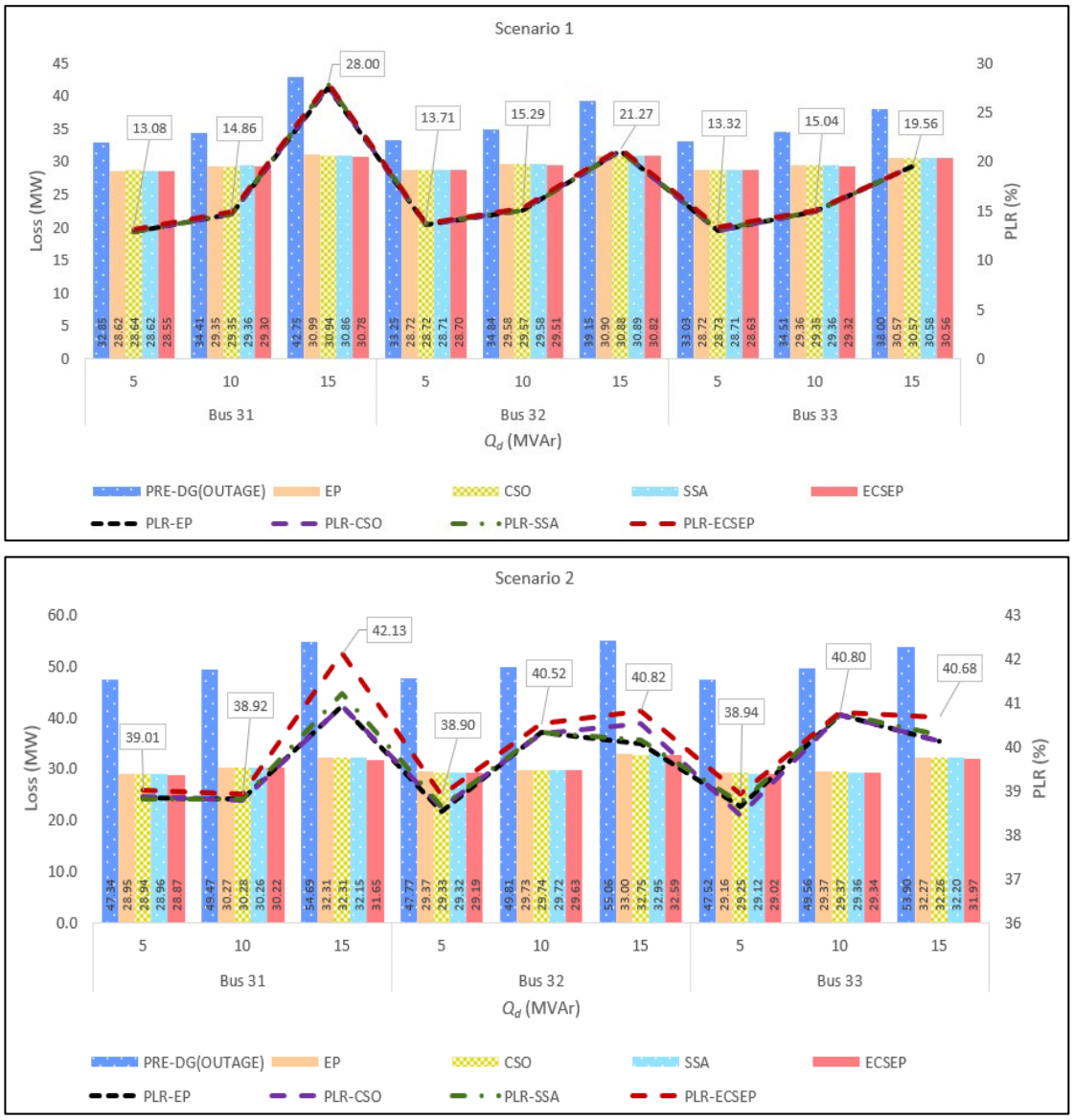


Figure 3.14 Comparison of Loss and *PLR* Results for Loss Minimization in DG Installation in IEEE 57-Bus RTS

It is also observed that Q_{d32} = 5 MVAr, ECSEP has the highest *PLR* of 13.71%, as against 13.65% for CSO and 13.66% for SSA. For each method and bus, ECSEP shows superior results as compared to other techniques as loss values are always less than that of EP, CSO and SSA. This trend is visible at all Q_d levels, which shows that

ECSEP has robust loss minimization capability. Once again, ECSEP shows high *PLR* values thus proving to be effective in mitigating power losses particularly during high reactive demand conditions.

In Scenario 2, ECSEP achieves a significant loss reduction at Q_{d31} = 15 MVAr, decreasing power losses from 54.69 MW in the pre-DG condition to 31.65 MW. This represents a substantial improvement in performance. Additionally, ECSEP demonstrates high *PLR* values, effectively mitigating power losses under increased reactive demand conditions. At Bus 31 with Q_{d31} = 15 MVAr, ECSEP achieves a *PLR* of 42.13%, indicating the highest among all methods. These values indicate that ECSEP not only reduces losses but also enhances the overall performance of the system by achieving a higher *PLR*. The graphs show that ECSEP maintains higher *PLR* percentages consistently across all load variations on the participating buses.

3.6.1.2 Voltage Security Improvement

Comparative studies were also conducted on the *FVSI* reduction involving both test models, i.e., IEEE 30-Bus RTS and IEEE 57-Bus RTS. The analysis focused on evaluating the impact of DG installation on system voltage stability, assessing the effectiveness of different optimisation techniques in reducing the *FVSI* values.

A. IEEE 30-Bus RTS

Figure 3.15 shows the performance of various optimisation methods: EP, CSO, SSA, and ECSEP in reducing *FVSI* and achieving Proportional *FVSI* Reduction (*PFR*) for IEEE 30-Bus RTS. The impact of each method on reducing *FVSI* is analysed across various buses and Q_d values.

The bar charts indicate the *FVSI* profiles, while the lines represent *PFR* values. For Scenario 1, at Bus 26 with Q_d = 10 MVAr, ECSEP achieves a notable reduction in *FVSI*, bringing it down to 0.241, a significant decrease compared to the pre-DG (Outage) value of 0.297. This reduction highlights the effectiveness of ECSEP in enhancing voltage stability.

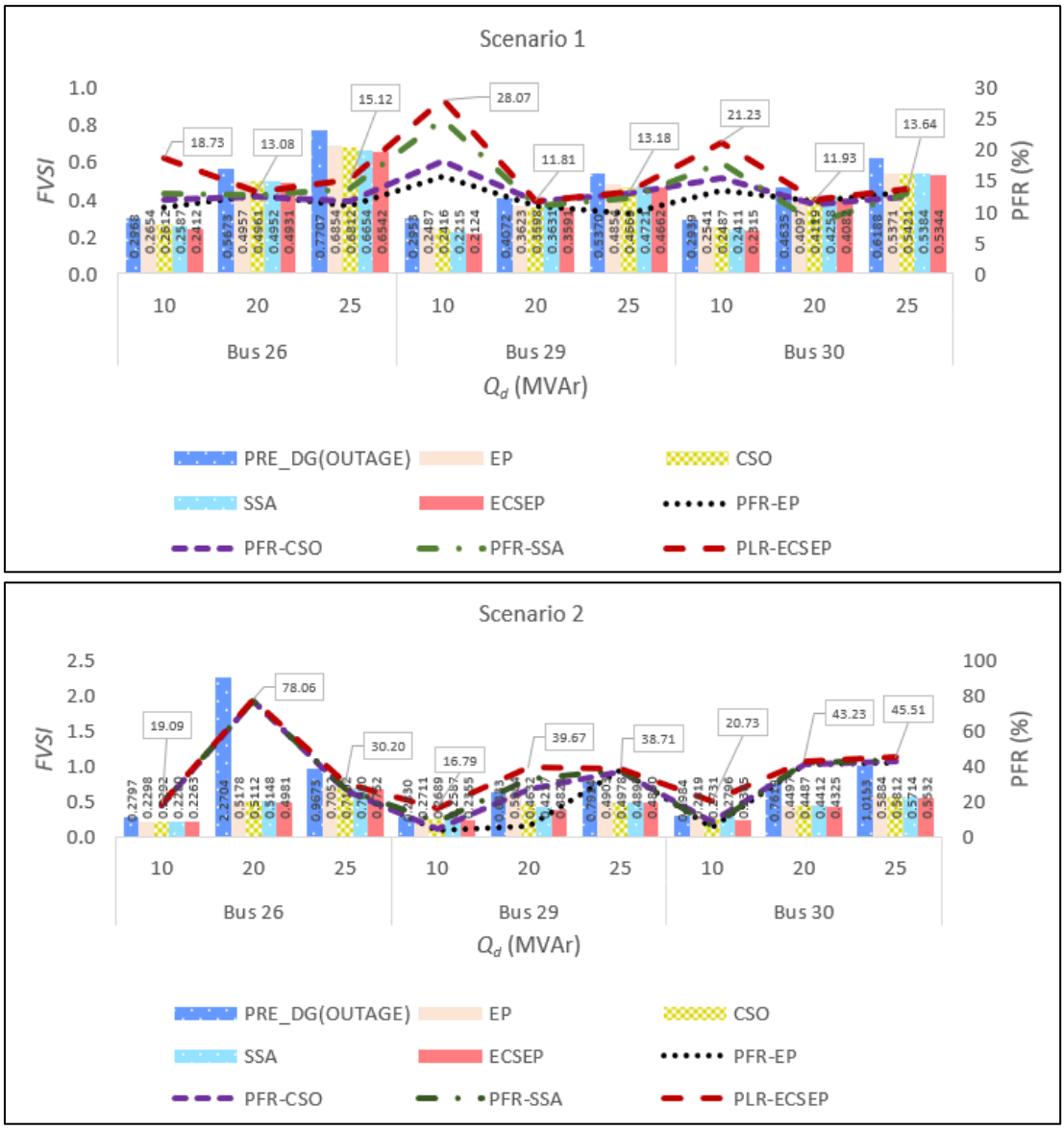


Figure 3.15 Comparison of *FVSI* and *PFR* Results for Voltage Security Improvement in DG Installation in IEEE 30-Bus RTS

In terms of *PFR*, ECSEP reaches 18.73%, which is the highest among all methods. For comparison, EP yields a *PFR* of 10.58%, while CSO and SSA achieve 11.99% and 12.84%, respectively. In Scenario 2, at Bus 26 with Q_d = 10 MVAr, the ECSEP method achieves a significant reduction in *FVSI*, decreasing it to 0.226 from the pre-DG (Outage) value of 0.280. In comparison, EP, CSO, and SSA yield *FVSI* values of 0.230, 0.229, and 0.228, respectively, all higher than ECSEP's result. For *PFR*, ECSEP achieves 19.09%, which is substantially higher than the *PFR* values of EP (17.84%), CSO (18.06%), and SSA (18.48%). This demonstrates the superior effectiveness of ECSEP in improving voltage stability, as indicated by the reduction in *FVSI*.

B. IEEE 57-Bus RTS

Figure 3.16 shows the results for comparative studies implemented in the IEEE 57-Bus RTS under two scenarios, each demonstrating the effectiveness of various optimisation methods: EP, CSO, SSA, and ECSEP in reducing the *FVSI* and improving *PFR* all the load variations at different buses.

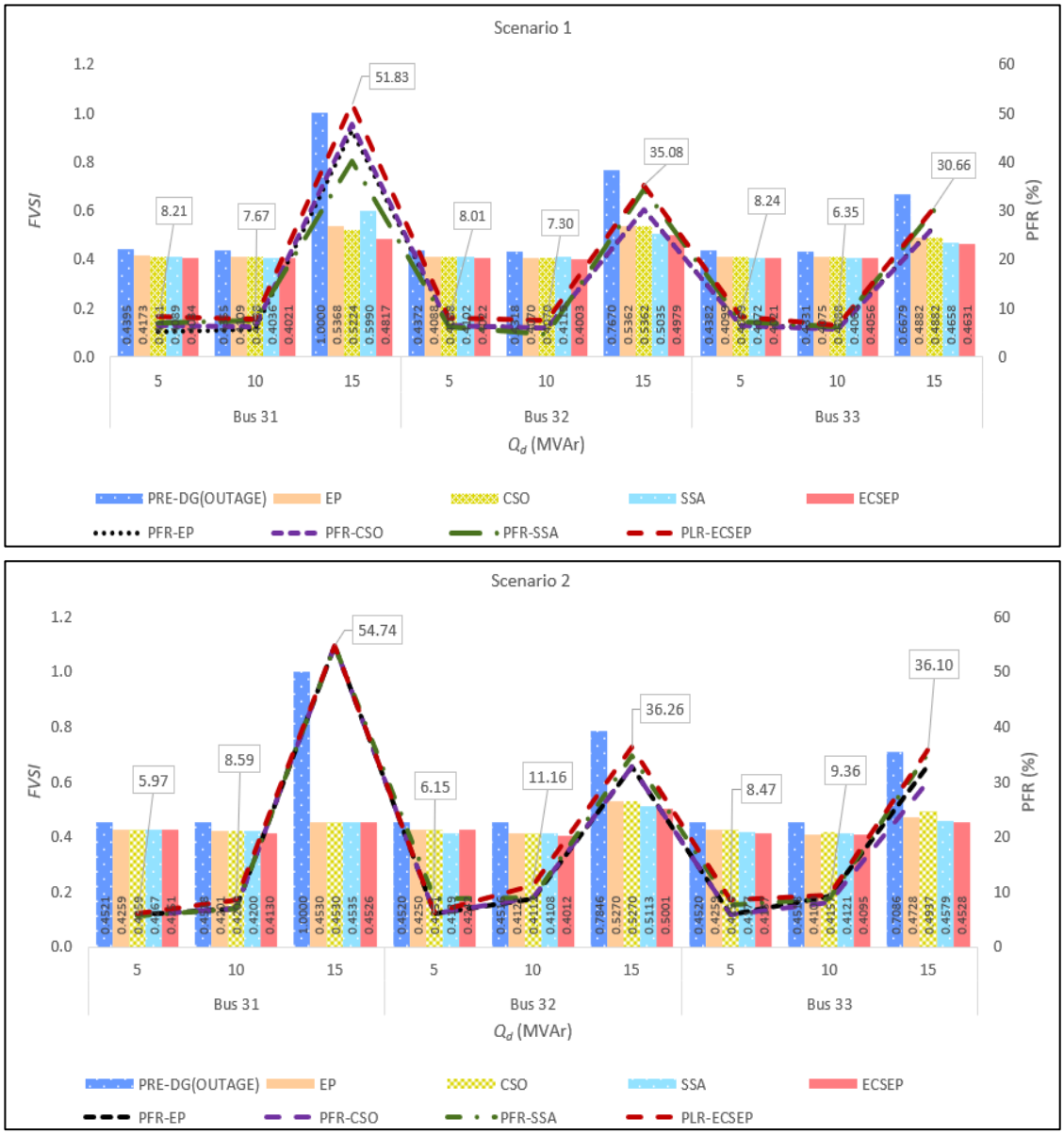


Figure 3.16 Comparison of *FVSI* and *PFR* Results for Voltage Security Improvement in DG Installation in IEEE 57-Bus RTS

In Scenario 1, at Q_{d31} = 15 MVAr, the ECSEP method achieves an *FVSI* value of 0.482, significantly reducing the instability risk from the pre-DG (Outage) value of 1.000. ECSEP's *PFR* reaches 51.83%, the highest among the methods

In Scenario 2, at Bus 31 with the Q_d = 15 MVAr, ECSEP continues to show strong performance with an *FVSI* of 0.453, substantially lower than the pre-DG value of 1.000. ECSEP achieves a *PFR* of 54.74%, indicating its exceptional ability to reduce instability in this scenario. These results demonstrate that ECSEP consistently outperforms other methods in both scenarios, achieving the most significant reductions in *FVSI* and the highest *PFR* values. This highlights the effectiveness of ECSEP in enhancing voltage stability and resilience across various loading conditions, making it a superior choice for DG planning in power systems.

3.6.2 Load Shedding Compensation Scheme

This study further extends to a comparative analysis of ECSEP against other optimization techniques: EP, CSO, and SSA within the load shedding compensation framework, focusing on loss reduction and voltage security enhancement in IEEE 30-Bus RTS and IEEE 57-Bus RTS.

3.6.2.1 Loss Minimization

A. IEEE 30-Bus RTS

Figure 3.17 presents the results of loss minimization using load shedding for the IEEE 30-Bus RTS under Scenario 1 and Scenario 2, emphasizing the impact of different optimisation techniques on loss reduction and *PLR*. The implementation of load shedding compensation scheme leads to a significant reduction in power loss solved using all methods, with ECSEP consistently achieving the lowest loss values compared to EP, CSO, and SSA. In Scenario 1, the highest *PLR* of 68.45% occurs at Bus 29 with Q_d = 25 MVAr, where the initial loss of 67.24 MW before the load shedding scheme is effectively reduced to 21.22 MW. Meanwhile, in Scenario 2, Q_{d30} = 25 MVAr records the highest *PLR* of 25.12%, with the loss decreasing from 28.33 MW to 21.22 MW after optimisation. The comparative results reveal that ECSEP provides a more effective load shedding performance, significantly reducing loss and obtained high *PLR* values.

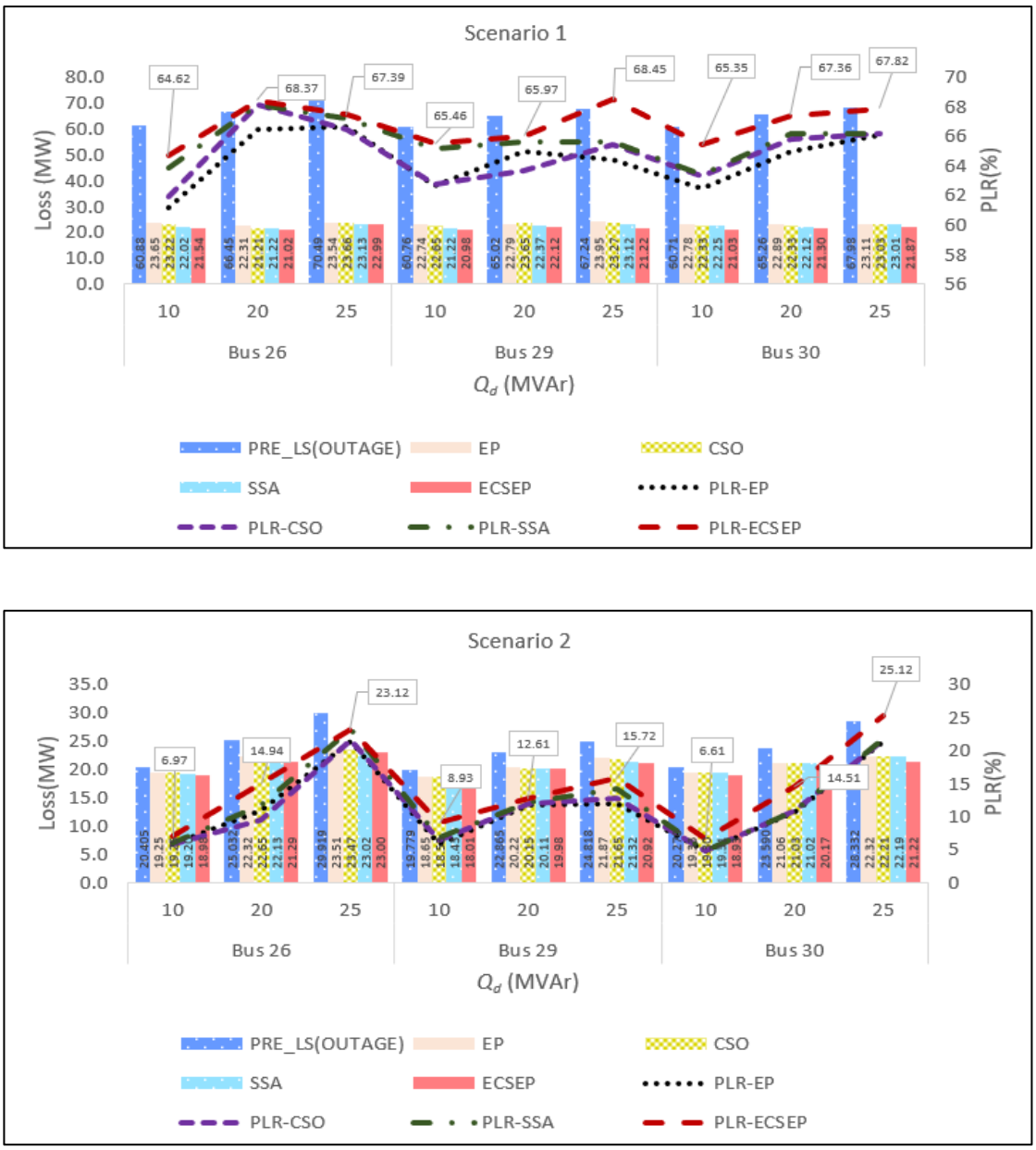


Figure 3.17 Comparison of Loss and *PLR* Results for Loss Minimization in Load Shedding Scheme in IEEE 30-Bus RTS

B. IEEE 57-Bus RTS

Figure 3.18 shows the comparison of Loss and *PLR* Results for Loss Minimization in Load shedding Scheme in IEEE 57-Bus RTS. In Scenario 1, at Bus 31 with a reactive power (Q_d) of 15 MVAr, the system losses decrease from 42.75 MW to 31.99 MW, resulting in the highest *PLR* of 25.17%. Conversely, in Scenario 2, the highest *PLR* of 43.71% is observed at Bus 32 with Q_d = 15 MVAr, where the system loss is reduced from 55.06 MW to 30.99 MW. These results highlight the effectiveness of load shedding in minimizing system losses and improving power system resilience.



Figure 3.18 Comparison of Loss and *PLR* Results for Loss Minimization in Load Shedding Scheme in IEEE 57-Bus RTS

3.6.2.2 Voltage Security Improvement

Load shedding was also implemented to enhance voltage security in the system. This approach was applied to both the IEEE 30-Bus RTS and IEEE 57-Bus RTS, with detailed discussions provided in the subsequent subchapters.

A. IEEE 30-Bus RTS

Figure 3.19 presents a comparison of FVSI and PFR results for voltage security improvement in the load shedding scheme applied to the IEEE 30-Bus RTS. In this system, FVSI values under reactive power variations were analysed using different optimisation techniques, with ECSEP consistently achieving the best results in both Scenario 1 and Scenario 2. In Scenario 1, ECSEP effectively improved voltage stability at Bus 30 with Qd = 10 MVAr, reducing the FVSI value from 0.294 to 0.225, resulting in a PFR of 23.31%.

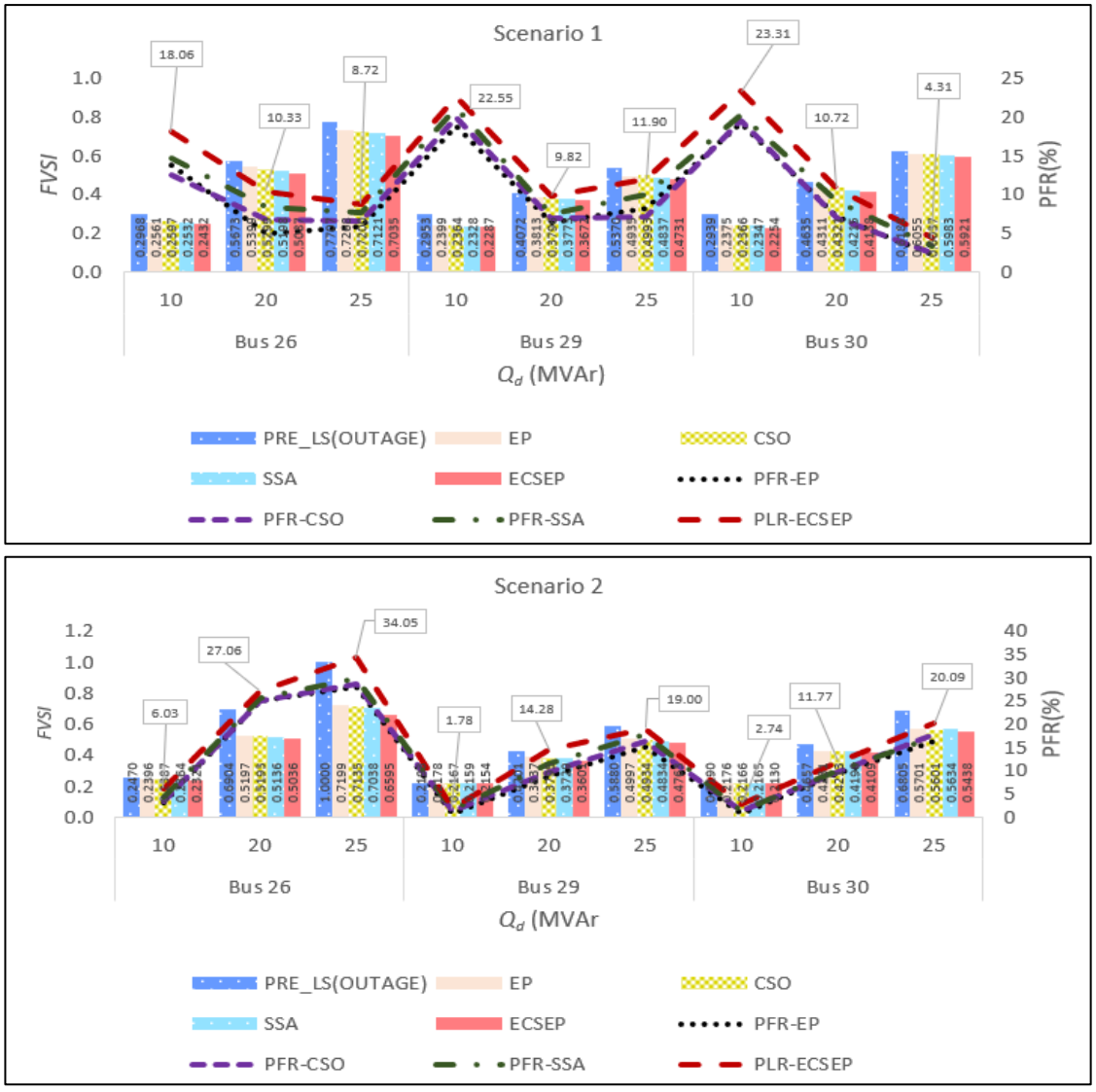


Figure 3.19 Comparison of *FVSI* and *PFR* Results for Voltage Security Improvement in Load Shedding Scheme in IEEE 30-Bus RTS

Similarly, in Scenario 2, ECSEP significantly enhanced stability at Bus 26 with Q_d = 25 MVAr, improving the *FVSI* value from 1.000 (highly unstable) to 0.659, achieving a *PFR* of 34.05%. These results highlight the effectiveness of ECSEP in mitigating voltage instability which led to system resilience improvement and successful grid hardening.

B. IEEE 57-Bus RTS

The final phase of the comparative study among the optimisation techniques focuses on analyzing *FVSI* and *PFR* results for voltage security improvement in the load shedding scheme applied to the IEEE 57-Bus RTS. Figure 3.20 illustrates the *FVSI* and *PFR* variations across different buses and reactive loading conditions.

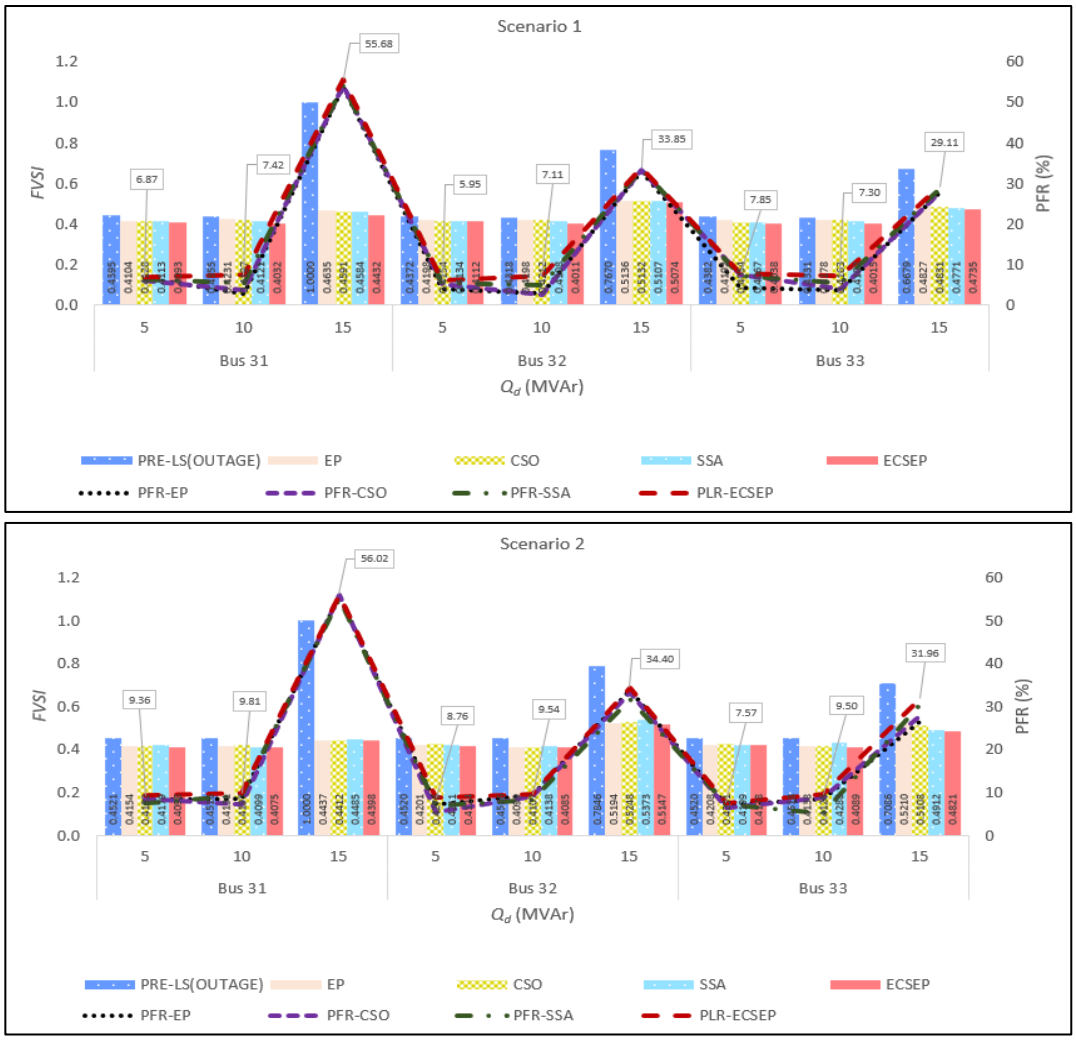


Figure 3.20 Comparison of *FVSI* and *PFR* Results for Voltage Security Improvement in Load shedding Scheme in IEEE 57-Bus RTS

Notably, Bus 31 with Q_d = 15 MVAr exhibits the highest *PFR* in both Scenario 1 and Scenario 2. Initially, before implementing the load shedding scheme, the *FVSI* value stands at 1.000, indicating an unstable system condition. However, with ECSEP optimizing the location and sizing of the buses and loads to be shed, the *FVSI* value is significantly reduced to 0.443 in Scenario 1 (*PFR* = 55.68%) and 0.440 in Scenario 2 (*PFR* = 56.02%).

The results show that ECSEP is able to improve the voltage stability of the system through the implementation of proper load shedding scheme. The large decrease in *FVSI* values shows that ECSEP has prevented the system from experiencing voltage collapse and has increased the system's robustness. Also, the increase in *PFR* indicates that the scheme is able to support grid stability in the face of changing reactive power requirements. Thus, it can be concluded that ECSEP has exhibited a reliable optimisation technique for load shedding schemes to improve voltage security in the IEEE 57-Bus RTS.

3.7 Summary

This chapter has presented the development of the Embedded Clonal Squirrel Evolutionary Programming (ECSEP) as a new hybrid algorithm to enhance the power system resilience. The newly proposed ECSEP optimisation technique managed to achieve the lowest loss and *FVSI* value in the implementation of DG installation and load shedding scheme as the initiatives in grid hardening strategy. The effectiveness of ECSEP has been validated via the implementation on the IEEE 30-bus and IEEE 57 bus RTS systems to determine the optimal location and capacity of DG units and load shedding scheme in grid hardening strategy. The results show that ECSEP has reduced transmission losses and improved voltage stability in small scale and medium scale transmission networks. Due to its hybrid structure ECSEP is able to maintain a balance between exploration and exploitation in order to find the optimal solutions to power system optimisation problems.

Therefore, the development and application of ECSEP offers a valid and effective optimisation tool for grid hardening strategies. Its effectiveness in reducing losses and improving stability makes it a suitable remedial action for practical power system applications to enhance grid resilience to disturbances. The findings from this study suggest that ECSEP can be a valuable tool for optimizing power system

operations, paving the way for future research on hybrid intelligent optimisation techniques in the field of power system resilience. The implementation of ECSEP in addressing the DG installation and load shedding schemes as grid hardening initiatives is demonstrated through its robustness under the influence of hurricane occurrences, denoted by Scenario 1 and Scenario 2, for both test models.

CHAPTER 4
MULTI-OBJECTIVE EMBEDDED CLONAL SQUIRREL EVOLUTIONARY PROGRAMMING ALGORITHM BASED TECHNIQUE FOR RESILIENCE IMPROVEMENT IN POWER SYSTEM

4.1 Introduction

Multi-Objective optimisation technique is important in power system planning and operation. This is due to the fact that, in single objective optimisation process, separate problems are solved independently. This leads to incomplete problems to be solved as the practical environment in power system community will have to consider several objective functions to be conducted concurrently. This chapter presents Multi-Objective Embedded Clonal Squirrel Evolutionary Programming (MOECSEP) algorithm-based technique for resilience improvement in power system. Similar scenarios and test systems are conducted to implement MOECSEP. Subsequent comparative studies will be ultimately conducted in the effort to highlight the superiority of the MOECSEP over benchmark techniques such as Multi-Objective Evolutionary Programming (MOEP) and Multi-Objective Squirrel Search (MOSS).

4.2 Weighted Sum Multi-Objective Optimisation

The study integrates DG installation with load shedding schemes into the IEEE 30-Bus RTS and IEEE 57-Bus RTS under two simulated hurricane scenarios. The test systems accurately depict real-world grid structures and serve as standard models for evaluating resilience in power systems. The systems show deteriorating voltage profiles and rising power losses particularly in weak buses and buses under critical load conditions during these extreme conditions. The study requires increasing reactive power demand at chosen weak buses to model post-disturbance scenarios which necessitates the implementation of resilience-enhancing measures.

The optimisation process aims to achieve two main objectives which include minimizing system power loss and also minimizing Fast Voltage Stability Index (*FVSI*) in one integrated fitness equation. A multi-objective optimisation framework is selected

to solve this problem. The weighted sum and pareto optimal methods stand as the most frequently used methods for solving multi-objective problems. The weighted-sum method serves this study because it provides straightforward results and works well with evolutionary algorithms to create a single objective function. The weighted sum method combines multiple fitness functions into a single composite objective function through the assignment of weighting coefficients to each fitness function. The approach enables users to adjust the relative importance between power loss reduction and voltage stability improvement. The proposed Multi-Objective Squirrel Evolutionary Programming (MOECSEP) can solve the single-objective problem which results from this formulation. The established formulation enables researchers to create optimal DG placement and load shedding strategies which improve system resilience against disruptive events.

In this study, the weighted-sum multi-objective technique provides an easy-to-use solution for multi-objective optimisation problems through the combination of multiple objective functions into one integrated fitness function. The general weighted-sum fitness function can be mathematically represented in Equation (4.1) and Equation (4.2):

$$F(x) = w_1 f_1(x) + w_2 f_2(x) + \cdots + w_n f_n(x) \tag{4.1}$$

$$O.F. = \min\big(F(x)\big) \; or \; \min\big(F(x)\big) \tag{4.2}$$

In weighted sum multi-objective optimization technique, the individual fitness is not independently optimized. The integrated fitness, $F(x)$ will be optimized, either to be minimized or maximized. Each fitness function $f_n(x)$ is assigned a corresponding weight coefficient w_n, which reflects its relative importance in the optimisation process. These weight coefficients typically range from 0.1 to 1.0, subject to their total summation must be equal led to 1.0. In this study the selection of weight coefficient is randomly chosen.

The weighted-sum method is incorporated into the proposed multi-objective Embedded Clonal Squirrel Evolutionary Programming (MOECSEP) to optimize the integrated fitness value leading to the evaluation of resilience index. Two fitness functions are considered in this study: *FVSI* and the total real power loss (Loss). These

are denoted as $f_1(x) = Loss$ and $f_2(x) = FVSI$, respectively. The integrated fitness function can be written in Equation (4.3):

$$O.F. = \min(w_1 Loss + w_2 FVSI) \tag{4.3}$$

where w_1 and w_2 are the weight coefficients assigned to each fitness function, subject to $w_1 + w_2$ =1. The unit for w_1 is $(MW)^{-1}$ and *FVSI* is unitless. The coefficients values are determined by their effect on system performance and usually fall between 0.1 and 0.9. This formulation allows for a flexible and balanced trade-off between voltage stability improvement and power loss reduction.

The research established three distinct weight coefficient schemes which served to optimize the multi-objective fitness function. The different weight configurations demonstrate how the two fitness functions of total system power loss and *FVSI* receive varying degrees of importance. The weight configurations follow these arrangements:

1) Case 1: $w_1 = 0.1, w_2 = 0.9$
2) Case 2: $w_1 = 0.5, w_2 = 0.5$
3) Case 3: $w_1 = 0.9, w_2 = 0.1$

The weight settings enable the assessment of trade-offs between fitness functions while showing how optimisation techniques perform with different priority preferences, thus enhancing the overall system resilience.

4.3 Research Framework for Resilience Improvement

In this study, the total power loss and Fast Voltage Stability Index (*FVSI*) are simultaneously optimised using a weighted-sum multi-objective approach integrated with the proposed Multi-Objective Embedded Clonal Squirrel Evolutionary Programming (MOECSEP) technique. The overall framework for the multi-objective optimisation implementation is illustrated in Figure 4.1. To evaluate the effectiveness of the proposed method, three optimisation techniques were employed: Multi-Objective Evolutionary Programming (MOEP), Multi-Objective Squirrel Search (MOSS), and the proposed MOECSEP. The aim is to evaluate the strength of MOECSEP over MOEP and MOSS. Each technique was utilized to determine the optimal placement and sizing of DG and optimal load shedding scheme under multi-objective optimisation

formulation. Subsequently, the resilience index is evaluated to determine the strength of the system. The performance of each optimisation technique is validated on the IEEE 30-Bus RTS and IEEE 57-Bus RTS. A comparative study on the results of each optimisation technique for each transmission network will be conducted.

This formulation enables the simultaneous reduction of system losses and enhancement of voltage security, contributing to improved power system resilience.

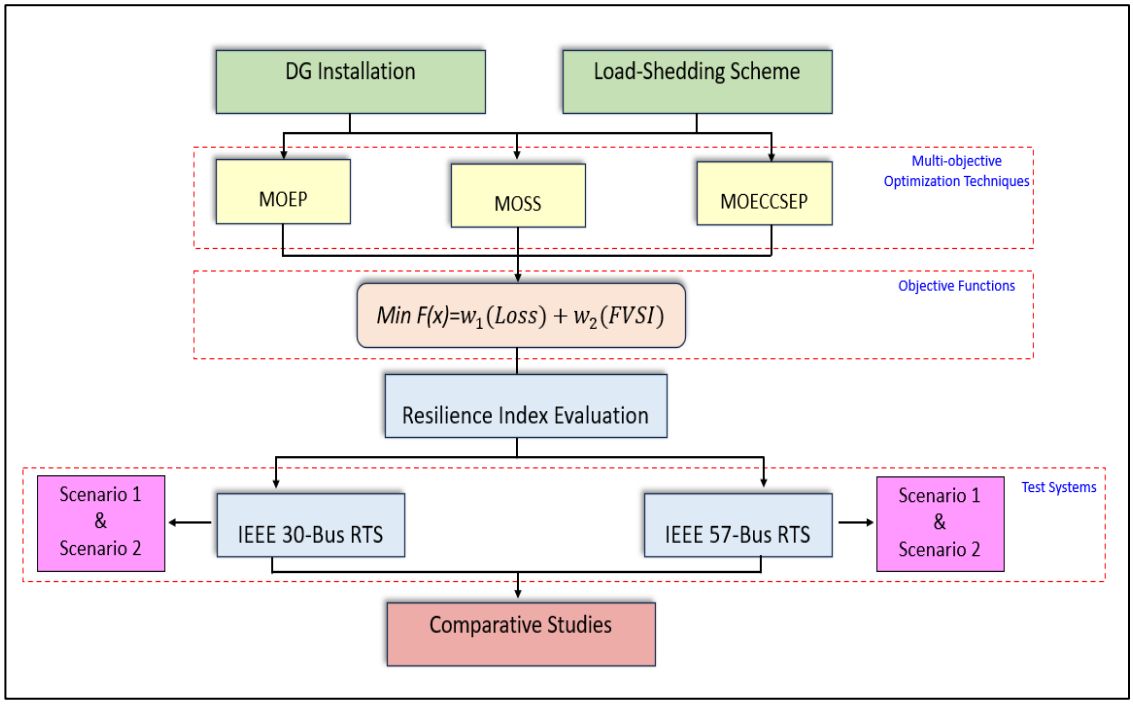


Figure 4.1 The Overall Research Framework for the Multi-Objective Optimisation Implementation

4.3.1 Multi-Objective Evolutionary Programming (MOEP) Algorithm in Power System Resilience Improvement

In this section, MOEP algorithm is utilized to determine the optimal installation of DG and load shedding scheme in the test systems. This technique is used as the benchmark for the proposed MOECSEP. The weight coefficient w_1 is assigned for total loss in the system and w_2 is assigned for $FVSI$ based on the three setting setups. The implementation of the MOEP technique for power system resilience improvement involves seven key steps: initialization, fitness 1 evaluation, mutation, fitness 2 evaluation, solution combination, tournament and selection, convergence checking, and

results recording (end). The flowchart of the MOEP algorithm is shown as in Figure 4.2.

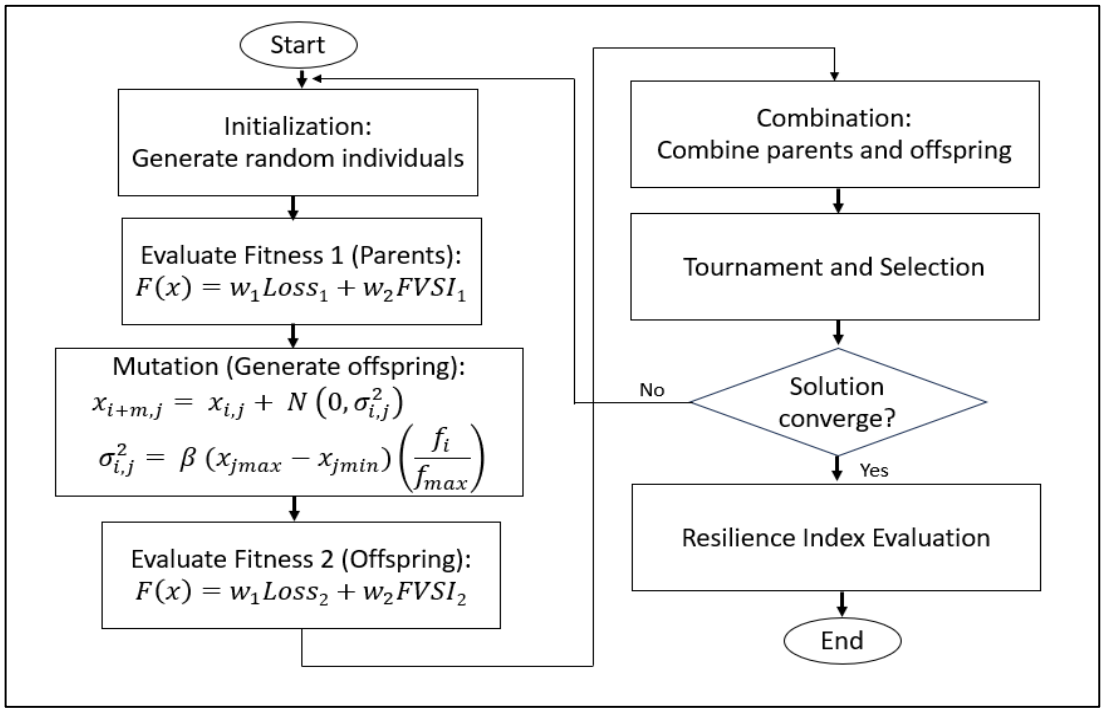


Figure 4.2 Flowchart of Multi-Objective Evolutionary Programming (MOEP) for Power System Resilience Improvement

4.3.2 Multi-objective Squirrel Search (MOSS) Algorithm in Power System Resilience Improvement

The following section explains how to solve multi-objective optimisation problems through the Multi-Objective Squirrel Search Algorithm (MOSS) which originates from the Squirrel Search Optimizer (SSO). The weighted sum method gets integrated into the SSO framework to handle power system resilience improvement multi-objective challenges. This study uses MOSS as its benchmark approach. The flowchart in Figure 4.3 demonstrates how the MOSS algorithm enhances power system resilience specifically through optimal DG installation and load shedding strategies.

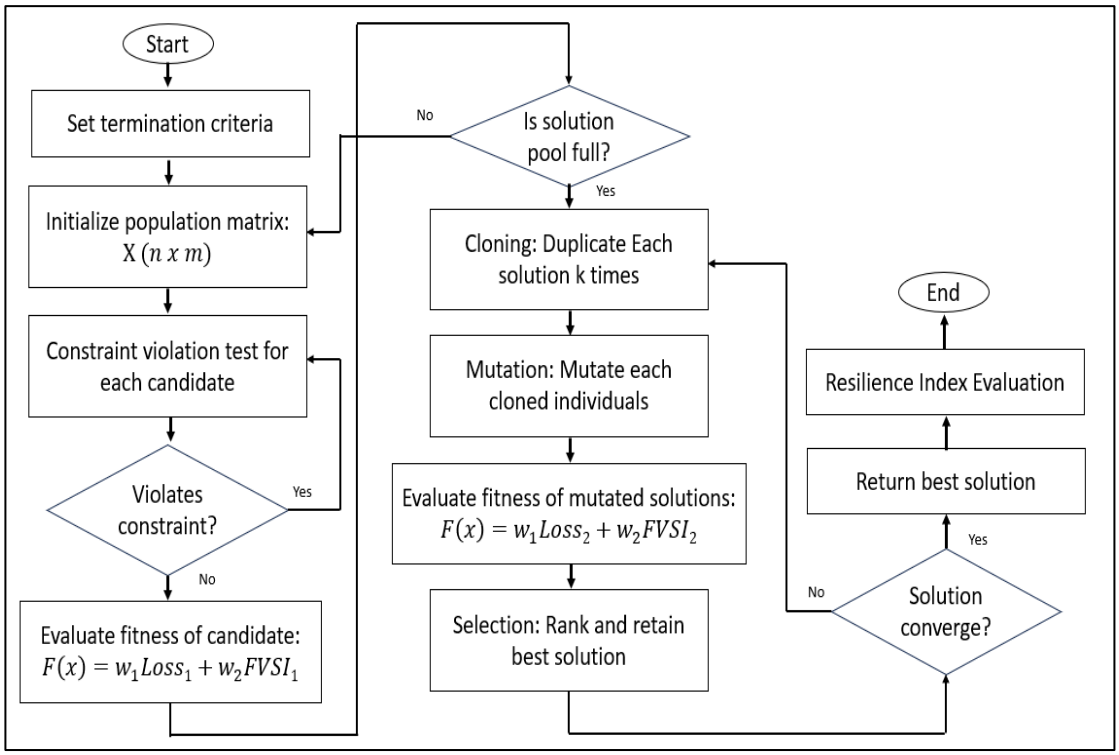


Figure 4.3 Flowchart of Multi-Objective Squirrel Search Algorithm (MOSS) for Power System Resilience Improvement

4.3.3 Proposed Multi-Objective Embedded Clonal Squirrel Evolutionary Programming (MOECSEP) in Power System Resilience Improvement

The study introduces a new multi-objective optimisation algorithm called Multi-Objective Embedded Clonal Squirrel Evolutionary Programming (MOECSEP). The MOECSEP algorithm extends the ECSEP framework to optimize DG installation and load shedding strategies simultaneously for enhancing power system resilience. The flowchart of the MOECSEP algorithm is presented in Figure 4.4, and the corresponding implementation steps are as follows:

Step 1: Initialize the population and calculate the initial system Loss and *FVSI*. During this process, random individuals are generated to represent the general locations for DG and the corresponding DG sizing. Random locations for load to undergo load shedding are also generated, followed by the sizing of P_d and Q_d for each random load. The general matrix equation for this phase can be written as:

$$[L_{DG11^m} L_{DG12^m} \ldots\ldots L_{DG1n^m} D_{G11^m} D_{G12^m} \ldots\ldots D_{G1n^m} L_{SH11^m} L_{SH12^m} \ldots\ldots L_{SH1k^m} P_{d11^m} P_{d12^m} \ldots P_{d11^m} \ldots P_{d1k^m} Q_{d11^m} Q_{d12^m}] \quad (4.4)$$

Where, n is number of DG to be installed, k is the number of loads to be shed and m is the number of individuals. For instance, for 3 units of DG to be installed into the system and 4 loads to be shed from the system, the control variables will be 6 for DG and 12 for load to be shed, making the total control variables of 18. If 20 individuals are required during this phase, apparently the total size of matrix would be 20 rows by 24 columns.

Step 2: Evaluate the pool filling condition. If the condition is not satisfied, regenerate the population.

Step 3: Fill in the population pool with valid candidate solutions.

Step 4: Clone the parent population to generate a larger solution pool. Let $X_{i,j}$ represent the solution matrix where i is the clone population size and j is the number of control variables.

Step 5: Redefine each individual in the population after cloning.

Step 6: Compute Fitness I using the weighted sum approach:

$$F_1(x) = w_1 Loss_1 + w_2 FVSI_1 \tag{4.5}$$

Step 7: Generate a random squirrel position to represent exploratory solution diversity.

Step 8: Update the position of each solution using the squirrel search equation to simulate natural foraging behaviour.

Step 9: Compute Fitness II:

$$F_2(x) = w_1 Loss_2 + w_2 FVSI_2 \tag{4.6}$$

Step 10: Perform a tournament selection process using an elitism strategy to preserve the best-performing solutions for the next generation.

Step 11: Check the convergence criterion. If satisfied, proceed to the final step. If not, return to Step 8 for further iterations.

Step 12: Terminate the algorithm and output the optimal solution for distributed generation installation and load shedding strategy that improves power system resilience.

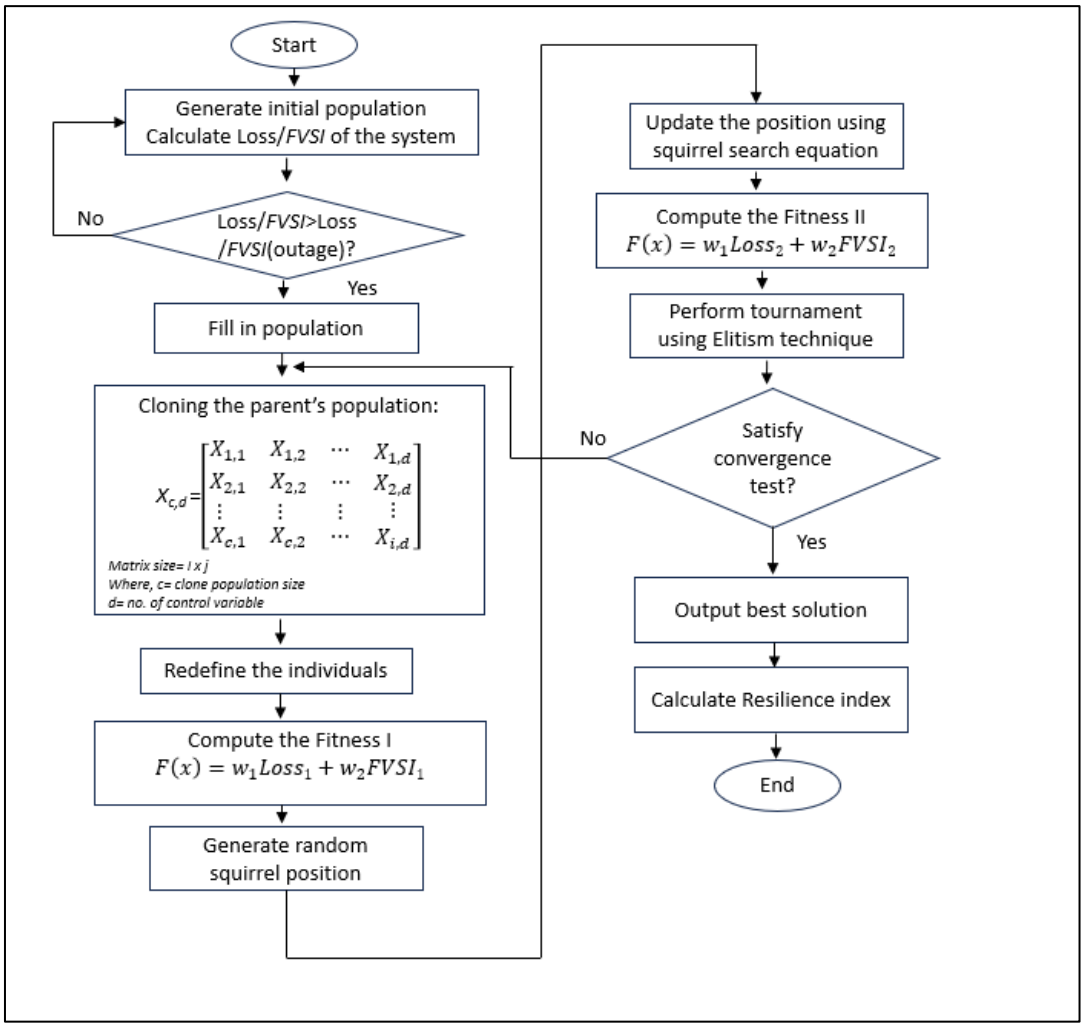


Figure 4.4 Flowchart of Multi-Objective Embedded Clonal Squirrel Evolutionary Programming (MOECSEP) for Power System Resilience Improvement

The MOECSEP algorithm, incorporating the weighted sum method, was applied to two test systems: the IEEE 30-Bus RTS and the IEEE 57-Bus RTS. The performance of the algorithm was evaluated under two distinct hurricane strike scenarios to assess its effectiveness in enhancing power system resilience. Three cases are arbitrarily configured to form 3 study cases. Case 1: $w_1 = 0.1, w_2 = 0.9$; Case 2: $w_1 = 0.5, w_2 = 0.5$ and Case 3: $w_1 = 0.9, w_2 = 0.1$. Two compensation strategies were employed in this study namely DG installation and load shedding schemes which were implemented independently. Additionally, the simulations accounted for the impact of increased reactive power demand (Q_d) at identified weak buses.

4.4 Results and Discussion

The simulation results of this study solved by the MOECSEP algorithm are presented and analysed in this section. The analysis is divided into two main sections which examine optimal DG installation and load shedding schemes implemented independently. The two standard test systems used for analysis are the IEEE 30-Bus RTS and the IEEE 57-Bus RTS. The MOECSEP algorithm performance evaluation focuses on its success in reducing power losses and enhancing voltage security in the system when hurricane strike scenarios are simulated. The algorithm demonstrates its effectiveness for system resilience improvement through DG unit placement and sizing analysis and load shedding decision optimisation in each test case.

4.4.1 Distributed Generation (DG) Installation

The study of multi-objective optimisation begins by implementing the proposed MOECSEP algorithm to find the optimal solution for DG installation. The study aims to discover both the best positions and optimal capacity levels for DG units which improve power system resilience. The research phase evaluates how DG affects system performance when operating under extreme conditions. The proposed method received validation through simulations performed on two reliability test systems which included the IEEE 30-Bus RTS and the IEEE 57-Bus RTS. The simulated hurricane strike scenarios caused line outages and voltage stability issues. The simulated conditions match actual disruptions which enables accurate evaluation of system responses and recovery abilities. The MOECSEP algorithm implements the weighted sum method as it was formulated to achieve simultaneous power loss and *FVSI* reduction. Each test system received two hurricane strike scenarios that simulated both power line failures and reactive power changes at essential buses.

4.4.1.1 DG Installation in IEEE 30-Bus RTS

The IEEE 30-Bus RTS underwent two hurricane strike simulations to evaluate DG effectiveness in solving a multi-objective optimisation problem. The optimisation goal involved minimizing power loss while reducing the *FVSI* value through integrated

fitness function optimisation. The study will also demonstrate how DG placement and sizing strategies improve system resilience during extreme weather disturbances.

A. Scenario 1

The integrated fitness function is characterized using three different weight coefficient configurations as previously discussed in Case 1, Case 2 and Case 3. The three configurations were used to study the trade-offs between power loss minimization and voltage stability improvement. This section presents detailed results from the simulation for each case. The MOECSEP algorithm produces the following overall results for DG installation under the weight coefficient configuration which prioritizes *FVSI* reduction over power loss minimization as tabulated in Table 4.1. The simulations were performed involving load variations at three load buses (Bus 26, Bus 29, and Bus 30) and for three levels of reactive power loading Q_d (10, 20, and 25 MVAr) to represent increasingly stressed conditions. The initial loss and *FVSI* values before any disturbance $Loss_{Set}$, $FVSI_{\mathrm{Set}}$ are listed in the first two rows. As expected, both the power losses and *FVSI* values increase with higher reactive power loading, indicating a more stressed system with greater vulnerability to voltage security. After the system is subjected to hurricane strike, which results in line outages and system stress, the power losses $Loss_{Out}$ and voltage stability index $FVSI_{Out}$ show significant deterioration across all buses and loading levels. For instance, at Bus 26 with a reactive power loading of Q_d = 25 MVAr, the system experiences a significant deterioration following the disturbance, where the power $Loss_{Out}$ increases sharply to 70.49 MW from the initial value of 22.27 MW $Loss_{Set}$, and the $FVSI_{\mathrm{Out}}$ escalates to 0.7707 from 0.6529 ($FVSI_{\mathrm{Set}}$). These results indicate a critically stressed and prone to unstable system condition, highlighting the closeness to vulnerability of the network under severe disruption. With the optimal placement and sizing of DGs determined by MOECSEP, a considerable improvement is observed. Power losses after DG installation $Loss_{DG}$ and corresponding *FVSI* values $FVSI_{DG}$ are significantly reduced compared to the outage condition. For example, at the same bus and loading, $Loss_{DG}$ is reduced to 23.23 MW from 70.49 MW, and $FVSI_{DG}$ drops to 0.7321 from 0.7707. This is resulted from the installation of 5DG units into the system, which implies that the compensation effort using DG installation is worth to ensure a stable system and lower power loss under the hurricane scenario.

Table 4.1
Results of MOECSEP Application in DG Installation for Scenario 1 Hurricane Strike for Case 1 in IEEE 30-Bus RTS

Bus	**26**			**29**			**30**		
Q_d	**10**	**20**	**25**	**10**	**20**	**25**	**10**	**20**	**25**
$Loss_{Set}$	18.23	20.25	22.27	18.12	19.39	20.53	18.11	19.55	20.93
$FVSI_{Set}$	0.2248	0.4919	0.6529	0.2111	0.3573	0.4646	0.2114	0.4073	0.5349
$Loss_{Out}$	60.88	66.45	70.49	60.76	65.02	67.24	60.71	65.26	67.98
$FVSI_{Out}$	0.2968	0.5673	0.7707	0.2953	0.4072	0.5370	0.2939	0.4635	0.6188
$Loss_{DG}$	18.25	20.35	23.23	19.35	19.70	21.25	19.86	22.22	23.22
$R1_{Loss}$	0.43	0.44	0.46	0.42	0.42	0.44	0.43	0.43	0.44
$R2_{Loss}$	0.43	0.44	0.49	0.47	0.43	0.46	0.49	0.52	0.52
$FVSI_{DG}$	0.2290	0.5012	0.7321	0.2546	0.3845	0.4932	0.2854	0.4238	0.5932
$R1_{FVSI}$	3.12	6.52	5.54	2.51	7.16	6.42	2.56	7.25	6.38
$R2_{FVSI}$	3.38	7.59	18.99	6.26	16.94	11.26	33.58	10.68	23.17
Loc_{DG1}	8	21	5	10	4	5	7	5	19
Loc_{DG2}	16	5	21	19	15	7	18	7	3
Loc_{DG3}	5	29	26	11	5	4	30	15	8
Loc_{DG4}	10	18	23	5	30	12	8	4	7
Loc_{DG5}	23	4	7	4	17	8	23	16	4
$Size_{DG1}$	9.89	71.46	62.95	86.94	69.09	13.69	94.53	40.49	13.81
$Size_{DG2}$	67.13	74.09	23.17	51.29	12.81	77.43	10.85	94.30	13.14
$Size_{DG3}$	95.98	50.16	17.00	47.81	48.64	45.91	44.50	46.57	48.80
$Size_{DG4}$	45.93	33.35	48.59	62.40	6.06	35.64	7.79	8.65	50.13
$Size_{DG5}$	43.55	20.24	50.33	42.32	43.61	45.80	32.77	15.94	42.60
F_{Set}	6.3556	7.1556	7.7425	6.3413	6.8690	7.2077	6.3350	6.9434	7.3548
F_{Total}	2.0306	2.4864	2.9821	2.1646	2.3158	2.5693	2.2432	2.6030	2.8554

*Notes: Unit for Q_d = MVAr, *FVSI* = p.u., Loss = MW and Size = MW

Focusing on Bus 26 with a reactive power loading of Q_d = 25 MVAr, the performance of the system before and after DG installation can be analysed through the resilience indices. The resilience index based on power loss before DG installation, $R1_{Loss}$, is 0.46, whereas after DG installation, $R2_{Loss}$ increases to 0.49. More notably, the voltage stability resilience shows a significant enhancement. The resilience index based on the *FVSI* prior to DG installation, $R1_{FVSI}$, is recorded at 5.54. With DG installation, this value dramatically increases to 18.99 ($R2_{FVSI}$). This indicates an increment of power system resilience characterized by *FVSI* within considerable resilience improvement due loss reduction. The optimal DG installation locations are identified as Bus 5, 21, 26, 23, and 7 for Loc_{DG1} to Loc_{DG5}, respectively. These buses were optimally identified by MOECSEP in reducing system losses and improving voltage stability when the system was subjected to the hurricane-induced disturbance

scenario. Correspondingly, the optimal DG sizes allocated to these locations are 62.95 MW, 23.17 MW, 17.00 MW, 48.59 MW, and 50.33 MW, respectively. The final row shows the combined fitness value for each case, computed using the weighted sum multi-objective optimisation process. For example, the F_{Total} for Q_{d26} = 25 MVAr decreases from 7.7425 to 2.9821. For Q_d variation at Buses 29 and 30, the same phenomena can be observed as tabulated in the Table 4.1 in terms of increment the resilience index, reduction in *FVSI* values and reduction in power loss. This generalises the impact of DG installation as the compensation strategy in improving the system performance and makes the system more resilient.

Table 4.2 presents the results of applying the MOECSEP algorithm to optimize DG installation for the IEEE 30-Bus RTS under Scenario 1 hurricane strike, using equal weight coefficients ($w_1 = 0.5$ and $w_2 = 0.5$) in Case 2.

Table 4.2
Results of MOECSEP Application in DG Installation for Scenario 1 Hurricane Strike for Case 2 in IEEE 30-Bus RTS

Bus	**26**			**29**			**30**		
Q_d	**10**	**20**	**25**	**10**	**20**	**25**	**10**	**20**	**25**
$Loss_{Set}$	18.23	20.25	22.27	18.12	19.39	20.53	18.11	19.55	20.93
$FVSI_{Set}$	0.2248	0.4919	0.6529	0.2111	0.3573	0.4646	0.2114	0.4073	0.5349
$Loss_{Out}$	60.88	66.45	70.49	60.76	65.02	67.24	60.71	65.26	67.98
$FVSI_{Out}$	0.2968	0.5673	0.7707	0.2953	0.4072	0.5370	0.2939	0.4635	0.6188
$Loss_{DG}$	19.22	22.37	24.33	19.37	22.35	22.98	20.35	20.32	23.67
$R1_{Loss}$	0.43	0.44	0.46	0.42	0.42	0.44	0.43	0.43	0.44
$R2_{Loss}$	0.46	0.51	0.53	0.47	0.52	0.52	0.50	0.45	0.53
$FVSI_{DG}$	0.2548	0.5324	0.6932	0.2635	0.3968	0.5364	0.2743	0.4132	0.5632
$R1_{FVSI}$	3.12	6.52	5.54	2.51	7.16	6.42	2.56	7.25	6.38
$R2_{FVSI}$	6.07	15.26	8.94	8.29	38.15	894.00	13.99	8.21	10.13
Loc_{DG1}	26	4	4	20	26	17	14	27	3
Loc_{DG2}	10	7	7	5	3	26	6	3	30
Loc_{DG3}	20	9	5	29	16	19	21	14	21
Loc_{DG4}	17	10	10	8	7	7	8	23	10
Loc_{DG5}	14	26	20	21	21	8	6	9	12
$Size_{DG1}$	84.32	49.84	98.06	89.92	63.60	48.62	44.33	23.57	90.53
$Size_{DG2}$	5.98	73.36	48.34	63.21	36.81	89.71	29.60	21.43	80.58
$Size_{DG3}$	26.43	28.72	69.57	12.50	79.39	28.64	39.28	69.12	34.54
$Size_{DG4}$	31.89	87.12	33.61	11.67	21.68	35.16	58.59	24.48	91.55
$Size_{DG5}$	37.92	81.01	53.91	76.53	79.57	44.80	65.51	81.63	69.44
F_{Set}	30.5907	33.5088	35.6298	30.5253	32.7161	33.8906	30.4995	32.8630	34.2990
F_{Total}	9.7351	11.4489	12.5092	9.8145	11.3755	11.7598	10.3143	10.3674	12.1143

*Notes: Unit for Q_d = MVAr, *FVSI* = p.u., Loss = MW and Size = MW

Across all buses and reactive power loading conditions, the implementation of DG led to noticeable improvements in system performance following the hurricane-induced disturbance. In general, with the increment in Q_d value at all the participating buses i.e. Buses 26, 29 and 30, the loss value increases for pre- and post- DG installation. The profiles of losses for pre-outage are lower than the post-outage profiles. With the installation of DGs into the system, the post-outage profiles are lower. This phenomenon occurs for all load variations at Buses 26. 29 and 30. With the DG installation, the resilience index values are also increased for all load variation at Buses 26, 29 and 30. For instance, at Q_{d29} = 10 MVAr, the power loss drastically increase from a pre-disturbance value of 18.12 MW ($Loss_{Set}$) to 60.76 MW after the outage ($Loss_{Out}$). Upon applying the optimised DG installation determined by the MOECSEP algorithm, the loss was significantly reduced to 19.37 MW ($Loss_{DG}$). Similarly, the *FVSI* increased from 0.2111 to 0.2953 due to the disruption, but was brought down to 0.2635 after DG placement. The corresponding resilience indices show this improvement clearly, where $R1_{Loss}$ = 0.42 increased to $R2_{Loss}$ = 0.47, and $R1_{FVSI}$ = 2.51 improved to $R2_{FVSI}$ = 8.29, indicating a strong recovery in both power loss and voltage stability.

The buses identified as the optimal locations for DG installation are Buses 20, 5, 29, 8, and 21, which correspond to Loc_{DG1} to Loc_{DG5}, respectively. These buses are selected to reduce the system vulnerability and improve the voltage stability under the Scenario 1 hurricane event. The corresponding DG sizes are 89.92 MW, 63.21 MW, 12.50 MW, 11.67 MW, and 76.53 MW, respectively as highlighted in the Table 4.2. The total fitness values (F_{Total}) observed at Q_{d29} = 10 MVAr is reduced from 30.5253 to 9.8145. These results demonstrate the MOECSEP algorithm is able to provide optimal DG placement that enhances system resilience. For Q_d variation at other load buses, the same phenomena can be observed as tabulated in the Table 4.2 in terms of increment in resilience index, reduction in *FVSI* values and reduction in power loss. This generalises the impact of DG installation as the compensation strategy in improving the system performance and makes the system more resilient.

Table 4.3 illustrates the effectiveness of the MOECSEP algorithm in minimizing power losses and enhancing voltage stability through DG installation under Scenario 1 hurricane strike, using a weighted configuration of ($w_1 = 0.9$ and $w_2 = 0.1$) in Case 3. At Bus 30 with Q_d = 25 MVAr, the system initially experienced a significant increase in power loss due to the hurricane-induced line outages, rising from 20.93 MW ($Loss_{Set}$) to 67.98 MW ($Loss_{Out}$). Following the application of the MOECSEP-optimised DG

placement, the loss was effectively reduced to 23.65 MW ($Loss_{DG}$). This resulted in an improvement in the loss-based resilience index from $R1_{Loss}$ = 0.44 to $R2_{Loss}$ = 0.53, confirming the algorithm ability to recover system efficiency after a disturbance. The *FVSI* value demonstrates a slight reduction, decreasing from 0.6188 ($FVSI_{Out}$) to 0.5532 ($FVSI_{DG}$) with DG installation.

Table 4.3
Results of MOECSEP Application in DG Installation for Scenario 1 Hurricane Strike for Case 3 in IEEE 30-Bus RTS

Bus	**26**			**29**			**30**		
Q_d	**10**	**20**	**25**	**10**	**20**	**25**	**10**	**20**	**25**
$Loss_{Set}$	18.23	20.25	22.27	18.12	19.39	20.53	18.11	19.55	20.93
$FVSI_{Set}$	0.2248	0.4919	0.6529	0.2111	0.3573	0.4646	0.2114	0.4073	0.5349
$Loss_{Out}$	60.88	66.45	70.49	60.76	65.02	67.24	60.71	65.26	67.98
$FVSI_{Out}$	0.2968	0.5673	0.7707	0.2953	0.4072	0.5370	0.2939	0.4635	0.6188
$Loss_{DG}$	20.36	23.65	26.24	20.31	23.55	22.57	23.85	22.47	23.65
$R1_{Loss}$	0.43	0.44	0.46	0.42	0.42	0.44	0.43	0.43	0.44
$R2_{Loss}$	0.50	0.55	0.59	0.50	0.57	0.51	0.65	0.52	0.53
$FVSI_{DG}$	0.2423	0.5038	0.6694	0.2235	0.3698	0.4765	0.2236	0.4198	0.5532
$R1_{FVSI}$	3.12	6.52	5.54	2.51	7.16	6.42	2.56	7.25	6.38
$R2_{FVSI}$	4.45	7.93	6.61	3.11	9.89	7.88	3.18	9.61	8.43
Loc_{DG1}	26	15	16	8	4	8	16	16	15
Loc_{DG2}	16	24	20	26	3	14	14	17	20
Loc_{DG3}	4	8	10	15	23	7	21	18	12
Loc_{DG4}	20	5	30	16	19	19	10	7	19
Loc_{DG5}	14	10	16	19	7	15	12	10	10
$Size_{DG1}$	70.12	38.06	26.61	81.75	21.35	58.75	83.10	94.21	51.64
$Size_{DG2}$	91.03	20.81	9.07	75.58	8.11	40.91	5.35	36.22	49.83
$Size_{DG3}$	76.22	92.85	94.78	46.22	38.88	98.91	52.97	35.21	81.52
$Size_{DG4}$	26.24	76.40	7.37	95.14	95.21	86.64	67.11	8.07	55.15
$Size_{DG5}$	4.74	61.66	50.07	63.27	94.75	63.40	3.46	57.19	85.40
F_{Set}	54.8258	59.8620	63.5170	54.7093	58.5631	60.5734	54.6640	58.7825	61.2432
F_{Total}	18.3450	21.3397	23.6816	18.3030	21.2302	20.3605	21.4851	20.2606	21.3428

*Notes: Unit for Q_d = MVAr, *FVSI* = p.u., Loss = MW and Size = MW

Correspondingly, the *FVSI*-based resilience index increased from $R1_{FVSI}$ = 6.38 to $R2_{FVSI}$ = 8.43. The optimal locations for DG placement include Bus 15, 20, 12, 19 and 10 which correspond to Loc_{DG1} to Loc_{DG5}. The optimal locations for DG placement managed to improve system voltage stability and network sensitivity after a disruptive hurricane event along with reducing the power loss. The respective DG sizes are 51.64 MW, 49.83 MW, 81.52 MW, 55.15 MW, and 85.40 MW. This result confirms the MOECSEP ability to solve multi-bus resilience reinforcement problems in a highly

stressed post-event situation. This particular case achieved a total fitness value F_{Total} reduction from 61.2432 to 21.3428 indicating a notable enhancement in the system. In this multi-objective optimisation, the priority is to minimize the F_{Total} rather than the *FVSI* and loss values independently. The resilience index is prioritized to be maximised. The results for other reactive load valuations for all the participating buses can be referred to the same table, i.e. Table 4.3.

B. Scenario 2

Table 4.4 tabulates the results of the MOECSEP-based optimisation for DG installation under Scenario 2 hurricane strike, where the weighted fitness function emphasizes voltage stability improvement ($w_1 = 0.1$ and $w_2 = 0.9$) in Case 1. In general, similar phenomenon is observed as those Scenario 1. With the increment in Q_d value at all the participating buses i.e. Buses 26, 29 and 30, the loss value increases for pre- and post- DG installation. The profiles of losses for pre-outage are lower than the post-outage profiles. With the installation of DGs into the system, the post-outage loss profiles are lower. This phenomenon occurs for all load variations at Buses 26, 29 and 30. With the DG installation, the resilience index values are also increased for all load variations at Buses 26, 29 and 30. For instance, at Q_{d26} = 10 MVAr, power loss ($Loss_{Se}$) is originally 18.23 MW while the corresponding *FVSI* ($FVSI_{\text{Set}}$) is 0.2248. When the system is subjected to hurricane-induced disturbance, the system experienced a deterioration in performance, where the power loss increased to 20.40 MW ($Loss_{Out}$) and *FVSI* increase to 0.2797 ($FVSI_{\text{Out}}$) as shown in the Table 4.4.

Following the application of the optimised DG solution derived from the MOECSEP algorithm, both indicators showed marked improvement: the power loss was reduced to 19.87 MW ($Loss_{DG}$) and ($FVSI_{\text{DG}}$) decreased to 0.2534. The loss-based resilience index increased from $R1_{Loss}$ = 8.38 before DG installation to $R2_{Loss}$ = 37.39 after DG compensation. Similarly, the *FVSI*-based resilience index improved significantly, rising from $R1_{FVSI}$ = 4.09 to $R2_{FVSI}$ = 9.63. The optimal DG placement determined for this condition includes Bus 29, 7, 21, 12, and 5, corresponding to Loc_{DG1} through Loc_{DG5}, respectively. The buses were selected based on their topological influence and sensitivity to voltage deviations during post-disturbance recovery. The DG capacities allocated at these locations are 21.34 MW (Bus 29), 19.59 MW (Bus 7), 23.80 MW (Bus 21), 18.68 MW (Bus 12), and 93.09 MW (Bus 5), respectively.

Table 4.4
Results of MOECSEP Application in DG Installation for Scenario 2 Hurricane Strike for Case 1 in IEEE 30-Bus RTS

Bus	**26**			**29**			**30**		
Q_d	**10**	**20**	**25**	**10**	**20**	**25**	**10**	**20**	**25**
$Loss_{Set}$	18.23	20.25	22.27	18.12	19.39	20.53	18.11	19.55	20.93
$FVSI_{Set}$	0.2248	0.4919	0.6529	0.2111	0.3573	0.4646	0.2114	0.4073	0.5349
$Loss_{Out}$	20.40	25.03	29.92	19.78	22.87	24.82	20.27	23.59	28.33
$FVSI_{Out}$	0.2797	1.0000	0.9673	0.2830	0.6333	0.7914	0.2984	0.7619	1.0000
$Loss_{DG}$	19.87	22.35	23.65	19.33	20.37	23.25	19.35	20.27	23.32
$R1_{Loss}$	8.38	4.24	2.91	10.89	5.57	4.78	8.38	0.26	2.83
$R2_{Loss}$	37.39	8.35	3.78	42.57	8.15	14.87	21.14	0.27	4.65
$FVSI_{DG}$	0.2534	0.5016	0.6724	0.2364	0.4123	0.5841	0.2914	0.4635	0.5432
$R1_{FVSI}$	4.09	0.97	2.08	2.94	1.29	1.42	2.43	1.15	1.15
$R2_{FVSI}$	9.63	1.01	2.28	5.07	1.87	2.82	41.63	1.55	1.19
Loc_{DG1}	29	5	8	7	11	9	15	5	5
Loc_{DG2}	7	3	4	17	3	7	14	8	19
Loc_{DG3}	21	12	3	5	8	5	7	13	13
Loc_{DG4}	12	10	10	24	23	18	6	28	6
Loc_{DG5}	5	14	5	15	5	22	5	19	29
$Size_{DG1}$	21.34	95.52	43.12	89.96	89.50	73.49	23.45	87.64	90.08
$Size_{DG2}$	19.59	72.65	56.61	28.76	11.89	62.58	20.09	80.38	17.47
$Size_{DG3}$	23.80	4.87	84.08	61.29	22.15	78.29	72.92	22.45	19.68
$Size_{DG4}$	18.68	18.68	8.35	32.71	58.07	26.10	58.20	23.00	63.75
$Size_{DG5}$	93.09	52.22	75.57	64.74	83.01	5.45	66.39	19.08	23.08
F_{Set}	2.2922	3.4032	3.8625	2.2326	2.8565	3.1941	2.2956	3.0447	3.7332
F_{Total}	2.2154	2.6868	2.9706	2.1453	2.4077	2.8511	2.1977	2.4437	2.8210

*Notes: Unit for Q_d = MVAr, *FVSI* = p.u., Loss = MW and Size = MW

This distribution pattern indicates the effectiveness of MOECSEP in performing coordinated, location-specific reinforcement of the system operational profile. Additionally, the total fitness value for this case, F_{Total} is 2.2154. These improvements confirm the effectiveness of the MOECSEP algorithm in enhancing both system efficiency and voltage stability. A severe condition situation can be observed at higher Q_d value. For instance, at Q_{d26} = 25 MVAr, the *FVSI* value abruptly increases from 0.6529 to 0.9673 due to hurricane event. This implies the system is prone to unsecure condition. But this condition has been alleviated through the DG installation where *FVSI* reduces to 0.6724. This phenomenon also highlights that the DG installation strategy managed to make the system more resilient where its value increases from 2.08 to 2.28 influenced by the loss reduction in the system. Similar phenomenon can also be experienced by the increment in resilience index due to *FVSI* reduction.

Table 4.5 provides the results of the MOECSEP algorithm applied to DG installation under Scenario 2 hurricane strike, using an equal weight configuration of ($w_1 = 0.5$ and $w_2 = 0.5$) in Case 2. A representative case can be observed at Bus 29 with Q_d = 20 MVAr, where the system experienced post-disturbance degradation due to hurricane-induced events. The pre-disturbance condition power loss is 19.39 MW and *FVSI* value is 0.3573. With a disturbance subjected to the system, these values worsened to 22.87 MW ($Loss_{Out}$) and 0.6333 ($FVSI_{Out}$), indicating reduced operational efficiency and heightened risk of voltage instability.

Table 4.5
Results of MOECSEP Application in DG Installation for Scenario 2 Hurricane Strike for Case 2 in IEEE 30-Bus RTS

Bus	**26**			**29**			**30**		
Q_d	**10**	**20**	**25**	**10**	**20**	**25**	**10**	**20**	**25**
$Loss_{Set}$	18.23	20.25	22.27	18.12	19.39	20.53	18.11	19.55	20.93
$FVSI_{Set}$	0.2248	0.4919	0.6529	0.2111	0.3573	0.4646	0.2114	0.4073	0.5349
$Loss_{Out}$	20.40	25.03	29.92	19.78	22.87	24.82	20.27	23.59	28.33
$FVSI_{Out}$	0.2797	1.0000	0.9673	0.2830	0.6333	0.7914	0.2984	0.7619	1.0000
$Loss_{DG}$	20.32	22.36	24.60	18.93	20.69	21.36	19.32	20.35	22.32
$R1_{Loss}$	8.38	4.24	2.91	10.89	5.57	4.78	8.38	0.26	2.83
$R2_{Loss}$	242.21	8.36	4.62	22.16	9.49	6.17	20.36	0.27	3.71
$FVSI_{DG}$	0.2687	0.5631	0.7312	0.2235	0.4102	0.5107	0.2935	0.4238	0.5637
$R1_{FVSI}$	4.09	0.28	2.08	2.94	1.29	1.42	2.43	1.15	1.11
$R2_{FVSI}$	24.43	0.33	3.10	3.76	1.84	1.82	59.90	1.25	1.25
Loc_{DG1}	9	9	3	16	4	25	7	3	29
Loc_{DG2}	8	4	10	18	7	7	23	14	26
Loc_{DG3}	5	3	29	4	18	3	3	26	7
Loc_{DG4}	29	27	7	8	16	8	26	8	2
Loc_{DG5}	10	23	5	20	3	26	19	7	24
$Size_{DG1}$	73.40	24.95	61.33	21.19	12.49	68.74	4.61	52.61	5.04
$Size_{DG2}$	16.83	24.18	33.31	8.42	78.15	35.49	4.78	74.56	96.00
$Size_{DG3}$	66.26	45.26	93.73	88.85	28.69	63.53	54.78	82.75	64.14
$Size_{DG4}$	47.03	32.25	69.77	85.82	34.30	92.94	29.77	32.89	57.34
$Size_{DG5}$	40.62	44.84	70.58	43.23	72.13	6.39	34.55	38.65	13.71
F_{Set}	10.3423	13.6513	15.4432	10.0312	11.7494	12.8048	10.2844	12.1760	14.6735
F_{Total}	10.2949	11.4598	12.6647	9.5745	10.5478	10.9336	9.8075	10.3890	11.4427

*Notes: Unit for Q_d = MVAr, *FVSI* = p.u., Loss = MW and Size = MW

The implementation of DG installation strategy solved using MOECSEP managed to significantly mitigated these effects, reducing the power loss to 20.69 MW and *FVSI* to 0.4102, as recorded in $Loss_{DG}$ and $FVSI_{DG}$, respectively. The improvement is further validated by the associated resilience indices. The loss-based resilience index

increased from $R1_{Loss}$ = 5.57 to $R2_{Loss}$ = 9.49 while the *FVSI*-based resilience index improved from $R1_{FVSI}$ = 1.29 to $R2_{FVSI}$ = 1.84. These values illustrate the system enhanced ability to recover both in terms of improved resilience and voltage security. The MOECSEP optimisation technique determined that Buses 4, 7, 18, 16, and 3 should receive DG installation as the most effective sites which correspond to Loc_{DG1} through Loc_{DG5}. The DG capacities assigned to these locations were 12.49 MW, 78.15 MW, 28.69 MW, 34.30 MW, and 72.13 MW, which demonstrates a proper distribution of capacities according to the operational requirements and importance of each bus. The total fitness value, F_{Total} is reduced from 11.7494 to 10.5478. In summary, the results reinforce the effectiveness of the MOECSEP algorithm in producing resilient and efficient DG placement strategies.

Table 4.6 summarizes the performance of the MOECSEP algorithm for DG installation under Scenario 2 hurricane strike, applying a multi-objective optimisation framework with a weighting scheme of $w_1 = 0.9$ and $w_2 = 0.1$ in Case 3. In general, the loss values increase as the reactive power loading at Buses 26. 29 and 30 were increased. This also leads to the increment of *FVSI* values, which implied voltage stability reduction. For instance, at Q_{d30} = 25 MVAr the post-outage system condition exhibits substantial degradation. The power loss escalated sharply from 20.93 MW to 28.33 MW, while the voltage stability index increases to a critical level worth 1.0000, indicating proximity to voltage collapse. With DG installation, *FVSI* improved from 1.0000 to 0.6312 implying enhancement in voltage stability. The corresponding *FVSI*-based resilience index improved from $R1_{FVSI}$ = 1.11 to $R2_{FVSI}$ = 1.64, suggesting enhanced system voltage robustness following DG compensation. Upon execution of the MOECSEP-based DG installation, the power loss was effectively mitigated to 23.46 MW. This reduction is reflected in the loss-based resilience indices, where the resilience index increased from 2.83 to 4.81, validating the DG contribution to system recovery from a loss perspective. The optimal DG locations identified by MOECSEP are Buses 2, 14, 12, 5, and 7, corresponding to Loc_{DG1} through Loc_{DG5}. The respective DG capacities to be allocated at each location are 52.93 MW at Bus 2, 17.61 MW at Bus 14, 14.67 MW at Bus 12, 64.76 MW at Bus 5, and 30.37 MW at Bus 7. This combination of distributed locations and tailored capacities illustrates the algorithm ability to deploy targeted resilience reinforcements while maintaining overall system efficiency. The total fitness value for this scenario has been reduced from 25.6001 to 21.1745.

Table 4.6
Results of MOECSEP Application in DG Installation for Scenario 2 Hurricane Strike for Case 3 in IEEE 30-Bus RTS

Bus	**26**			**29**			**30**		
Q_d	**10**	**20**	**25**	**10**	**20**	**25**	**10**	**20**	**25**
$Loss_{Set}$	18.23	20.25	22.27	18.12	19.39	20.53	18.11	19.55	20.93
$FVSI_{Set}$	0.2248	0.4919	0.6529	0.2111	0.3573	0.4646	0.2114	0.4073	0.5349
$Loss_{Out}$	20.40	25.03	29.92	19.78	22.87	24.82	20.27	23.59	28.33
$FVSI_{Out}$	0.2797	1.0000	0.9673	0.2830	0.6333	0.7914	0.2984	0.7619	1.0000
$Loss_{DG}$	18.94	22.33	24.33	18.93	20.94	22.24	18.98	23.24	23.46
$R1_{Loss}$	8.38	4.24	2.91	10.89	5.57	4.78	8.38	0.26	2.83
$R2_{Loss}$	12.89	8.25	4.35	22.36	10.85	8.61	14.75	0.32	4.81
$FVSI_{DG}$	0.2398	0.5123	0.7102	0.2243	0.3865	0.5321	0.2236	0.4321	0.6312
$R1_{FVSI}$	4.09	0.28	2.08	2.94	1.29	1.42	2.43	1.15	1.11
$R2_{FVSI}$	6.01	0.29	2.76	3.82	1.57	2.05	2.99	1.31	1.64
Loc_{DG1}	17	17	18	8	4	25	7	3	2
Loc_{DG2}	8	23	16	30	7	7	23	14	14
Loc_{DG3}	7	5	10	23	18	3	3	26	12
Loc_{DG4}	12	2	17	7	16	8	26	8	5
Loc_{DG5}	20	18	14	10	3	26	19	7	7
$Size_{DG1}$	7.72	52.01	4.53	71.58	12.49	68.74	4.61	52.61	52.93
$Size_{DG2}$	42.49	8.01	4.14	22.26	78.15	35.49	4.78	74.56	17.61
$Size_{DG3}$	84.11	35.21	15.33	86.12	28.69	63.53	54.78	82.75	14.67
$Size_{DG4}$	63.35	6.33	76.70	60.15	34.30	92.94	29.77	32.89	64.76
$Size_{DG5}$	94.48	4.22	6.17	53.89	72.13	6.39	34.55	38.65	30.37
F_{Set}	18.3924	22.7559	27.0239	17.8298	20.6422	22.4155	18.2731	21.3072	25.6001
F_{Total}	17.0660	20.1451	21.9636	17.0619	18.8815	20.0648	17.1075	20.9551	21.1745

*Notes: Unit for Q_d = MVAr, *FVSI* = p.u., Loss = MW and Size = MW

Table 4.7 presents the comparative results of F_{Total} values under Scenario 1 for reactive load variations at all the three buses (26, 29, and 30) at varying reactive load levels (10, 20, and 25 MVAr). The weight configurations used are: $w_1 = 0.1, w_2 = 0.9$, in Case 1; $w_1 = 0.5, w_2 = 0.5$ in Case 2 and $w_1 = 0.9, w_2 = 0.1$ in Case 3. Among the three configurations, the lowest F_{Total} values across all buses and load levels were consistently achieved in Case 1 ($w_1 = 0.1$ and $w_2 = 0.9$). For example, at Bus 30 with Q_d = 25 MVAr, the lowest F_{Total} is 2.8554. It implies that the fitness in much influenced by the factor of loss rather than the *FVSI* value.

At Q_{d30} = 25 MVAr, the performance of different weight coefficient configurations was evaluated under both Scenario 1 and Scenario 2. In Scenario 1, the total fitness value F_{Total} recorded for the weight setting $w_1 = 0.1, w_2 = 0.9$ was 2.8554, which was the lowest among all three configurations, indicating the most suitable setting of weight coefficient. For the balanced weight setting $w_1 = 0.5, w_2 = 0.5$, the

F_{Total} increased to 12.1143, while the configuration with $w_1 = 0.9, w_2 = 0.1$ resulted in the highest value of 21.3428. A similar trend was observed in Scenario 2, where the F_{Total} values for the respective configurations were 2.8210, 11.4427, and 21.1745. Across both Scenario 1 and Scenario 2, the weight coefficient configuration of $w_1 = 0.1$ and $w_2 = 0.9$ consistently outperformed the other settings in minimizing F_{Total}.

Table 4.7
Comparative Results of F_{Total} for DG Installation Using MOECSEP in IEEE 30-Bus RTS

Bus		**26**			**29**			**30**		
Q_d		**10**	**20**	**25**	**10**	**20**	**25**	**10**	**20**	**25**
Scenario 1										
F_{Total}	**w_1=0.1 w_2=0.9**	2.0306	2.4864	2.9821	2.1646	2.3158	2.5693	2.2432	2.6030	2.8554
	w_1=0.5 w_2=0.5	9.7351	11.4489	12.5092	9.8145	11.3755	11.7598	10.3143	10.3674	12.1143
	w_1=0.9 w_2=0.1	18.3450	21.3397	23.6816	18.3030	21.2302	20.3605	21.4851	20.2606	21.3428
Scenario 2										
F_{Total}	**w_1=0.1 w_2=0.9**	2.2154	2.6868	2.9706	2.1453	2.4077	2.8511	2.1977	2.4437	2.8210
	w_1=0.5 w_2=0.5	10.2949	11.4598	12.6647	9.5745	10.5478	10.9336	9.8075	10.3890	11.4427
	w_1=0.9 w_2=0.1	17.0660	20.1451	21.9636	17.0619	18.8815	20.0648	17.1075	20.9551	21.1745

4.4.1.2 DG Installation in IEEE 57-Bus RTS

The proposed DG installation strategy is also evaluated under large-scale system to observe the feasibility and robustness of the proposed MOECSEP in addressing the resilience index improvement. The study was also implemented on IEEE 57-Bus RTS under two hurricane scenarios. These scenarios introduced severe disturbances by triggering line outages and altering reactive power demands to test the system operational resilience and voltage security. The optimisation process was proposed to minimize transmission losses while improving the voltage stability in the system indicated by the reduction in *FVSI* value. For this implementation, three buses were subjected to reactive load variation namely Bus 5, Bus 10, and Bus 15. The simulations evaluated three reactive power loading levels (Q_d): 10, 20, and 25 MVAr, corresponding

to progressively higher system stress. For each bus and loading, the placement and sizing of the DG were optimised using the MOECSEP algorithm.

A. Scenario 1

Table 4.8 presents the results of DG installation optimised using the MOECSEP algorithm for Scenario 1 hurricane strike on the IEEE 57-Bus RTS, under a weight configuration prioritizing power loss minimization i.e. $w_1 = 0.9, w_2 = 0.1$. In general, with the increment in Q_d value at all participating buses i.e. Buses 31, 32 and 33, the loss value increases for pre- and post- DG installation. The profiles of losses for pre-outage are lower than the post-outage profiles. With the installation of DGs into the system, the post-outage loss profiles are lower. This phenomenon occurs for all load variations at Buses 31, 32 and 33. With the DG installation, the resilience index values are also increased for all load variations at these buses. For instance, Q_{d33} = 15 MVAr, the system exhibits an initial power loss of 30.55 MW ($Loss_{Set}$) and a corresponding *FVSI* value of 0.4613. However, once the hurricane-induced disruption is applied, the system performance significantly degrades, with power loss rising to 38.00 MW ($Loss_{Out}$) and voltage security index increasing sharply to 0.6679 ($FVSI_{\mathrm{Out}}$), reflecting a critical instability level. With the implementation of the optimal DG installation, the system performance improves. The post-installation power loss ($Loss_{DG}$) is reduced to 31.24 MW, and the *FVSI* drops to 0.4732 ($FVSI_{\mathrm{DG}}$), showing recovery from the extreme disturbance. Apparently, this is the optimal combination of *FVSI* and loss in one equivalent fitness equation. The resilience indices support these findings, where $R1_{Loss}$ prior to DG installation is 4.10 and increases to $R2_{Loss}$ = 4.62, implying improvement in system resilience. Particularly, the voltage stability-based resilience shows positive progression, with $R1_{FVSI}$ = 2.23 increasing to $R2_{FVSI}$ = 2.43 after DG installation, highlighting the algorithm ability to reduce the severity in voltage insecurity. The MOECSEP algorithm successfully determined the best DG placement and sizing methods for Scenario 1 hurricane strike conditions which identified Buses 32, 7, 10, 55, and 14 for DG installation correspond to Loc_{DG1} through Loc_{DG5}.

Table 4.8
Results of MOECSEP Application in DG Installation for Scenario 1 Hurricane Strike for Case 1 in IEEE 57-Bus RTS

Bus	**31**			**32**			**33**		
Q_d	**5**	**10**	**15**	**5**	**10**	**15**	**5**	**10**	**15**
$Loss_{Set}$	28.46	29.22	30.56	28.67	29.42	30.66	28.56	29.30	30.55
$FVSI_{Set}$	0.4028	0.3977	0.4339	0.4005	0.3948	0.4973	0.4016	0.3960	0.4613
$Loss_{Out}$	32.85	34.41	42.75	33.25	34.84	39.15	33.03	34.51	38.00
$FVSI_{Out}$	0.4395	0.4355	1.0000	0.4372	0.4318	0.7370	0.4382	0.4331	0.6679
$Loss_{DG}$	29.32	30.01	31.55	29.32	30.72	31.65	29.04	30.32	31.24
$R1_{Loss}$	6.49	5.63	2.51	6.25	5.44	3.61	6.38	5.62	4.10
$R2_{Loss}$	8.31	6.82	2.82	7.46	7.47	4.22	7.27	7.24	4.62
$FVSI_{DG}$	0.4065	0.4036	0.5023	0.4135	0.4007	0.5097	0.4132	0.4068	0.4732
$R1_{FVSI}$	10.98	10.52	0.77	10.91	10.67	2.07	10.97	10.67	2.23
$R2_{FVSI}$	12.32	12.65	1.01	17.45	12.88	2.24	16.53	15.47	2.43
Loc_{DG1}	49	52	35	23	44	13	50	51	32
Loc_{DG2}	48	35	46	44	48	16	38	23	7
Loc_{DG3}	29	6	50	28	41	10	19	18	10
Loc_{DG4}	18	12	52	10	10	11	26	11	55
Loc_{DG5}	13	49	41	18	18	5	44	28	14
$Size_{DG1}$	79.66	1.56	46.12	19.94	56.71	62.59	90.31	74.21	34.53
$Size_{DG2}$	42.93	32.68	29.13	81.76	40.72	39.72	39.03	76.06	60.98
$Size_{DG3}$	48.44	69.89	73.64	15.24	14.86	53.92	7.90	43.92	60.46
$Size_{DG4}$	21.72	46.79	71.86	65.93	61.61	6.32	13.70	17.74	12.96
$Size_{DG5}$	64.57	62.17	28.70	64.51	69.92	64.97	49.33	39.62	54.29
F_{Set}	3.6806	3.8333	5.1753	3.7188	3.8722	4.5781	3.6975	3.8410	4.4009
F_{Total}	3.2980	3.3645	3.6068	3.3043	3.4331	3.6240	3.2756	3.3986	3.5497

*Notes: Unit for Q_d = MVAr, $FVSI$ = p.u., Loss = MW and Size = MW

The DG sizes to be installed at the respective locations are 34.53 MW, 60.98 MW, 60.46 MW, 12.96 MW, and 54.29 MW. The system achieved better post-disturbance voltage profiles and reduced total system losses through the strategic placement of diverse DG capacities across different locations. The final fitness value for this case is F_{Total} is 3.5497 reduction from 4.4009. These results demonstrate that even under severe loading and disturbance conditions, the MOECSEP algorithm effectively enhances system resilience by restoring power flow performance and improving voltage security at critical buses such as Bus 33. The results for other loading conditions involving all the three buses can be referred to the same table.

Table 4.9
Results of MOECSEP Application in DG Installation for Scenario 1 Hurricane Strike for Case 2 in IEEE 57-Bus RTS

Bus	**31**			**32**			**33**		
Q_d	**5**	**10**	**15**	**5**	**10**	**15**	**5**	**10**	**15**
$Loss_{Set}$	28.46	29.22	30.56	28.67	29.42	30.66	28.56	29.30	30.55
$FVSI_{Set}$	0.4028	0.3977	0.4339	0.4005	0.3948	0.4973	0.4016	0.3960	0.4613
$Loss_{Out}$	32.85	34.41	42.75	33.25	34.84	39.15	33.03	34.51	38.00
$FVSI_{Out}$	0.4395	0.4355	1.0000	0.4372	0.4318	0.7370	0.4382	0.4331	0.6679
$Loss_{DG}$	29.45	30.22	31.52	29.04	30.20	31.32	29.21	30.12	31.22
$R1_{Loss}$	6.49	5.63	2.51	6.25	5.44	3.61	6.38	5.62	4.10
$R2_{Loss}$	8.67	7.20	2.81	6.89	6.52	4.00	7.65	6.85	4.61
$FVSI_{DG}$	0.4132	0.4136	0.4531	0.4093	0.3991	0.5013	0.4103	0.4156	0.4716
$R1_{FVSI}$	10.98	10.52	0.27	10.91	10.67	2.07	10.97	10.67	2.23
$R2_{FVSI}$	15.71	18.89	0.28	14.67	12.20	2.13	14.71	23.75	2.40
Loc_{DG1}	38	31	47	8	41	28	56	51	27
Loc_{DG2}	10	50	25	29	12	41	49	43	20
Loc_{DG3}	31	3	18	47	29	38	50	44	47
Loc_{DG4}	12	17	57	54	53	32	47	32	29
Loc_{DG5}	44	18	15	35	35	50	29	55	53
$Size_{DG1}$	36.86	22.58	63.05	56.70	92.40	66.60	63.16	82.13	18.18
$Size_{DG2}$	42.39	51.01	61.63	57.56	72.09	1.15	88.47	15.54	26.38
$Size_{DG3}$	32.72	81.79	0.06	98.77	66.65	79.48	27.27	4.11	14.55
$Size_{DG4}$	71.35	22.04	0.08	72.84	69.96	56.09	43.64	34.36	13.60
$Size_{DG5}$	57.68	54.37	77.33	11.11	2.50	28.86	76.65	11.00	86.93
F_{Set}	16.6449	17.4244	22.3991	16.8454	17.6337	19.9424	16.7347	17.4728	19.3327
F_{Total}	14.9325	15.3156	15.9890	14.7232	15.3019	15.9131	14.8121	15.2660	15.8468

*Notes: Unit for Q_d = MVAr, *FVSI* = p.u., Loss = MW and Size = MW

Table 4.9 tabulates the performance of the MOECSEP algorithm in optimizing DG installation for Scenario 1 hurricane strike on the IEEE 57-Bus RTS, using an equal weight configuration ($w_1 = 0.5, w_2 = 0.5$) to balance power loss minimization and voltage security improvement. In general, similar phenomenon can be experienced as those in Case 1 where the increment in Q_d value at all the participating buses i.e. Buses 31, 32 and 33, the loss value increases for pre- and post- DG installation. The profiles of losses for pre-outage are lower than the post-outage profiles. With the installation of DGs into the system, the post-outage loss profiles are lower. This phenomenon occurs for all load variations at Buses 31, 32 and 33. With the DG installation, the resilience index values are also increased for all load variations at these buses. For instance, at Q_{d32} = 10 MVAr, the pre-disturbance power loss is 29.42 MW ($Loss_{Set}$), while the $FVSI_{\text{Set}}$ is 0.3948, indicating a moderately loaded but secure condition. Due to hurricane

event, the system experiences performance deterioration, with power loss increasing to 34.84 MW ($Loss_{Out}$) and $FVSI_{\mathrm{Out}}$ rising to 0.4318 reflecting a reduction in voltage security.

In post-DG installation, the power loss is reduced to 30.20 MW ($Loss_{DG}$), the loss and *FVSI* are concurrently reduced. More importantly, the voltage security index reduces from 0.4318 to 0.3991 ($FVSI_{\mathrm{DG}}$), showing a clear recovery trend in system security. This improvement is further supported by the voltage-based resilience indices, where $R1_{FVSI}$ is 10.67 before DG and increases significantly to $R2_{FVSI}$ = 12.20 after DG installation. Meanwhile, the power loss resilience also improves slightly from $R1_{Loss}$ = 5.44 to $R2_{Loss}$ = 6.52, reflecting the algorithm effectiveness in optimising the DG installation. The optimal buses selected for DG placement were 41, 12, 29, 53, and 35, listed under Loc_{DG1} to Loc_{DG5}, respectively. These buses were identified based on their strategic influence on system recovery post-hurricane. The DG capacities allocated to these locations were 92.40 MW at Bus 41, 72.09 MW at Bus 12, 66.65 MW at Bus 29, 69.96 MW at Bus 53, and 2.50 MW at Bus 35. The total fitness value for this case, F_{Total} is reduced from 17.6337 to 15.3019 and the results confirm the capability of the MOECSEP technique to enhance power system resilience for reactive power variation at Bus 32 under a moderate reactive load and balanced objective setting, particularly in terms of voltage security recovery following a severe disturbance. The results for other loading conditions involving all the three buses can be referred to the same table.

Table 4.10 presents the results of the proposed MOECSEP algorithm applied to DG installation in the IEEE 57-Bus RTS under Scenario 1 hurricane strike when $w_1 = 0.9$ and $w_2 = 0.1$. In general, similar phenomenon can be experienced as those in previous case where the increment in Q_d value at all the participating buses i.e. Buses 31, 32 and 33, the loss value increases for pre- and post-DG installation. The profiles of losses for pre-outage are lower than the post-outage profiles. With the installation of DGs into the system, the post-outage loss profiles are lower. This phenomenon occurs for all load variations at Buses 31, 32 and 33. With the DG installation, the resilience index values are also increased for all load variations at theses buses. At Q_{d31} = 15 MVAr, the system recorded a power loss of 30.56 MW ($Loss_{Set}$) and an *FVSI* value of 0.4339 ($FVSI_{\mathrm{Set}}$), before the hurricane strike. Upon the hurricane disruption, the power loss increases to 42.75 MW ($Loss_{Out}$), while the *FVSI* further deteriorates to 1.0000 ($FVSI_{\mathrm{Out}}$), signalling the onset of severe voltage security risk and weakened system performance

Table 4.10
Results of MOECSEP Application in DG Installation for Scenario 1 Hurricane Strike for Case 3 in IEEE 57-Bus RTS

Bus	**31**			**32**			**33**		
Q_d	**5**	**10**	**15**	**5**	**10**	**15**	**5**	**10**	**15**
$Loss_{Set}$	28.46	29.22	30.56	28.67	29.42	30.66	28.56	29.30	30.55
$FVSI_{Set}$	0.4028	0.3977	0.4339	0.4005	0.3948	0.4973	0.4016	0.3960	0.4613
$Loss_{Out}$	32.85	34.41	42.75	33.25	34.84	39.15	33.03	34.51	38.00
$FVSI_{Out}$	0.4395	0.4355	1.0000	0.4372	0.4318	0.7370	0.4382	0.4331	0.6679
$Loss_{DG}$	29.53	30.24	31.57	29.75	30.69	30.91	29.21	29.93	31.24
$R1_{Loss}$	6.49	5.63	2.51	6.25	5.44	3.61	6.38	5.62	4.10
$R2_{Loss}$	8.90	7.24	2.82	8.50	7.39	3.75	7.65	6.54	4.62
$FVSI_{DG}$	0.4115	0.4014	0.4432	0.4091	0.4008	0.5013	0.4099	0.4035	0.4721
$R1_{FVSI}$	10.98	10.52	0.27	10.91	10.67	2.07	10.97	10.67	2.23
$R2_{FVSI}$	14.70	11.77	0.28	14.56	12.93	2.13	14.48	13.63	2.41
Loc_{DG1}	47	32	38	23	37	53	47	29	38
Loc_{DG2}	29	55	19	18	12	50	54	53	32
Loc_{DG3}	27	8	26	11	10	20	12	32	8
Loc_{DG4}	20	29	12	49	43	18	8	55	17
Loc_{DG5}	47	47	14	12	12	26	27	12	10
$Size_{DG1}$	26.38	57.56	53.74	94.71	94.53	40.49	13.81	21.34	18.03
$Size_{DG2}$	14.55	98.77	51.44	24.43	10.85	94.30	13.14	19.59	39.85
$Size_{DG3}$	13.60	72.84	10.34	95.32	44.50	46.57	48.80	23.80	37.17
$Size_{DG4}$	1.15	88.47	15.54	63.21	7.79	8.65	50.13	18.68	32.47
$Size_{DG5}$	79.48	27.27	4.11	2.78	32.77	15.94	42.60	93.09	58.97
F_{Set}	29.6092	31.0154	38.6825	29.9719	31.3951	35.3067	29.7719	31.1045	34.2645
F_{Total}	26.6194	27.2538	28.4547	26.8196	27.6569	27.8730	26.3331	26.9817	28.1618

*Notes: Unit for Q_d = MVAr, *FVSI* = p.u., Loss = MW and Size = MW

To mitigate this impact, the MOECSEP algorithm determines an optimal DG installation strategy that reduces the *FVSI* and maintains a reasonable loss level. The post-DG installation *FVSI* is improved to 0.4432 ($FVSI_{DG}$), and while the power loss reduces to 31.57 MW ($Loss_{DG}$). The resilience index based on power loss ($R1_{Loss}$) is 2.51, and after DG implementation, this improves marginally to $R2_{Loss}$ = 2.82, indicating a slight enhancement in energy efficiency recovery. More significant improvement is observed in voltage resilience, where $R1_{FVSI}$ = 0.27 increases to $R2_{FVSI}$ = 0.28, showing the DG effectiveness in restoring voltage conditions even in high-stress scenarios. The algorithm identified Buses 38, 19, 26, 12, and 14 as the optimal locations for DG installation, listed as Loc_{DG1} to Loc_{DG5}. The system selected these buses because the buses had the most significant influence on voltage stability and power flow. The optimal DG sizes are 53.74 MW, 51.44 MW, 10.34 MW, 15.54 MW, and 4.11 MW for

each bus respectively. The final combined fitness value for this case is F_{Total} is reduced from 38.6825 to 28.4547. The results for other loading conditions involving all the three buses can be referred to the same table.

B. Scenario 2

This study further extends the evaluation of the proposed MOECSEP algorithm by applying it to Scenario 2 hurricane strikes on the IEEE 57-Bus RTS, focusing on DG installation performance under varying reactive power loading involving Buses 31, 32 and 33 for Cases 1, 2 and 3. Table 4.11, presents the results of MOECSEP application in DG installation for Scenario 2 hurricane strike of Case 1 with $w_1 = 0.1$ and $w_2 = 0.9$ in the IEEE 57-Bus RTS. In general, similar phenomenon can be witnessed as those in previous scenario where the increment in Q_d value at all the participating buses i.e. Buses 31, 32 and 33 has caused increasing trend in power loss. This phenomenon occurs in both the pre- and post- DG installation. The profiles of losses for pre-outage are lower than the post-outage profiles as hurricane can cause outages of several transmission lines in the system. This has caused current increase, leading to the increment in power loss. With the installation of DGs into the system, the loss profiles are lower than those before DGs were installed into the system. This phenomenon occurs for all load variations at Buses 31, 32 and. 33. With the DG installation, the resilience index values are also increased for all load variations at these buses which indicates that the system is getting more resilient. Apparently, the increment in resilience index is more explicit at the lower loading conditions.

As Q_{d33} = 15 MVAr, the *FVSI* values increases from 0.4613 to 0.7086 due to the hurricane event in the system. With DG installation into the system, this effort managed to reduce the *FVSI* value to 0.4802 ($FVSI_{\mathrm{DG}}$), implying voltage security improvement. This has also improved the voltage security resilience from $R1_{FVSI}$ = 1.87 to $R2_{FVSI}$ = 2.10. The loss-based resilience index has also been increased from The $R1_{Loss}$ = 1.31 to $R2_{Loss}$ = 1.47 with DG installation. The load buses identified as the optimal DG locations are Buses 55, 18, 25, 49, and 15 which corresponded to Loc_{DG1} through Loc_{DG5}. The selection of these buses was based on their ability to provide active power support and stabilize system performance during post-disturbance recovery. The DG sizes to be installed at these buses are 20.83 MW (Bus 55), 53.58 MW (Bus 18), 25.00 MW (Bus 25), 85.54 MW (Bus 49), and 65.10 MW (Bus 15). This strategy has reduced the total

fitness value (F_{Total}) from 6.0279 to 3.6387.

Table 4.11
Results of MOECSEP Application in DG Installation for Scenario 2 Hurricane Strike for Case 1 in IEEE 57-Bus RTS

Bus	**31**			**32**			**33**		
Q_d	**5**	**10**	**15**	**5**	**10**	**15**	**5**	**10**	**15**
$Loss_{Set}$	28.46	29.22	30.56	28.67	29.42	30.66	28.56	29.30	30.55
$FVSI_{Set}$	0.4028	0.3977	0.4339	0.4005	0.3948	0.4973	0.4016	0.3960	0.4613
$Loss_{Out}$	47.34	49.47	54.69	47.77	49.81	55.06	47.52	49.56	53.90
$FVSI_{Out}$	0.4521	0.4518	1.0000	0.4520	0.4516	0.7846	0.4520	0.4518	0.7086
$Loss_{DG}$	29.37	30.68	31.24	29.85	30.68	32.07	29.64	30.40	32.06
$R1_{Loss}$	1.51	1.44	1.27	1.50	1.44	1.26	1.51	1.45	1.31
$R2_{Loss}$	1.63	1.63	1.33	1.67	1.60	1.39	1.66	1.59	1.47
$FVSI_{DG}$	0.4103	0.4001	0.4431	0.4196	0.4103	0.5157	0.4104	0.4015	0.4802
$R1_{FVSI}$	8.17	7.35	0.77	7.78	6.95	1.73	7.97	7.10	1.87
$R2_{FVSI}$	9.82	7.74	0.80	12.95	9.93	1.92	9.87	7.98	2.10
Loc_{DG1}	12	49	43	18	49	23	6	6	55
Loc_{DG2}	14	12	12	26	51	37	53	17	18
Loc_{DG3}	28	15	33	12	35	12	50	41	25
Loc_{DG4}	32	40	55	55	43	10	20	44	49
Loc_{DG5}	7	30	50	35	19	28	38	10	15
$Size_{DG1}$	92.28	26.78	95.32	41.26	77.84	22.52	54.52	45.79	20.83
$Size_{DG2}$	42.14	50.98	19.01	25.38	21.43	51.50	16.13	1.39	53.58
$Size_{DG3}$	3.61	93.90	17.26	77.99	38.49	55.22	36.35	37.54	25.00
$Size_{DG4}$	16.99	12.60	85.44	80.89	95.02	33.85	33.49	58.39	85.54
$Size_{DG5}$	56.47	28.81	38.32	20.97	35.09	48.22	33.26	67.57	65.10
F_{Set}	5.1409	5.3532	6.3694	5.1836	5.3876	6.2124	5.1590	5.3626	6.0279
F_{Total}	3.3061	3.4285	3.5228	3.3628	3.4377	3.6707	3.3331	3.4012	3.6387

*Notes: Unit for Q_d = MVAr, $FVSI$ = p.u., Loss = MW and Size = MW

Variation in the weight coefficient value in Case 2 are presented in Table 4.12. From the Table 4.12, the increment in Q_d value at all the participating buses i.e. Buses 31, 32 and 33 has caused increasing trend in power loss. This phenomenon occurs in both the pre- and post- DG installation. The profiles of losses for pre-outage are lower than the post-outage profiles as hurricane can cause outages of several transmission lines in the system. This has caused current increase, leading to the increment in power loss. With the installation of DGs into the system, the loss profiles are lower than those before DGs were installed into the system. This phenomenon occurs for all load variations at Buses 31, 32 and. 33.

Table 4.12
Results of MOECSEP Application in DG Installation for Scenario 2 Hurricane Strike for Case 2 in IEEE 57-Bus RTS

Bus	**31**			**32**			**33**		
Q_d	**5**	**10**	**15**	**5**	**10**	**15**	**5**	**10**	**15**
$Loss_{Set}$	28.46	29.22	30.56	28.67	29.42	30.66	28.56	29.30	30.55
$FVSI_{Set}$	0.4028	0.3977	0.4339	0.4005	0.3948	0.4973	0.4016	0.3960	0.4613
$Loss_{Out}$	47.34	49.47	54.69	47.77	49.81	55.06	47.52	49.56	53.90
$FVSI_{Out}$	0.4521	0.4518	1.0000	0.4520	0.4516	0.7846	0.4520	0.4518	0.7086
$Loss_{DG}$	29.47	30.86	30.89	29.65	30.00	31.37	29.32	30.96	30.68
$R1_{Loss}$	1.51	1.44	1.27	1.50	1.44	1.26	1.51	1.45	1.31
$R2_{Loss}$	1.65	1.66	1.30	1.64	1.51	1.32	1.61	1.66	1.32
$FVSI_{DG}$	0.4125	0.4086	0.4483	0.4196	0.4008	0.5014	0.4093	0.4039	0.4724
$R1_{FVSI}$	8.17	7.35	0.71	7.78	6.95	1.73	7.97	7.10	1.87
$R2_{FVSI}$	10.42	9.46	0.75	12.95	7.89	1.77	9.59	8.43	2.00
Loc_{DG1}	13	52	51	55	32	18	49	18	12
Loc_{DG2}	19	29	23	14	7	26	51	11	10
Loc_{DG3}	51	41	18	35	23	12	35	28	28
Loc_{DG4}	17	17	11	46	44	55	43	32	51
Loc_{DG5}	15	31	28	50	28	35	19	7	14
$Size_{DG1}$	83.60	27.24	74.21	95.32	41.26	41.26	77.84	50.98	19.01
$Size_{DG2}$	60.24	94.71	76.06	19.01	25.38	25.38	21.43	93.90	17.26
$Size_{DG3}$	62.32	24.43	43.92	17.26	77.99	77.99	38.49	12.60	85.44
$Size_{DG4}$	83.86	95.32	17.74	6.32	13.70	80.89	95.02	54.52	45.79
$Size_{DG5}$	67.16	47.69	39.62	64.97	49.33	20.97	35.09	16.13	1.39
F_{Set}	23.8961	24.9588	27.8704	24.1100	25.1317	27.9234	23.9872	25.0058	27.3050
F_{Total}	14.9405	15.6367	15.6702	15.0357	15.1998	15.9348	14.8668	15.6828	15.5769

*Notes: Unit for Q_d = MVAr, *FVSI* = p.u., Loss = MW and Size = MW

With the DG installation, the resilience index values are also increased for all load variations at these buses which indicates that the system is getting more resilient. *FVSI* values at all the loading conditions increase with the outage of several transmission lines due to hurricane i this scenario. With DG installation the *FVSI* values reduce, indicating improvement in voltage security. For instance, at Q_{d33} = 15 MVAR, its *FVSI* value reduces from 0.7086 to 0.4724 with DG installation. It also reduces its power loss from 53.90 MW to 30.68 MW with this effort. This has increased the *FVSI* based resilience index from 1.87 to 2.00 indicating more resilient condition. The loss-based resilience index also increases from $R1_{Loss}$ = 1.31 to $R2_{Loss}$ = 1.32. The optimal locations for DG installation are Buses 12, 10, 28, 51, and 14 as per Loc_{DG1} through Loc_{DG5}. The amount of respective DG capacities to be installed in the system at the optimal buses are 19.01 MW, 17.26 MW, 85.44 MW, 45.79 MW, and 1.39 MW. The

total fitness value, F_{Total} has been reduced from 27.3050 to 15.5769.

Table 4.13
Results of MOECSEP Application in DG Installation for Scenario 2 Hurricane Strike for Case 3 in IEEE 57-Bus RTS

Bus	**31**			**32**			**33**		
Q_d	**5**	**10**	**15**	**5**	**10**	**15**	**5**	**10**	**15**
$Loss_{Set}$	28.46	29.22	30.56	28.67	29.42	30.66	28.56	29.30	30.55
$FVSI_{Set}$	0.4028	0.3977	0.4339	0.4005	0.3948	0.4973	0.4016	0.3960	0.4613
$Loss_{Out}$	47.34	49.47	54.69	47.77	49.81	55.06	47.52	49.56	53.90
$FVSI_{Out}$	0.4521	0.4518	1.0000	0.4520	0.4516	0.7846	0.4520	0.4518	0.7086
$Loss_{DG}$	29.36	30.68	30.87	29.46	30.32	31.85	29.63	30.04	31.85
$R1_{Loss}$	1.51	1.44	1.27	1.50	1.44	1.26	1.51	1.45	1.31
$R2_{Loss}$	1.63	1.63	1.30	1.61	1.56	1.37	1.66	1.54	1.44
$FVSI_{DG}$	0.4193	0.4008	0.4436	0.4077	0.4031	0.5006	0.4093	0.4009	0.4691
$R1_{FVSI}$	8.17	7.35	0.71	7.78	6.95	1.73	7.97	7.10	1.87
$R2_{FVSI}$	12.78	7.86	0.74	9.20	8.31	1.76	9.59	7.88	1.96
Loc_{DG1}	3	27	47	12	8	23	55	32	20
Loc_{DG2}	44	6	18	7	41	18	18	5	8
Loc_{DG3}	31	56	51	20	19	29	10	20	15
Loc_{DG4}	19	32	11	37	32	12	8	17	19
Loc_{DG5}	15	50	8	47	14	37	23	10	47
$Size_{DG1}$	63.38	22.16	44.37	73.61	17.54	4.53	71.58	62.40	6.06
$Size_{DG2}$	30.87	78.92	54.40	32.82	92.24	4.14	22.26	42.32	43.61
$Size_{DG3}$	78.94	19.35	49.34	63.26	3.77	15.33	86.12	73.64	15.24
$Size_{DG4}$	33.08	64.38	39.33	75.64	86.31	76.70	60.15	71.86	65.93
$Size_{DG5}$	14.79	18.97	32.29	99.10	66.97	6.17	53.89	20.40	19.01
F_{Set}	42.6513	44.5643	49.3294	43.0364	44.8758	49.6344	42.8153	44.6489	48.5820
F_{Total}	26.4687	27.6550	27.8293	26.5523	27.3298	28.7161	26.7096	27.0747	28.7158

*Notes: Unit for Q_d = MVAr, *FVSI* = p.u., Loss = MW and Size = MW

Adjustment of the weight coefficients in case 3 was further conducted to the system. Table 4.13 presents the results of the MOECSEP algorithm under Scenario 2 hurricane event for this case. Same phenomenon is also experienced as those in the previous case in terms of reduction in loss and *FVSI* with the DG installation and increment in resilience index. At Q_{d31} = 5 MVAr, the pre-disturbance system condition records a power loss of 28.46 MW ($Loss_{Set}$) and an *FVSI* value of 0.4028 ($FVSI_{Set}$). Following the hurricane-induced disturbance, the system performance declines, with power loss increasing to 47.34 MW ($Loss_{Out}$) and *FVSI* rising to 0.4521 ($FVSI_{\mathrm{Out}}$).

With DG installation optimised by MOECSEP, the power loss slightly increases to 29.36 MW ($Loss_{DG}$). The *FVSI* value reduces to 0.4193 ($FVSI_{\mathrm{DG}}$), indicating a modest gain in voltage stability. From a resilience perspective, the system shows improvement

in power loss recovery, with $R1_{Loss}$ = 1.51 and $R2_{Loss}$ = 1.63. Voltage security resilience, on the other hand, increases more significantly from $R1_{FVSI}$ = 8.17 to $R2_{FVSI}$ = 12.78, reflecting better post-event system stability. The MOECSEP algorithm identified Buses 3, 44, 31, 19 and 15 as the optimal locations for DG placement which denoted by Loc_{DG1} to Loc_{DG5}. The DG sizes to be installed at each location were different, based on what the system needed. The largest DG needs to be placed at Bus 31 worth 78.94 MW, followed by 63.38 MW at Bus 3, while smaller units need to be placed at Bus 15 (14.79 MW), Bus 44 (30.87 MW) and Bus 19 (33.08 MW). The total fitness function value, F_{Total} for this case has been reduced from 42.6513 to 26.4687.

Table 4.14 summarizes the results for comparative of F_{Total} for DG installation into the system when reactive load variations were subjected to Bus 31, Bus 32, and Bus 33 in the IEEE 57-Bus RTS under both Scenario 1 and Scenario 2. The evaluation was conducted using three different weight configurations: $w_1 = 0.1, w_2 = 0.9$ (Case 1); $w_1 = 0.5, w_2 = 0.5$ (Case 2); and $w_1 = 0.9, w_2 = 0.1$ (Case 3), which reflect different priorities between voltage security index (*FVSI*) and power loss minimization. At all the reactive power variations (Q_d = 5, 10, and 15 MVAr), the lowest F_{Total} values are consistently achieved when the optimisation gives higher emphasis to voltage security, as seen in the weight configuration of $w_1 = 0.1, w_2 = 0.9$ (Case 1).

For instance, at Q_{d33} = 15 MVAr, the minimum F_{Total} recorded under Scenario 1 is 3.1239, while the values increase considerably to 15.8468 and 28.1618 for the balanced ($w_1 = 0.5, w_2 = 0.5$) and loss-prioritized ($w_1 = 0.9, w_2 = 0.1$) configurations, respectively. A similar pattern emerges under Scenario 2, where the same bus and loading combination yields F_{Total} values of 3.6387, 15.5769, and 28.7158 for the respective weight settings. This trend concludes that when system resilience and voltage security are prioritized in the optimisation process, MOECSEP delivers significantly improved performance in minimizing the overall fitness value. These findings affirm that the $w_1 = 0.1, w_2 = 0.9$ (Case 1) configuration is the most effective and reliable choice for DG optimisation using MOECSEP which in turns enhancing system resilience under severe disturbance scenarios.

Table 4.14
Comparative Results of F_{Total} for DG Installation Using MOECSEP in IEEE 57-Bus RTS

Bus		**31**			**32**			**33**		
Q_d		**5**	**10**	**15**	**5**	**10**	**15**	**5**	**10**	**15**
Scenario 1										
F_{Total}	**w_1=0.1 w_2=0.9**	2.9321	3.0013	3.1547	2.9321	3.0725	3.1652	2.9037	3.0325	3.1239
	w_1=0.5 w_2=0.5	14.9325	15.3156	15.9890	14.7232	15.3019	15.9131	14.8121	15.2660	15.8468
	w_1=0.9 w_2=0.1	26.6194	27.2538	28.4547	26.8196	27.6569	27.8730	26.3331	26.9817	28.1618
Scenario 2										
F_{Total}	**w_1=0.1 w_2=0.9**	3.3061	3.4285	3.5288	3.3628	3.4377	3.6707	3.3331	3.4012	3.6387
	w_1=0.5 w_2=0.5	14.9405	15.6367	15.6702	15.0357	15.1998	15.9348	14.8668	15.6828	15.5769
	w_1=0.9 w_2=0.1	26.4687	27.6550	27.8293	26.5523	27.3298	28.7161	26.7096	27.0747	28.7158

4.4.2 Load shedding Compensation Scheme

The study of multi-objective optimisation is further extended to the implementation of the proposed MOECSEP algorithm in optimal load shedding strategies. The objective is to identify the suitable load curtailment for locations and sizing that enhance system resilience without compromising overall stability. The validation process involves simulation on the IEEE 30-Bus RTS and IEEE 57-Bus RTS under predefined hurricane strike scenarios. The simulation models actual operational conditions through the activation of specific line failures and changes in reactive power requirements. The MOECSEP algorithm employs the weighted sum approach to simultaneously minimize power losses and improve voltage stability, characterized by the reduction in *FVSI* value. The results show that strategic load shedding plays a significant role in enhancing resilience by maintaining system operation and decreasing the stress on critical components during high-impact disturbances.

4.4.2.1 Load Shedding in IEEE 30-Bus RTS

The IEEE 30-Bus RTS underwent two hurricane event simulations to evaluate the effectiveness of load shedding strategies for solving the multi-objective optimisation problem. The optimisation process focused on minimizing system losses together with improving voltage stability through coordinated load curtailment actions as measured by the *FVSI*. The simulations demonstrate how strategic load shedding locations combined with proper shedding amounts enhance system resilience when dealing with severe weather disruptions. The concurrent optimisation of loss and voltage security index in multi-objective mode allows us to determine the best combination indicated by the value of F_{Total} in the system.

A. Scenario 1

The multi-objective optimisation for load shedding analysis was conducted under three different weight coefficient combinations, Case 1, Case 2 and Case 3 as defined earlier. Table 4.15 tabulates the results of MOECSEP application in load shedding Scheme for Scenario 1 Hurricane Strike under Case 1 in IEEE 30-Bus RTS. Reactive power loadings variations were again subjected to the three similar buses: Bus

26, Bus 29, and Bus 30, under three different levels of reactive power demand (Q_d = 10, 20, and 25 MVAr). The initial system conditions prior to any disturbance, denoted as $Loss_{Set}$ and $FVSI_{Set}$, reflect baseline performance under normal operation. As expected, both power loss and voltage instability increase as Q_d rises, indicating the system is prone to vulnerability. At Q_{d26} = 20 MVAr, the power loss increases from an initial value of 20.25 MW ($Loss_{Set}$) to 66.45 MW ($Loss_{Out}$) following the simulated hurricane-induced disruption, while the *FVSI* deteriorates from 0.4919 ($FVSI_{\text{Set}}$) to 0.5673 ($FVSI_{\text{Out}}$). These values imply the tendency of the system towards instability for further Q_d increment.

Table 4.15
Results of MOECSEP Application in Load shedding Scheme for Scenario 1 Hurricane Strike for Case 1 in IEEE 30-Bus RTS

Bus	**26**			**29**			**30**		
Q_d	**10**	**20**	**25**	**10**	**20**	**25**	**10**	**20**	**25**
$Loss_{Set}$	18.23	20.25	22.27	18.12	19.39	20.53	18.11	19.55	20.93
$FVSI_{Set}$	0.2248	0.4919	0.6529	0.2111	0.3573	0.4646	0.2114	0.4073	0.5349
$Loss_{Out}$	60.88	66.45	70.49	60.76	65.02	67.24	60.71	65.26	67.98
$FVSI_{Out}$	0.2968	0.5673	0.7707	0.2953	0.4072	0.5370	0.2939	0.4635	0.6188
$Loss_{LS}$	18.27	20.56	22.30	18.45	19.92	21.01	19.04	21.03	21.07
$R1_{Loss}$	0.43	0.44	0.46	0.42	0.42	0.44	0.43	0.43	0.44
$R2_{Loss}$	0.43	0.45	0.46	0.44	0.44	0.45	0.46	0.48	0.45
$FVSI_{LS}$	0.2431	0.4997	0.6875	0.2278	0.3745	0.4851	0.2387	0.4187	0.5488
$R1_{FVSI}$	3.12	6.52	5.54	2.51	7.16	6.42	2.56	7.25	6.38
$R2_{FVSI}$	4.53	7.39	8.26	3.37	11.45	9.35	4.32	9.35	7.84
Loc_{LS1}	29	18	22	14	23	14	9	10	4
Loc_{LS2}	9	27	19	15	9	7	23	21	6
Loc_{LS3}	7	16	25	6	7	9	25	27	7
Loc_{LS4}	22	17	27	30	28	28	17	17	20
P_{dLS1}	91.99	80.64	76.90	16.45	49.87	44.25	154.40	55.89	5.90
P_{dLS2}	41.93	36.49	63.49	35.74	15.71	75.96	23.85	27.79	94.46
P_{dLS3}	79.16	21.12	89.61	179.77	100.41	117.13	78.47	70.34	135.69
P_{dLS4}	51.81	99.87	87.81	28.63	93.14	33.42	19.44	36.75	22.95
Q_{dLS1}	6.57	15.34	48.63	66.93	2.88	5.20	73.46	138.62	47.21
Q_{dLS2}	48.83	63.02	11.27	3.04	74.02	138.15	29.23	16.45	57.81
Q_{dLS3}	24.32	61.60	37.72	4.52	13.57	152.38	28.26	8.60	34.55
Q_{dLS4}	38.45	0.02	38.24	43.87	117.74	142.67	28.16	72.08	64.74
F_{Set}	6.3556	7.1556	7.7425	6.3413	6.8690	7.2077	6.3350	6.9434	7.3548
F_{Total}	2.1002	2.5145	2.9191	2.1494	2.3862	2.7305	2.2389	2.5974	2.7182

*Notes: Unit for Q_d = MVAr, P_d = MW, *FVSI* = p.u., Loss = MW and Size = MW

To mitigate this impact, the load shedding scheme was implemented, optimised by MOECSEP algorithm which identifies the optimal load shedding level and location that enhances the system performance. At Q_{d26} = 20 MVAR, with load shedding implementation, the system exhibits improved outcomes, with power loss after load curtailment ($Loss_{LS}$) significantly reduced from 66.45 MW to 20.56 MW and the *FVSI* ($FVSI_{\mathrm{LS}}$) reduced from 0.5673 to 0.4997. In terms of resilience index based on power loss before load shedding ($R1_{Loss}$) is 0.44, and post-load shedding ($R2_{Loss}$) is 0.45. The voltage stability-based resilience shows more visible improvement, where the index based on *FVSI* before shedding ($R1_{FVSI}$) is 6.52 and increases to 7.39 ($R2_{FVSI}$) after load shedding. The optimal locations to undergo load shedding are Buses 18, 27, 16, and 17 denoted by Loc_{LS1} to Loc_{LS4}, respectively. The corresponding active power (P_d) values to be shed at these locations were 80.64 MW (Bus 18), 36.49 MW (Bus 27), 21.12 MW (Bus 16), and 99.87 MW (Bus 17), as listed in P_{dLS1} to P_{dLS4}. The reactive power (Q_d) values to be shed at the same buses were 15.34 MVAr, 63.02 MVAr, 61.60 MVAr, and 0.02 MVAr, respectively. The total fitness function value F_{Total} for this scheme is reduced from 7.1556 to 2.5145, reflecting the balanced performance achieved by the algorithm in minimizing losses and enhancing voltage stability under stressed conditions.

In Table 4.16, under the balanced weight configuration in Case 2, the impact of load shedding when Q_{d29} was subjected to of 25 MVAr can be observed. Prior to any disruption, the system shows a base power loss ($Loss_{Set}$) of 20.53 MW and *FVSI* value of 0.4646. However, when the hurricane scenario is experienced which led to line outages, the power loss escalates to 67.24 MW ($Loss_{Out}$), while the voltage stability index also worsens, increasing to 0.5370 ($FVSI_{\mathrm{Out}}$). These changes reflect the increased burden on the system caused by the external disturbance. Following this, load shedding is optimised using the MOECSEP algorithm to mitigate the effects of the disruption.

With load shedding implementation, the power loss is reduced to 21.33 MW ($Loss_{LS}$), showing substantial loss reduction compared to the disturbed state. Similarly, the *FVSI* value reduces to 0.4745 ($FVSI_{\mathrm{LS}}$), indicating a positive shift in voltage stability. When assessed using resilience indices, the power loss-based resilience before and after load shedding $R1_{Loss}$ and $R2_{Loss}$ are 0.44 and 0.46 respectively. While the *FVSI*-based resilience $R1_{FVSI}$ is significantly increased from at 6.42 and improves to 7.59 ($R2_{FVSI}$). The algorithm identified four optimal buses, Buses 25, 4, 7 and 12 denoted by Loc_{LS1} to Loc_{LS4}, respectively, for implementing load shedding.

Table 4.16
Results of MOECSEP Application in Load shedding Scheme for Scenario 1 Hurricane Strike for Case 2 in IEEE 30-Bus RTS

Bus	**26**			**29**			**30**		
Q_d	**10**	**20**	**25**	**10**	**20**	**25**	**10**	**20**	**25**
$Loss_{Set}$	18.23	20.25	22.27	18.12	19.39	20.53	18.11	19.55	20.93
$FVSI_{Set}$	0.2248	0.4919	0.6529	0.2111	0.3573	0.4646	0.2114	0.4073	0.5349
$Loss_{Out}$	60.88	66.45	70.49	60.76	65.02	67.24	60.71	65.26	67.98
$FVSI_{Out}$	0.2968	0.5673	0.7707	0.2953	0.4072	0.5370	0.2939	0.4635	0.6188
$Loss_{LS}$	18.24	20.36	22.35	19.63	20.25	21.33	20.38	20.22	22.03
$R1_{Loss}$	0.43	0.44	0.46	0.42	0.42	0.44	0.43	0.43	0.44
$R2_{Loss}$	0.43	0.44	0.46	0.48	0.45	0.46	0.51	0.45	0.48
$FVSI_{LS}$	0.2385	0.5031	0.6945	0.2247	0.3684	0.4745	0.2214	0.4181	0.5431
$R1_{FVSI}$	3.12	6.52	5.54	2.51	7.16	6.42	2.56	7.25	6.38
$R2_{FVSI}$	4.09	7.84	9.11	3.18	9.49	7.59	3.05	9.21	7.17
Loc_{LS1}	9	12	10	7	6	25	7	7	12
Loc_{LS2}	12	10	28	20	3	4	9	29	28
Loc_{LS3}	7	28	26	4	10	7	4	12	6
Loc_{LS4}	21	17	10	24	27	12	10	10	10
P_{dLS1}	10.64	61.63	109.11	97.23	43.56	19.32	19.70	23.08	20.15
P_{dLS2}	59.00	54.88	20.74	14.77	16.45	115.99	10.96	13.46	29.09
P_{dLS3}	117.17	66.06	16.19	92.84	59.63	70.53	100.79	166.07	159.65
P_{dLS4}	86.30	19.75	112.51	19.32	86.11	27.61	107.24	143.61	43.65
Q_{dLS1}	103.38	100.72	19.41	98.25	50.82	48.04	53.20	39.67	184.85
Q_{dLS2}	1.53	116.50	99.47	4.25	75.40	110.31	154.29	11.84	2.17
Q_{dLS3}	72.90	31.42	2.01	122.67	164.42	24.42	126.58	156.58	26.60
Q_{dLS4}	2.74	140.77	168.34	56.01	63.12	45.40	162.42	23.27	147.26
F_{Set}	30.5907	33.5088	35.6298	30.5253	32.7161	33.8906	30.4995	32.8630	34.2990
F_{Total}	9.2370	10.4298	11.5198	9.9284	10.3116	10.9008	10.3030	10.3184	11.2876

*Notes: Unit for Q_d = MVAr, P_d = MW, *FVSI* = p.u., Loss = MW and Size = MW

The active power (P_d) values to be shed at the respective locations were 19.32 MW (Bus 25), 115.99 MW (Bus 4), 70.53 MW (Bus 7), and 27.61 MW (Bus 12). Similarly, the reactive power (Q_d) values shed at these locations were 48.04 MVAr, 110.31 MVAr, 24.42 MVAr, and 45.40 MVAr, respectively. The total weighted fitness function value (F_{Total}) for this case is reduced from 33.8906 to 10.9008.

The results for Case 3 are tabulated in Table 4.17. Under the load shedding scheme guided by the MOECSEP algorithm with a weight configuration of $w_1 = 0.9, w_2 = 0.1$, the performance at Bus 30 with a reactive demand of 20 MVAr reveals several important insights. Initially, the system operates with a baseline power loss ($Loss_{Set}$) of 19.55 MW and a corresponding *FVSI* of 0.4073. Under the influence of hurricane, the system experiences deterioration, with power loss rising to 65.26 MW

($Loss_{Out}$) and voltage stability index increasing to 0.4635 ($FVSI_{Out}$).

Table 4.17
Results of MOECSEP Application in Load shedding Scheme for Scenario 1 Hurricane Strike for Case 3 in IEEE 30-Bus RTS

Bus	**26**			**29**			**30**		
Q_d	**10**	**20**	**25**	**10**	**20**	**25**	**10**	**20**	**25**
$Loss_{Set}$	18.23	20.25	22.27	18.12	19.39	20.53	18.11	19.55	20.93
$FVSI_{Set}$	0.2248	0.4919	0.6529	0.2111	0.3573	0.4646	0.2114	0.4073	0.5349
$Loss_{Out}$	60.88	66.45	70.49	60.76	65.02	67.24	60.71	65.26	67.98
$FVSI_{Out}$	0.2968	0.5673	0.7707	0.2953	0.4072	0.5370	0.2939	0.4635	0.6188
$Loss_{LS}$	18.23	20.35	24.15	19.63	21.57	21.83	19.21	21.24	22.52
$R1_{Loss}$	0.43	0.44	0.46	0.42	0.42	0.44	0.43	0.43	0.44
$R2_{Loss}$	0.43	0.44	0.52	0.48	0.50	0.48	0.46	0.48	0.50
$FVSI_{LS}$	0.2384	0.5013	0.6745	0.2213	0.3699	0.4831	0.2255	0.4121	0.5521
$R1_{FVSI}$	3.12	6.52	5.54	2.51	7.16	6.42	2.56	7.25	6.38
$R2_{FVSI}$	4.08	7.60	7.01	2.99	9.92	8.96	3.30	8.02	8.28
Loc_{LS1}	17	25	24	29	11	27	13	27	12
Loc_{LS2}	4	12	7	13	7	12	7	11	7
Loc_{LS3}	27	29	5	11	24	13	24	18	10
Loc_{LS4}	10	9	27	21	20	11	5	24	9
P_{dLS1}	55.89	15.71	178.98	25.20	12.52	85.38	91.09	97.23	43.56
P_{dLS2}	27.79	100.41	36.36	40.56	29.21	6.07	78.29	14.77	16.45
P_{dLS3}	70.34	93.14	20.71	150.10	47.99	20.45	12.73	92.84	59.63
P_{dLS4}	36.75	2.88	36.50	14.19	163.76	99.95	93.35	19.32	86.11
Q_{dLS1}	66.93	2.88	0.55	73.42	43.17	1.94	0.55	92.21	157.99
Q_{dLS2}	3.04	74.02	4.12	79.76	51.59	53.16	4.12	43.17	84.31
Q_{dLS3}	4.52	13.57	43.94	167.49	63.07	112.90	43.94	51.59	6.67
Q_{dLS4}	43.87	117.74	40.18	2.50	33.35	4.46	40.18	63.07	173.48
F_{Set}	54.8258	59.8620	63.5170	54.7093	58.5631	60.5734	54.6640	58.7825	61.2432
F_{Total}	16.4322	18.3694	21.8062	17.6928	19.4483	19.6994	17.3153	19.1588	20.3209

*Notes: Unit for Q_d = MVAr, P_d = MW, $FVSI$ = p.u., Loss = MW and Size = MW

Upon applying the optimised load shedding strategy, the system shows improvement. The post- load shedding power loss ($Loss_{LS}$) drops to 21.24 MW, and the $FVSI$ ($FVSI_{LS}$) slightly decrease to 0.4121, reflecting a modest enhancement in voltage security. The resilience indices $R1_{Loss}$ and $R2_{Loss}$ are recorded at 0.43 and 0.48, respectively, indicating better loss resilience after load shedding. For $FVSI$-based resilience, $R1_{FVSI}$ is 7.25 and slightly increases to 8.02 ($R2_{FVSI}$). The optimal locations for load curtailment are Buses 27, 11, 18, and 24, denoted by Loc_{LS1} through Loc_{LS4}, respectively. The corresponding P_d to be shed at these locations are 97.23 MW, 14.77 MW, 92.84 MW, and 19.23 MW, indicating a well-distributed curtailment across high-impact areas. Likewise, the Q_d values to be shed at these buses are 92.21 MVAr, 43.17

MVAr, 51.59 MVAr, and 63.07 MVAr, respectively. The total fitness value, F_{Total} for this case is reduced from 58.7825 to 19.1588. Thus, Table 4.17 confirm that load shedding remains an effective resilience-enhancing strategy, particularly when optimised through a multi-objective framework.

B. Scenario 2

The results for Scenario 2 of the hurricane implemented in IEEE 30-Bus RTS, are tabulated in Table 4.18 under Case 1 with the weight coefficient of $w_1 = 0.1, w_2 = 0.9$.

Table 4.18
Results of MOECSEP Application in Load shedding Scheme for Scenario 2 Hurricane Strike for Case 1 in IEEE 30-Bus RTS

Bus	**26**			**29**			**30**		
Q_d	**10**	**20**	**25**	**10**	**20**	**25**	**10**	**20**	**25**
$Loss_{Set}$	18.23	20.25	22.27	18.12	19.39	20.53	18.11	19.55	20.93
$FVSI_{Set}$	0.2248	0.4919	0.6529	0.2111	0.3573	0.4646	0.2114	0.4073	0.5349
$Loss_{Out}$	20.40	25.03	29.92	19.78	22.87	24.82	20.27	23.59	28.33
$FVSI_{Out}$	0.2797	1.0000	0.9673	0.2830	0.6333	0.7914	0.2984	0.7619	1.0000
$Loss_{LS}$	19.45	20.98	22.73	18.79	20.33	21.54	18.99	20.60	21.02
$R1_{Loss}$	8.38	4.24	2.91	10.89	5.57	4.78	8.38	0.26	2.83
$R2_{Loss}$	20.43	5.18	3.16	18.92	8.00	6.58	14.80	0.27	2.88
$FVSI_{LS}$	0.2451	0.5143	0.6756	0.2256	0.4028	0.4731	0.2314	0.4126	0.5547
$R1_{FVSI}$	4.09	0.97	2.08	2.94	1.29	1.42	2.43	1.15	1.15
$R2_{FVSI}$	7.08	1.06	2.32	3.93	1.75	1.49	3.45	1.18	1.25
Loc_{LS1}	10	17	7	22	10	28	21	7	9
Loc_{LS2}	27	7	12	17	15	3	17	21	6
Loc_{LS3}	9	6	6	10	9	25	7	24	7
Loc_{LS4}	27	22	9	25	28	6	28	10	17
P_{dLS1}	178.98	91.09	25.21	74.36	140.15	101.63	12.52	85.38	26.70
P_{dLS2}	36.36	78.29	40.56	137.19	9.95	46.48	29.21	6.07	139.63
P_{dLS3}	20.71	12.73	150.10	62.00	22.13	58.74	47.99	20.45	22.23
P_{dLS4}	36.50	93.35	14.19	1.84	80.41	92.21	163.76	99.95	116.71
Q_{dLS1}	73.42	0.55	91.78	20.73	42.19	43.17	1.94	7.75	145.89
Q_{dLS2}	79.76	4.12	192.65	104.16	32.56	51.59	53.16	12.06	17.91
Q_{dLS3}	167.48	43.94	46.94	155.14	62.88	63.07	112.90	46.77	2.83
Q_{dLS4}	2.50	40.18	39.50	44.11	41.36	33.35	4.46	72.36	63.03
F_{Set}	5.1409	5.3532	6.3694	5.1836	5.3876	6.2124	5.1590	5.3626	6.0279
F_{Total}	2.1659	2.5612	2.8813	2.0817	2.3951	2.5800	2.1070	2.4312	2.6017

*Notes: Unit for Q_d = MVAr, P_d = MW, *FVSI* = p.u., Loss = MW and Size = MW

At Q_{d30} = 20 MVAr, the system initially exhibits a base power loss of 19.55 MW ($Loss_{Set}$) and an *FVSI* value of 0.4073 ($FVSI_{Set}$) before hurricane was experienced by

the system. Following the hurricane-induced disturbance, the network experiences a deterioration where power loss increases to 23.59 MW ($Loss_{Out}$), while the *FVSI* rises to 0.7619 ($FVSI_{\text{Out}}$). After applying the optimised load shedding solution, the power loss is reduced to 20.60 MW ($Loss_{LS}$), and voltage security improves with a reduced $FVSI_{\text{LS}}$ value to 0.4126. The resilience indices, $R1_{Loss}$, which captures the resilience of the system prior to load shedding, is 0.26, while $R2_{Loss}$ after load shedding slightly increases to 0.27. However, the *FVSI*-based resilience index improves from $R1_{FVSI}$ = 1.15 to $R2_{FVSI}$ = 1.18, demonstrating positive enhancement in power system resilience. The algorithm determined Bus 7, 21, 24, and 10 as the optimal locations for load shedding which correspond to Loc_{LS1} through Loc_{LS4}. The required active power to be shed (P_{dLS1} to P_{dLS4}) are 85.38 MW, 6.07 MW, 20.45 MW, and 99.95 MW, while the reactive power to be shed (Q_{dLS1} to Q_{dLS4}) are 7.75 MVAr, 12.06 MVAr, 46.77 MVAr, and 72.36 MVAr, respectively. The total fitness value (F_{Total}) for this case is reduced from 5.3626 to 2.4312.

In Table 4.19, the performance of the MOECSEP algorithm under the influence of Scenario 2 hurricane conditions is assessed using an equal weighting scheme of $w_1 = 0.5, w_2 = 0.5$ (Case 2). Focusing on Bus 29 with a reactive power loading of Q_d = 20 MVAr, the system initial condition prior to the disturbance records a power loss ($Loss_{Set}$) of 19.39 MW and a corresponding $FVSI_{\text{Set}}$ value of 0.3573. However, the simulated hurricane strike leads to performance deterioration, with the power loss increasing to 22.87 MW ($Loss_{Out}$) and *FVSI* rising to 0.6333 ($FVSI_{\text{Out}}$). After implementing the optimised load shedding strategy, the system shows recovery.

With the implementation of multi-objective load shedding, the power loss reduces to 19.53 MW ($Loss_{LS}$), and the *FVSI* improves to 0.3742 ($FVSI_{\text{LS}}$), both approaching pre-disturbance levels. The improvement is also reflected in the resilience metrics. The power loss resilience index improves from $R1_{Loss}$ = 5.57 to $R2_{Loss}$ = 5.86, indicating a stronger system ability to recover from power loss. Similarly, the *FVSI*-based resilience index also shows enhancement, with $R1_{FVSI}$ = 1.29 increasing to $R2_{FVSI}$ = 1.44. Buses 14, 7, 9, and 28 were identified as the optimal locations for load curtailment, assigned as Loc_{LS1} to Loc_{LS4}, respectively. The active power to be shed are at these buses are 2.88 MW, 74.02 MW, 13.57 MW, and 117.74 MW. In parallel, the reactive power to be shed are 5.20 MVAr at Bus 14, 138.15 MVAr at Bus 7, 152.38 MVAr at Bus 9, and 142.67 MVAr at Bus 28, indicating substantial support at these locations in maintaining system voltage stability. The final combined fitness value,

F_{Total} is reduced from 11.7494 to 9.9528.

Table 4.19
Results of MOECSEP Application in Load shedding Scheme for Scenario 2 Hurricane Strike for Case 2 in IEEE 30-Bus RTS

Bus	**26**			**29**			**30**		
Q_d	**10**	**20**	**25**	**10**	**20**	**25**	**10**	**20**	**25**
$Loss_{Set}$	18.23	20.25	22.27	18.12	19.39	20.53	18.11	19.55	20.93
$FVSI_{Set}$	0.2248	0.4919	0.6529	0.2111	0.3573	0.4646	0.2114	0.4073	0.5349
$Loss_{Out}$	20.40	25.03	29.92	19.78	22.87	24.82	20.27	23.59	28.33
$FVSI_{Out}$	0.2797	1.0000	0.9673	0.2830	0.6333	0.7914	0.2984	0.7619	1.0000
$Loss_{LS}$	18.25	21.89	22.98	18.64	19.53	21.00	18.93	20.35	21.03
$R1_{Loss}$	8.38	4.24	2.91	10.89	5.57	4.78	8.38	0.26	2.83
$R2_{Loss}$	8.45	6.98	3.31	16.29	5.86	5.51	14.14	0.27	2.88
$FVSI_{LS}$	0.2454	0.5127	0.7014	0.2350	0.3742	0.4714	0.2341	0.4321	0.5541
$R1_{FVSI}$	4.09	0.28	2.08	2.94	1.29	1.42	2.43	1.15	1.11
$R2_{FVSI}$	7.15	0.29	2.64	4.90	1.44	1.47	3.64	1.31	1.20
Loc_{LS1}	21	17	12	3	14	4	28	10	24
Loc_{LS2}	17	10	10	10	7	21	7	12	7
Loc_{LS3}	10	28	25	20	9	6	12	9	25
Loc_{LS4}	7	21	4	9	28	17	20	28	12
P_{dLS1}	73.46	2.88	5.20	66.93	2.88	178.98	25.20	154.40	49.86
P_{dLS2}	29.23	74.02	138.14	3.04	74.02	36.36	40.56	23.85	15.72
P_{dLS3}	28.26	13.55	152.37	4.52	13.57	20.71	150.10	78.47	100.42
P_{dLS4}	28.16	117.74	142.66	43.87	117.74	36.50	14.19	19.44	93.14
Q_{dLS1}	73.42	91.78	31.34	42.19	5.20	73.42	0.55	73.42	138.62
Q_{dLS2}	79.76	192.64	106.66	32.56	138.15	79.75	4.12	79.76	16.45
Q_{dLS3}	167.49	46.93	18.28	62.88	152.38	167.48	43.94	167.49	8.60
Q_{dLS4}	2.50	39.50	167.03	41.36	142.67	2.50	40.18	2.50	72.08
F_{Set}	10.3423	13.6513	15.4432	10.0312	11.7494	12.8048	10.2844	48.3360	14.6735
F_{Total}	9.2454	11.2031	11.8424	9.4352	9.9528	10.7373	9.5829	10.3931	10.7906

*Notes: Unit for Q_d = MVAr, P_d = MW, *FVSI* = p.u., Loss = MW and Size = MW

In Table 4.20, the performance of the MOECSEP algorithm under Scenario 2 of the hurricane strike is evaluated with a weight configuration that prioritizes power loss minimization with $w_1 = 0.9, w_2 = 0.1$ (Case 3). At Bus 30 with a reactive power demand of Q_d = 25 MVAr, the system pre-disturbance condition shows a baseline power loss ($Loss_{Set}$) of 20.93 MW and an initial *FVSI* value of 0.5349. Following the hurricane impact, the system becomes significantly stressed, leading the power loss rises to 28.33 MW ($Loss_{Out}$), and the voltage stability index deteriorates to 1.0000 ($FVSI_{\text{Out}}$), highlighting an increase in system vulnerability.

Table 4.20
Results of MOECSEP Application in Load shedding Scheme for Scenario 2 Hurricane Strike for Case 3 in IEEE 30-Bus RTS

Bus	**26**			**29**			**30**		
Q_d	**10**	**20**	**25**	**10**	**20**	**25**	**10**	**20**	**25**
$Loss_{Set}$	18.23	20.25	22.27	18.12	19.39	20.53	18.11	19.55	20.93
$FVSI_{Set}$	0.2248	0.4919	0.6529	0.2111	0.3573	0.4646	0.2114	0.4073	0.5349
$Loss_{Out}$	20.40	25.03	29.92	19.78	22.87	24.82	20.27	23.59	28.33
$FVSI_{Out}$	0.2797	1.0000	0.9673	0.2830	0.6333	0.7914	0.2984	0.7619	1.0000
$Loss_{LS}$	18.93	20.65	22.98	18.65	19.68	21.03	18.97	20.85	21.82
$R1_{Loss}$	8.38	4.24	2.91	10.89	5.57	4.78	8.38	0.26	2.83
$R2_{Loss}$	12.85	4.71	3.31	16.53	6.19	5.54	14.60	0.28	3.35
$FVSI_{LS}$	0.2250	0.5027	0.6751	0.2186	0.3812	0.4721	0.2232	0.4125	0.5518
$R1_{FVSI}$	4.09	0.28	2.08	2.94	1.29	1.42	2.43	1.15	1.11
$R2_{FVSI}$	4.11	0.28	2.31	3.39	1.51	1.48	2.97	1.18	1.19
Loc_{LS1}	18	24	27	5	7	12	6	25	12
Loc_{LS2}	13	11	12	24	29	28	3	4	5
Loc_{LS3}	10	9	5	11	12	6	10	7	9
Loc_{LS4}	27	28	10	13	10	27	27	12	18
P_{dLS1}	19.32	26.70	7.42	10.64	49.86	55.90	19.70	23.08	25.20
P_{dLS2}	115.99	139.63	41.34	59.00	15.72	27.81	10.96	13.46	40.56
P_{dLS3}	70.53	22.23	116.37	117.17	100.42	70.35	100.79	166.07	150.09
P_{dLS4}	27.61	116.71	130.31	86.30	93.14	36.75	107.24	143.61	14.19
Q_{dLS1}	98.25	50.82	39.67	184.85	2.88	47.21	73.42	91.78	20.73
Q_{dLS2}	4.25	75.40	11.84	2.17	74.02	57.81	79.76	192.65	104.16
Q_{dLS3}	122.67	164.42	156.58	26.60	13.55	34.55	167.48	46.94	155.14
Q_{dLS4}	56.01	63.12	23.27	147.26	117.74	64.74	2.50	39.50	44.11
F_{Set}	18.3924	22.7559	27.0239	17.8298	20.6422	22.4155	18.2731	86.3952	25.6001
F_{Total}	17.0614	18.6368	20.7508	16.8081	17.7538	18.9701	17.0964	18.8081	19.6944

*Notes: Unit for Q_d = MVAr, P_d = MW, $FVSI$ = p.u., Loss = MW and Size = MW

Once the optimised load shedding solution is applied, the power loss is brought down to 21.82 MW ($Loss_{LS}$), showing substantial improvement relative to the disrupted condition. The voltage security index also improves, with $FVSI_{LS}$ reduced to 0.5518. The resilience index based on power loss ($R1_{Loss}$ = 2.83) shows a slight gain after load shedding with $R2_{Loss}$ increasing to 3.35, reflecting modest enhancement in power loss resilience. The voltage stability resilience values increase from $R1_{FVSI}$ = 1.11 to $R2_{FVSI}$ = 1.19. The MOECSEP algorithm identified four optimal buses for curtailment. These are Buses 12, 5, 9, and 18, denoted by Loc_{LS1} through Loc_{LS4}, respectively. The associated active power shedding (P_{dLS1} to P_{dLS4}) values are 25.20 MW (Bus 12), 40.56 MW (Bus 5), 150.09 MW (Bus 9), and 14.19 MW (Bus 18). Correspondingly, the reactive power shedding (Q_{dLS1} to Q_{dLS4}) at these locations are 20.73 MVAr, 104.16

MVAr, 155.14 MVAr, and 44.11 MVAr, respectively, further confirming the importance of these buses in maintaining system voltage resilience. All the changes in system variables have led to the reduction in total fitness value, F_{Total} from 25.6001 to 19.6944, is the highest among the three weight configurations. Results of other reactive load values can be referred to the same table.

Table 4.21 presents a comparative analysis of the total fitness values F_{Total} derived from the MOECSEP load shedding scheme applied to the IEEE 30-Bus RTS. The results are evaluated under two hurricane strike scenarios, under reactive load variations at three buses (Bus 26, 29, and 30), and three different reactive power loading levels, Q_d (10, 20, and 25 MVAr). The analysis further considers three cases under distinct weight configurations: ($w_1 = 0.1, w_2 = 0.9$ (Case 1); $w_1 = 0.5, w_2 = 0.5$ (Case 2) and $w_1 = 0.9, w_2 = 0.1$ (Case 3)).

In Scenario 1, the total fitness values, F_{Total} reveal that the weight configuration of Case 1 consistently produces the lowest F_{Total} values across all buses and reactive loading levels. For example, at Q_{d30} = 20 MVAr, the F_{Total} is 2.4801 under this configuration, which is significantly lower compared to 10.3184 and 19.1588 for the weight settings in Case 2 and Case 3 respectively. Similar trends are observed at Buses 26 and 29. Therefore, the weight coefficient $w_1 = 0.1, w_2 = 0.9$ is identified as the most effective configuration for the MOECSEP algorithm in Scenario 1. The results from Scenario 2 reaffirm the effectiveness of the weight configuration of Case 1 in minimizing F_{Total}. Under this setting, the fitness values remain the lowest for all buses and Q_d levels when compared to the other two configurations. Thus Case 1 with $w_1 = 0.1, w_2 = 0.9$ exhibit the best choice in achieving the lowest total values in multi-objective optimisation.

Table 4.21
Comparative Results of F_{Total} for Load shedding Scheme Using MOECSEP in IEEE 30-Bus RTS

Bus		**26**			**29**			**30**		
Q_d		**10**	**20**	**25**	**10**	**20**	**25**	**10**	**20**	**25**
Scenario 1										
F_{Total}	**w_1=0.1 w_2=0.9**	2.0453	2.5060	2.8490	2.0502	2.3295	2.5378	2.1186	2.4801	2.6005
	w_1=0.5 w_2=0.5	9.2370	10.4298	11.5198	9.9284	10.3116	10.9008	10.3030	10.3184	11.2876
	w_1=0.9 w_2=0.1	16.4322	18.3694	21.8062	17.6928	19.4483	19.6994	17.3153	19.1588	20.3209
Scenario 2										
F_{Total}	**w_1=0.1 w_2=0.9**	2.1659	2.5612	2.8813	2.0817	2.3951	2.5800	2.1070	2.4312	2.6017
	w_1=0.5 w_2=0.5	9.2454	11.2031	11.8424	9.4352	9.9528	10.7373	9.5829	10.3931	10.7906
	w_1=0.9 w_2=0.1	17.0614	18.6368	20.7508	16.8081	17.7538	18.9701	17.0964	18.8081	19.6944

4.4.2.2 Load shedding in IEEE 57-Bus RTS

Optimal load shedding scheme was also conducted to the second test model under both hurricane scenarios. in addressing both the power loss and voltage security. The IEEE 57-Bus RTS was subjected to two hurricane strike to assess the effectiveness of load shedding strategies in addressing the formulated multi-objective optimisation problem. The optimisation process aimed to reduce overall system power losses while simultaneously enhancing voltage security, evaluated using the *FVSI*, through carefully coordinated load curtailment or load shedding actions.

A. Scenario 1

Table 4.22 presents the results of the MOECSEP algorithm applied to load shedding optimisation under Scenario 1 hurricane conditions in the IEEE 57-Bus RTS. The study was conducted using a Case 1 with weight configuration of $w_1 = 0.1, w_2 = 0.9$. The study includes the variation of Q_d at three critical buses: Bus 31, Bus 32, and Bus 33 each tested under increasing reactive load levels (Q_d = 5, 10, and 15 MVAr). For instance, at Bus 33 with Q_d = 15 MVAr, the *FVSI* degrades to 0.7086 ($FVSI_{\text{Out}}$) when the system was subjected to the disturbance but reduces to 0.4731 ($FVSI_{\text{LS}}$) following MOECSEP-based load shedding initiative. Similarly, voltage-based resilience shows clear enhancement, with $R1_{FVSI}$ = 2.23 increasing to $R2_{FVSI}$ = 2.43, highlighting the effectiveness of the scheme in restoring voltage security post-event. The optimal buses optimised by MOECSEP for curtailment are Buses 48, 35, 10, and 1.

The corresponding active power to be shed are 66.84 MW (Bus 48), 90.17 MW (Bus 35), 83.58 MW (Bus 10), and 38.28 MW (Bus 1), respectively. Alongside, the reactive power to be shed are 38.28 MVAr, 57.32 MVAr, 144.00 MVAr, and 54.17 MVAr. This has caused the reduction of the total fitness value from 4.4409 to 3.5124. These values reflect the algorithm ability to maintain performance consistency even under increasing system stress.

Table 4.22
Results of MOECSEP Application in Load Shedding Scheme for Scenario 1 Hurricane Strike for Case 1 in IEEE 57-Bus RTS

Bus	**31**			**32**			**33**		
Q_d	**5**	**10**	**15**	**5**	**10**	**15**	**5**	**10**	**15**
$Loss_{Set}$	28.46	29.22	30.56	28.67	29.42	30.66	28.56	29.30	30.55
$FVSI_{Set}$	0.4028	0.3977	0.4339	0.4005	0.3948	0.4973	0.4016	0.3960	0.4613
$Loss_{Out}$	47.34	49.47	54.69	47.77	49.81	55.06	47.52	49.56	53.90
$FVSI_{Out}$	0.4521	0.4518	1.0000	0.4520	0.4516	0.7846	0.4520	0.4518	0.7086
$Loss_{LS}$	29.32	29.94	31.30	29.64	30.63	31.27	29.33	30.65	30.87
$R1_{Loss}$	6.49	5.63	2.51	6.25	5.44	3.61	6.38	5.62	4.10
$R2_{Loss}$	8.31	6.69	2.73	8.19	7.29	3.97	7.92	7.95	4.33
$FVSI_{LS}$	0.4130	0.4098	0.4452	0.4135	0.4013	0.5009	0.4106	0.4067	0.4731
$R1_{FVSI}$	10.98	10.52	0.77	10.91	10.67	2.07	10.97	10.67	2.23
$R2_{FVSI}$	15.58	15.95	0.80	17.45	13.16	2.12	14.88	15.41	2.43
Loc_{LS1}	38	50	16	45	46	45	17	55	48
Loc_{LS2}	11	30	55	21	35	21	27	43	35
Loc_{LS3}	29	43	43	31	13	31	37	21	10
Loc_{LS4}	51	57	39	41	14	41	21	31	1
P_{dLS1}	93.71	5.33	130.61	168.79	34.42	57.50	40.32	82.85	66.84
P_{dLS2}	112.14	34.84	60.56	21.24	163.89	177.08	96.31	195.99	90.17
P_{dLS3}	41.38	162.69	98.76	20.84	189.05	122.68	83.37	128.94	83.58
P_{dLS4}	154.54	56.78	98.73	47.57	52.56	12.50	156.88	13.08	28.79
Q_{dLS1}	130.06	179.48	38.75	15.91	27.09	163.39	106.79	114.03	38.28
Q_{dLS2}	195.25	38.01	5.11	30.18	122.75	85.37	10.44	128.12	57.23
Q_{dLS3}	33.13	129.18	173.56	175.70	21.49	15.34	45.12	121.01	144.00
Q_{dLS4}	77.46	95.50	154.96	6.07	62.92	37.08	62.51	14.93	54.17
F_{Set}	3.6806	3.8333	5.1753	3.7188	3.8722	4.5781	3.6975	3.8410	4.4009
F_{Total}	3.3037	3.3626	3.5305	3.3357	3.4246	3.5776	3.3023	3.4315	3.5124

*Notes: Unit for Q_d = MVAr, P_d = MW, *FVSI* = p.u., Loss = MW and Size = MW

Overall, the findings support the conclusion that the $w_1 = 0.1, w_2 = 0.9$ (Case 1) configuration is highly effective in enhancing system resilience through load shedding.

This study further extends the evaluation of the proposed MOECSEP algorithm by applying it to Scenario 1 hurricane events on the IEEE 57-Bus RTS, with a focus on load shedding performance under different weight coefficient configurations. In general, power loss will increase accordingly as we increased the Q_d value at the subjected loads. The results under Case 2 and Case 3 are tabulated in Table 4.23 and Table 4.24. Under the balanced weight configuration (Table 4.23), the system achieves a post-load shedding *FVSI* value of 0.4713 ($FVSI_{LS}$), with voltage security resilience improving from $R1_{FVSI} = 2.23$ to $R2_{FVSI} = 2.40$.

Table 4.23
Results of MOECSEP Application in Load Shedding Scheme for Scenario 1 Hurricane Strike for Case 2 in IEEE 57-Bus RTS

Bus	**31**			**32**			**33**		
Q_d	**5**	**10**	**15**	**5**	**10**	**15**	**5**	**10**	**15**
$Loss_{Set}$	28.46	29.22	30.56	28.67	29.42	30.66	28.56	29.30	30.55
$FVSI_{Set}$	0.4028	0.3977	0.4339	0.4005	0.3948	0.4973	0.4016	0.3960	0.4613
$Loss_{Out}$	47.34	49.47	54.69	47.77	49.81	55.06	47.52	49.56	53.90
$FVSI_{Out}$	0.4521	0.4518	1.0000	0.4520	0.4516	0.7846	0.4520	0.4518	0.7086
$Loss_{LS}$	28.96	30.65	30.97	29.36	29.86	30.93	29.86	29.98	30.93
$R1_{Loss}$	6.49	5.63	2.51	6.25	5.44	3.61	6.38	5.62	4.10
$R2_{Loss}$	7.45	8.15	2.63	7.54	6.01	3.76	9.43	6.62	4.38
$FVSI_{LS}$	0.4117	0.4011	0.4484	0.4101	0.4006	0.5014	0.4114	0.4034	0.4713
$R1_{FVSI}$	10.98	10.52	0.77	10.91	10.67	2.07	10.97	10.67	2.23
$R2_{FVSI}$	14.81	11.66	0.81	15.13	12.84	2.13	15.35	13.58	2.40
Loc_{LS1}	45	17	48	11	4	38	25	16	17
Loc_{LS2}	21	27	35	29	14	11	13	55	50
Loc_{LS3}	31	37	10	30	29	29	14	43	15
Loc_{LS4}	41	21	1	18	15	51	4	39	40
P_{dLS1}	132.25	83.41	35.11	57.61	152.90	31.40	19.28	122.30	61.53
P_{dLS2}	84.20	42.26	90.53	57.61	15.69	138.99	31.79	52.17	107.04
P_{dLS3}	3.69	80.67	53.54	73.13	24.61	118.03	188.99	7.13	108.65
P_{dLS4}	122.55	21.71	81.74	197.38	23.25	88.59	164.21	143.60	160.62
Q_{dLS1}	96.35	72.33	90.88	92.12	173.71	84.41	188.99	20.12	20.42
Q_{dLS2}	64.91	19.27	190.79	6.17	66.80	130.81	164.21	101.02	22.25
Q_{dLS3}	24.94	40.70	191.69	79.56	99.06	0.59	31.03	62.50	52.55
Q_{dLS4}	103.03	77.37	96.39	122.86	70.28	124.63	8.16	40.70	135.80
F_{Set}	16.6449	17.4244	22.3991	16.8454	17.6337	19.9424	16.7347	17.4728	19.3327
F_{Total}	14.6864	15.5266	15.7108	14.8858	15.1319	15.7165	15.1374	15.1935	15.7024

*Notes: Unit for Q_d = MVAr, P_d = MW, $FVSI$ = p.u., Loss = MW and Size = MW

Meanwhile, the loss-based resilience rises slightly from $R1_{Loss}$ = 4.10 to $R2_{Loss}$ = 4.38, indicating moderate performance across both fitness function. The four optimal buses identified for load shedding were Buses 17, 50, 15, and 40. The corresponding active power to undergo load shedding are 61.53 MW at Bus 17, 107.04 MW at Bus 50, 108.65 MW at Bus 15, and 160.62 MW at Bus 40. The reactive power for load shedding at these same buses were 20.42 MVAr, 22.25 MVAr, 52.55 MVAr, and 135.80 MVAr, respectively. This scheme leads to total fitness value (F_{Total}) reduction for this case from 19.3327 to 15.7024.

Table 4.24
Results of MOECSEP Application in Load Shedding Scheme for Scenario 1 Hurricane Strike for Case 3 in IEEE 57-Bus RTS

Bus	**31**			**32**			**33**		
Q_d	**5**	**10**	**15**	**5**	**10**	**15**	**5**	**10**	**15**
$Loss_{Set}$	28.46	29.22	30.56	28.67	29.42	30.66	28.56	29.30	30.55
$FVSI_{Set}$	0.4028	0.3977	0.4339	0.4005	0.3948	0.4973	0.4016	0.3960	0.4613
$Loss_{Out}$	47.34	49.47	54.69	47.77	49.81	55.06	47.52	49.56	53.90
$FVSI_{Out}$	0.4521	0.4518	1.0000	0.4520	0.4516	0.7846	0.4520	0.4518	0.7086
$Loss_{LS}$	29.37	29.58	30.99	29.33	30.63	31.70	29.89	29.87	30.94
$R1_{Loss}$	6.49	5.63	2.51	6.25	5.44	3.61	6.38	5.62	4.10
$R2_{Loss}$	8.43	6.13	2.63	7.47	7.29	4.26	9.53	6.44	4.38
$FVSI_{LS}$	0.4084	0.4015	0.4468	0.4079	0.4015	0.5006	0.4100	0.4008	0.4723
$R1_{FVSI}$	10.98	10.52	0.77	10.91	10.67	2.07	10.97	10.67	2.23
$R2_{FVSI}$	13.13	11.81	0.81	13.92	13.25	2.12	14.54	12.41	2.41
Loc_{LS1}	38	3	15	13	6	7	16	6	7
Loc_{LS2}	31	24	6	19	9	6	14	9	6
Loc_{LS3}	34	12	9	5	4	9	24	4	9
Loc_{LS4}	26	7	7	8	3	12	18	3	12
P_{dLS1}	157.54	129.07	104.87	134.01	193.38	19.82	149.48	92.89	193.38
P_{dLS2}	173.43	99.51	134.54	179.61	170.09	168.24	124.03	188.19	170.09
P_{dLS3}	89.45	27.66	51.24	82.47	173.50	158.49	170.53	10.01	173.50
P_{dLS4}	24.91	68.10	19.55	150.97	62.32	66.28	87.39	152.30	62.32
Q_{dLS1}	79.93	22.04	27.55	7.00	29.67	188.01	97.46	154.04	29.67
Q_{dLS2}	23.25	15.01	158.23	131.72	199.51	130.12	12.40	165.56	199.51
Q_{dLS3}	62.16	18.98	79.25	159.37	127.90	167.04	182.84	25.07	127.90
Q_{dLS4}	64.72	34.25	27.65	15.14	93.61	37.46	47.43	3.17	93.61
F_{Set}	29.6092	31.0154	38.6825	29.9719	31.3951	35.3067	29.7719	31.1045	34.2645
F_{Total}	26.4697	26.6658	27.9327	26.4359	27.6084	28.5789	26.9453	26.9263	27.8891

*Notes: Unit for Q_d = MVAr, P_d = MW, *FVSI* = p.u., Loss = MW and Size = MW

Table 4.24 shows the results of MOECSEP application in load shedding scheme for Scenario 1 for Case 1 where the weightage is $w_1 = 0.9,\ w_2 = 0.1$. From Table 4.24, at Bus 33 with reactive power loading at 15 MVAr, the system experience *FVSI* improvement, with $FVSI_{LS}$ = 0.4723, and resilience values of $R1_{FVSI}$ = 2.23 and $R2_{FVSI}$ = 2.41. The loss-based resilience also experience improvement, increasing from $R1_{Loss}$ = 4.10 to $R2_{Loss}$ = 4.38. The MOECSEP developed an optimal load shedding plan by choosing four essential buses which included Buses 7, 6, 9 and 12. The active power to be shed at Bus 7 worth 193.38 MW while Bus 6, 9 and 12 require 170.09 MW, 173.50 MW and 62.32 MW. The required reactive power to be shed at these buses are 29.67 MVAr, 199.51 MVAr, 127.90 MVAr, and 93.61 MVAr, respectively. The buses experienced major power reductions because power reduction at these buses was

essential for achieving voltage stability and relieving network stress after the hurricane event. This initiative leads to the reduction of total fitness value from 34.2645 to 27.8891. Further results can be explored from the same table.

B. Scenario 2

In Scenario 2, where hurricane has affected different lines in the system; MOECSEP was also implemented to address the voltage stability improvement and loss minimisation. Table 4.25 presents the performance of the MOECSEP algorithm in implementing a load shedding scheme under Scenario 2 hurricane conditions in the IEEE 57-Bus RTS, for Case 1 with a weight configuration of $w_1 = 0.1,\ w_2 = 0.9$. Generally, the hurricane event in Scenario 2 has caused the increment of power loss and *FVSI* values in the system regardless of any Q_d values. The reactive power demand at Bus 31 worth 15 MVAR can be used to explain the phenomenon. At this Q_d value, the system initially exhibits a power loss of 30.56 MW ($Loss_{Set}$) and a pre-disturbance voltage security index of 0.4339 ($FVSI_{\mathrm{Set}}$). Following the Scenario 2 hurricane disturbance, the power loss increases to 30.88 MW ($Loss_{Out}$) and the *FVSI* value rises to 1.0000 ($FVSI_{\mathrm{Out}}$), indicating severe system degradation. After applying the optimised load shedding strategy, the post-curtailment power loss is 30.88 MW ($Loss_{LS}$), while the voltage security index reduces to 0.4414 ($FVSI_{LS}$). The resilience analysis reflects the effectiveness of the load shedding action: $R1_{Loss}$= 1.27 improves to $R2_{Loss}$ = 1.30, suggesting a modest gain in power loss recovery. Improvement is also observed in voltage resilience, with $R1_{FVSI}$ = 0.77 increasing to $R2_{FVSI}$ = 0.79. The algorithm identified Buses 51, 45, 49, and 36 as the optimal locations for load curtailment.

The corresponding active power reductions at these buses were 111.09 MW (Bus 51), 52.01 MW (Bus 45), 114.86 MW (Bus 49), and 63.70 MW (Bus 36). Meanwhile, the reactive power shedding values are 85.97 MVAr, 91.05 MVAr, 102.51 MVAr, and 34.09 MVAr, respectively. This effort managed to minimise the total fitness value to F_{Total} = 3.4850 from its original value of 6.3694.

Table 4.25
Results of MOECSEP Application in Load Shedding Scheme for Scenario 2 Hurricane Strike for Case 1 in IEEE 57-Bus RTS

Bus	**31**			**32**			**33**		
Q_d	**5**	**10**	**15**	**5**	**10**	**15**	**5**	**10**	**15**
$Loss_{Set}$	28.46	29.22	30.56	28.67	29.42	30.66	28.56	29.30	30.55
$FVSI_{Set}$	0.4028	0.3977	0.4339	0.4005	0.3948	0.4973	0.4016	0.3960	0.4613
$Loss_{Out}$	47.34	49.47	54.69	47.77	49.81	55.06	47.52	49.56	53.90
$FVSI_{Out}$	0.4521	0.4518	1.0000	0.4520	0.4516	0.7846	0.4520	0.4518	0.7086
$Loss_{LS}$	29.44	29.89	30.88	29.17	30.23	31.63	29.30	30.85	31.53
$R1_{Loss}$	1.51	1.44	1.27	1.50	1.44	1.26	1.51	1.45	1.31
$R2_{Loss}$	1.65	1.53	1.30	1.57	1.54	1.35	1.61	1.65	1.41
$FVSI_{LS}$	0.4120	0.4007	0.4414	0.4109	0.4015	0.5123	0.4168	0.4018	0.4705
$R1_{FVSI}$	8.17	7.35	0.77	7.78	6.95	1.73	7.97	7.10	1.87
$R2_{FVSI}$	10.27	7.84	0.79	10.00	8.01	1.88	11.84	8.04	1.98
Loc_{LS1}	17	48	51	43	48	38	25	5	5
Loc_{LS2}	27	35	45	31	30	52	13	45	38
Loc_{LS3}	37	10	49	46	43	43	14	23	1
Loc_{LS4}	21	1	36	33	18	15	4	4	15
P_{dLS1}	83.47	55.88	111.09	11.06	65.37	70.71	72.28	1.98	66.57
P_{dLS2}	42.30	27.80	52.01	114.70	19.87	30.03	128.86	126.98	104.31
P_{dLS3}	80.71	70.33	114.86	158.55	60.87	167.90	43.70	50.41	16.46
P_{dLS4}	21.74	36.74	63.70	0.13	6.48	3.03	58.51	145.79	161.53
Q_{dLS1}	72.38	138.62	85.97	35.11	93.19	19.09	70.10	160.17	136.32
Q_{dLS2}	19.35	16.46	91.05	121.11	10.01	127.34	28.91	35.06	118.95
Q_{dLS3}	40.75	8.61	102.51	165.41	74.55	72.72	63.67	184.03	40.81
Q_{dLS4}	77.38	72.09	34.09	14.53	68.15	101.30	82.09	82.00	40.06
F_{Set}	5.1409	5.3532	6.3694	5.1836	5.3876	6.2124	5.1590	5.3626	6.0279
F_{Total}	3.3152	3.3500	3.4850	3.2864	3.3845	3.6243	3.3053	3.4468	3.5763

*Notes: Unit for Q_d = MVAr, P_d = MW, *FVSI* = p.u., Loss = MW and Size = MW

Adjustment of weight coefficient values as in Case 2 can be reflected in Table 4.26 for IEEE 57-Bus RTS, where equal emphasis is placed on minimizing power losses and enhancing voltage security. The discussion here centres on Bus 32 with Q_d = 15 MVAr, a case representing a high-stress condition for resilience assessment. At this loading level, the system initially records a power loss of 30.66 MW ($Loss_{Set}$) and an *FVSI* of 0.4973 ($FVSI_{Set}$) under pre-disturbance conditions.

Table 4.26
Results of MOECSEP Application in Load Shedding Scheme for Scenario 2 Hurricane Strike for Case 2 in IEEE 57-Bus RTS

Bus	**31**			**32**			**33**		
Q_d	**5**	**10**	**15**	**5**	**10**	**15**	**5**	**10**	**15**
$Loss_{Set}$	28.46	29.22	30.56	28.67	29.42	30.66	28.56	29.30	30.55
$FVSI_{Set}$	0.4028	0.3977	0.4339	0.4005	0.3948	0.4973	0.4016	0.3960	0.4613
$Loss_{Out}$	47.34	49.47	54.69	47.77	49.81	55.06	47.52	49.56	53.90
$FVSI_{Out}$	0.4521	0.4518	1.0000	0.4520	0.4516	0.7846	0.4520	0.4518	0.7086
$Loss_{LS}$	28.96	30.52	30.97	29.21	30.53	30.99	29.86	29.98	30.89
$R1_{Loss}$	1.51	1.44	1.27	1.50	1.44	1.26	1.51	1.45	1.31
$R2_{Loss}$	1.58	1.61	1.30	1.57	1.58	1.29	1.69	1.53	1.34
$FVSI_{LS}$	0.4097	0.4011	0.4485	0.4116	0.4001	0.5067	0.4143	0.4036	0.4785
$R1_{FVSI}$	8.17	7.35	0.77	7.78	6.95	1.73	7.97	7.10	1.87
$R2_{FVSI}$	9.66	7.91	0.81	10.19	7.77	1.82	10.99	8.37	2.08
Loc_{LS1}	50	38	16	27	48	38	25	5	16
Loc_{LS2}	30	29	55	32	30	52	13	45	23
Loc_{LS3}	43	17	43	4	43	43	14	23	45
Loc_{LS4}	57	51	39	50	18	15	4	4	15
P_{dLS1}	85.03	0.24	42.47	12.39	81.15	140.74	58.84	98.70	114.56
P_{dLS2}	82.64	42.39	98.54	170.58	14.55	36.39	162.18	182.78	31.84
P_{dLS3}	168.85	113.78	85.43	83.05	63.95	45.22	187.31	41.45	189.05
P_{dLS4}	7.21	104.84	20.14	135.83	21.76	133.29	71.01	151.14	164.27
Q_{dLS1}	22.63	139.65	37.72	46.47	5.09	108.41	42.85	65.15	31.08
Q_{dLS2}	177.98	12.91	197.22	97.31	90.45	166.34	34.64	32.09	8.22
Q_{dLS3}	136.85	22.60	163.67	150.71	53.75	170.44	77.06	151.71	68.72
Q_{dLS4}	82.36	66.74	20.36	125.30	148.35	29.68	55.52	100.44	22.00
F_{Set}	23.8961	24.9588	27.8704	24.1100	25.1317	27.9234	23.9872	25.0058	27.3050
F_{Total}	14.6864	15.4626	15.7070	14.8127	15.4672	15.7491	15.1347	15.1934	15.6858

*Notes: Unit for Q_d = MVAr, P_d = MW, *FVSI* = p.u., Loss = MW and Size = MW

Following the hurricane disruption, power loss increases significantly to 55.06 MW ($Loss_{Out}$), while the *FVSI* increases to 0.7846 ($FVSI_{Out}$), indicating voltage security degradation. The application of the MOECSEP-based load shedding strategy results in a reduced post-curtailment power loss of 30.99 MW ($Loss_{LS}$) and improved *FVSI* performance of 0.5067 ($FVSI_{LS}$). The resilience indices further illustrate the system recovery capability. Power loss resilience slightly increases from $R1_{Loss}$ = 1.26 to $R2_{Loss}$ = 1.29, while the voltage security resilience improves more substantially from $R1_{FVSI}$ = 1.73 to $R2_{FVSI}$ = 1.82, reflecting successful mitigation of post-disturbance voltage instability. The algorithm identified Buses 38, 52, 43, and 15 as optimal curtailment locations. The respective active power shedding values were 140.74 MW, 36.39 MW, 45.22 MW, and 133.29 MW. In parallel, the reactive power to be shed are 108.41

MVAr, 166.34 MVAr, 170.44 MVAr, and 29.68 MVAr. The total fitness value has been reduced to 15.7491 from its original value of 27.9234. These results indicate that for high reactive demand at Bus 32, the MOECSEP algorithm, when applied with a balanced weight setting, effectively mitigates the impacts of severe disturbances by simultaneously improving voltage conditions and reducing losses in the system.

Table 4.27
Results of MOECSEP Application in Load Shedding Scheme for Scenario 2 Hurricane Strike for Case 3 in IEEE 57-Bus RTS

Bus	**31**			**32**			**33**		
Q_d	**5**	**10**	**15**	**5**	**10**	**15**	**5**	**10**	**15**
$Loss_{Set}$	28.46	29.22	30.56	28.67	29.42	30.66	28.56	29.30	30.55
$FVSI_{Set}$	0.4028	0.3977	0.4339	0.4005	0.3948	0.4973	0.4016	0.3960	0.4613
$Loss_{Out}$	47.34	49.47	54.69	47.77	49.81	55.06	47.52	49.56	53.90
$FVSI_{Out}$	0.4521	0.4518	1.0000	0.4520	0.4516	0.7846	0.4520	0.4518	0.7086
$Loss_{LS}$	29.02	30.55	30.96	29.01	30.99	31.64	29.65	30.85	31.63
$R1_{Loss}$	1.51	1.44	1.27	1.50	1.44	1.26	1.51	1.45	1.31
$R2_{Loss}$	1.58	1.61	1.30	1.55	1.65	1.35	1.66	1.65	1.42
$FVSI_{LS}$	0.4087	0.4006	0.4435	0.4197	0.4007	0.5013	0.4198	0.4014	0.4773
$R1_{FVSI}$	8.17	7.35	0.77	7.78	6.95	1.73	7.97	7.10	1.87
$R2_{FVSI}$	9.42	7.82	0.80	12.99	7.87	1.77	13.04	7.96	2.06
Loc_{LS1}	7	19	6	11	10	24	8	6	19
Loc_{LS2}	13	11	13	16	14	14	11	11	5
Loc_{LS3}	8	5	8	14	13	11	13	12	12
Loc_{LS4}	12	7	7	17	17	16	6	9	6
P_{dLS1}	33.40	61.76	80.73	43.21	162.84	142.02	73.13	74.72	140.83
P_{dLS2}	124.05	67.66	33.80	27.55	141.62	175.81	197.38	43.92	115.50
P_{dLS3}	174.38	97.97	13.66	19.55	38.62	71.88	28.81	187.29	54.22
P_{dLS4}	17.61	156.29	111.58	99.65	61.72	17.97	120.43	62.91	119.80
Q_{dLS1}	74.72	34.33	91.36	138.24	124.62	32.21	1.10	66..7533	6.65
Q_{dLS2}	43.92	118.93	94.31	157.24	1.14	83.36	95.94	171.25	57.26
Q_{dLS3}	187.29	31.29	19.02	27.55	183.25	60.32	127.80	22.40	26.49
Q_{dLS4}	62.91	78.09	121.32	82.47	178.37	115.21	49.05	164.74	148.34
F_{Set}	42.6513	44.5643	49.3294	43.0364	44.8758	49.6344	42.8153	44.6489	48.5820
F_{Total}	26.1564	27.5322	27.9117	26.1521	27.9269	28.5220	26.7253	27.8080	28.5106

*Notes: Unit for Q_d = MVAr, P_d = MW, *FVSI* = p.u., Loss = MW and Size = MW

This final part of the simulation results for this section assesses the performance of the MOECSEP load shedding strategy under Scenario 2 hurricane conditions using a power-loss-focused in Case 3 with weight configuration $w_1 = 0.9,\ w_2 = 0.1$. The results are summarized in Table 4.27, which evaluates load shedding responses across reactive power variation involving Bus 31, Bus 32, and Bus 33 for three levels of

reactive demand. This discussion highlights the outcome for Bus 32 with Q_d = 10 MVAr, as indicated in the shaded portion of the Table 4.27. Under this loading condition, the system experiences a baseline power loss of 29.42 MW ($Loss_{Set}$) and a pre-disturbance *FVSI* of 0.3948 ($FVSI_{Set}$). Upon the hurricane disturbance, the power loss increases significantly to 49.81 MW ($Loss_{Out}$) and *FVSI* rises to 0.4516 ($FVSI_{Out}$), reflecting a moderately stressed condition. Upon executing the MOECSEP-based load shedding scheme, the system power loss is reduced to 30.99 MW ($Loss_{LS}$). At the same time, the *FVSI* value reduces to 0.4007 ($FVSI_{LS}$). In terms of resilience, the power loss metric shows improvement, with $R1_{Loss}$ = 1.44 improving to $R2_{Loss}$ = 1.65. Voltage security resilience shows a slight improvement as well, increasing from $R1_{FVSI}$ = 6.95 to $R2_{FVSI}$ = 7.87. The four buses identified as the optimal curtailment locations were Buses 10, 14, 13, and 17. The active power for load shedding values at these locations are 162.84 MW at Bus 10, 141.62 MW at Bus 14, 38.62 MW at Bus 13, and 61.72 MW at Bus 17. Concurrently, the reactive power curtailment for theses buses amounted to 124.62 MVAr, 1.14 MVAr, 183.25 MVAr, and 178.37 MVAr, respectively. However, the overall optimisation cost is reflected in the total fitness value of F_{Total} = 27.9269 which has been reduced from 44.8758. This highlights the need for careful selection of objective weightings in resilience planning, particularly when both energy efficiency and voltage stability must be balanced under extreme weather scenarios.

Table 4.28 summarizes the comparative studies of F_{Total} results for DG installation with respect to reactive load variations at Bus 31, Bus 32, and Bus 33 in the IEEE 57-Bus RTS under both Scenario 1 and Scenario 2. In Scenario 1, at Q_{d33} = 15 MVAr, the results highlight the impact of the weight coefficient settings on the overall fitness performance F_{Total}. When more emphasis is given to voltage security improvement $w_1 = 0.1,\ w_2 = 0.9$, the lowest fitness value is recorded worth F_{Total} = 3.5124. This reflects the effectiveness of prioritizing the *FVSI* in enhancing system resilience. As the weight shifts toward a balanced configuration $w_1 = 0.5,\ w_2 = 0.5$, the total fitness increases moderately to F_{Total} = 15.7024, indicating a trade-off between minimizing voltage security and reducing power losses. The highest value is observed when loss minimization dominates $w_1 = 0.9,\ w_2 = 0.1$, reaching F_{Total} of 27.8891. Thus, setting higher weigh to *FVSI* will lead to the lowest total fitness value, while high weight coefficient on loss can cause high F_{Total} in the system regardless of any load subjected to the system.

Under Scenario 2, the same pattern is observed with slight variations in

performance. When voltage security is given greater importance $w_1 = 0.1,\ w_2 = 0.9$, with reactive power increment at Bus 33 yields a slightly increased minimum fitness value of F_{Total} =3.5763. For the balanced setting $w_1 = 0.5,\ w_2 = 0.5$, the fitness value remains consistent with Scenario 1, recording F_{Total} = 15.6858. This consistency implies robustness of the MOECSEP algorithm in balancing voltage and loss under different grid conditions. The maximum total fitness cost occurs again when more importance is placed on power loss minimization $w_1 = 0.9,\ w_2 = 0.1$, reaching F_{Total} = 28.5106, slightly higher than in Scenario 1. This increase reflects a heightened sensitivity of the power system to real power losses under stressed conditions, reinforcing the importance of strategic weight tuning post-disturbance. The MOECSEP algorithm demonstrates strong adaptability to different weight strategies, but prioritizing voltage security yields the most reliable and stable outcomes under extreme conditions.

Table 4.28
Comparative Results of F_{Total} for Load Shedding Scheme Using MOECSEP in IEEE 57-Bus RTS

Bus		**31**			**32**			**33**		
Q_d		**5**	**10**	**15**	**5**	**10**	**15**	**5**	**10**	**15**
Scenario 1										
F_{Total}	**w_1=0.1 w_2=0.9**	3.3037	3.3626	3.5305	3.3357	3.4246	3.5776	3.3023	3.4315	3.5124
	w_1=0.5 w_2=0.5	14.6864	15.5266	15.7108	14.8858	15.1319	15.7165	15.1374	15.1935	15.7024
	w_1=0.9 w_2=0.1	26.4697	26.6658	27.9327	26.4359	27.6084	28.5789	26.9453	26.9263	27.8891
Scenario 2										
F_{Total}	**w_1=0.1 w_2=0.9**	3.3152	3.3500	3.4850	3.2864	3.3845	3.6243	3.3053	3.4468	3.5763
	w_1=0.5 w_2=0.5	14.6864	15.4626	15.7070	14.8127	15.4672	15.7491	15.1347	15.1934	15.6858
	w_1=0.9 w_2=0.1	26.1564	27.5322	27.9117	26.1521	27.9269	28.5220	26.7253	27.8080	28.5106

4.5 Comparative Studies for DG Installation

This section presents a comprehensive comparative analysis of DG installation outcomes across two benchmark power system models, namely the IEEE 30-Bus and IEEE 57-RTS. The primary objective is to evaluate and compare the effectiveness of the proposed Multi-Objective Evolutionary Clonal Squirrel Search Algorithm (MOECSEP) against two established optimisation techniques: Multi-Objective Evolutionary Programming (MOEP) and Multi-Objective Squirrel Search Algorithm (MOSS). The comparison is performed under identical simulation conditions and performance objectives, which include the minimization of power losses and the enhancement of voltage security through DG installation. By applying each algorithm to both test systems under multiple reactive power loading scenarios, this section aims to highlight the relative strengths and capabilities of the proposed MOECSEP technique in terms of achieving the lowest total fitness value, along with the associated *FVSI* and loss as compared to MOSS and MOEP as the benchmarked multi-objective optimization techniques.

4.5.1 Comparative Studies for DG Installation in IEEE 30-Bus RTS

This section presents a comparative analysis of three multi-objective optimisation techniques: MOEP, MOSS, and MOECSEP for DG installation across selected buses in the IEEE 30-Bus RTS. The comparison is based on total power loss after DG placement ($Loss_{DG}$), the Fast Voltage Stability Index ($FVSI_{\mathrm{DG}}$), and the combined fitness value (F_{Total}) under two distinct scenarios. The emphasize concerns more on F_{Total} rather the individual *FVSI* value and power loss. However, the achievement of minimal F_{Total}, will conventionally lead to low *FVSI* and power loss in the system.

Table 4.29 tabulates the performance comparison of multi-objective optimisation algorithms for DG installation in the IEEE 30-Bus RTS, using weight coefficients of Case 1 with $w_1 = 0.1$ and $w_2 = 0.9$. Under Scenario 1, the proposed MOECSEP algorithm consistently demonstrates superior performance across all Q_d levels. For example, at Bus 30 with Q_d =25 MVAr, MOECSEP achieves the lowest total fitness value of F_{Total} = 2.8554, compared to 2.9459 by MOEP and 2.9118 by MOSS. The corresponding power loss is 23.22 MW, which is also lower than MOEP (23.98

MW) and MOSS (23.78 MW), indicating that MOECSEP is more effective in minimizing real power loss while enhancing voltage security. In terms of *FVSI*, MOECSEP yields 0.5932, which is lower than both MOEP (0.6084) and MOSS (0.6007), showing better voltage security.

Table 4.29
Performance Comparison of Multi-Objective Optimisation Algorithms for DG Installation in IEEE 30-Bus RTS for Case 1

Bus	**26**			**29**			**30**		
Q_d	**10**	**20**	**25**	**10**	**20**	**25**	**10**	**20**	**25**
MOEP									
Scenario 1									
$Loss_{DG}$	18.43	21.37	23.96	19.56	20.64	22.99	21.33	23.65	23.98
$FVSI_{DG}$	0.2498	0.5325	0.7421	0.2732	0.3901	0.5123	0.2901	0.4435	0.6084
F_{Total}	2.0678	2.6158	3.0642	2.2022	2.4146	2.7597	2.3936	2.7646	2.9459
Scenario 2									
$Loss_{DG}$	20.32	23.66	24.13	19.45	22.22	24.37	20.21	22.04	24.03
$FVSI_{DG}$	0.2685	0.6519	0.6921	0.2521	0.4523	0.6087	0.2953	0.5121	0.6128
F_{Total}	2.2738	2.9526	3.0354	2.1721	2.6286	2.9843	2.2871	2.6645	2.9548
MOSS									
Scenario 1									
$Loss_{DG}$	18.65	20.98	23.87	19.79	20.23	22.66	20.25	23.12	23.78
$FVSI_{DG}$	0.2365	0.5300	0.7495	0.2721	0.3821	0.5236	0.2893	0.4325	0.6007
F_{Total}	2.0781	2.5754	3.0618	2.2234	2.3670	2.7371	2.2859	2.7014	2.9188
Scenario 2									
$Loss_{DG}$	20.03	23.49	23.47	19.42	21.32	24.32	20.12	21.23	24.00
$FVSI_{DG}$	0.2687	0.6412	0.6875	0.2436	0.4511	0.5932	0.2937	0.5012	0.5932
F_{Total}	2.2451	2.9258	2.9656	2.1616	2.5381	2.9661	2.2768	2.5742	2.9336
MOECSEP									
Scenario 1									
$Loss_{DG}$	18.25	20.35	23.23	19.35	19.70	21.25	19.86	22.22	23.22
$FVSI_{DG}$	0.2290	0.5012	0.7321	0.2546	0.3845	0.4932	0.2854	0.4238	0.5932
F_{Total}	2.0306	2.4864	2.9821	2.1646	2.3158	2.5693	2.2432	2.6030	2.8554
Scenario 2									
$Loss_{DG}$	19.87	22.35	23.65	19.33	20.37	23.25	19.35	20.27	23.32
$FVSI_{DG}$	0.2534	0.5016	0.6724	0.2364	0.4123	0.5841	0.2914	0.4635	0.5432
F_{Total}	2.2154	2.6868	2.9706	2.1453	2.4077	2.8511	2.1977	2.4437	2.8210

Under Scenario 2, where the system faces more stressed conditions, MOECSEP continues to outperform the other two techniques. For Bus 30 at Q_d = 25 MVAr, MOECSEP records the lowest fitness value of F_{Total}=2.8210 with a reduced power loss of 23.32 MW and improved *FVSI* of 0.5432. In contrast, MOEP and MOSS yield higher loss values of 24.03 MW and 24.00 MW, respectively, along with higher fitness costs, indicating less effective mitigation. The reduced loss and *FVSI* values indicate that MOECSEP performs better when the system is under stress. Results for other reactive power loadings involving all the subjected loads for all scenarios by all the optimization techniques can be referred to the same table. This phenomenon technically causes the

increment of power system resilience when referred to the results in the earlier sections (Sections 4.4.1.1).

4.5.2 Comparative Studies for DG Installation in IEEE 57-Bus RTS

This study proceeds with the performance comparison of multi-objective algorithms for DG installation in IEEE 57-Bus RTS with weight coefficient in Case 1 with $w_1 = 0.1$ and $w_2 = 0.9$. In general, increment of Q_d at all load buses will increase the power loss in the system. The performance comparison is tabulated in Table 4.30. Under Scenario 1, the MOECSEP algorithm exhibits superior performance compared to the other two techniques. At Q_{d31}=15 MVAr, it achieves the lowest total fitness value of F_{Total} = 3.6068, compared to 3.7848 by MOEP and 3.7000 by MOSS.

Table 4.30
Performance Comparison of Multi-Objective Optimisation Algorithms for DG Installation in IEEE 57-Bus RTS for Case 1

Bus	**31**			**32**			**33**		
Q_d	**5**	**10**	**15**	**5**	**10**	**15**	**5**	**10**	**15**
MOEP									
Scenario 1									
$Loss_{DG}$	30.99	31.93	32.93	30.93	31.85	32.54	30.96	31.96	32.84
$FVSI_{DG}$	0.4137	0.4162	0.5463	0.4236	0.4197	0.5236	0.4207	0.4132	0.5014
F_{Total}	3.4710	3.5677	3.7848	3.4745	3.5623	3.7255	3.4750	3.5681	3.7356
Scenario 2									
$Loss_{DG}$	32.24	32.33	33.70	32.60	32.10	33.08	30.90	32.30	33.84
$FVSI_{DG}$	0.4197	0.4176	0.4631	0.4268	0.4287	0.5415	0.4287	0.4193	0.5164
F_{Total}	3.6021	3.6088	3.7865	3.6439	3.5956	3.7950	3.4755	3.6071	3.8491
MOSS									
Scenario 1									
$Loss_{DG}$	30.93	31.06	32.21	30.15	30.96	32.52	30.33	31.24	32.33
$FVSI_{DG}$	0.4124	0.4068	0.5320	0.4196	0.4136	0.5193	0.4199	0.4193	0.4932
F_{Total}	3.4643	3.4726	3.7000	3.3931	3.4686	3.7195	3.4107	3.5011	3.6764
Scenario 2									
$Loss_{DG}$	31.54	31.64	33.52	31.04	31.04	33.03	30.39	31.56	33.64
$FVSI_{DG}$	0.4193	0.4125	0.4536	0.4204	0.4218	0.5247	0.4293	0.4121	0.5016
F_{Total}	3.5310	3.5348	3.7606	3.4819	3.4832	3.7751	3.4258	3.5273	3.8157
MOECSEP									
Scenario 1									
$Loss_{DG}$	29.32	30.01	31.55	29.32	30.72	31.65	29.04	30.32	31.24
$FVSI_{DG}$	0.4065	0.4036	0.5023	0.4135	0.4007	0.5097	0.4132	0.4068	0.4732
F_{Total}	3.2980	3.3645	3.6068	3.3043	3.4331	3.6240	3.2756	3.3986	3.5497
Scenario 2									
$Loss_{DG}$	29.37	30.68	31.24	29.85	30.68	32.07	29.64	30.40	32.06
$FVSI_{DG}$	0.4103	0.4001	0.4431	0.4196	0.4103	0.5157	0.4104	0.4015	0.4802
F_{Total}	3.3061	3.4285	3.5228	3.3628	3.4377	3.6707	3.3331	3.4012	3.6387

This indicates that MOECSEP is more effective in minimizing the total fitness value, especially when higher priority is given to voltage stability. In terms of *FVSI*, MOECSEP records a value of 0.5023, which is lower than MOEP (0.5463) and MOSS (0.5320), highlighting better voltage stability. Furthermore, the power loss is also the lowest for MOECSEP at 31.55 MW, compared to 32.93 MW (MOEP) and 32.21 MW (MOSS). These findings validate the effectiveness of the proposed MOECSEP technique achieving the lowest F_{Total}, along with the lowest *FVSI* and power loss with DG installation which in turns maintaining system efficiency and voltage integrity under heavy loading. This phenomenon can also be witnessed for other reactive power loading values.

The performance trend continues in Scenario 2, where the system is under stress due to a disturbance. MOECSEP again records the lowest fitness value of F_{Total} = 3.5338, followed by MOSS (3.7606) and MOEP (3.7865). Apparently MOECSEP consistently outperformed both MOEP and MOSS in achieving the lowest F_{Total} in the system through the DG installation. This improvement illustrates MOECSEP adaptability and robustness under contingency conditions due to hurricanes in two scenarios. The *FVSI* value with MOECSEP is 0.4431, significantly lower than MOEP (0.4631) and MOSS (0.4536). Meanwhile, power loss is also lowest under MOECSEP at 31.24 MW, compared to 33.70 MW (MOEP) and 33.52 MW (MOSS), reaffirming its superiority in reducing system losses and maintaining voltage performance during adverse conditions. The comparative results for Q_{d31} = 15 MVAr clearly demonstrate that MOECSEP consistently outperforms MOEP and MOSS in both hurricane scenarios. With lower fitness values, reduced power losses, and improved voltage security indices, MOECSEP proves to be the most effective optimisation method for DG installation. These outcomes suggest that MOECSEP is well-suited for enhancing system resilience and operational reliability in heavily loaded buses within large-scale power networks like the IEEE 57-Bus RTS. This phenomenon technically causes the increment of power system resilience when referred to the results in the earlier sections (Sections 4.4.1.2). The complete results for other reactive power loadings for all subjected buses using all the optimization techniques can be referred to the same table for both hurricane scenarios.

4.6 Comparative Studies for Load Shedding Scheme

This section focuses on the comparative analysis of load shedding schemes applied to two standard power system models, the IEEE 30-Bus and IEEE 57-Bus RTS. The purpose of this study is to assess the performance of the proposed MOECSEP in comparison with MOEP and MOSS. All three algorithms are evaluated under identical hurricane-induced disturbance scenarios to determine their effectiveness in minimizing power loss and enhancing voltage security in an integrated fitness equation termed F_{Total} through optimal load curtailment strategy. The simulations are conducted across various reactive power demand levels and load buses to reflect different operating stress conditions. This comparison helps show how well MOECSEP improves system resilience compared to the other methods when facing severe disturbances.

4.6.1 Comparative Studies for Load Shedding in IEEE 30-Bus RTS

Table 4.31 tabulates the performance comparison of three multi-objective optimization techniques: MOEP, MOSS, and MOECSEP, applied to load shedding schemes in the IEEE 30-Bus RTS. Results are presented for both Scenario 1 and Scenario 2. In general, the increment of Q_d at all load buses will increase the power loss and *FVSI* in the system for all subjected load buses in both scenarios. In Scenario 1, at Q_{d29} = 25 MVAr, MOECSEP achieves the lowest power loss at 21.01 MW, compared to 22.65 MW for MOEP and 21.96 MW for MOSS. This indicates that MOECSEP is more efficient in minimizing system losses during load shedding execution. In terms of voltage security, MOECSEP achieves an $FVSI_{LS}$ value of 0.4851, which is also significantly lower than MOEP (0.5169) and MOSS (0.5127). This improvement reflects MOECSEP effectiveness in enhancing voltage security of the system. The total fitness value further confirms MOECSEP superiority, with the lowest F_{Total} = 2.5378, as compared to 2.7305 (MOEP) and 2.6576 (MOSS). Even *FVSI* and power loss have been integrated in one combined fitness equation, the implementation of load shedding scheme managed to satisfy both loss and *FVSI* reductions. This phenomenon technically causes the increment of power system resilience when referred to the results in the earlier sections (Sections 4.4.2.1). Under Scenario 2, MOECSEP continues to outperform the other algorithms. At Q_{d29} = 25 MVAr, it achieves the lowest system loss at 21.54 MW, outperforming MOEP (22.64 MW) and MOSS (22.78 MW). The

corresponding $FVSI_{LS}$ is 0.4731 for MOECSEP, again lower than MOEP (0.5014) and MOSS (0.4932), suggesting stronger voltage security performance.

Table 4.31
Performance Comparison of Multi-Objective Optimization Algorithms for Load Shedding Scheme in IEEE 30-Bus RTS for Case 1

Bus	**26**			**29**			**30**		
Q_d	**10**	**20**	**25**	**10**	**20**	**25**	**10**	**20**	**25**
MOEP									
Scenario 1									
$Loss_{LS}$	18.39	20.44	22.51	19.32	20.32	22.65	20.22	22.03	22.04
$FVSI_{LS}$	0.2904	0.5224	0.7425	0.2415	0.3934	0.5169	0.2415	0.4379	0.5715
F_{Total}	2.1002	2.5145	2.9191	2.1494	2.3862	2.7305	2.2389	2.5974	2.7182
Scenario 2									
$Loss_{LS}$	20.03	21.70	24.25	19.03	21.56	22.64	19.32	23.65	23.55
$FVSI_{LS}$	0.2518	0.5264	0.7124	0.2531	0.4285	0.5014	0.2435	0.4632	0.5876
F_{Total}	2.2299	2.6436	3.0666	2.1311	2.5421	2.7152	2.1516	2.7820	2.8837
MOSS									
Scenario 1									
$Loss_{LS}$	18.42	20.43	22.44	18.99	20.36	21.96	21.03	21.99	21.93
$FVSI_{LS}$	0.2659	0.5124	0.7120	0.2378	0.3815	0.5127	0.2531	0.4328	0.5531
F_{Total}	2.0816	2.5043	2.8847	2.1128	2.3796	2.6576	2.3311	2.5890	2.6910
Scenario 2									
$Loss_{LS}$	20.23	21.04	23.25	18.93	20.84	22.78	19.24	22.56	22.36
$FVSI_{LS}$	0.2497	0.5287	0.6934	0.2347	0.4321	0.4932	0.2397	0.4215	0.5932
F_{Total}	2.2479	2.5797	2.9486	2.1044	2.4732	2.7223	2.1394	2.6358	2.7698
MOECSEP									
Scenario 1									
$Loss_{LS}$	18.27	20.56	22.30	18.45	19.92	21.01	19.04	21.03	21.07
$FVSI_{LS}$	0.2431	0.4997	0.6875	0.2278	0.3745	0.4851	0.2387	0.4187	0.5488
F_{Total}	2.0453	2.5060	2.8490	2.0502	2.3295	2.5378	2.1186	2.4801	2.6005
Scenario 2									
$Loss_{LS}$	19.45	20.98	22.73	18.79	20.33	21.54	18.99	20.60	21.02
$FVSI_{LS}$	0.2451	0.5143	0.6756	0.2256	0.4028	0.4731	0.2314	0.4126	0.5547
F_{Total}	2.1659	2.5612	2.8813	2.0817	2.3951	2.5800	2.1070	2.4312	2.6017

As for the fitness value, MOECSEP reports F_{Total} = 2.5800 as the lowest F_{Total} value as compared to MOEP (2.7152) and MOSS (2.7223). The comparative results at Bus 29 with Q_d = 25 MVAr clearly show that MOECSEP consistently delivers the best performance among the three optimization methods. It achieves the lowest system losses, improved voltage security, and lowest total fitness values in both scenarios. These results confirm that MOECSEP is effective in carrying out load shedding and improving the resilience and performance of the IEEE 30-Bus RTS under disruptive events. This finding leads to the significant improvement of power system resilience as previously discussed in Section 4.4.2.1. The results for other reactive power loadings for both scenarios involving all the optimization techniques can be referred to the same table.

4.6.2 Comparative Studies for Load Shedding in IEEE 57-Bus RTS

Table 4.32 presents the results for comparative performance of three multi-objective optimization algorithms, MOEP, MOSS, and MOECSEP for load shedding schemes implemented in the IEEE 57-Bus RTS under Case 1 with the weight setting $w_1 = 0.1$ and $w_2 = 0.9$. In general, the implementation of MOECSEP in the load implementation exhibits its superiority as shown in the Table 4.32 in terms of achieving the lowest F_{Total}, along with the lowest *FVSI* and power loss values.

Table 4.32
Performance Comparison of Multi-Objective Optimization Algorithms for Load Shedding Scheme in IEEE 57-Bus RTS for Case 1

Bus	**31**			**32**			**33**		
Q_d	**5**	**10**	**15**	**5**	**10**	**15**	**5**	**10**	**15**
MOEP									
Scenario 1									
$Loss_{LS}$	29.99	30.55	32.33	30.24	31.04	32.63	30.91	31.04	31.35
$FVSI_{LS}$	0.4193	0.4188	0.5127	0.4199	0.4189	0.5327	0.4177	0.4186	0.4932
F_{Total}	3.3767	3.4316	3.6939	3.4017	3.4805	3.7426	3.4671	3.4806	3.5791
Scenario 2									
$Loss_{LS}$	29.85	30.94	31.85	29.89	30.91	32.83	30.45	31.96	32.89
$FVSI_{LS}$	0.4276	0.4196	0.4508	0.4185	0.4126	0.5146	0.4199	0.4198	0.4935
F_{Total}	3.3702	3.4721	3.5909	3.3654	3.4626	3.7463	3.4231	3.5742	3.7333
MOSS									
Scenario 1									
$Loss_{LS}$	29.85	30.02	31.98	29.86	30.94	32.00	30.85	30.94	31.23
$FVSI_{LS}$	0.4185	0.4154	0.5073	0.4186	0.4130	0.5178	0.4157	0.4098	0.4815
F_{Total}	3.3619	3.3762	3.6541	3.3631	3.4652	3.6657	3.4588	3.4625	3.5568
Scenario 2									
$Loss_{LS}$	29.96	30.64	31.64	29.65	30.63	32.35	29.89	31.52	32.64
$FVSI_{LS}$	0.4214	0.4113	0.4532	0.4188	0.4124	0.5173	0.4173	0.4039	0.4835
F_{Total}	3.3756	3.4337	3.5714	3.3422	3.4343	3.7010	3.3649	3.5159	3.6987
MOECSEP									
Scenario 1									
$Loss_{LS}$	29.32	29.94	31.3	29.64	30.63	31.27	29.33	30.65	30.87
$FVSI_{LS}$	0.4130	0.4098	0.4452	0.4135	0.4013	0.5009	0.4106	0.4067	0.4731
F_{Total}	3.3037	3.3626	3.5305	3.3357	3.4246	3.5776	3.3023	3.4315	3.5124
Scenario 2									
$Loss_{LS}$	29.44	29.89	30.88	29.17	30.23	31.63	29.30	30.85	31.53
$FVSI_{LS}$	0.4120	0.4007	0.4414	0.4109	0.4015	0.5123	0.4168	0.4018	0.4705
F_{Total}	3.3152	3.3500	3.4850	3.2864	3.3845	3.6243	3.3053	3.4468	3.5763

For example, in Scenario 1, Bus 33 with a reactive demand of Q_d =10 MVAr, witnesses MOECSEP algorithm delivers the best performance in terms of achieving the lowest F_{Total}, along with the lowest *FVSI* and power loss values. It achieves the lowest post-shedding system loss of 30.65 MW, compared to 31.04 MW under MOEP and

30.94 MW under MOSS. This indicates a more efficient reduction of active power resulted by the load shedding process.

From a voltage security perspective, MOECSEP yields the lowest $FVSI_{LS}$ value of 0.4067, outperforming both MOEP (0.4186) and MOSS (0.4098). This result highlights MOECSEP effectiveness in maintaining a more stable voltage profile during hurricane scenario. The total fitness value, F_{Total} , which combines both loss and voltage stability considerations, is also achieves the lowest value for MOECSEP worth 3.4315, followed by MOSS at 3.4625 and MOEP at 3.4806. These results clearly demonstrate MOECSEP consistently exhibits superior capability in delivering a balanced and resilient load shedding strategy.

In Scenario 2, the MOECSEP techniques continue to outperform the other two algorithms. It records the lowest system loss at 30.85 MW, which is lower than 31.96 MW (MOEP) and 31.52 MW (MOSS). The $FVSI_{LS}$ value remains the lowest for MOECSEP at 0.4018, while MOEP and MOSS record slightly higher values of 0.4198 and 0.4039, respectively. Furthermore, MOECSEP reports the most optimal total fitness value at 3.4468, compared to 3.5159 for MOSS and 3.5742 for MOEP. The comparative results at Bus 33 with Q_d = 10 MVAr validate that the MOECSEP technique consistently outperforms MOEP and MOSS in both scenarios. Therefore, MOECSEP proves to be the most effective strategy for load shedding at critical load buses in the IEEE 57-Bus RTS. This finding leads to the significant improvement of power system resilience as previously discussed. The results for other reactive power loadings for both scenarios involving all the optimization techniques can be referred to the same table.

4.7 Summary

This chapter has presented the study on Multi-Objective Embedded Clonal Squirrel Evolutionary Programming (MOECSEP) algorithm-based technique for resilience improvement in power system. The proposed MOECSEP algorithm has been formulated and consecutively demonstrated significant effectiveness in enhancing the resilience and operational performance of power systems. Through comprehensive simulations on the IEEE 30-Bus and 57-Bus RTS, the algorithm was applied to optimize two key strategies: DG installation and load shedding schemes, under two disturbance scenarios due to hurricane.

The results indicate that MOECSEP consistently outperformed benchmark algorithms such as MOEP and MOSS in minimizing system power loss and improving voltage stability, particularly under high load conditions. The integration of *FVSI* and power loss confined in F_{Total} has managed to exhibit the outstanding performance over MOEP and MOSS in both DG installation and load shedding strategies. The algorithm achieved a good balance between reducing losses and improving stability, as shown by its lower fitness values at all critical buses. This in turn improving the power system resilience even hurricane scenarios have been experienced by the system.

On the overall, the MOECSEP technique has proven to be a reliable and adaptive solution for resilience improvement, capable of responding efficiently to system disturbances and maintaining grid performance. Its hybridized optimisation structure positions it as a valuable tool for strategic planning in modern and future power systems, especially in the face of increasing uncertainty and extreme events.

CHAPTER 5
EMBEDDED CLONAL SQUIRREL EVOLUTIONARY PROGRAMMING (ECSEP)-BASED COMPOSITE STRATEGY FOR ENHANCING POWER SYSTEM SURVIVABILITY

5.1 Introduction

Electricity demand continues to grow rapidly, and when combined with the increasing frequency of natural disasters, it places significant stress on modern power networks, making power system survivability essential to keep critical services running during extreme conditions. An electrical power system demonstrates survivability through its ability to preserve vital operational tasks or restore vital loads at a fast pace after experiencing severe disturbances like natural disasters and equipment breakdowns and cyber-attacks.

The power system community now places greater emphasis on survivability because high-impact low-frequency events like hurricanes and wildfires and coordinated attacks frequently result in extensive power outages. The implementation of survivability measures protects critical infrastructure operations while improving disaster readiness and supports worldwide targets for dependable and protected energy delivery. The concept of survivability guides smart grid development through adaptive control systems and distributed resources which need proper planning and design and operational strategies.

This chapter presents a Composite Survivability Strategy (CSS) for power systems under extreme disturbance scenarios. To preserve the survivability of power system, DG installation and load shedding scheme is proposed. The proposed approach integrates DG installation and load shedding schemes, optimised using the developed Embedded Clonal Squirrel Evolutionary Programming (ECSEP) technique in the earlier chapter. The study is divided into two key objectives: minimizing total system power loss and reducing the *FVSI*, each evaluated under pre-outage and post-outage conditions simulating hurricane-induced line outages. The strategy is applied to two benchmark test systems: the IEEE 30-Bus and IEEE 57-Bus RTS.

Through this approach, the chapter demonstrates how supply-side reinforcement (via DG installation) and demand-side adjustment (via load shedding) can be co-

optimised to provide a balanced and effective strategy for improving survivability of power system. The outcomes are expected to offer valuable insights for future power system planning, particularly in designing grids that are robust, flexible, and capable of sustaining critical functions during catastrophic events.

5.2 Power System Survivability

Power system survivability refers to the capability of an electric power network to sustain the delivery of essential services during, and to rapidly recover after, extreme disturbances. Unlike conventional power system reliability, which primarily measures the frequency and duration of outages under normal operating conditions, survivability focuses on high-impact, low-probability events that can severely impair system performance, such as hurricanes, earthquakes, cyberattacks, cascading line failures, or large-scale equipment malfunctions. A survivable power system is one that can withstand severe disruptions without complete service collapse, isolate faults to prevent cascading failures, protect critical loads such as hospitals and emergency services, reconfigure operational pathways in real-time using network topology changes, and restore service rapidly after partial or total outages.

Survivability is closely related to but distinct from reliability and resilience. While reliability deals with the likelihood of uninterrupted service under normal or moderately stressed conditions, resilience focuses on the ability to adapt, absorb, and recover from disturbances while maintaining acceptable service levels. Survivability in this research is treated as a more event-specific, performance-oriented measure, targeting the system ability to maintain core functionality during the most severe and disruptive scenarios. It therefore incorporates both preventive measures, such as strategic DG placement and robust system design, and corrective actions, such as intelligent load shedding (LS) and network reconfiguration, to ensure minimal service disruption. Several technological and operational measures can be applied to strengthen power system survivability. DG provides local energy sources that can continue to supply loads when central generation is disrupted. Intelligent load shedding ensures that critical loads are given priority while non-essential demand is reduced to maintain stability. Thus, the role of ECSEP is crucial and relevant to ensure power system survivability.

In this research, survivability is quantified using two primary performance indicators, namely total real power loss and *FVSI*, as both indicators directly capture the effects of DG installation and load shedding strategies under extreme conditions. Minimizing system loss ensures efficient energy transfer even during outages, while reducing *FVSI* reflects improved voltage security and stability margins under stressed operations. Although DG installation and the load shedding scheme individually contribute to enhancing system performance, their combined application through a composite strategy leverages the strengths of both approaches: DG installation provides local supply support that reduces dependency on stressed transmission lines, whereas the load shedding scheme acts as a corrective mechanism to stabilize voltages and prevent cascading failures.

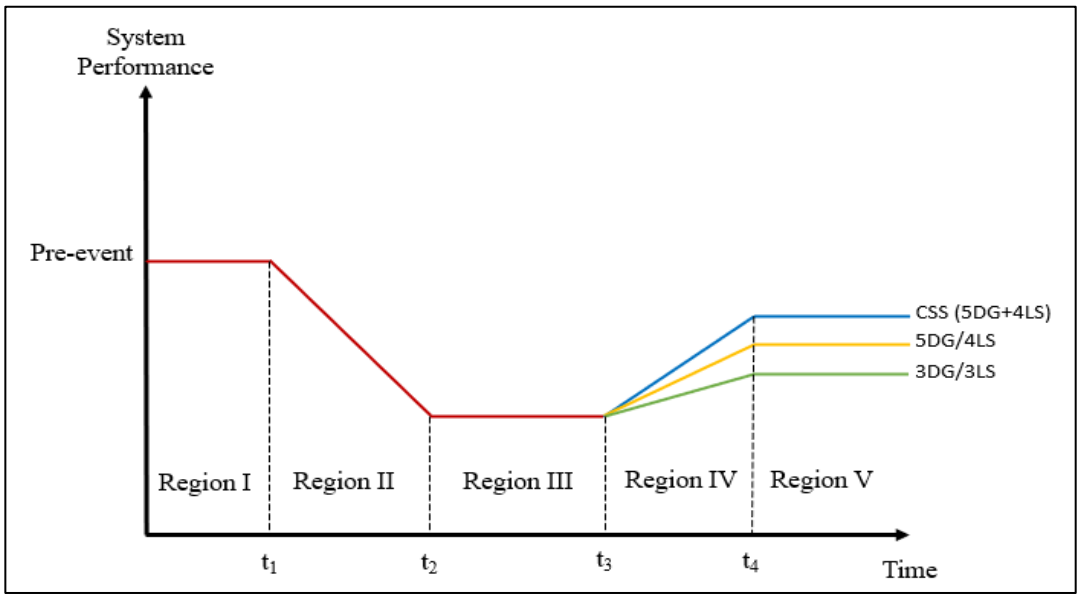


Figure 5.1 Conceptual Survivability Curve under Different Compensation Strategies

Figure 5.1 illustrates the general progression of system performance over time in response to an extreme disturbance. At the initial stage (Region I: $t < t_1$) the system operates under normal steady-state conditions with stable performance. When the outage occurs at t_2 (Region II: $t_1 < t < t_2$), a sharp decline in performance is observed, representing the immediate impact of the disturbance on network functionality. Without corrective measures, the system remains in a degraded state until t_3 (Region III: $t_2 < t < t_3$), when compensation techniques are applied to initiate recovery. The recovery trajectory from t_3 to t_4 (Region IV: $t_3 < t < t_4$), reflects the effectiveness of different

strategies in restoring the system to an acceptable performance level. At (Region V: $t > t_4$), the system has reached the secure region.

Studies have been conducted to evaluate the impact of stand-alone techniques such as DG installation and the load shedding scheme in various configurations. For instance, cases with three DG installations (3DG) and five DG installations (5DG) were tested to evaluate the extent to which additional distributed generation capacity enhances performance recovery. Similarly, load shedding schemes at three locations (3LS) and four locations (4LS) were examined to determine how strategic demand curtailment contributes to system stabilization under stressed operating conditions. These stand-alone applications demonstrate partial improvements in performance, with higher DG capacity or increased load shedding generally yielding better results compared to smaller configurations. However, the improvements achieved individually remain limited in scope.

To overcome these limitations, the Composite Survivability Strategy (CSS) was formulated by combining 5DG installation with the 4LS scheme in a coordinated manner. This integrated approach influences the strengths of both supply-side reinforcement and demand-side adjustment, enabling a more balanced and effective response to disturbances. As shown in the figure, the CSS achieves the highest post-recovery performance at t_4 compared to the stand-alone cases. This clearly demonstrates that co-optimizing DG installation and load shedding scheme produces superior survivability outcomes, ensuring faster recovery, improved stability margins, and a more reliable post-event operating state for the power system.

The proposed ECSEP algorithm plays a central role in this composite strategy by simultaneously optimizing DG installation placement and load shedding scheme allocation. Its chaotic component enhances global search diversity, the cloning operator preserves high-quality solutions, and the squirrel search mechanism accelerates convergence, enabling robust configurations even under severe outage scenarios. During hurricane-induced disturbances simulated on the IEEE 30-Bus RTS and IEEE 57-Bus RTS, the network experiences severe voltage instability and increased power losses due to multiple line outages. Without compensation, the *FVSI* approaches instability thresholds, leading to a high risk of cascading failures. By applying the ECSEP-based composite strategy, DG installation and load shedding scheme actions are coordinated to mitigate these adverse effects, maintaining acceptable *FVSI* values and restoring network performance close to pre-outage conditions. The framework

provides both technical resilience and operational continuity for essential facilities including hospitals and emergency services and communication infrastructure during disruptions which demonstrates the real-world value of this approach.

Table 5.1
Configuration of DG Installation and LS Strategies Parameters for Simulation Cases

DG Installation										
Parameters										
Cases	**L_1**	**L_2**	**L_3**	**L_4**	**L_5**	**S_1**	**S_2**	**S_3**	**S_4**	**S_5**
1DG	1	0	0	0	0	1	0	0	0	0
2DG	1	1	0	0	0	1	1	0	0	0
3DG	1	1	1	0	0	1	1	1	0	0
4DG	1	1	1	1	0	1	1	1	1	0
5DG	1	1	1	1	1	1	1	1	1	1

Load Shedding Scheme												
Parameters												
Cases	**L_1**	**L_2**	**L_3**	**L_4**	**P_{d1}**	**P_{d2}**	**P_{d3}**	**P_{d4}**	**Q_{d1}**	**Q_{d2}**	**Q_{d3}**	**Q_{d4}**
1LS	1	0	0	0	1	0	0	0	1	0	0	0
2LS	1	1	0	0	1	1	0	0	1	1	0	0
3LS	1	1	1	0	1	1	1	0	1	1	1	0
4LS	1	1	1	1	1	1	1	1	1	1	1	1

Table 5.1 tabulates the parameter configurations considered for DG installation and load shedding scheme in the simulation study. The simulation study uses the parameter settings from Table 5.1 to evaluate DG installation and load shedding scheme performance. These parameters are applied to evaluate the performance of the system under various DG and load shedding scenarios. The DG installation parameters consist of two categories: location variables (L_1-L_5), which specify the optimal locations for DG placement and sizing variables (S_1-S_5), which define the active power output of the installed DG units. The simulation cases are progressively arranged from 1DG to 5DG, representing the incremental addition of DG units to the system. The load shedding scheme comprises three categories of parameters: location variables (L_1-L_5), which indicate the buses subjected to load shedding; active power to be shed from the system (P_{d1}-P_{d4}); and reactive power to be shed from the system (Q_{d1}-Q_{d4}). The simulation considers four progressive load shedding scenarios, designated as 1LS, 2LS, 3LS and 4LS. The organized system design enables researchers to study on how DG systems and

load shedding methods affect power system performance when used separately and together.

The Table 5.1 shows '1' as an indicator that the parameter remains active for optimisation while ECSEP will search for it to meet the defined objective functions. The value '0' in the Table 5.1 indicates that the parameter stays outside the search area for that specific case thus remaining inactive during optimisation. For instance, a single DG installation involves two parameters, namely the location and size of the DG unit, while a single load shedding scheme requires three parameters confining: the location of the curtailed bus, active power to be shed (P_d), and reactive power to be shed (Q_d). Consequently, the total number of parameters that need to be optimised by ECSEP is directly determined by the number of DG units and load shedding schemes tabulated in a given case.

The CSS system integrates DG installation methods with load shedding schemes to create an integrated solution which boosts power system resilience against extreme disturbances. The study implements CSS through the implementation of 5DG units together with 4LS schemes conducted concurrently. The 5DG scheme depends on 10 parameters which include DG unit locations L_1 *to* L_5 and their active power sizing S_1 *to* S_5. The 4LS scheme needs 12 parameters to operate because each load shedding scheme requires 3 parameters which include L_1 *to* L_4, P_{d1} to P_{d4} and Q_{d1} to Q_{d4}. The 22 decision parameters in the CSS framework enable the optimization algorithm to simultaneously determine the optimal locations and sizes of DG, as well as the load shedding locations and their corresponding power reduction levels. The extensive parameterization allows the optimisation algorithm to link supply-side reinforcement with demand-side adjustment for better loss reduction and voltage stability improvement during severe disturbances.

5.3 Algorithm for Power System Survivability

The development of an effective algorithm for power system survivability is essential to ensure that the grid can withstand and recover from severe disturbances while maintaining the electricity delivery of critical services. This study defines survivability through two main aspects which include enduring rare high-impact events like hurricane-caused power outages and implementing fast and efficient preventive and corrective measures for system recovery. A computational system must exist to find the

best operational methods which reduce system performance decline and enhance recovery speed after disruptions.

The proposed survivability algorithm combines DG installation with intelligent load shedding through an integrated optimisation system that optimizes both preventive and corrective actions to boost system performance when facing contingency situations. The system uses total power loss and *FVSI* as performance indicators for decision-making because both indicators represent power transfer efficiency and voltage security levels. The algorithm achieves better operational performance and voltage stability through simultaneous optimisation during pre-outage and post-outage periods.

The study implements ECSEP as its optimisation technique to solve the problem. ECSEP combines the global search capability of the squirrel search algorithm with the local exploitation ability of evolutionary programming, enhanced by chaotic cloning for population diversity. Through iterative simulation of contingency conditions in the IEEE 30-Bus and IEEE 57-Bus RTS, the algorithm determines the most effective DG placements and load shedding schemes to improve survivability outcomes.

Figure 5.2 illustrates the overall procedure for implementing the ECSEP algorithm in the CSS, which integrates 5DG installations and 4LS schemes. The process begins by defining the parameters of the system, followed by obtaining the pre-outage and post-outage values to establish baseline performance before optimisation. The system generates random individuals that represent DG placement and LS scheme schemes before applying cloning to maintain high-quality solutions. The system evaluates the fitness values (Fitness I) of the redefined individuals to select the most promising candidates.

The algorithm introduces random squirrel positions to boost exploration and prevent early convergence. The algorithm updates candidate positions through the to choose the most successful candidates from both the 5DG and 4LS schemes. The position of each candidate is subsequently updated using the squirrel search equation, and new offspring fitness values (Fitness II) are calculated. The algorithm performs a tournament selection process performs this cycle repeatedly until it fulfils convergence requirements or reaches its predefined maximum number of iterations. The RI value is compared with a predefined threshold value to determine the survivability of the system. If the RI is greater than or equal to the specified threshold, the system is considered survivable. Otherwise, the system is classified as not survivable, and the optimization

process is repeated until the optimal solution that satisfies the survivability criterion is achieved.

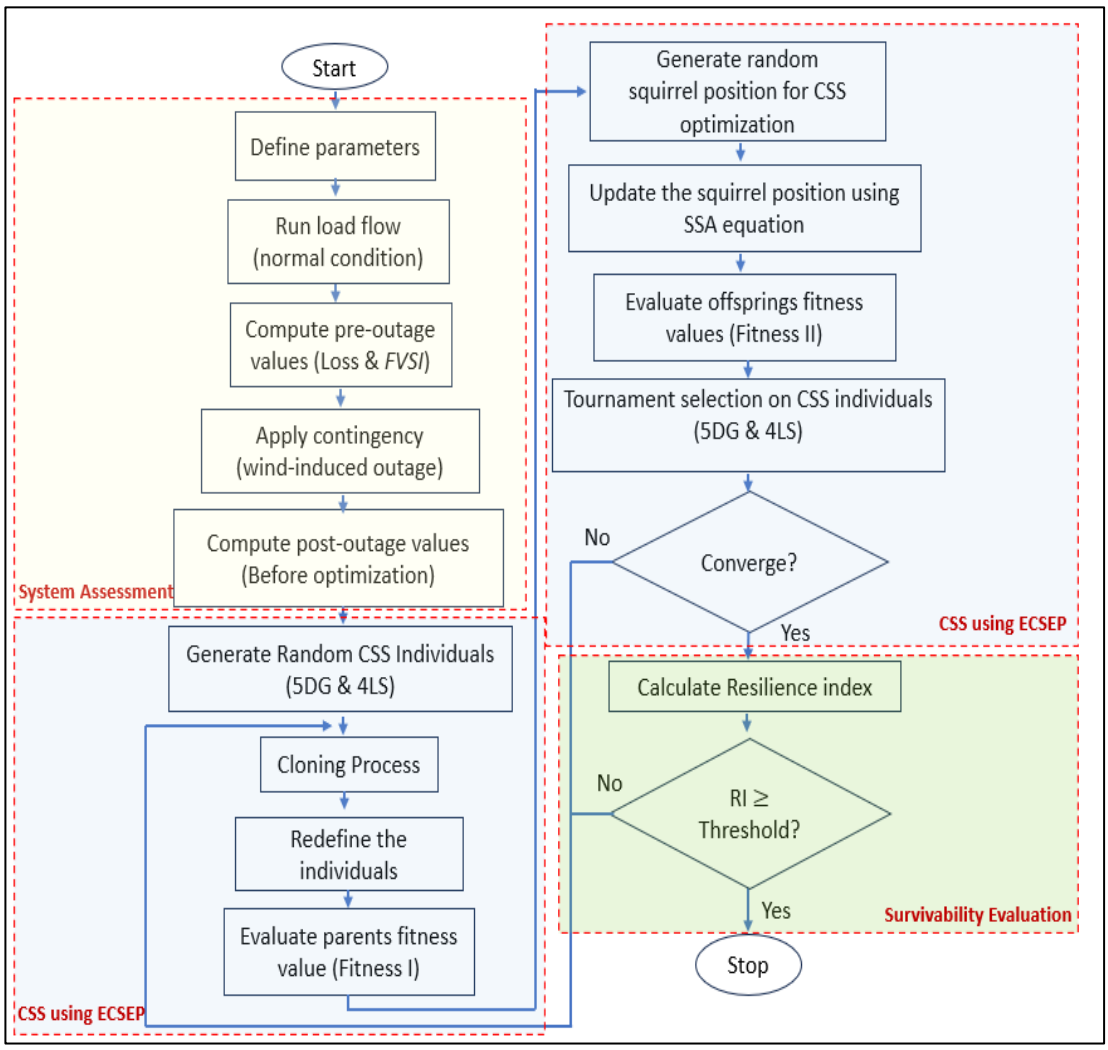


Figure 5.2 Flowchart of the ECSEP-Based Composite Survivability Strategy (CSS) with 5DG and 4LS

The process then terminates, providing the optimal scheme of DG installation and load shedding scheme that minimizes system loss and improves voltage stability, thereby enhancing overall system survivability.

5.4 Power System Survivability Strategy Framework

The power system survivability strategy framework developed in this research provides a comprehensive approach in maintaining essential grid operations during and after severe disturbances. The framework combines the preventive and corrective

measures which work together to protect the system from extreme events and restore operations quickly with minimal impact on essential power supply. The preventive measures include DG placement optimisation for network strength enhancement and transmission line stress reduction and emergency power supply during central generation failures. Network strength enhancement is achieved through the strategic placement of DG units that provide localized generation support, improving voltage stability and increasing the system's ability to withstand disturbances. Transmission line stress reduction occurs when power is generated closer to load canters, thereby reducing long-distance power transfers, lowering line loading levels, and minimizing transmission losses. Furthermore, DG units serve as emergency power sources during contingencies such as central generation failures or transmission outages, enabling localized supply support and maintaining service continuity to critical loads. Collectively, these capabilities contribute to improving the overall survivability and resilience of the power system. The intelligent load shedding system performs corrective actions by choosing non-essential power cuts and stop system breakdowns after disturbances.

The framework targets high-risk low-chance events through hurricane power outages which function as the primary disturbance model in this research. The simulation environment implements the IEEE 30-Bus and IEEE 57-Bus RTS systems to analyse transmission infrastructure fragility curves for contingency condition modelling. System performance is quantified using two key survivability metrics: total real power loss, which reflects the operational efficiency of power transfer and the *FVSI*, which assesses the system proximity to voltage instability. Both metrics are evaluated in pre-outage and post-outage conditions to capture the extent of performance degradation and recovery potential.

The optimisation process for both preventive and corrective actions is carried out simultaneously using the ECSEP algorithm. This hybrid technique combines the global exploration ability of the Squirrel Search Algorithm (SSA), the local exploitation capability of Evolutionary Programming (EP), and diversity preservation through chaotic cloning. By embedding both DG installation and load shedding decisions into a unified search space, the ECSEP-based framework ensures a balanced trade-off between loss minimization and voltage stability improvement. The output of this strategy framework is an optimised operational plan that enhances the system’s

survivability index, ensuring sustained supply to critical loads and rapid restoration of service pathways even under severe contingency conditions.

Figure 5.3 presents the overall framework of the proposed power system survivability strategy. The framework is divided into two main branches: stand-alone techniques and the Composite Survivability Strategy (CSS). The stand-alone techniques involve the independent application of DG installation and load shedding schemes, which are tested on the IEEE 30-Bus and IEEE 57-Bus RTS systems under two outage scenarios. In contrast, the CSS integrates DG installation and load shedding into a unified approach to enhance system performance under disturbance conditions. The performance of each compensation technique is evaluated based on two system performance indicators, namely power loss and the *FVSI*. These indicators are used to assess the effectiveness of the compensation strategies in improving system operational stability after an outage.

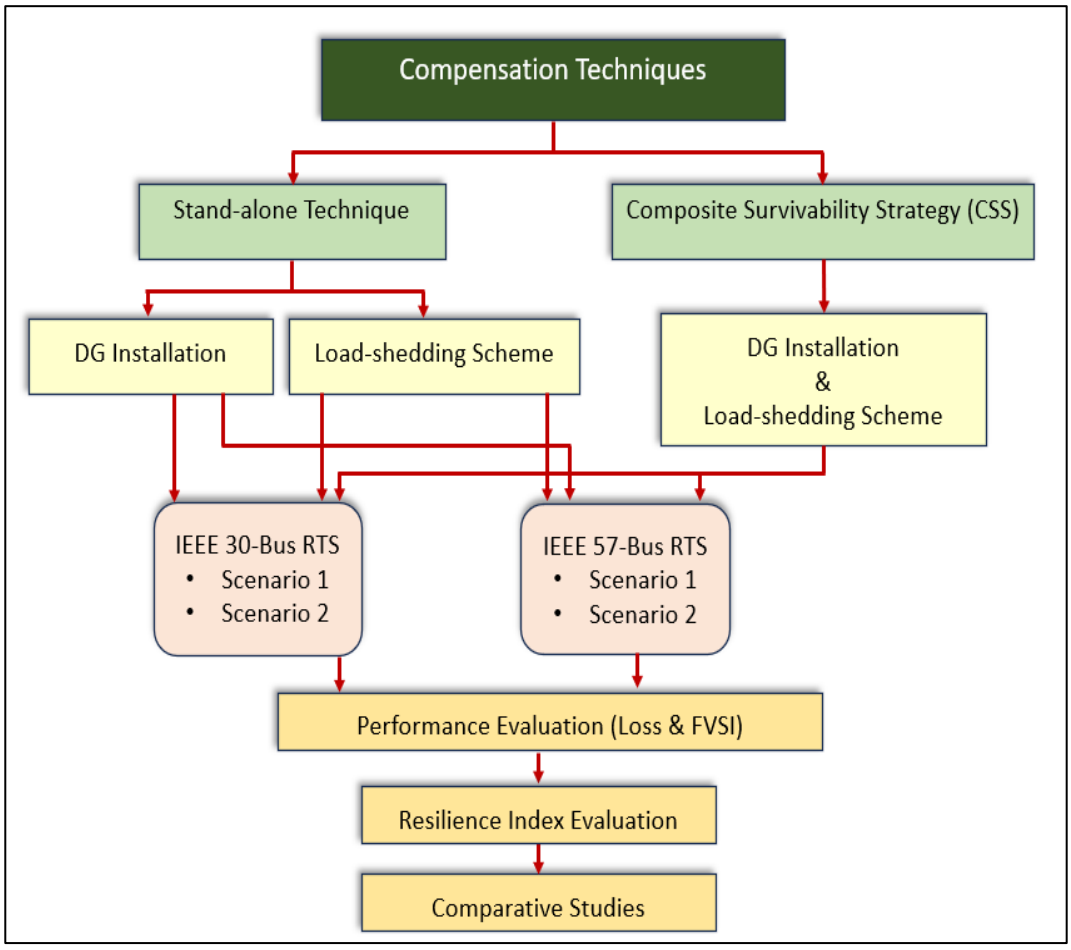


Figure 5.3 Power System Survivability Strategy Framework: Compensation Techniques and Evaluation Process

Following the performance evaluation, the RI is calculated to quantify the survivability level of the power system under the applied compensation strategies. The RI provides an integrated measure of system performance under disturbed conditions and reflects the ability of the system to maintain acceptable operating conditions. The calculated RI is then compared with a predefined survivability threshold to determine whether the system can sustain stable operation under the given scenario. Finally, the results obtained from both test systems and compensation strategies are compared through a comparative analysis to identify the approach that provides the most effective improvement in power system survivability and resilience.

5.5 Results and Discussion

This section presents the results obtained from the implementation of the proposed optimal composite survivability strategy in power system. The strategy integrates DG installation and intelligent load shedding within the ECSEP optimisation framework, aiming to enhance system performance during and after severe disturbances. The evaluation is carried out on the IEEE 30-Bus and IEEE 57-Bus RTS under simulated hurricane-induced outage scenarios.

The results are discussed in terms of the two primary survivability performance objective functions: total real power loss and the *FVSI*. Both metrics are examined in pre-outage and post-outage conditions to capture the effectiveness of the proposed strategy in mitigating performance degradation. Comparative analyses with benchmark optimisation techniques are also provided to demonstrate the superiority of the proposed approach in achieving balanced improvements in both loss reduction and voltage stability. The following subsections present detailed findings for both IEEE 30-Bus RTS and IEEE 57-Bus RTS. Eventually, decision can be made by the power system operators or planners to choose which strategy is viable to maintain the survivability of their systems.

5.5.1 Composite Survivability Strategy in IEEE 30-Bus RTS

This section presents the implementation and evaluation of the proposed composite survivability strategy on the IEEE 30-Bus RTS. For the IEEE 30-Bus RTS, simulation studies were conducted with a focus on reactive power load at Bus 26, where

the reactive loading, Q_d , is 25 MVAr. This bus was selected as it represents one of the weakest nodes in the test system as stated in Chapter 3, Chapter 4 and also agreed by Ismail in [189]. The CSS, integrating two compensation schemes, DG installation and load shedding was implemented using the ECSEP algorithm. Comparative analyses with benchmark optimisation methods are also included to validate the superiority of the proposed ECSEP-based composite approach.

5.5.1.1 Loss Minimization

Two scenarios, representing different hurricane event conditions, were simulated and analysed to evaluate loss minimization. The trend of loss reduction was examined by comparing several loss values: the baseline loss before the event occurrence ($Loss_{Set}$), the loss following the event ($Loss_{Out}$), the loss after DG installation ($Loss_{DG}$), the loss after applying the load shedding scheme ($Loss_{LS}$), and the loss achieved through the composite survivability strategy ($Loss_{CSS}$). In addition, the corresponding R1 and R2 values were assessed for each loss condition to provide a comprehensive performance evaluation. R1 is the resilience index before strategy implementation and R2 is the resilience index after strategy implementation.

Table 5.2 presents the performance of different survivability strategies at Bus 26 with a reactive loading of Q_d = 25 MVAr. The baseline system loss before the line outage event was recorded due to hurricane as $Loss_{Set}$ = 22.26 MW, which subsequently increased significantly to $Loss_{Out}$ = 70.49 MW due to the event occurrence of Scenario 1, highlighting the system vulnerability under stressed conditions. When DG was integrated into the system, the system loss reduced to 22.33 MW, accompanied by resilience indices $R1_{DG}$ = 0.462 and $R2_{DG}$ = 0.464.

Table 5.2
Performance of DG Installation, Load Shedding, and Composite Survivability Strategy in Terms of Loss Reduction and Resilience Indices (*R1, R2*) for the IEEE 30-Bus RTS at Q_{d26} = 25 MVAr

	$Loss_{DG}$	$R1_{DG}$	$R2_{DG}$	$Loss_{LS}$	$R1_{LS}$	$R2_{LS}$	$Loss_{CSS}$	$R1_{CSS}$	$R2_{CSS}$
Scenario 1	22.33	0.462	0.464	22.99	0.462	0.484	22.32	0.462	0.463
Scenario 2	22.27	2.910	2.914	23.47	2.910	3.638	22.27	2.910	2.911

Notes: $Loss_{Set}$ = 22.26 MW; $Loss_{Out}$ (Scenario 1) = 70.49 MW; $Loss_{Out}$ (Scenario 2) = 29.92 MW

The load shedding scheme causes the reduction in loss to 22.99 MW within Scenario 1, with resilience indices $R1_{LS}$ of 0.462 and $R2_{LS}$ = 0.484. On the other hand, CSS, which integrates DG installation and load shedding, achieved the most favourable result with a system loss of 22.32 MW. The resilience indices ($R1_{CSS}$ = 0.462, $R2_{CSS}$ = 0.463) further support that CSS provides a balanced solution in maintaining stability while minimizing loss. This implies that the strategies manage to make the system survives within Scenario 1.

For Scenario 2, the $Loss_{Set}$ was originally 22.26 MW before any hurricane affected the system. With hurricane occurrence the system loss is increased to 29.92 MW ($Loss_{Out}$). When DG was integrated into the system, the system loss reduces to 22.27 MW, with corresponding resilience indices of $R1_{DG}$ = 2.910 and $R2_{DG}$ = 2.914. This indicates that DG integration was able to restore the system close to its pre-event condition while maintaining relatively stable resilience performance. The load shedding scheme resulted in a loss of 23.47 MW, with the corresponding resilience indices of $R1_{LS}$ = 2.910 and $R2_{LS}$ of 3.638. These results indicate that load shedding was also able to minimize loss while simultaneously enhancing system resilience, demonstrating its effectiveness in alleviating system stress under this scenario. The CSS achieved the most favourable results, with a system loss of 22.27 MW and resilience indices of $R1_{CSS}$ = 2.910 and $R2_{CSS}$ = 2.911.

These values highlight the effectiveness of CSS in not only minimizing loss but also ensuring balanced resilience indices across the system. Overall, the results confirm that while DG installation and load shedding individually enhance system resilience, the composite strategy delivers superior performance, achieving the lowest loss value and ensuring stable resilience levels. This demonstrates the effectiveness of integrating multiple survivability schemes for improving power system performance under extreme event conditions. In terms of system survivability indicated by their resilience index, load shedding is better than DG integration and CSS strategies. This allows the power system operators to choose which strategy is preferrable for their system in both scenarios. Figure 5.4 presents the percentage loss reduction (*PLR*) performance of three mitigation strategies: DG installation, load shedding scheme, and the CSS in the IEEE 30-Bus RTS. The *PLR* values indicate the effectiveness of each strategy in reducing total system losses under two distinct event conditions. In Scenario 1, the *PLR* values were consistently high, with CSS achieving the highest reduction of 68.34%, followed closely by DG at 68.32% and load shedding at 67.39%. These results highlight that,

under the conditions defined for Scenario 1, the application of any of the strategies provides significant improvement in system resilience. The superior performance of CSS reflects the benefit of integrating DG and LS measures, which enhances the system overall survivability looking at the loss reduction.

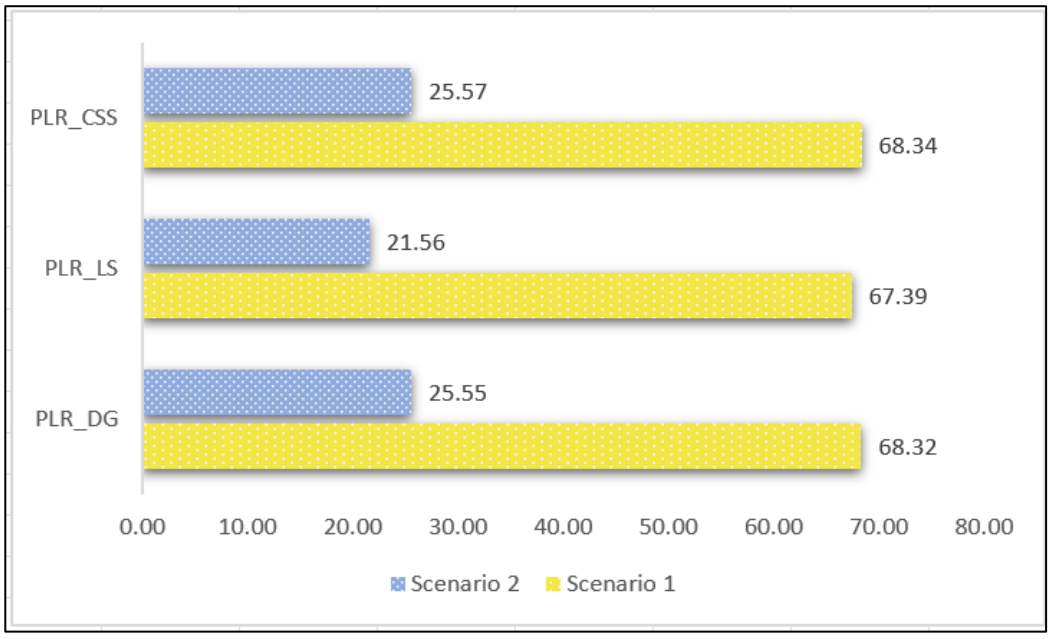


Figure 5.4 Percentage of Loss Reduction (*PLR*) for DG, LS, and CSS Strategies under Scenario 1 and Scenario 2 in IEEE 30-Bus RTS

In Scenario 2, CSS exhibited the highest *PLR* of 25.57%, with DG integration or installation closely following at 25.55%, while LS achieved a *PLR* of 21.56%. Although the improvements were more modest, the outcomes emphasize the continued value of deploying these strategies to reduce system losses during adverse conditions. The CSS approach again provided the best result in terms of loss reduction, demonstrating its effectiveness as a comprehensive strategy even when the system is exposed to more severe disruptions.

Figure 5.5 shows the system loss profile during Scenario 1 under three compensation strategies: DG installation, load shedding scheme and the CSS. At the pre-outage stage (t_1), all strategies start at the same baseline of 22.27 MW. During the outage (t_2), losses rise sharply to 70.49 MW for all cases, indicating that the disturbance initially affects the system equally regardless of the applied strategy. Differences emerge during the recovery stage (t_3). Both DG and CSS successfully reduce the transmission loss to 22.33 MW and 22.32 MW, respectively, demonstrating their

effectiveness in restoring system performance. In contrast, load shedding scheme achieves only 22.99 MW, which is higher than both DG installation and CSS, reflecting its relatively weaker capability in minimizing losses. By the post-recovery stage (t_4), all strategies converge to the same steady-state level of 22.27 MW. Nevertheless, CSS demonstrates the most efficient recovery path, outperforming load shedding scheme and matching the strong performance of DG installation.

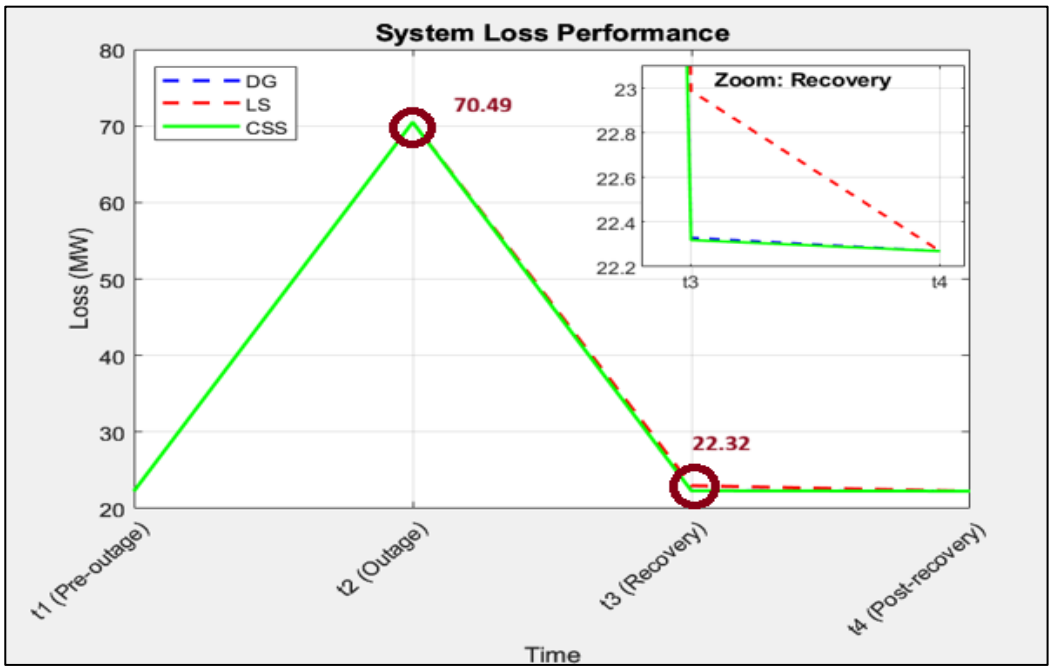


Figure 5.5 Loss Profile under Different Compensation Strategies in IEEE 30-Bus RTS for Scenario 1

Figure 5.6 illustrates the loss profile for Scenario 2 under the same three compensation strategies. At the pre-outage stage (t_1), all strategies again begin at 22.27 MW. During the outage (t_2), the losses increased moderately to 29.92 MW, which is considerably lower than in Scenario 1, reflecting the different severity of the disturbance. At the recovery stage (t_3), DG installation and CSS again restore the system to the pre-outage condition at 22.27 MW, showing strong effectiveness in loss minimization. On the other hand, load shedding scheme records a higher recovery loss of 23.47 MW, consistent with the results observed in Scenario 1, and indicating its lower efficiency compared to DG installation and CSS.

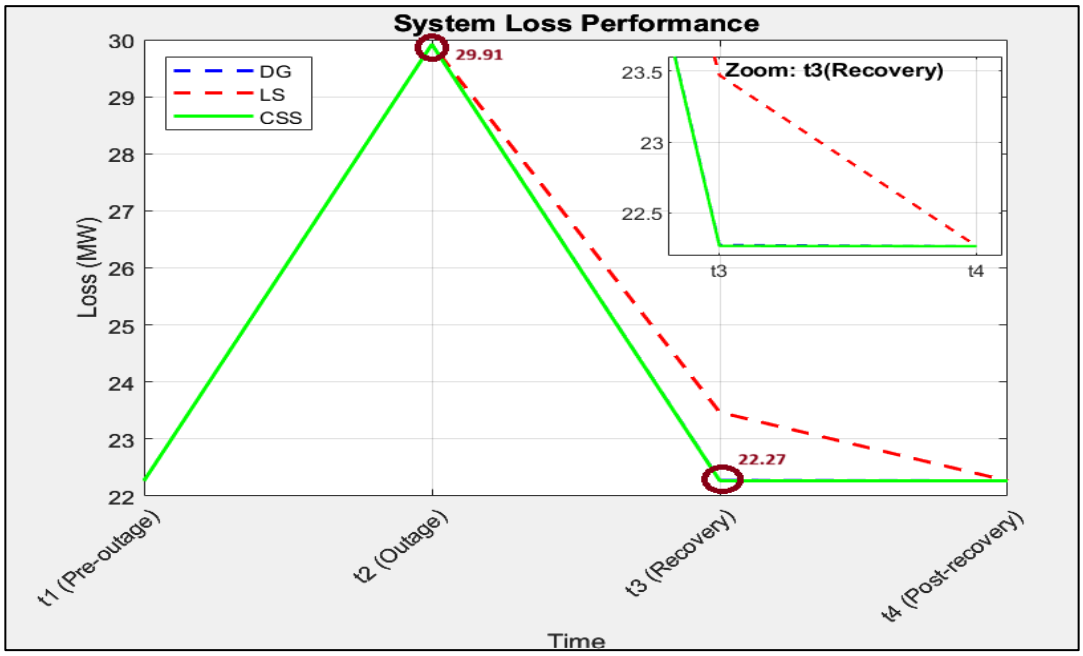


Figure 5.6 Loss Profile under Different Compensation Strategies in IEEE 30-Bus RTS for Scenario 2

By the post-recovery stage (t_4), the loss values converge across all strategies at 22.27 MW indicating system stabilization. Similar to Scenario 1, CSS exhibits the best performance, maintaining minimal losses throughout the disturbance period, followed closely by DG installation, while load shedding remains the least effective approach.

5.5.1.2 Voltage Stability Improvement

In addition to loss minimization, the CSS also emphasizes the improvement of voltage stability within the IEEE 30-Bus RTS. To comprehensively evaluate this aspect, two distinct scenarios were simulated and analysed with respect to the *FVSI* variation. The *FVSI* values serve as the critical indicators to system vulnerability, allowing a detailed assessment of how the proposed strategies contribute in maintaining voltage stability under different operating conditions.

Table 5.3
Performance of DG Installation, Load Shedding, and Composite Survivability Strategy in Terms of Voltage Stability Improvement and Resilience Indices (*R1, R2*) for the IEEE 30-Bus RTS at Bus 26 with Q_d = 25 MVAr

	$FVSI_{DG}$	$R1_{DG}$	$R2_{DG}$	$FVSI_{LS}$	$R1_{LS}$	$R2_{LS}$	$FVSI_{CSS}$	$R1_{CSS}$	$R2_{CSS}$
Scenario 1	0.6542	5.542	5.615	0.7035	5.542	10.469	0.6532	5.542	5.559
Scenario 2	0.6752	2.077	2.312	0.6595	2.077	2.142	0.6546	2.077	2.093

Notes: $FVSI_{Set}$ = 0.6529 p.u.; $FVSI_{Out}$ (Scenario 1) = 0.7707 p.u.; $FVSI_{Out}$ (Scenario 2) = 0.9673 p.u.

Table 5.3 tabulates the performance of DG installation, load shedding, and CSS in improving voltage stability and resilience at Q_{d26} = 25 MVAr. In Scenario 1, the baseline *FVSI* value before the event was 0.6529, it increases to 0.7707 after the event, indicating reduced voltage stability. With DG installation, the $FVSI_{DG}$ reduced to 0.6542, accompanied by $R1_{DG}$ = 5.542 and $R2_{DG}$ = 5.615. The load shedding scheme improved the $FVSI_{LS}$ to 0.7035 with $R1_{LS}$ = 5.542 and $R2_{LS}$ = 10.469, demonstrating that load shedding effectively reduced instability compared to the post-event condition. The CSS strategy managed to achieve the best outcome with $FVSI_{CSS}$ = 0.6532, nearly identical to the baseline, supported by $R1_{CSS}$ = 5.542 and $R2_{CSS}$ of 5.559. Apparently, LS strategy achieves better resilience over DG and CSS. In terms of voltage stability improvement, CSS apparently outperformed LS and DG strategies.

In Scenario 2, the baseline *FVSI* before the event was 0.6529, which increases sharply to 0.9673 after the event, reflecting severe instability. The integration of DG reduced the index to $FVSI_{DG}$ = 0.6752, with resilience indices $R1_{DG}$ = 2.077 and $R2_{DG}$ = 2.312, indicating improved system stability. The load shedding scheme further improved the stability margin with $FVSI_{LS}$ = 0.6595, with the corresponding resilience of $R1_{LS}$ = 2.077 and $R2_{LS}$ = 2.142, highlighting its effectiveness in relieving system stress. The CSS once again delivered the most favourable result with $FVSI_{CSS}$ = 0.6546, resilience indices of $R1_{CSS}$ = 2.077 and $R2_{CSS}$ = 2.093, confirming its robustness in restoring the system close to its pre-event condition. This demonstrates the effectiveness of combining DG installation and load shedding in reducing system vulnerability and enhancing post-disturbance voltage recovery.

On the overall, the results demonstrate that while both DG installation and load shedding improve voltage stability and resilience, the CSS consistently provides the most effective performance by restoring *FVSI* values nearly to the baseline and maintaining stable resilience indices across both scenarios. Figure 5.7 presents the results for percentage reduction in *FVSI* for DG, LS and CSS strategies in IEEE 30-Bus RTS. The results highlight how each strategy contributes to improving system performance under different conditions.

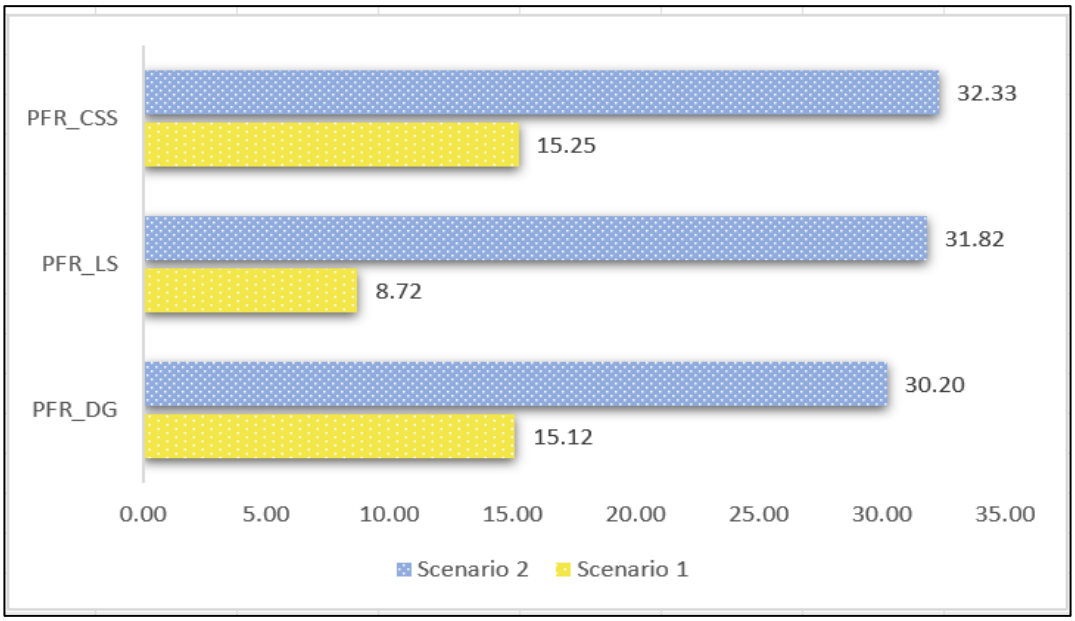


Figure 5.7 Percentage of *FVSI* Reduction (*PFR*) for DG, LS, and CSS Strategies under Scenario 1 and Scenario 2 in IEEE 30-Bus RTS

In Scenario 1, the reduction values were modest, with CSS and DG giving almost the same results at 15.25% and 15.12%, while LS recorded a lower value of 8.72%. These results show that the compensation strategies are effective in reducing *FVSI*, with CSS showing a slight advantage due to the combined effect of DG and LS.

In Scenario 2, substantial reduction in *FVSI* values can be observed. CSS achieved the largest reduction at 32.33%, followed closely by LS strategy of 31.82% and DG of 30.20%. This indicates that all strategies worked well in improving voltage stability, with CSS being dominant as compared to LS and DG strategies. The results confirm that combining DG and LS provides a stronger effect compared to applying the strategies individually.

Figure 5.8, the results of *FVSI* profile under different compensation strategies for Scenario 1, implemented in IEEE 30-Bus RTS are presented. The *FVSI* profile shown in Figure 5.8 reveals the varying effectiveness of the three compensation approaches. All strategies begin at the same stability level during the pre-outage period ($t_1 = 0.6529$) and experience a sharp deterioration during the outage ($t_2 = 0.7707$).

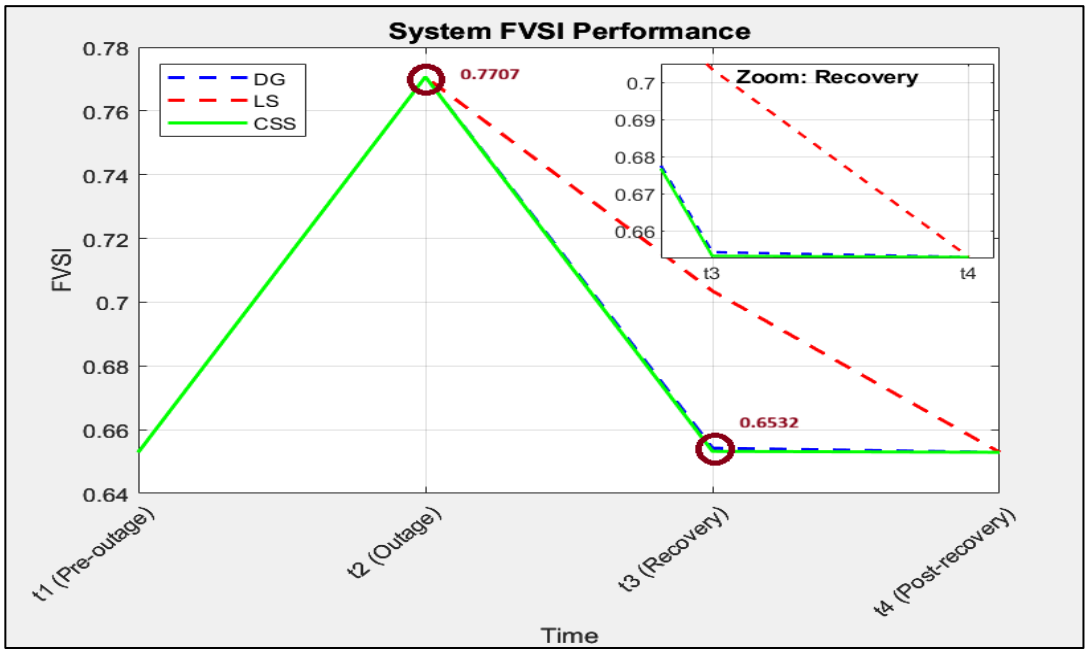


Figure 5.8 *FVSI* Profile under Different Compensation Strategies in IEEE 30-Bus RTS for Scenario 1

The critical distinction arises at the recovery stage (t_3). The composite survivability strategy (CSS) and DG installation rapidly drive the *FVSI* back close to the pre-disturbance condition (0.6532 and 0.6542, respectively), highlighting their ability to stabilize the system effectively. By contrast, the LS strategy lags behind with a higher *FVSI* value of 0.7035, suggesting slower and less efficient stabilization. Once the system reaches the post-recovery state (t_4), all strategies converge to the same value of 0.6529, restoring the system to its initial condition. Nevertheless, the evidence is clear: CSS consistently demonstrates superior performance during recovery, outperforming the LS and DG strategies while offering a more balanced resilience improvement. Figure 5.9 depicts the *FVSI* profile of the IEEE 30-Bus RTS involving all the compensation strategies in Scenario 2. Scenario 2 shows a similar pattern but with some differences. *FVSI* values for all strategies start at 0.6529 in the pre-outage stage (t_1) and rise to 0.9673 during the outage (t_2), reflecting a sharper stress level compared to Scenario 1. When the system moves into recovery (t_3), CSS again shows the strongest stabilizing effect, reducing *FVSI* to 0.6546. DG strategy performs reasonably well at 0.6752, while the LS strategy records 0.6595, slightly better than in Scenario 1 but still inferior to CSS. At the post-recovery stage (t_4), the *FVSI* values of all strategies settle back to 0.6529, indicating complete restoration. However, the comparative analysis underlines a consistent finding: CSS delivers the best recovery

performance by ensuring the lowest *FVSI* during the transient phase, reinforcing its role as the most robust approach for enhancing voltage stability in the IEEE 30-Bus RTS.

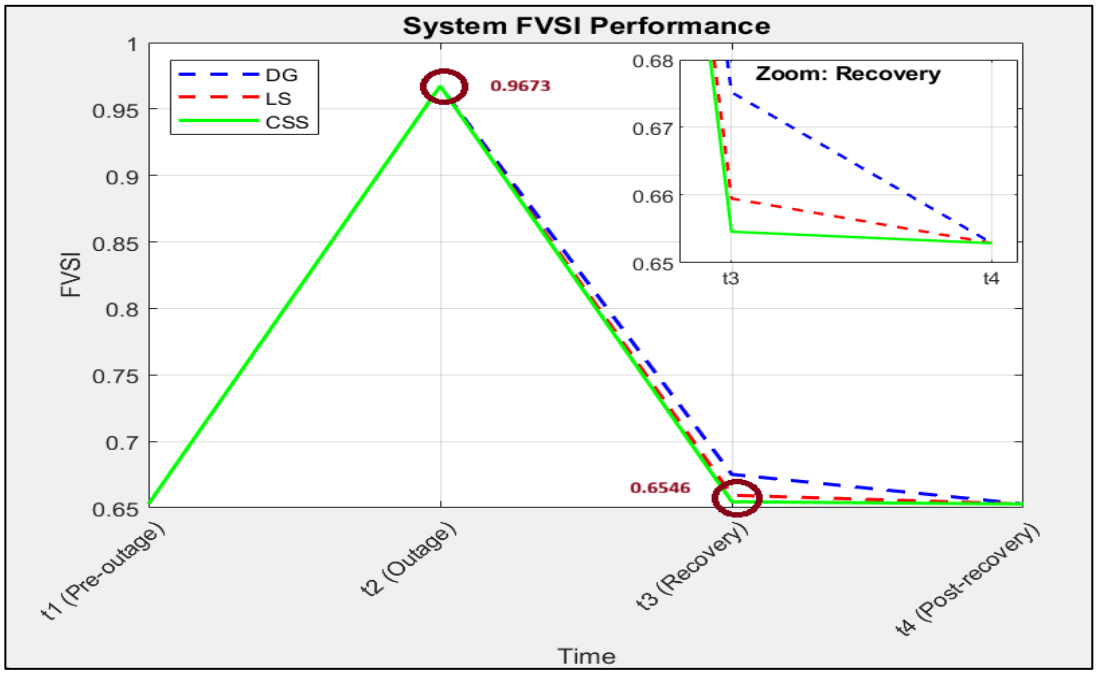


Figure 5.9 *FVSI* Profile under Different Compensation Strategies in IEEE 30-Bus RTS for Scenario 2

5.5.2 Composite Survivability Strategy in IEEE 57-Bus RTS

Similar study was conducted on IEEE 57-Bus RTS to investigate the performance of the proposed strategies when implemented on a larger system. Two similar objective functions were considered: loss minimization and voltage stability improvement. Two distinct scenarios were simulated to examine the impact DG, LS and CSS under different hurricane and outage conditions termed Scenario 1 and Scenario 2 as those conducted in IEEE 30-Bus RTS. For this test system, the simulation was centred on Q_{d33} = 15MVAr, which was selected as it represents one of the weakest nodes in the network.

5.5.2.1 Loss minimization

In the case of the IEEE 57-Bus RTS, the evaluation of loss minimization was carried out through the simulation of two scenarios reflecting different hurricane disturbances. The analysis considered the variation in system losses across several

stages, starting with the baseline loss prior to the disturbance ($Loss_{Set}$), followed by the loss recorded immediately after the event occurrence ($Loss_{Out}$).

Table 5.4
Performance of DG Installation, Load Shedding, and Composite Survivability Strategy in Terms of Loss Reduction and Resilience Indices (*R1, R2*) for the IEEE 57-Bus RTS at Q_{d33} = 15 MVAr

	$Loss_{DG}$	$R1_{DG}$	$R2_{DG}$	$Loss_{LS}$	$R1_{LS}$	$R2_{LS}$	$Loss_{CSS}$	$R1_{CSS}$	$R2_{CSS}$
Scenario 1	30.56	4.101	4.112	31.25	4.101	4.635	30.55	4.101	4.102
Scenario 2	31.97	1.308	1.458	31.00	1.308	1.354	30.98	1.308	1.351

Notes: $Loss_{Set}$ = 30.55 MW; $Loss_{Out}$ (Scenario 1) = 38.00 MW; $Loss_{Out}$ (Scenario 2) = 53.90 MW

Subsequent assessments included the impact of DG installation strategy ($Loss_{DG}$), the application of LS strategy ($Loss_{LS}$), followed by CSS ($Loss_{CSS}$). Alongside these loss values, the corresponding resilience indicators R1 and R2 were also computed, enabling a thorough assessment of system behaviour and the effectiveness of the applied strategies under the tested conditions.

Table 5.4 tabulates the performance of DG installation, LS, and the CSS in terms of loss reduction and resilience indices with reactive power loading subjected to Bus 33 in IEEE 57-Bus RTS with Q_d = 15 MVAr. In Scenario 1, the baseline system loss before the disturbance was $Loss_{Set}$ = 30.55 MW, which increased to $Loss_{Out}$ = 38.00 MW after the event. This increase reflects the vulnerability of the system when subjected to hurricane. With DG installation, the loss was reduced to 30.56 MW, with the corresponding resilience indices of $R1_{DG}$ = 4.101 and $R2_{DG}$ = 4.112, demonstrating the ability of DG to restore the system to near pre-event conditions. The LS strategy resulted in a slightly higher loss of 31.25 MW, with resilience indices of $R1_{LS}$ = 4.101 and $R2_{LS}$ = 4.635, showing that while load shedding mitigated the impact of the event, its effectiveness was lower compared to DG. The CSS achieved the best outcome, restoring the loss to 30.55 MW, with resilience indices of $R1_{CSS}$ = 4.101 and $R2_{CSS}$ = 4.102, confirming that CSS provides the most balanced and effective recovery under Scenario 1. In terms if resilience improvement, LS strategy could be a better choice.

In Scenario 2, the baseline system loss is $Loss_{Set}$ = 30.55 MW, which increased significantly to $Loss_{Out}$ = 53.90 MW after the disturbance, indicating severe stress on Bus 33. With DG installation strategy, the system loss was reduced to 31.97 MW, with the corresponding resilience indices of $R1_{DG}$ = 1.308 and $R2_{DG}$ = 1.458. The load shedding scheme further improved system performance with a loss of 31.00 MW, and

resilience indices $R1_{LS}$ = 1.308 and $R2_{LS}$ = 1.354, showing enhanced resilience compared to the post-event condition. The CSS again provided the most effective solution, reducing the loss to 30.98 MW, supported by resilience indices $R1_{CSS}$ = 1.308 and $R2_{CSS}$ = 1.351, which closely match the baseline values. This result confirms that CSS consistently achieves superior recovery by minimizing losses and maintaining balanced resilience indices even under severe event conditions. Taken together, the results from both scenarios highlight that although DG installation and LS individually contribute to improving system resilience, the CSS remains the most effective, as it consistently restores the system close to its pre-disturbance condition while ensuring stable resilience indices.

Figure 5.10 shows the results for percentage of loss reduction (*PLR*) achieved using DG installation, load shedding technique, and the CSS for the IEEE 57-Bus RTS under two scenarios. The results reflect how each compensation strategy helps reduce system losses during disruptive events. In Scenario 1, the *PLR* values were moderate, ranging between 17.75% and 19.60%. CSS recorded the highest reduction at 19.60%, followed by DG at 19.56%, while LS gives a slightly lower value of 17.75%. These values confirm that all three techniques are effective in power system loss reduction, with CSS giving a marginal advantage because of its combined approach.

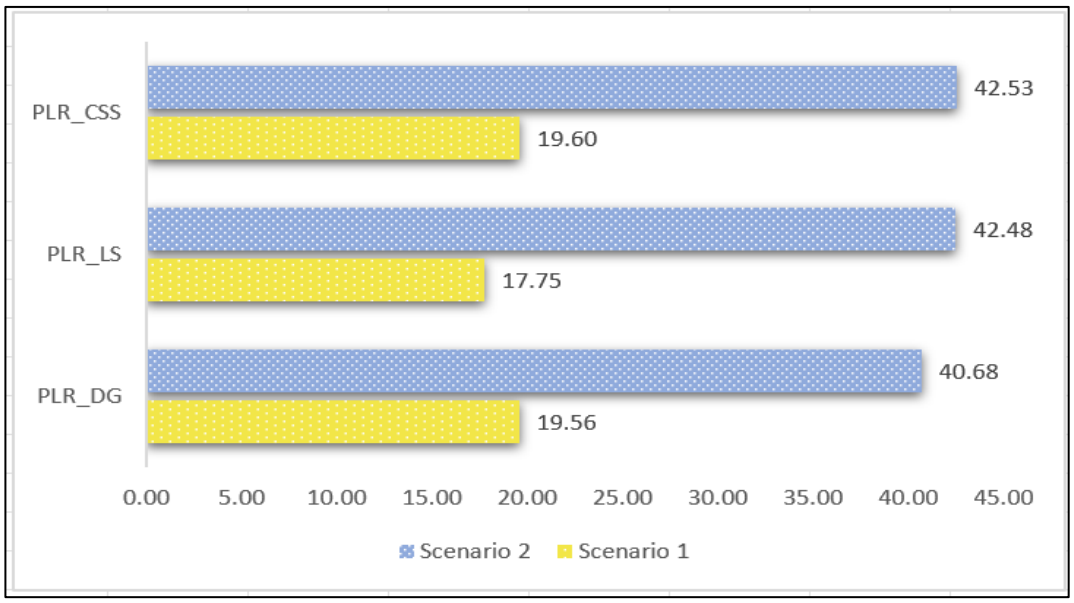


Figure 5.10 Percentage Loss Reduction (*PLR*) for DG, LS, and CSS Strategies under Scenario 1 and Scenario 2 in IEEE 57-Bus RTS

In Scenario 2, the performance of all strategies improved significantly. CSS achieved the highest reduction at 42.53%, with LS strategy showing a very close result at 42.48%, and DG at 40.68%. These higher percentages indicate that the mitigation strategies worked very effectively in reducing losses when the system was subjected to more severe conditions. The consistently strong result of CSS again shows the benefit of integrating DG and LS strategies into a composite strategy.

The loss profile of the IEEE 57-Bus RTS under various compensation strategies in Scenario 1 is presented in Figure 5.11. In Scenario 1, the system loss begins at 30.55 MW during the pre-outage stage (t_1). Once the outage occurs at t_2, losses increase to 38.00 MW across all three strategies, showing that the immediate impact of the disturbance is consistent regardless of the applied technique. The real difference appears at the recovery stage (t_3). Here, the LS strategy registers the highest loss at 31.25 MW, indicating that although it helps relieve system stress, it is less efficient in restoring the system to its pre-disturbance state.

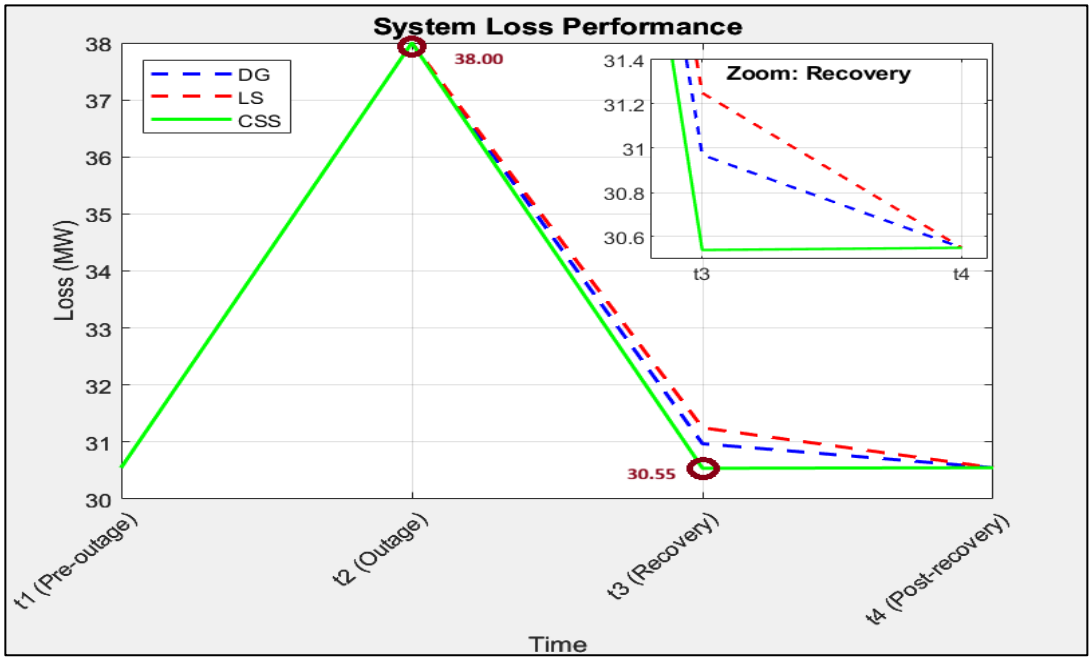


Figure 5.11 Loss Profile under Different Compensation Strategies in IEEE 57-Bus RTS for Scenario 1

DG installation shows slightly better results with 30.56 MW, while the CSS achieves the lowest recovery loss of 30.55 MW. This confirms CSS as the most effective technique in reducing transient losses. By the post-recovery stage (t_4), all strategies return to the same level of 30.55 MW, highlighting that while all methods

ultimately stabilize the system, CSS provides the smoothest and most efficient path to recovery.

Figure 5.12 shows the results for loss profile under different compensation strategies in IEEE 57-Bus RTS (Scenario 2). Scenario 2 displays a more severe disturbance compared to Scenario 1, with the outage (t_2) pushing system losses up to 53.90 MW for all strategies. At the recovery stage (t_3), the differences between the methods become clearer. The LS strategy exhibits a recovery loss of 31.00 MW, performing slightly better than in Scenario 1 but still not the most effective option. DG installation shows a higher loss of 31.97 MW, suggesting that in this scenario, generation support alone struggles to minimize losses efficiently.

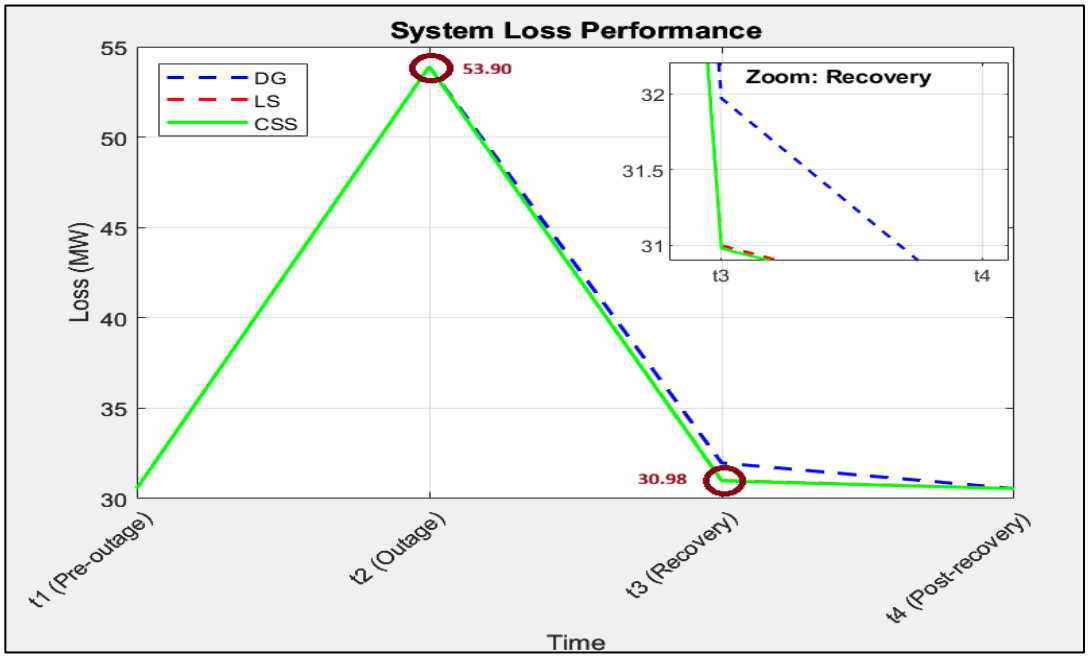


Figure 5.12 Loss Profile under Different Compensation Strategies in IEEE 57-Bus RTS for Scenario 2

CSS once again demonstrates its strength by producing the lowest recovery loss of 30.98 MW, confirming that the integration of both DG installation and load shedding provides the best balance between supply restoration and demand relief. At the post-recovery stage (t_4), the system stabilizes at 30.55 MW for all strategies, but CSS clearly delivers the most favourable recovery performance.

5.5.2.2 Voltage Stability Improvement

For the IEEE 57-Bus RTS, the evaluation of the CSS was extended beyond loss minimization to include its impact on voltage stability enhancement. Two similar scenarios were also subjected to capture the effect of hurricane-induced disturbances, and the system response was analysed using the *FVSI*.

Table 5.5 presents the performance of DG installation, load shedding, and the CSS in terms of voltage stability improvement and resilience indices at Bus 33 of the IEEE 57-Bus RTS with Q_d = 15 MVAr. In Scenario 1, the initial *FVSI* before the event was $FVSI_{\text{Set}}$ = 0.4613, which increased to $FVSI_{\text{Out}}$= 0.6679 following the disturbance, indicating a decline in voltage stability.

Table 5.5
Performance of DG, LS and CSS Strategy on Voltage Stability Improvement and Resilience Indices (*R1, R2*) for the IEEE 57-Bus RTS at Q_{d33} = 15 MVAr

	$FVSI_{DG}$	$R1_{DG}$	$R2_{DG}$	$FVSI_{LS}$	$R1_{LS}$	$R2_{LS}$	$FVSI_{CSS}$	$R1_{CSS}$	$R2_{CSS}$
Scenario 1	0.4631	2.233	2.261	0.4735	2.233	2.436	0.4629	2.233	2.258
Scenario 2	0.4635	1.865	1.891	0.4821	1.865	2.128	0.4627	1.865	1.882

Notes: $FVSI_{\text{Set}}$ = 0.4613 p.u.; $FVSI_{Out}$ (Scenario 1) = 0.6679 p.u.; $FVSI_{Out}$ (Scenario 2) = 0.7086 p.u.

The $FVSI_{Set}$ is originally 0.4613 before any occurrence of hurricane events termed Scenario 1 and Scenario 2. When hurricane occurs in Scenario 1, the *FVSI* ($FVSI_{Out}$) increases to 0.6679. This value reduces to 0.4631 with the DG installation strategy while LS strategy reduces its value to 0.4735 and CSS reduces its value to 0.4629. Apparently, CSS exhibits the best result in terms of *FVSI* reduction. In terms of resilience index values, DG scheme increases its value from 2.233 to 2.261, showing that DG was able to restore the system very close to its baseline stability level. The LS strategy reduces its *FVSI* value from 0.6679 to $FVSI_{LS}$ of 0.4735, with resilience indices worth $R1_{LS}$ = 2.233 and $R2_{LS}$ = 2.436. On the other hand, CSS strategy achieved the most favourable performance, reducing the $FVSI_{\text{CSS}}$ to 0.4629, with resilience indices of $R1_{CSS}$ = 2.233 and $R2_{CSS}$ = 2.258, confirming its ability to restore system stability with a balanced resilience profile. In terms of achieving the highest resilience index, LS strategy performs the best, followed by DG and CSS.

In Scenario 2, the baseline *FVSI* was $FVSI_{Set}$ = 0.4613, which increase significantly to $FVSI_{Out}$ = 0.7086 with the presence of hurricane, reflecting severe voltage instability and reduced stability margin. With DG installation strategy, the

$FVSI_{DG}$ is reduced to 0.4635, and the resilience indices are $R1_{DG}$ = 1.865 and $R2_{DG}$ = 1.891, demonstrating effective recovery of the system toward stable operation. The LS strategy further alleviated stress, producing an $FVSI_{LS}$ of 0.4821, with $R1_{LS}$ = 1.865 and $R2_{LS}$ = 2.128, showing improvements relative to the post-event condition. The CSS once again delivered the best result, achieving $FVSI_{CSS}$ of 0.4627, very close to the baseline, with resilience indices $R1_{CSS}$ = 1.865 and $R2_{CSS}$ = 1.882, confirming its robustness in restoring voltage stability under severe event conditions.

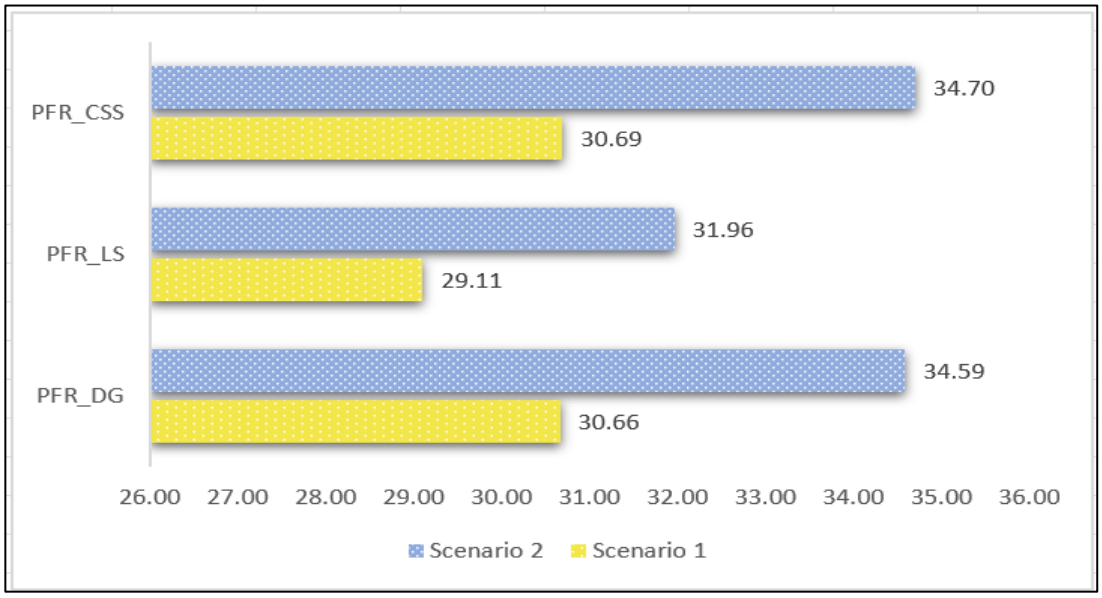


Figure 5.13 Percentage *FVSI* Reduction (*PFR*) for DG, LS and CSS Strategies under Scenario 1 and Scenario 2 in IEEE 57-Bus RTS

The percentage of *FVSI* reduction (*PFR*) involving the DG installation, LS and CSS strategies for IEEE 57-Bus RTS under two scenarios is shown in Figure 5.13. The compensation strategies show their effectiveness in reducing the *FVSI* values which helps maintain voltage stability during system disruptions. In Scenario 1, the reduction values were moderate. CSS achieved a *PFR* of 30.69%, while DG installation exhibits 30.66%, showing almost identical performance. LS strategy gave a slightly lower reduction of 29.11%. These results confirm that all three strategies provided effective support in reducing *FVSI*, with CSS offering a small advantage because of its integrated approach. In Scenario 2, the *PFR* values were higher compared to Scenario 1. CSS produced the largest reduction at 34.70%, followed closely by DG installation strategy at 34.59%, while LS strategy gives 31.96%. This indicates that under more severe conditions, all strategies were successful in reducing the *FVSI* value, with CSS again

delivering the best performance. The consistent advantage of CSS highlights the benefit of combining DG and LS strategy to enhance system resilience.

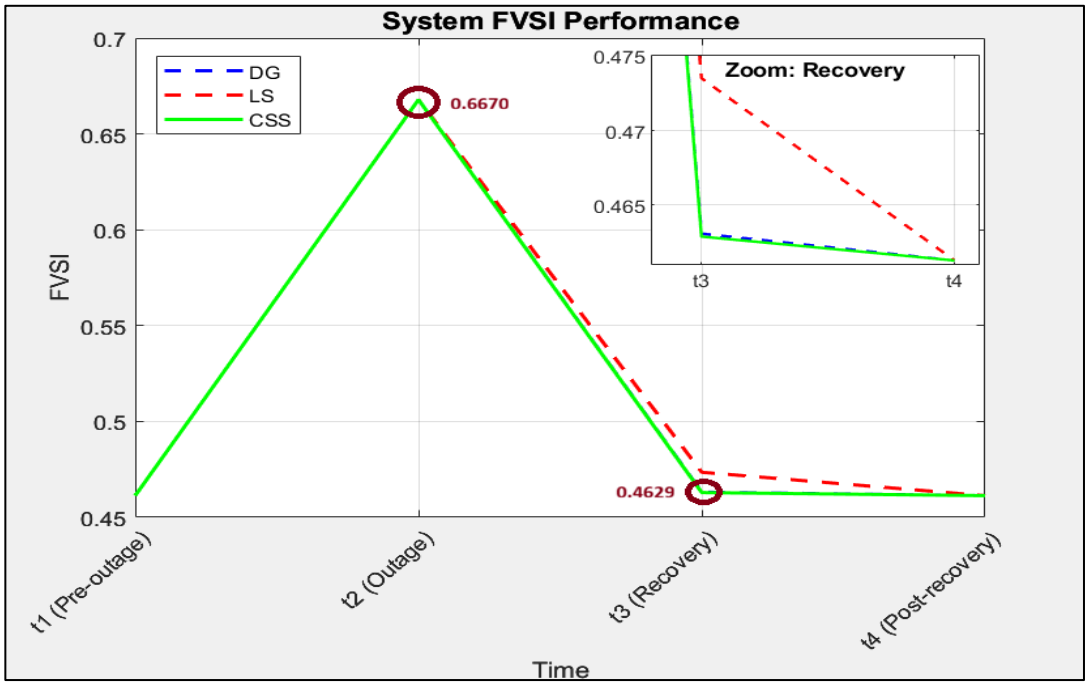


Figure 5.14 *FVSI* Profile under Different Compensation Strategies in IEEE 57-Bus RTS for Scenario 1

Figure 5.14 shows the *FVSI* profile under different compensation strategies in IEEE 57-Bus RTS (Scenario 1). In Scenario 1, the *FVSI* profile begins at the same baseline value of 0.4613 for all strategies during the pre-outage stage (t_1). When outage occurs (t_2), *FVSI* rises sharply to 0.6679, indicating a weakened voltage stability condition across all methods. The system behaviour during the recovery stage (t_3) highlights the difference between compensation strategies. DG installation and CSS are both able to return the *FVSI* close to its initial value, recording 0.4631 and 0.4629 respectively. By comparison, the load shedding scheme produces a noticeably higher *FVSI* of 0.4735, showing that while it reduces the stress on the system, it is less capable of fully restoring voltage stability. At the post-recovery stage (t_4), *FVSI* values for all strategies converge back to 0.4613, but the more effective and smoother recovery achieved by CSS demonstrates its superiority in maintaining system stability compared to the other strategies.

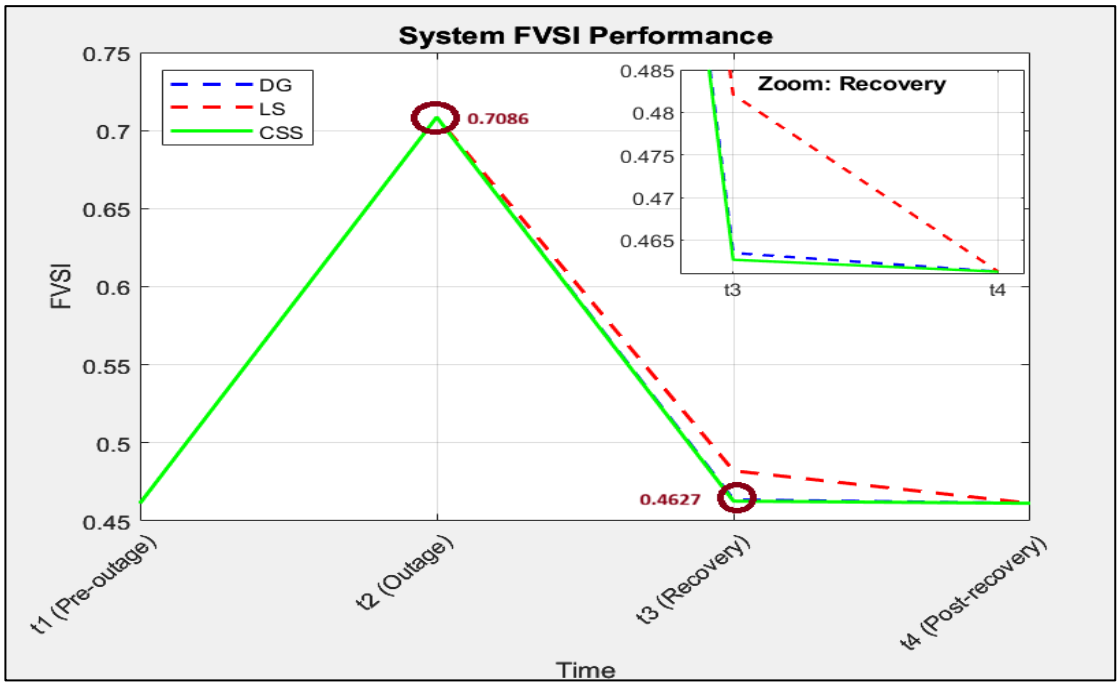


Figure 5.15 *FVSI* Profile under Different Compensation Strategies in IEEE 57-Bus RTS for Scenario 2

Figure 5.15 illustrates the *FVSI* profile for different compensation strategies in the IEEE 57-Bus RTS under Scenario 2. Scenario 2 follows a similar general trend, starting with an *FVSI* of 0.4613 at the pre-outage stage (t_1) and escalating to 0.7086 during the outage (t_2), which represents a more severe stability deterioration than Scenario 1. The recovery phase (t_3) provides a clearer difference between the strategies. CSS delivers the best outcome, reducing *FVSI* to 0.4627, closely followed by DG installation at 0.4635. The LS strategy, however, records a significantly higher *FVSI* of 0.4821, again demonstrating its ability to restore the system to a stable state. At the post-recovery stage (t_4), all methods stabilize at 0.4613, but CSS consistent ability to maintain the lowest *FVSI* during recovery which confirms its role as the most reliable strategy for improving voltage stability in the IEEE 57-Bus RTS.

5.6 Summary

This chapter presented the effectiveness of DG installation, LS and CSS strategies in improving system resilience for both the IEEE 30-Bus and IEEE 57-Bus RTS test systems. Two distinct scenarios were simulated to represent different hurricane-induced event conditions, and the system performance was analysed in terms of loss minimization and voltage stability improvement.

For the IEEE 30-Bus RTS, the results demonstrated that both DG installation and LS strategy contributed to reducing power losses and enhancing resilience. However, the CSS consistently outperformed the individual strategies (DG and LS), reducing loss values close to the baseline condition while maintaining stable resilience indices (R1 and R2). A similar trend was observed in voltage stability analysis, where *FVSI* values deteriorated significantly after events but were effectively restored by the CSS, achieving values nearly identical to the pre-event baseline.

The evaluation was extended to the IEEE 57-Bus RTS, a larger and more complex test system. Here, the same two scenarios were simulated. Results revealed that DG installation and LS strategies individually provided improvements, but the CSS consistently delivered the lowest loss values and the most stable *FVSI* indices. The comparative outcomes across both test systems confirm that while DG installation and LS strategy are valuable resilience-enhancing measures, the integration of both in the CSS framework provides the most robust solution. The CSS not only minimizes real power losses but also strengthens voltage stability, thereby ensuring a balanced and comprehensive enhancement of power system survivability under extreme event conditions.

CHAPTER 6
CONCLUSION AND RECOMMENDATION

6.1 Conclusion

This thesis has presented Embedded Clonal Squirrel Evolutionary Programming (ECSEP) for resilience improvement in power system planning. The first objective has been successfully achieved through the derivation of a new optimisation technique termed ECSEP for grid hardening in power systems. By integrating chaotic mapping and cloning processes into the Squirrel Search Algorithm with Evolutionary Programming, the proposed ECSEP demonstrated improved exploration and exploitation capabilities. The technique was applied to minimize transmission losses and enhance system stability through optimal DG placement and load shedding decisions, conducted independently. Results revealed that the proposed ECSEP performed well when validated on IEEE 30-Bus RTS and IEEE 57-Bus RTS. Comparative studies against conventional algorithms confirmed that ECSEP outperforms its counterparts, i.e. EP, CSO and SSA thereby validating its feasibility as a robust optimisation tool for grid hardening applications.

The second objective has been successfully achieved by formulating the Multi-Objective Embedded Clonal Squirrel Evolutionary Programming (MOECSEP) technique for power system planning. The formulation employed weighted-sum multi-objective technique to minimize the total fitness confining system losses and improve voltage security. The results across multiple test systems demonstrated that MOECSEP achieves balanced trade-offs between the two objectives, producing superior fitness values compared to other evolutionary-based methods. This capability highlights the significance of the technique for addressing conflicting planning criteria in modern power system operation.

The third objective has been successfully realized through the development of the Composite Survivability Strategy (CSS) for grid hardening by integrating intelligent DG installation with load shedding using ECSEP. This strategy introduced a coordinated optimisation framework to simultaneously allocate DG and perform load shedding in order to enhance resilience and operational efficiency. The results showed that CSS consistently provided the highest improvement in resilience indices, reduced

power losses and improve voltage stability. This highlights the advantage of a combined strategy over standalone measures, offering system operators a more effective tool for survivability planning.

In summary, this thesis has comprehensively addressed all three research objectives, demonstrating the effectiveness of the proposed techniques for resilience improvement in power system planning. The first objective introduced the novel ECSEP algorithm, which proved capable of minimizing transmission losses and enhancing system stability through independent DG placement and load shedding, outperforming benchmark algorithms such as EP, CSO, and SSA. The second objective extended this foundation by formulating MOECSEP, a weighted-sum multi-objective framework that successfully balanced conflicting goals of loss minimization and voltage security, consistently delivering superior fitness values across multiple test systems. Building on these results, the third objective established the Composite Survivability Strategy (CSS), which integrated DG installation and load shedding in a coordinated manner to provide the most significant improvements in resilience indices, loss reduction, and voltage stability. Collectively, the findings affirm that the proposed ECSEP-based methodologies not only achieved the intended objectives but also outperformed conventional approaches, thereby offering a robust and practical toolset for modern grid hardening and survivability planning.

6.2 Research Contribution

Based on the verifications, analyses, and discussions conducted in this thesis, the key contributions of the research are summarized as follows:

a) Development of ECSEP Technique

This research introduces a novel optimisation technique, Squirrel Evolutionary Programming (ECSEP), specifically designed for grid hardening in power systems. By integrating chaotic mapping and cloning operators into the Squirrel Evolutionary Programming framework, the technique enhances exploration and exploitation capabilities while mitigating premature convergence. ECSEP was successfully applied to identify the optimal location and sizing of DG and to perform load shedding compensation in the IEEE 30-Bus and IEEE 57-Bus Reliability Test Systems. Comparative evaluations with benchmark algorithms (EP, CSO, SSA) confirmed that

ECSEP consistently outperforms existing approaches in minimizing system losses and improving voltage stability, thereby providing a strong foundation for resilience-oriented optimisation.

b) Formulation of MOECSEP for Multi-Objective Optimisation

Building on the single-objective formulation, this study extends ECSEP into a multi-objective framework, termed MOECSEP, using the weighted-sum approach. The technique addresses the trade-off between minimizing power system losses and enhancing voltage stability, both of which are critical for resilience improvement. Applied to standard IEEE test systems under various scenarios, MOECSEP demonstrated its capability to deliver balanced and optimal solutions across conflicting objectives. Results confirmed that MOECSEP achieves superior combined fitness values compared to other evolutionary-based multi-objective techniques, thereby validating its suitability as a tool for resilience-oriented system planning and operation.

c) Development of a Composite Survivability Strategy (CSS)

A significant contribution of this thesis is the development of a Composite Survivability Strategy (CSS) that integrates intelligent DG installation with load shedding within the ECSEP framework. Unlike standalone approaches, the CSS provides a coordinated optimisation strategy to simultaneously minimize system losses, enhance voltage stability, and improve resilience indices under disruptive events such as line outages and contingencies. Results revealed that CSS consistently outperforms individual DG or LS strategies, highlighting its effectiveness as a survivability-oriented planning methodology for modern power systems.

d) Resilience-Oriented Planning Framework

Finally, this study contributes a resilience-oriented planning framework that explicitly links optimisation techniques with resilience indices. By incorporating resilience as a planning criterion alongside traditional objectives of loss minimization and voltage stability improvement, the thesis provides a holistic methodology for grid hardening. This framework demonstrates how ECSEP-based strategies can be systematically employed to strengthen system survivability under high-impact, low-probability events, offering both technical rigor and operational practicality for future power system resilience planning.

6.3 Recommendation for Future Works

Building upon the findings of this study, several directions are recommended for future research to further strengthen the applicability and impact of the proposed ECSEP-based techniques. One important extension is the application of the developed methods to larger and more complex power systems, such as the IEEE-118 Bus, IEEE-300 Bus, or even utility-scale networks. This would provide valuable insights into the scalability of the algorithms and their performance under diverse network topologies, ranging from weakly meshed to highly interconnected grids. In addition, the techniques may be extended to alternative problem formulations beyond grid hardening. For instance, the proposed optimisation framework can be applied to unit commitment, economic dispatch, renewable energy scheduling, microgrid optimisation, and transmission expansion planning. Incorporating stochastic and probabilistic models that explicitly capture the uncertainties of renewable energy generation and load fluctuations will also enhance the robustness of the solutions in real-world environments.

Another promising direction involves the integration of energy storage systems alongside distributed generation and load shedding. The coordinated optimisation of storage sizing and placement with DG units could offer enhanced flexibility, enabling systems to absorb excess renewable generation during normal conditions and provide backup support during extreme events. This aligns with the growing role of storage in enabling resilient and sustainable power systems. Furthermore, future studies could adapt the techniques for real-time and dynamic applications, where computational efficiency becomes critical. Leveraging high-performance computing, surrogate modelling, or machine-learning-assisted optimisation may reduce execution times, making the methods suitable for real-time resilience enhancement. Extending the framework to include dynamic aspects such as frequency stability or cascading failures would further improve the comprehensiveness of resilience evaluation.

The increasing penetration of renewable energy sources also highlights the need to adapt the proposed approaches to renewable-dominated grids. Hybrid strategies that combine DG, storage, demand response, and flexible loads could be explored to enhance system survivability under variable and uncertain operating conditions. In addition, resilience planning should not only address physical threats such as natural disasters but also cyber-physical vulnerabilities. Extending the proposed framework to consider cyber-attack scenarios, including false data injection or intrusion into control

systems, would improve its relevance to modern smart grids. This calls for cyber–physical co-optimisation approaches that jointly address physical and cyber resilience.

From a methodological perspective, the adoption of more advanced multi-criteria decision-making approaches beyond the weighted-sum method may provide further flexibility in handling conflicting objectives. Pareto-based evolutionary techniques, fuzzy logic, and other decision-support frameworks could allow operators to explore a wider range of trade-offs between resilience, cost, and environmental considerations. To bridge the gap between research and practice, it is also recommended that the proposed techniques be tested in collaboration with utility companies, where regulatory, economic, and policy constraints can be incorporated into the survivability planning process. Finally, the development of a dedicated software toolbox implementing ECSEP, MOECSEP, and CSS would support system planners and operators in adopting these techniques in real-world applications. These directions provide a pathway for extending the contributions of this thesis towards more comprehensive, practical, and future-ready solutions for power system resilience enhancement.

REFERENCES

[1] M. Panteli and P. Mancarella, “Influence of extreme weather and climate change on the resilience of power systems: Impacts and possible mitigation strategies,” Jun. 29, 2015, *Elsevier Ltd*. doi: 10.1016/j.epsr.2015.06.012.

[2] U.S. Department of Energy, “Hurricane Katrina Situation Reports,” Washington, D.C., USA, 2006.

[3] R. J. Campbell, “Weather-Related Power Outages and Electric System Resiliency,” Washington, D.C., 2012.

[4] FEMA, “After-Action Report: Hurricane Maria,” Washington, D.C., USA, 2018.

[5] R. Yang and Y. Li, “Resilience assessment and improvement for electric power transmission systems against typhoon disasters: A data-model hybrid driven approach,” *Energy Reports*, vol. 8, pp. 10923–10936, Nov. 2022, doi: 10.1016/j.egyr.2022.08.226.

[6] “National Infrastructure Advisory Council A Framework for Establishing Critical Infrastructure Resilience Goals Final Report and Recommendations by the Council,” 2010.

[7] Y. Xu *et al.*, “A review of resilience enhancement strategies in renewable power system under HILP events,” *Energy Reports*, vol. 9, pp. 200–209, May 2023, doi: 10.1016/j.egyr.2022.12.128.

[8] C. Zhang, Y. F. Li, H. Zhang, Y. Wang, Y. Huang, and J. Xu, “Distributionally robust resilience optimization of post-disaster power system considering multiple uncertainties,” *Reliab. Eng. Syst. Saf.*, vol. 251, Nov. 2024, doi: 10.1016/j.ress.2024.110367.

[9] National Centers for Environmental Information (NCEI), “Billion-Dollar Weather and Climate Disasters,” 2024.

[10] G. Jiménez-Estévez, A. Navarro-Espinosa, R. Palma-Behnke, L. Lanuzza, and N. Velázquez, “Achieving resilience at distribution level: Learning from isolated community microgrids,” *IEEE Power and Energy Magazine*, vol. 15, no. 3, pp. 64–73, May 2017, doi: 10.1109/MPE.2017.2662328.

[11] S. F. Abrar, N. Al Masood, and M. J. Alam, “An adaptive load shedding methodology for renewable integrated power systems,” *Heliyon*, vol. 10, no. 21, Nov. 2024, doi: 10.1016/j.heliyon. 2024.e40043.

[12] A. Rezaee Jordehi, “Allocation of distributed generation units in electric power

systems: A review," Apr. 01, 2016, *Elsevier Ltd*. doi: 10.1016/j.rser.2015.11.086.

[13] P. Paliwal, N. P. Patidar, and R. K. Nema, "Planning of grid integrated distributed generators: A review of technology, objectives and techniques," 2014, *Elsevier Ltd*. doi: 10.1016/j.rser.2014.07.200.

[14] Y. Xu, C. C. Liu, K. P. Schneider, F. K. Tuffner, and D. T. Ton, "Microgrids for service restoration to critical load in a resilient distribution system," *IEEE Trans. Smart Grid*, vol. 9, no. 1, pp. 426–437, Jan. 2018, doi: 10.1109/TSG.2016.2591531.

[15] D. D. Woods, "Essential Characteristics of Resilience," in *Resilience Engineering: Concepts and Precepts*, E. Hollnagel, D. D. Woods, and N. Leveson, Eds. Aldershot, U.K.: Ashgate Publishing Ltd., 2006, pp. 21–34.

[16] M. Panteli, C. Pickering, S. Wilkinson, R. Dawson, and P. Mancarella, "Power System Resilience to Extreme Weather: Fragility Modeling, Probabilistic Impact Assessment, and Adaptation Measures," *IEEE Transactions on Power Systems*, vol. 32, no. 5, pp. 3747–3757, Sep. 2017, doi: 10.1109/TPWRS.2016.2641463.

[17] L. Ma, "Multi-Scale Methodologies for Probabilistic Assessment of Structural and Functional Performance of Power Transmission Systems under Hurricanes," 2021.

[18] M. A. Mohamed, T. Chen, W. Su, and T. Jin, "Proactive Resilience of Power Systems against Natural Disasters: A Literature Review," *IEEE Access*, vol. 7, pp. 163778–163795, 2019, doi: 10.1109/ACCESS.2019.2952362.

[19] M. Mahzarnia, M. P. Moghaddam, and M.-R. Haghifam, "A novel three-stage risk-based scheme to improve power system resilience against hurricane," *Computers & Electrical Engineering*, vol. 93, p. 107309, Jul. 2021, doi: 10.1016/j.compeleceng.2021.107309.

[20] M. Mahzarnia, M. Parsa Moghaddam, P. Siano, and M. R. Haghifam, "A comprehensive assessment of power system resilience to a hurricane using a two-stage analytical approach incorporating risk-based index," *Sustainable Energy Technologies and Assessments*, vol. 42, Dec. 2020, doi: 10.1016/j.seta.2020.100831.

[21] Massoud Amin, "Toward self-healing energy infrastructure systems," in *IEEE Computer Applications in Power*, 2001, pp. 20–28. [Online]. Available: http://www.nerc.com/dawg;

[22] B. Walker, C. S. Holling, S. R. Carpenter, and A. Kinzig, "Resilience,

Adaptability and Transformability in Social-ecological Systems," 2004. [Online]. Available: http://www.ecologyandsociety.org/vol9/iss2/art5

[23] T. E. K. Zidane *et al.*, "Power systems and microgrids resilience enhancement strategies: A review," Jan. 01, 2025, *Elsevier Ltd*. doi: 10.1016/j.rser.2024.114953.

[24] F. Amini, S. Ghassemzadeh, N. Rostami, and V. S. Tabar, "Electrical energy systems resilience: A comprehensive review on definitions, challenges, enhancements and future proceedings," *IET Renewable Power Generation*, May 2023, doi: 10.1049/rpg2.12705.

[25] S. Afzal, H. Mokhlis, H. Azil Lllias, N. Nadzirah Mansor, and H. Shareef, "State-of-the-art review on power system resilience and assessment techniques," *IET Generation, Transmission and Distribution*, vol. 14, no. 25, pp. 6107–6121, Dec. 2020, doi: 10.1049/iet-gtd.2020.0531.

[26] M. Chaudry, P. Ekins, K. Ramachandran, A. Shakoor, J. Skea, G. Strbac, X. Wang, and J. Whitaker, *Building a Resilient UK Energy System*, Research Report, Ref. UKERC/RR/HQ/2011/001. London, U.K.: UK Energy Research Centre (UKERC), Apr. 14, 2011.

[27] S. Afzal, H. Mokhlis, H. A. Illias, N. N. Mansor, A. S. M. Khairuddin, and M. K. N. M. Sarmin, "A Comparative Analysis of Flow-Based Resilience Indices Using Topological and Load Flow Models," in *3rd IEEE International Virtual Conference on Innovations in Power and Advanced Computing Technologies, i-PACT 2021*, Institute of Electrical and Electronics Engineers Inc., 2021. doi: 10.1109/i-PACT52855.2021.9696618.

[28] D. Henry and J. Emmanuel Ramirez-Marquez, "Generic metrics and quantitative approaches for system resilience as a function of time," *Reliab. Eng. Syst. Saf.*, vol. 99, pp. 114–122, Mar. 2012, doi: 10.1016/j.ress.2011.09.002.

[29] M. H. Nejati Amiri and F. Guéniat, "Towards a framework for measurements of power systems resiliency: Comprehensive review and development of graph and vector-based resilience metrics," Aug. 15, 2024, *Elsevier Ltd*. doi: 10.1016/j.scs.2024.105517.

[30] E. D. Vugrin, A. R. Castillo, and C. A. Silva-Monroy, *Resilience Metrics for the Electric Power System: A Performance-Based Approach*, SAND2017-1493, Sandia National Laboratories, Albuquerque, NM, USA, Feb. 2017. doi: 10.2172/1367499.

[31] J.-P. Watson *et al.*, “SANDIA REPORT Conceptual Framework for Developing Resilience Metrics for the Electricity, Oil, and Gas Sectors in the United States,” 2015. [Online]. Available: http://www.ntis.gov/help/ordermethods.asp?loc=7-4-0#online

[32] M. Panteli, P. Mancarella, D. N. Trakas, E. Kyriakides, and N. D. Hatziargyriou, “Metrics and Quantification of Operational and Infrastructure Resilience in Power Systems,” *IEEE Transactions on Power Systems*, vol. 32, no. 6, pp. 4732–4742, Nov. 2017, doi: 10.1109/TPWRS.2017.2664141.

[33] H. Raoufi, V. Vahidinasab, and K. Mehran, “Power systems resilience metrics: A comprehensive review of challenges and outlook,” Nov. 02, 2020, *MDPI*. doi: 10.3390/su12229698.

[34] Q. Lyu *et al.*, “Research on Offline and Online Evaluation of Disaster Resilience for Distribution Systems,” in *2020 4th International Conference on HVDC, HVDC 2020*, Institute of Electrical and Electronics Engineers Inc., Nov. 2020, pp. 425–429. doi: 10.1109/HVDC50696.2020.9292736.

[35] D. Luo *et al.*, “Evaluation Method of Distribution Network Resilience Focusing on Critical Loads,” *IEEE Access*, vol. 6, pp. 61633–61639, 2018, doi: 10.1109/ACCESS.2018.2872941.

[36] A. Kwasinski, “Quantitative model and metrics of electrical grids’ resilience evaluated at a power distribution level,” *Energies (Basel).*, vol. 9, no. 2, 2016, doi: 10.3390/en9020093.

[37] J. Najafi, A. Peiravi, and J. M. Guerrero, “Power distribution system improvement planning under hurricanes based on a new resilience index,” *Sustain. Cities Soc.*, vol. 39, pp. 592–604, May 2018, doi: 10.1016/j.scs.2018.03.022.

[38] C. Wang, P. Ju, F. Wu, X. Pan, and Z. Wang, “A systematic review on power system resilience from the perspective of generation, network, and load,” Oct. 01, 2022, *Elsevier Ltd*. doi: 10.1016/j.rser.2022.112567.

[39] A. K. Erenoğlu, I. Sengor, and O. Erdinç, “Power System Resiliency: A Comprehensive Overview from Implementation Aspects and Innovative Concepts,” Sep. 01, 2024, *Elsevier Ltd*. doi: 10.1016/j.nexus.2024.100311.

[40] A. Mohanty *et al.*, “Power system resilience and strategies for a sustainable infrastructure: A review,” Oct. 01, 2024, *Elsevier B.V.* doi: 10.1016/j.aej.2024.06.092.

[41] J. H. Lin and Y. K. Wu, “Review of Power System Resilience Concept, Assessment, and Enhancement Measures,” Feb. 01, 2024, *Multidisciplinary Digital Publishing Institute (MDPI)*. doi: 10.3390/app14041428.

[42] S. Paul, A. Poudyal, S. Poudel, A. Dubey, and Z. Wang, “Resilience assessment and planning in power distribution systems: Past and future considerations,” Jan. 01, 2024, *Elsevier Ltd*. doi: 10.1016/j.rser.2023.113991.

[43] D. Chattopadhyay and M. Panteli, “Integrating resilience in power system planning: A note for practitioners,” *Electricity Journal*, vol. 35, no. 9, Nov. 2022, doi: 10.1016/j.tej.2022.107201.

[44] R. Arghandeh, A. Von Meier, L. Mehrmanesh, and L. Mili, “On the definition of cyber-physical resilience in power systems,” May 01, 2016, *Elsevier Ltd*. doi: 10.1016/j.rser.2015.12.193.

[45] E. Hossain, S. Roy, N. Mohammad, N. Nawar, and D. R. Dipta, “Metrics and enhancement strategies for grid resilience and reliability during natural disasters,” May 15, 2021, *Elsevier Ltd*. doi: 10.1016/j.apenergy.2021.116709.

[46] M. Ouyang and L. Dueñas-Osorio, “Multi-dimensional hurricane resilience assessment of electric power systems,” *Structural Safety*, vol. 48, pp. 15–24, May 2014, doi: 10.1016/j.strusafe.2014.01.001.

[47] M. Ghanbari and J. Jiang, “Resilience Metrics in Power & Control Systems: Comparative Analysis,” in *IFAC-PapersOnLine*, Elsevier B.V., Jun. 2024, pp. 699–704. doi: 10.1016/j.ifacol.2024.07.301.

[48] E. Rosales-Asensio, J. L. Elejalde, A. Pulido-Alonso, and A. Colmenar-Santos, “Resilience Framework, Methods, and Metrics for the Prioritization of Critical Electrical Grid Customers,” *Electronics (Switzerland)*, vol. 11, no. 14, Jul. 2022, doi: 10.3390/electronics11142246.

[49] H. Wang, B. Wang, P. Luo, F. Ma, Y. Zhou, and M. A. Mohamed, “State Evaluation Based on Feature Identification of Measurement Data: for Resilient Power System,” *CSEE Journal of Power and Energy Systems*, vol. 8, no. 4, pp. 983–992, Jul. 2022, doi: 10.17775/CSEEJPES.2021.01270.

[50] S. Zuloaga, V. Vittal, J. Zhang, L. Mays, and M. Wu, “Coordinated Operation of the Electric Power System with Water Distribution Systems: Modeling, Control, Simulation, and Quantification of Resilience,” 2020.

[51] T. Phillips, T. McJunkin, C. Rieger, J. Gardner, and H. Mehrpouyan, “An Operational Resilience Metric for Modern Power Distribution Systems,” in *Proc.*

IEEE 20th Int. Conf. Software Quality, Reliability and Security Companion (QRS-C), Macau, China, Dec. 2020, pp. 334–342, doi: 10.1109/QRS-C51114.2020.00065.

[52] H. H. Willis and K. Loa, "Measuring the Resilience of Energy Distribution Systems," 2015. [Online]. Available: www.rand.org/giving/contribute

[53] I. Zunnurain, Y. Sang, P. Mandal, M. Velez-Reyes, and J. Espiritu, "Improving the resilience of large-scale power systems using distributed static series compensators," *International Journal of Electrical Power and Energy Systems*, vol. 145, Feb. 2023, doi: 10.1016/j.ijepes.2022.108702.

[54] F. Hasanzad and H. Rastegar, "Application of optimal hardening for improving resilience of integrated power and natural gas system in case of earthquake," *Reliab. Eng. Syst. Saf.*, vol. 223, Jul. 2022, doi: 10.1016/j.ress.2022.108476.

[55] Z. Li, M. Shahidehpour, F. Aminifar, A. Alabdulwahab, and Y. Al-Turki, "Networked Microgrids for Enhancing the Power System Resilience," Jul. 01, 2017, *Institute of Electrical and Electronics Engineers Inc.* doi: 10.1109/JPROC.2017.2685558.

[56] A. Hussain, V. H. Bui, and H. M. Kim, "Microgrids as a resilience resource and strategies used by microgrids for enhancing resilience," Apr. 15, 2019, *Elsevier Ltd*. doi: 10.1016/j.apenergy.2019.02.055.

[57] R. Eskandarpour and A. Khodaei, "Machine Learning Based Power Grid Outage Prediction in Response to Extreme Events," *IEEE Transactions on Power Systems*, vol. 32, no. 4, pp. 3315–3316, Jul. 2017, doi: 10.1109/TPWRS.2016.2631895.

[58] K. Fatima, H. Shareef, and A. A. Bajwa, "An insight into power system resilience and its confounding traits," Institute of Electrical and Electronics Engineers (IEEE), Nov. 2022, pp. 226–231. doi: 10.1109/isemantic55962.2022.9920458.

[59] A. A. Bajwa, H. Mokhils, S. Mekhilef, M. Mubin, N. N. Mansor, and H. A. Illias, "Sequential Service Restoration of Distribution System Considering Interdependent Critical Loads," in *3rd IEEE International Virtual Conference on Innovations in Power and Advanced Computing Technologies, i-PACT 2021*, Institute of Electrical and Electronics Engineers Inc., 2021. doi: 10.1109/i-PACT52855.2021.9696953.

[60] B. Li, R. Roche, and A. Miraoui, "A temporal-spatial natural disaster model for power system resilience improvement using DG and lines hardening," in *Proc.*

IEEE Manchester PowerTech, Manchester, U.K., Jun. 2017, pp. 1–6, doi: 10.1109/PTC.2017.7980851.

[61] E. Hollnagel, *Safety-II in practice: Developing the resilience potentials*. Taylor and Francis, 2017. doi: 10.4324/9781315201023.

[62] C. Chen, J. Wang, and D. Ton, "Modernizing Distribution System Restoration to Achieve Grid Resiliency Against Extreme Weather Events: An Integrated Solution," *Proceedings of the IEEE*, vol. 105, no. 7, pp. 1267–1288, Jul. 2017, doi: 10.1109/JPROC.2017.2684780.

[63] Z. Bie, Y. Lin, G. Li, and F. Li, "Battling the Extreme: A Study on the Power System Resilience," *Proceedings of the IEEE*, vol. 105, no. 7, pp. 1253–1266, Jul. 2017, doi: 10.1109/JPROC.2017.2679040.

[64] M. Panteli and P. Mancarella, "The grid: Stronger, bigger, smarter?: Presenting a conceptual framework of power system resilience," *IEEE Power and Energy Magazine*, vol. 13, no. 3, pp. 58–66, May 2015, doi: 10.1109/MPE.2015.2397334.

[65] R. J. Campbell, "CRS Report for Congress Weather-Related Power Outages and Electric System Resiliency Specialist in Energy Policy Weather-Related Power Outages and Electric System Resiliency Congressional Research Service Weather-Related Power Outages and Electric System Resiliency Congressional Research Service," 2012. [Online]. Available: www.crs.gov

[66] R. Nateghi, "Multi-Dimensional Infrastructure Resilience Modeling: An Application to Hurricane-Prone Electric Power Distribution Systems," *IEEE Access*, vol. 6, pp. 13478–13489, Jan. 2018, doi: 10.1109/ACCESS.2018.2792680.

[67] G. V. Iswaran, M. Hedman, V. Vittal, and R. Ayyanar, "Comprehensive Framework Based on Dynamic and Steady State Analysis to Evaluate Power System Resilience Against Natural Calamities," 2022.

[68] J. Zhou, D. W. Coit, F. A. Felder, and S. Tsianikas, "Combined optimization of system reliability improvement and resilience with mixed cascading failures in dependent network systems," *Reliability Engineering & System Safety*, vol. 237, Art. no. 109376, Sep. 2023, doi: 10.1016/j.ress.2023.109376.

[69] J. Pilatásig, D. Carrión, and M. Jaramillo, "Resilience Maximization in Electrical Power Systems through Switching of Power Transmission Lines," *Energies (Basel).*, vol. 15, no. 21, p. 8138, Nov. 2022, doi: 10.3390/en15218138.

[70] S. Ma, B. Chen, and Z. Wang, “Resilience enhancement strategy for distribution systems under extreme weather events,” *IEEE Trans. Smart Grid*, vol. 9, no. 2, pp. 1442–1451, 2018, doi: 10.1109/TSG.2016.2591885.

[71] R. Eskandarpour, A. Khodaei, and A. Arab, “Improving power grid resilience through predictive outage estimation,” in Proc. 2017 North American Power Symposium (NAPS), Morgantown, WV, USA, Sep. 2017, pp. 1–5, doi: 10.1109/NAPS.2017.8107262.

[72] T. Ridwan Billah Kushal, M. S. Illindala, J. Wang, and A. J. Conejo, “Decision analysis of cyber-physical resilience in power systems,” in *Proc. IEEE Power & Energy Society General Meeting (PESGM)*, Washington, DC, USA, Jul. 2021, pp. 1–5, doi: 10.1109/PESGM46819.2021.9638074.

[73] “Center, N.H.: Saffir-Simpson Hurricane Wind Scale. https://www.nhc. noaa.gov/aboutsshws.php (2023). Accessed 15, May 2023.”

[74] R. Yang and Y. Li, “Resilience assessment and improvement for electric power transmission systems against typhoon disasters: A data-model hybrid driven approach,” *Energy Reports*, vol. 8, pp. 10923–10936, Nov. 2022, doi: 10.1016/j.egyr.2022.08.226.

[75] N. Bhusal, M. Gautam, M. Abdelmalak, and M. Benidris, “Modeling of Natural Disasters and Extreme Events for Power System Resilience Enhancement and Evaluation Methods,” in *2020 International Conference on Probabilistic Methods Applied to Power Systems, PMAPS 2020 - Proceedings*, Institute of Electrical and Electronics Engineers Inc., Aug. 2020. doi: 10.1109/PMAPS47429.2020.9183679.

[76] S. S. Puhan, R. Sharma, and M. K. Mallick, “Ensuring grid resilience: Voltage stability analysis and contingency ranking in electric power systems,” *e-Prime - Advances in Electrical Engineering, Electronics and Energy*, vol. 9, Sep. 2024, doi: 10.1016/j.prime.2024.100696.

[77] Y. Xu *et al.*, “A review of resilience enhancement strategies in renewable power system under HILP events,” *Energy Reports*, vol. 9, pp. 200–209, May 2023, doi: 10.1016/j.egyr.2022.12.128.

[78] A. A. Ogunsina, M. O. Petinrin, O. O. Petinrin, E. N. Offornedo, J. O. Petinrin, and G. O. Asaolu, “Optimal distributed generation location and sizing for loss minimization and voltage profile optimization using ant colony algorithm,” *SN Appl. Sci.*, vol. 3, no. 2, Feb. 2021, doi: 10.1007/s42452-021-04226-y.

[79] M. Nasir, A. Rezaee Jordehi, M. Tostado-Véliz, S. A. Mansouri, E. R. Sanseverino, and M. Marzband, "Two-stage stochastic-based scheduling of multi-energy microgrids with electric and hydrogen vehicles charging stations, considering transactions through pool market and bilateral contracts," *Int. J. Hydrogen Energy*, 2023, doi: 10.1016/j.ijhydene.2023.03.003.

[80] A. Keane *et al.*, "State-of-the-art techniques and challenges ahead for distributed generation planning and optimization," 2013. doi: 10.1109/TPWRS.2012.2214406.

[81] P. Paliwal, N. P. Patidar, and R. K. Nema, "Planning of grid integrated distributed generators: A review of technology, objectives and techniques," 2014, *Elsevier Ltd*. doi: 10.1016/j.rser.2014.07.200.

[82] A. Rezaee Jordehi, "Allocation of distributed generation units in electric power systems: A review," Apr. 01, 2016, *Elsevier Ltd*. doi: 10.1016/j.rser.2015.11.086.

[83] Y. Xu, C. C. Liu, K. P. Schneider, F. K. Tuffner, and D. T. Ton, "Microgrids for service restoration to critical load in a resilient distribution system," *IEEE Trans. Smart Grid*, vol. 9, no. 1, pp. 426–437, Jan. 2018, doi: 10.1109/TSG.2016.2591531.

[84] H. Gao, Y. Chen, Y. Xu, and C. C. Liu, "Resilience-Oriented Critical Load Restoration Using Microgrids in Distribution Systems," *IEEE Trans. Smart Grid*, vol. 7, no. 6, pp. 2837–2848, Nov. 2016, doi: 10.1109/TSG.2016.2550625.

[85] X. Liu, M. Shahidehpour, Z. Li, X. Liu, Y. Cao, and Z. Bie, "Microgrids for Enhancing the Power Grid Resilience in Extreme Conditions," *IEEE Trans. Smart Grid*, vol. 8, no. 2, pp. 589–597, Mar. 2017, doi: 10.1109/TSG.2016.2579999.

[86] G. Jiménez-Estévez, A. Navarro-Espinosa, R. Palma-Behnke, L. Lanuzza, and N. Velázquez, "Achieving resilience at distribution level: Learning from isolated community microgrids," *IEEE Power and Energy Magazine*, vol. 15, no. 3, pp. 64–73, May 2017, doi: 10.1109/MPE.2017.2662328.

[87] A. A. Bajwa, H. Mokhlis, S. Mekhilef, and M. Mubin, "Enhancing power system resilience leveraging microgrids: A review," May 01, 2019, *American Institute of Physics Inc.* doi: 10.1063/1.5066264.

[88] T. T. H. Pham, Y. Bésanger, and N. Hadjsaid, "New challenges in power system restoration with large scale of dispersed generation insertion," *IEEE Transactions on Power Systems*, vol. 24, no. 1, pp. 398–406, 2009, doi:

10.1109/TPWRS.2008.2009477.

[89] A. A. Bajwa, H. Mokhlis, S. Mekhlief, M. Mubin, M. M. Azam, and S. Sarwar, "Resilience-oriented service restoration modelling interdependent critical loads in distribution systems with integrated distributed generators," *IET Generation, Transmission and Distribution*, vol. 15, no. 8, pp. 1257–1272, Apr. 2021, doi: 10.1049/gtd2.12100.

[90] M. Hamidieh and M. Ghassemi, "Microgrids and resilience: A review," *IEEE Access*, vol. 10, pp. 106059–106080, 2022, doi: 10.1109/ACCESS.2022.3211511.

[91] D. K. Mishra, M. J. Ghadi, L. Li, J. Zhang, and M. J. Hossain, "Active distribution system resilience quantification and enhancement through multi-microgrid and mobile energy storage," *Appl. Energy*, vol. 311, Apr. 2022, doi: 10.1016/j.apenergy.2022.118665.

[92] D. Baghbanzadeh, J. Salehi, F. S. Gazijahani, M. Shafie-khah, and J. P. S. Catalão, "Resilience improvement of multi-microgrid distribution networks using distributed generation," *Sustainable Energy, Grids and Networks*, vol. 27, Sep. 2021, doi: 10.1016/j.segan.2021.100503.

[93] G. Zhang, F. Zhang, X. Zhang, Z. Wang, K. Meng, and Z. Y. Dong, "Mobile Emergency Generator Planning in Resilient Distribution Systems: A Three-Stage Stochastic Model with Nonanticipativity Constraints," *IEEE Trans. Smart Grid*, vol. 11, no. 6, pp. 4847–4859, Nov. 2020, doi: 10.1109/TSG.2020.3003595.

[94] M. A. Mostafa, M. E. El-Hawary, G. A. N. Mbamalu, M. M. Mansour, K. M. El-Nagar, and A. M. El-Arabaty, "A computational comparison of steady state load shedding approaches in electric power systems," *IEEE Transactions on Power Systems*, vol. 12, no. 1, pp. 30–37, Feb. 1997, doi: 10.1109/59.574931.

[95] L. P. Moji, P. A. Hohne, K. Kusakana, and B. P. Numbi, "Optimal operation of a hybrid multisource energy system considering grid load shedding," *Energy Reports*, vol. 8, pp. 151–161, Nov. 2022, doi: 10.1016/j.egyr.2022.10.063.

[96] P. Singh, R. Arya, L. S. Titare, P. Purey, and L. D. Arya, "Value aided optimal load shedding accounting voltage stability consideration employing Crow Search Algorithm with modification based on Lampinen's criterion," *Appl. Soft Comput.*, vol. 143, Aug. 2023, doi: 10.1016/j.asoc.2023.110391.

[97] N. Al Masood, A. Jawad, and S. Banik, "A RoCoF-constrained underfrequency load shedding scheme with static voltage stability-based zoning approach,"

Sustainable Energy, Grids and Networks, vol. 35, Sep. 2023, doi: 10.1016/j.segan.2023.101080.

[98] A. Arief, M. B. Nappu, and Z. Y. Dong, "Dynamic under-voltage load shedding scheme considering composite load modeling," *Electric Power Systems Research*, vol. 202, Jan. 2022, doi: 10.1016/j.epsr.2021.107598.

[99] F. Elyasichamazkoti, S. Teimourzadeh, and F. Aminifar, "Optimal Distribution of Power Grid Under-Frequency Load Shedding With Security Considerations," *IEEE Transactions on Power Systems*, vol. 37, no. 5, pp. 4110–4112, Sep. 2022, doi: 10.1109/TPWRS.2022.3181856.

[100] X. Yu, L. Qin, Q. Chen, S. He, and G. Huang, "Integrated Energy System Resilience Assessment Based on Load Shedding Methodology," in *Proceedings - 2022 Power System and Green Energy Conference, PSGEC 2022*, Institute of Electrical and Electronics Engineers Inc., 2022, pp. 347–355. doi: 10.1109/PSGEC54663.2022.9881095.

[101] S. F. Abrar, N. Al Masood, and M. J. Alam, "An adaptive load shedding methodology for renewable integrated power systems," *Heliyon*, vol. 10, no. 21, Nov. 2024, doi: 10.1016/j.heliyon. 2024.e40043.

[102] J. Liu, X. Zhuan, L. Shang, S. Su, and Q. Xie, "A load-shedding preplan strategy for unplanned microgrid islanding considering frequency security constraints," *International Journal of Electrical Power and Energy Systems*, vol. 170, Sep. 2025, doi: 10.1016/j.ijepes.2025.110932.

[103] M. A. Kabir, A. H. Chowdhury, and N. Al Masood, "A dynamic-adaptive load shedding methodology to improve frequency resilience of power systems," *International Journal of Electrical Power and Energy Systems*, vol. 122, Nov. 2020, doi: 10.1016/j.ijepes.2020.106169.

[104] T. Amraee and H. Saberi, "Controlled islanding using transmission switching and load shedding for enhancing power grid resilience," *International Journal of Electrical Power and Energy Systems*, vol. 91, pp. 135–143, Oct. 2017, doi: 10.1016/j.ijepes.2017.01.029.

[105] J. Ouyang, S. Bi, A. Zhang, S. Xu, and J. Wang, "Emergency frequency control method for power system containing wind generation based on coordination of frequency-autonomous-response, constant-power-control-switching and generator-tripping or load-shedding," *International Journal of Electrical Power and Energy Systems*, vol. 162, Nov. 2024, doi: 10.1016/j.ijepes.2024.110290.

[106] A. Abbasizadeh and E. Azad-Farsani, “Cyber-constrained load shedding for smart grid resilience enhancement,” *Reliab. Eng. Syst. Saf.*, vol. 243, Mar. 2024, doi: 10.1016/j.ress.2023.109886.

[107] R. Eskandarpour and A. Khodaei, “Machine Learning Based Power Grid Outage Prediction in Response to Extreme Events,” *IEEE Transactions on Power Systems*, vol. 32, no. 4, pp. 3315–3316, Jul. 2017, doi: 10.1109/TPWRS.2016.2631895.

[108] G. Patsakis, *Enhancing Power System Resilience through Computational Optimization*, Ph.D. dissertation, Dept. Industrial Engineering and Operations Research, University of California, Berkeley, Berkeley, CA, USA, 2020.

[109] L. Gong, *Parallel Optimization Based Operational Planning to Enhance the Resilience of Large-Scale Power Systems*, Ph.D. dissertation, Dept. Electrical and Computer Engineering, Mississippi State University, Starkville, MS, USA, 2020.

[110] M. A. Muhammad, H. Mokhlis, K. Naidu, A. Amin, J. F. Franco, and M. Othman, “Distribution Network Planning Enhancement via Network Reconfiguration and DG Integration Using Dataset Approach and Water Cycle Algorithm,” *Journal of Modern Power Systems and Clean Energy*, vol. 8, no. 1, pp. 86–93, Jan. 2020, doi: 10.35833/MPCE.2018.000503.

[111] M. Yehia, D. Allam, and A. F. Zobaa, “A Novel Hybrid Fuzzy-Metaheuristic Strategy for Estimation of Optimal Size and Location of the Distributed Generators,” *Energy Reports*, vol. 8, pp. 12408–12425, Nov. 2022, doi: 10.1016/j.egyr.2022.09.019.

[112] S. A. ChithraDevi, L. Lakshminarasimman, and R. Balamurugan, “Stud Krill herd Algorithm for multiple DG placement and sizing in a radial distribution system,” *Engineering Science and Technology, an International Journal*, vol. 20, no. 2, pp. 748–759, Apr. 2017, doi: 10.1016/j.jestch.2016.11.009.

[113] S. Sharma, S. Bhattacharjee, and A. Bhattacharya, “Quasi-Oppositional Swine Influenza Model Based Optimization with Quarantine for optimal allocation of DG in radial distribution network,” *International Journal of Electrical Power and Energy Systems*, vol. 74, pp. 348–373, Jan. 2016, doi: 10.1016/j.ijepes.2015.07.034.

[114] S. A. Salimon, G. A. Adepoju, I. G. Adebayo, O. B. Adewuyi, and S. O. Amuda, “Simultaneous Placement and Sizing of Distributed Generation Units and Shunt

Capacitors on Radial Distribution Systems Using Cuckoo Search Algorithm," *Current Journal of Applied Science and Technology*, pp. 43–58, Jun. 2021, doi: 10.9734/cjast/2021/v40i1231380.

[115] Z. Abdmouleh, A. Gastli, L. Ben-Brahim, M. Haouari, and N. A. Al-Emadi, "Review of optimization techniques applied for the integration of distributed generation from renewable energy sources," 2017, *Elsevier Ltd*. doi: 10.1016/j.renene.2017.05.087.

[116] A. Fathy, "Efficient energy valley optimization approach for reconfiguring thermoelectric generator system under non-uniform heat distribution," *Renew. Energy*, vol. 217, p. 119177, Nov. 2023, doi: 10.1016/j.renene.2023.119177.

[117] M. Azizi, U. Aickelin, H. A. Khorshidi, and M. Baghalzadeh Shishehgarkhaneh, "Energy valley optimizer: a novel metaheuristic algorithm for global and engineering optimization," *Sci. Rep.*, vol. 13, no. 1, Dec. 2023, doi: 10.1038/s41598-022-27344-y.

[118] S. A. Shaaya, I. Musirin, S. I. Sulaiman, and M. H. Mansor, "Immunized-Evolutionary Algorithm Based Technique for Loss Control in Transmission System with MultiLoad Increment," *Indonesian Journal of Electrical Engineering and Computer Science*, vol. 17, no. 2, pp. 941–949, 2019, doi: 10.11591/ijeecs.

[119] C. Zhang, Y. F. Li, H. Zhang, Y. Wang, Y. Huang, and J. Xu, "Distributionally robust resilience optimization of post-disaster power system considering multiple uncertainties," *Reliab. Eng. Syst. Saf.*, vol. 251, Nov. 2024, doi: 10.1016/j.ress.2024.110367.

[120] J. C. Silva Chavez, A. Zamora-Mendez, M. R. Arrieta Paternina, J. F. Yrena Heredia, and R. Cardenas-Javier, "A hybrid optimization framework for the non-convex economic dispatch problem via meta-heuristic algorithms," *Electric Power Systems Research*, vol. 177, Dec. 2019, doi: 10.1016/j.epsr.2019.105999.

[121] B. Li and A. Mostafavi, "Unraveling fundamental properties of power system resilience curves using unsupervised machine learning," *Energy and AI*, vol. 16, May 2024, doi: 10.1016/j.egyai.2024.100351.

[122] M. Akmal Muhamad Hapiz *et al.*, "Hybrid-Swarm Evolutionary Programming Based Technique for Optimal Placement and Sizing DGPV for Loss Control in Power System," vol. 71, no. 3, 2022, [Online]. Available: http://philstat.org.ph

[123] S. Kansal, V. Kumar, and B. Tyagi, "Hybrid approach for optimal placement of

multiple DGs of multiple types in distribution networks," *International Journal of Electrical Power and Energy Systems*, vol. 75, pp. 226–235, Feb. 2016, doi: 10.1016/j.ijepes.2015.09.002.

[124] A. El-Fergany, "Optimal allocation of multi-type distributed generators using backtracking search optimization algorithm," *International Journal of Electrical Power and Energy Systems*, vol. 64, pp. 1197–1205, 2015, doi: 10.1016/j.ijepes.2014.09.020.

[125] O. Krejcar, P. Kukuliac, L. K. Cheng, A. Selamat, and J. Horak, "Deep-Learning Pre-Processing for Improvement Of K-Means Cluster Analysis of Seniors' Walkability in Hradec Kralove And Ostrava (Two Middle-Sized Czech Cities)," *Journal of Advanced Research in Computing and Applications Journal homepage*, vol. 28, pp. 1–11, 2022, [Online]. Available: https://akademiabaru.com/submit/index.php/arca/index

[126] N. L. Ismail, "Computational Intelligence Based Technique for Fuel Cost Minimization in Small and Bulk Power," *International Journal of Advanced Trends in Computer Science and Engineering*, vol. 9, no. 1.2, pp. 45–50, Apr. 2020, doi: 10.30534/ijatcse/2020/0891.22020.

[127] D. B. Fogel, *Evolutionary Computation: Toward a New Philosophy of Machine Intelligence*. New York, NY, USA: IEEE Press, 1995.

[128] S. B. S. Z. Abidin, M. M. Othman, M. Ahmadipour, and K. Hasan, "Optimal Allocation of Photovoltaic (PV) System Incorporating Energy Storage System (ESS) using Evolutionary Programming (EP) for Power System Reliability," in *2023 IEEE 3rd International Conference in Power Engineering Applications: Shaping Sustainability Through Power Engineering Innovation, ICPEA 2023*, Institute of Electrical and Electronics Engineers Inc., 2023, pp. 362–367. doi: 10.1109/ICPEA56918.2023.10093165.

[129] N. T. E. M. Jailaini, M. M. Othman, M. Ahmadipour, and K. Hasan, "Optimal Allocation of Photovoltaic (PV) System Considering Weather Conditions using Evolutionary Programming (EP) for Enhanced Power System Resiliency," in *2023 IEEE 3rd International Conference in Power Engineering Applications: Shaping Sustainability Through Power Engineering Innovation, ICPEA 2023*, Institute of Electrical and Electronics Engineers Inc., 2023, pp. 368–373. doi: 10.1109/ICPEA56918.2023.10093211.

[130] A. R. Ochi, S. G. Mahmud, and M. Margala, "Quantum-Inspired Evolutionary

Programming: A Case Study on Optimum Power Generation Scheduling," in *Proceedings of the IEEE Dallas Circuits and Systems Conference, DCAS*, Institute of Electrical and Electronics Engineers Inc., 2025. doi: 10.1109/DCAS65331.2025.11045496.

[131] S. A. S. Mustaffa, I. Musirin, M. M. Othman, and N. H. Rosli, "Multi DGPV installation in transmission system for loss minimization," in *2017 4th International Conference on Industrial Engineering and Applications, ICIEA 2017*, Institute of Electrical and Electronics Engineers Inc., Jun. 2017, pp. 350–354. doi: 10.1109/IEA.2017.7939236.

[132] F. P. Mahdi, P. Vasant, V. Kallimani, J. Watada, P. Y. S. Fai, and M. Abdullah-Al-Wadud, "A holistic review on optimization strategies for combined economic emission dispatch problem," Jan. 01, 2018, *Elsevier Ltd*. doi: 10.1016/j.rser.2017.06.111.

[133] A. B. Mashudi, M. M. Othman, M. Ahmadipour, and K. Hasan, "Generation Expansion Planning Considering Photovoltaic (PV) and Wind turbine Systems Using Optimization of Evolutionary Programming (EP) Technique," in *2023 IEEE 3rd International Conference in Power Engineering Applications: Shaping Sustainability Through Power Engineering Innovation, ICPEA 2023*, Institute of Electrical and Electronics Engineers Inc., 2023, pp. 307–312. doi: 10.1109/ICPEA56918.2023.10093202.

[134] N. F. Ibrahim, I. Musirin, N. Z. Mohamad, N. A. M. Kamari, M. N. Abdullah, and F. B. Zakaria, "Integrated Immune Chaotic Evolutionary Programming (IICEP) for Integrating Battery Energy Storage System in Transmission Network," in *2024 IEEE 4th International Conference in Power Engineering Applications: Powering the Future: Innovations for Sustainable Development, ICPEA 2024*, Institute of Electrical and Electronics Engineers Inc., 2024, pp. 182–186. doi: 10.1109/ICPEA60617.2024.10498731.

[135] M. A. Kamalrolzaman, I. Musirin, M. H. Mansor, R. H. Salimin, N. L. Ismail, and N. A. Mohamed Kamari, "Integrated Grasshopper Algorithm-Evolutionary Programming Technique for Distributed Energy Resources Allocation," in *2022 IEEE International Conference on Power and Energy: Advancement in Power and Energy Systems towards Sustainable and Resilient Energy Supply, PECon 2022*, Institute of Electrical and Electronics Engineers Inc., 2022, pp. 316–321. doi: 10.1109/PECon54459.2022.9988769.

[136] N. Y. Dahlan, N. Romeli, and S. S. Sivaraju, “Energy Efficiency Policy Evaluation Model using Hybrid Evolutionary Programming (EP) - Artificial Neural Network (ANN) for Measurement and Verification Baseline Development,” in *Proceedings - International Conference on Augmented Intelligence and Sustainable Systems, ICAISS 2022*, Institute of Electrical and Electronics Engineers Inc., 2022, pp. 110–115. doi: 10.1109/ICAISS55157.2022.10011025.

[137] S. Gore, Y. Bhapkar, J. Ghadge, S. Gore, and S. K. Singha, “Evolutionary Programming for Dynamic Resource Management and Energy Optimization in Cloud Computing,” in *Proceedings of 3rd International Conference on Advanced Computing Technologies and Applications, ICACTA 2023*, Institute of Electrical and Electronics Engineers Inc., 2023. doi: 10.1109/ICACTA58201.2023.10393769.

[138] H. Tian, S. C. Chen, and M. L. Shyu, “Evolutionary Programming Based Deep Feature and Model Selection for Visual Data Classification,” in *Proceedings - 3rd International Conference on Multimedia Information Processing and Retrieval, MIPR 2020*, Institute of Electrical and Electronics Engineers Inc., Aug. 2020, pp. 61–66. doi: 10.1109/MIPR49039.2020.00020.

[139] Dolganov Anton, “Application of the Evolutionary Programming for Indirect Evaluation of Blood Pressure based on Heart Rate Variability Parameters,” in *Ural Symposium on Biomedical Engineering, Radioelectronics and Information Technology (USBEREIT)*, IEEE, 2020, pp. 139–142.

[140] J. Zhang, Z. Gao, S. Li, J. Zhao, and W. Song, “Improved intelligent clonal optimizer based on adaptive parameter strategy,” *Mathematical Biosciences and Engineering*, vol. 19, no. 10, pp. 10275–10315, 2022, doi: 10.3934/mbe.2022481.

[141] Y. Zhang and H. Zhang, “Enhancing Robot Path Planning Through a Twin-Reinforced Chimp Optimization Algorithm and Evolutionary Programming Algorithm,” *IEEE Access*, vol. 12, pp. 170057–170078, 2024, doi: 10.1109/ACCESS.2023.3337602.

[142] V. Sahargahi, V. Majidnezhad, S. T. Afshord, and Y. Jafari, “An intelligent chaotic clonal optimizer,” *Appl. Soft Comput.*, vol. 115, Jan. 2022, doi: 10.1016/j.asoc.2021.108126.

[143] L. Lian, “Reactive power optimization based on adaptive multi-objective

optimization artificial immune algorithm," *Ain Shams Engineering Journal*, vol. 13, no. 5, Sep. 2022, doi: 10.1016/j.asej.2021.101677.

[144] F. P. A. Lima, A. D. P. Lotufo, and C. R. Minussi, "Disturbance detection for optimal database storage in electrical distribution systems using artificial immune systems with negative selection," *Electric Power Systems Research*, vol. 109, pp. 54–62, Apr. 2014, doi: 10.1016/j.epsr.2013.12.010.

[145] L. W. De Oliveira, E. J. De Oliveira, F. V. Gomes, I. C. Silva, A. L. M. Marcato, and P. V. C. Resende, "Artificial Immune Systems applied to the reconfiguration of electrical power distribution networks for energy loss minimization," *International Journal of Electrical Power and Energy Systems*, vol. 56, pp. 64–74, 2014, doi: 10.1016/j.ijepes.2013.11.008.

[146] N. Bayar, S. Darmoul, S. Hajri-Gabouj, and H. Pierreval, "Fault detection, diagnosis and recovery using Artificial Immune Systems: A review," Nov. 01, 2015, *Elsevier Ltd*. doi: 10.1016/j.engappai.2015.08.006.

[147] A. Y. Hatata, G. Osman, and M. M. Aladl, "An optimization method for sizing a solar/wind/battery hybrid power system based on the artificial immune system," *Sustainable Energy Technologies and Assessments*, vol. 27, pp. 83–93, Jun. 2018, doi: 10.1016/j.seta.2018.03.002.

[148] S. S. F. Souza, R. Romero, J. Pereira, and J. T. Saraiva, "Artificial immune algorithm applied to distribution system reconfiguration with variable demand," *International Journal of Electrical Power and Energy Systems*, vol. 82, pp. 561–568, Nov. 2016, doi: 10.1016/j.ijepes.2016.04.038.

[149] M. Basu, "Artificial immune system for combined heat and power economic dispatch," *International Journal of Electrical Power and Energy Systems*, vol. 43, no. 1, pp. 1–5, Dec. 2012, doi: 10.1016/j.ijepes.2012.05.016.

[150] M. Basu, "Artificial immune system for fixed head hydrothermal power system," *Energy*, vol. 36, no. 1, pp. 606–612, 2011, doi: 10.1016/j.energy.2010.09.057.

[151] O. A. Ahmed, K. H. Chong, S. P. Koh, C. T. Yaw, and J. Pasupuleti, "Artificial immune systems (GA-AIS) enabled power loss mitigation in distributed generation: X3PAIS optimization approaches," *Heliyon*, vol. 10, no. 18, Sep. 2024, doi: 10.1016/j.heliyon. 2024.e37332.

[152] H. S. Bernardino and H. J. C. Barbosa, "Artificial Immune Systems for Optimization," in *Nature-Inspired Algorithms for Optimisation*, R. Chiong, Ed. Berlin, Germany: Springer, 2009, pp. 389–411, doi: 10.1007/978-3-642-00267-

0_14.

[153] M. Jain, V. Singh, and A. Rani, “A novel nature-inspired algorithm for optimization: Squirrel search algorithm,” *Swarm Evol. Comput.*, vol. 44, pp. 148–175, Feb. 2019, doi: 10.1016/j.swevo.2018.02.013.

[154] L. Zhu, Y. Zhou, R. Jiang, and Q. Su, “Surgical cases assignment problem using a multi-objective squirrel search algorithm,” *Expert Syst. Appl.*, vol. 235, Jan. 2024, doi: 10.1016/j.eswa.2023.121217.

[155] M. Dhaini and N. Mansour, “Squirrel search algorithm for portfolio optimization,” *Expert Syst. Appl.*, vol. 178, Sep. 2021, doi: 10.1016/j.eswa.2021.114968.

[156] V. P. Sakthivel and P. D. Sathya, “Single and multi-area multi-fuel economic dispatch using a fuzzified squirrel search algorithm,” *Protection and Control of Modern Power Systems*, vol. 6, no. 1, Dec. 2021, doi: 10.1186/s41601-021-00188-w.

[157] M. Basu, “Squirrel search algorithm for multi-region combined heat and power economic dispatch incorporating renewable energy sources,” *Energy*, vol. 182, pp. 296–305, Sep. 2019, doi: 10.1016/j.energy.2019.06.087.

[158] V. P. Sakthivel, M. Suman, and P. D. Sathya, “Combined economic and emission power dispatch problems through multi-objective squirrel search algorithm,” *Appl. Soft Comput.*, vol. 100, Mar. 2021, doi: 10.1016/j.asoc.2020.106950.

[159] D. E. Wekesa, K. K. Kaberere, and I. N. Muisvo, “Optimization of Reactive Power Dispatch for improvement of Voltage Stability Using Hybrid Differential Squirrel Search Algorithm,” in *2024 IEEE PES/IAS PowerAfrica, PowerAfrica 2024*, Institute of Electrical and Electronics Engineers Inc., 2024. doi: 10.1109/PowerAfrica61624.2024.10759391.

[160] T. Yuan, J. Ding, and T. Tu, “An improved squirrel search algorithm for optimization,” in *Proc. 41st Chinese Control Conf. (CCC)*, Hefei, China, Jul. 2022, pp. 3230–3235, doi: 10.23919/CCC55666.2022.9901595.

[161] F. Artuğer, “Innovative nonlinear component generator inspired by squirrel search algorithm,” *Integration*, vol. 104, Sep. 2025, doi: 10.1016/j.vlsi.2025.102466.

[162] M. Y. Javed *et al.*, “Improving the efficiency of photovoltaic-thermoelectric generator system using novel flying squirrel search optimization algorithm: Hybrid renewable and thermal energy system (RTES) for electricity generation,”

Process Safety and Environmental Protection, vol. 187, pp. 104–116, Jul. 2024, doi: 10.1016/j.psep.2024.04.093.

[163] Y. Huang *et al.*, "Multi-objective optimization of campus microgrid system considering electric vehicle charging load integrated to power grid," *Sustain. Cities Soc.*, vol. 98, Nov. 2023, doi: 10.1016/j.scs.2023.104778.

[164] H. Yang, X. Zhang, Y. Chu, Y. Ma, and D. Zhang, "Multi-objective-based demand response strategy optimization considering differential demand on reliability of power system," *International Journal of Electrical Power and Energy Systems*, vol. 152, Oct. 2023, doi: 10.1016/j.ijepes.2023.109202.

[165] A. Selim, S. Kamel, A. S. Alghamdi, and F. Jurado, "Optimal Placement of DGs in Distribution System Using an Improved Harris Hawks Optimizer Based on Single- And Multi-Objective Approaches," *IEEE Access*, vol. 8, pp. 52815–52829, 2020, doi: 10.1109/ACCESS.2020.2980245.

[166] A. Zeinalzadeh, Y. Mohammadi, and M. H. Moradi, "Optimal multi objective placement and sizing of multiple DGs and shunt capacitor banks simultaneously considering load uncertainty via MOPSO approach," *International Journal of Electrical Power and Energy Systems*, vol. 67, pp. 336–349, 2015, doi: 10.1016/j.ijepes.2014.12.010.

[167] H. P. C, K. Subbaramaiah, and P. Sujatha, "Optimal DG unit placement in distribution networks by multi-objective whale optimization algorithm & its techno-economic analysis," *Electric Power Systems Research*, vol. 214, Jan. 2023, doi: 10.1016/j.epsr.2022.108869.

[168] M. H. Mansor, I. Musirin, and M. M. Othman, "Multi-objective immune-commensal-evolutionary programming for total production cost and total system loss minimization via integrated economic dispatch and distributed generation installation," *Energies (Basel).*, vol. 14, no. 22, Nov. 2021, doi: 10.3390/en14227733.

[169] S. Kansal, V. Kumar, and B. Tyagi, "Optimal placement of different type of DG sources in distribution networks," *International Journal of Electrical Power and Energy Systems*, vol. 53, no. 1, pp. 752–760, 2013, doi: 10.1016/j.ijepes.2013.05.040.

[170] Z. H. Leghari, M. Y. Hassan, D. M. Said, Z. A. Memon, and S. Hussain, "An efficient framework for integrating distributed generation and capacitor units for simultaneous grid-connected and islanded network operations," *Int. J. Energy*

Res., vol. 45, no. 10, pp. 14920–14958, Aug. 2021, doi: 10.1002/er.6768.

[171] Y. Shen, W. Hu, M. Liu, F. Yang, and X. Kong, "Energy storage optimization method for microgrid considering multi-energy coupling demand response," *J. Energy Storage*, vol. 45, Jan. 2022, doi: 10.1016/j.est.2021.103521.

[172] H. Parsadust, H. Lotfi, and M. E. Hajiabadi, "A Dual-Objective Approach to Load Management: Telecommunication Switch Optimization with Distributed Generation Integration," *Processes*, vol. 13, no. 3, Mar. 2025, doi: 10.3390/pr13030716.

[173] Y. Wang, C. Chen, J. Wang, and R. Baldick, "Research on Resilience of Power Systems under Natural Disasters - A Review," Mar. 01, 2016, *Institute of Electrical and Electronics Engineers Inc.* doi: 10.1109/TPWRS.2015.2429656.

[174] S. A. Ismail *et al.*, "Comparative Analysis for Loss Control in Power Transmission System via Composite Compensation Scheme," in *2024 IEEE 4th International Conference in Power Engineering Applications: Powering the Future: Innovations for Sustainable Development, ICPEA 2024*, Institute of Electrical and Electronics Engineers Inc., 2024, pp. 151–156. doi: 10.1109/ICPEA60617.2024.10498705.

[175] F. Amini, S. Ghassemzadeh, N. Rostami, and V. S. Tabar, "Electrical energy systems resilience: A comprehensive review on definitions, challenges, enhancements and future proceedings," *IET Renewable Power Generation*, May 2023, doi: 10.1049/rpg2.12705.

[176] Y. Tan, *Power System Resilience under Natural Disasters*, Ph.D. dissertation, Dept. Electrical Engineering, University of Washington, Seattle, WA, USA, 2018.

[177] Z. Mat Yasin, *Performance Improvement Through Optimal Location and Sizing of Distributed Generation*, Ph.D. dissertation, Faculty of Electrical Engineering, Universiti Teknologi MARA, Shah Alam, Selangor, Malaysia, 2014.

[178] A. Abdullah *et al.*, "Effect of multi-unit and multi-type DG installation using integrated optimization technique in distribution power system planning," *Alexandria Engineering Journal*, vol. 107, pp. 895–914, Nov. 2024, doi: 10.1016/j.aej.2024.09.006.

[179] J. A. Laghari, H. Mokhlis, M. Karimi, A. H. A. Bakar, and H. Mohamad, "Computational Intelligence based techniques for islanding detection of distributed generation in distribution network: A review," 2014, *Elsevier Ltd*.

doi: 10.1016/j.enconman.2014.08.024.

[180] E. Lo Cascio, D. Borelli, F. Devia, and C. Schenone, “Future distributed generation: An operational multi-objective optimization model for integrated small scale urban electrical, thermal and gas grids,” *Energy Convers. Manag.*, vol. 143, pp. 348–359, 2017, doi: 10.1016/j.enconman.2017.04.006.

[181] M. M. Aman, G. B. Jasmon, A. H. A. Bakar, and H. Mokhlis, “A new approach for optimum DG placement and sizing based on voltage stability maximization and minimization of power losses,” *Energy Convers. Manag.*, vol. 70, pp. 202–210, 2013, doi: 10.1016/j.enconman.2013.02.015.

[182] S. Abdi and K. Afshar, “Application of IPSO-Monte Carlo for optimal distributed generation allocation and sizing,” *International Journal of Electrical Power and Energy Systems*, vol. 44, no. 1, pp. 786–797, Jan. 2013, doi: 10.1016/j.ijepes.2012.08.006.

[183] C. L. T. Borges and D. M. Falcão, “Optimal distributed generation allocation for reliability, losses, and voltage improvement,” *International Journal of Electrical Power and Energy Systems*, vol. 28, no. 6, pp. 413–420, Jul. 2006, doi: 10.1016/j.ijepes.2006.02.003.

[184] E. D. Melaku, E. S. Bayu, C. Roy, A. Ali, and B. Khan, “Distribution network forecasting and expansion planning with optimal location and sizing of solar photovoltaic-based distributed generation,” *Computers and Electrical Engineering*, vol. 110, Sep. 2023, doi: 10.1016/j.compeleceng.2023.108862.

[185] S. A. Shaaya, “Immunized- Brainstorm-Evolutionary Programming Technique for DG Installation and Power Scheduling with Economic Impact in Transmission System,” 2022.

[186] M. Muftić Dedović, S. Avdaković, M. Musić, and I. Kuzle, “Enhancing power system stability with adaptive under frequency load shedding using synchrophasor measurements and empirical mode decomposition,” *International Journal of Electrical Power and Energy Systems*, vol. 160, Sep. 2024, doi: 10.1016/j.ijepes.2024.110133.

[187] H. Saadat, *Power System Analysis*. McGraw-Hill, 2004.

[188] N. R. H. Abdullah, I. Musirin, and M. M. Othman, “Transmission Loss Minimization Using Evolutionary Programming Considering UPFC Installation Cost,” *International Review of Electrical Engineering,* vol. 5, pp. 1189–1203, 2010.

[189] I. Bin Musirin, “Novel Techniques for Voltage Stability Assessment and Improvement in Power System,” 2003.

[190] I. Musirin and T. K. Abdul Rahman, “Novel fast voltage stability index (FVSI) for voltage stability analysis in power transmission system,” in *2002 Student Conference on Research and Development: Globalizing Research and Development in Electrical and Electronics Engineering, SCOReD 2002 - Proceedings*, Institute of Electrical and Electronics Engineers Inc., 2002, pp. 265–268. doi: 10.1109/SCORED.2002.1033108.

[191] Y. Mohammadi Darestani and A. Shafieezadeh, “Multi-dimensional wind fragility functions for wood utility poles,” *Eng. Struct.*, vol. 183, pp. 937–948, Mar. 2019, doi: 10.1016/j.engstruct.2019.01.048.

[192] Y. Almoghathawi and K. Barker, “Component importance measures for interdependent infrastructure network resilience,” *Comput. Ind. Eng.*, vol. 133, pp. 153–164, Jul. 2019, doi: 10.1016/j.cie.2019.05.001.

[193] N. G. Bingel, “Wood Pole Strength and Loading-Key to Resiliency, Require Programs,” *Natural Gas & Electricity*, vol. 34, no. 3, pp. 12–15, Oct. 2017, doi: 10.1002/gas.22009.

APPENDICES

APPENDIX 1

Linedata and Busdata of IEEE 30-Bus RTS

Linedata:

Bus nl	Bus nr	R (p.u.)	X (p.u.)	1/2B (p.u.)	Line code
[1	2	0.0192	0.0575	0.02640	1
1	3	0.0452	0.1852	0.02040	1
2	4	0.0570	0.1737	0.01840	1
3	4	0.0132	0.0379	0.00420	1
2	5	0.0472	0.1983	0.02090	1
2	6	0.0581	0.1763	0.01870	1
4	6	0.0119	0.0414	0.00450	1
5	7	0.0460	0.1160	0.01020	1
6	7	0.0267	0.0820	0.00850	1
6	8	0.0120	0.0420	0.00450	1
6	9	0.0	0.2080	0.0	0.978
6	10	0	.5560	0	0.969
9	11	0	.2080	0	1
9	10	0	.1100	0	1
4	12	0	.2560	0	0.932
12	13	0	.1400	0	1
12	14	.1231	.2559	0	1
12	15	.0662	.1304	0	1
12	16	.0945	.1987	0	1
14	15	.2210	.1997	0	1
16	17	.0824	.1923	0	1
15	18	.1073	.2185	0	1
18	19	.0639	.1292	0	1
19	20	.0340	.0680	0	1
10	20	.0936	.2090	0	1
10	17	.0324	.0845	0	1
10	21	.0348	.0749	0	1
10	22	.0727	.1499	0	1
21	22	.0116	.0236	0	1
15	23	.1000	.2020	0	1
22	24	.1150	.1790	0	1
23	24	.1320	.2700	0	1
24	25	.1885	.3292	0	1
25	26	.2544	.3800	0	1
25	27	.1093	.2087	0	1
28	27	0	.3960	0	0.968
27	29	.2198	.4153	0	1
27	30	.3202	.6027	0	1
29	30	.2399	.4533	0	1
8	28	.0636	.2000	0.0214	1
6	28	.0169	.0599	0.065	1];

Note: Line code = 1 for lines; > 1 or <1 tr. tap at bus nl

Busdata:

IEEE 30-BUS TEST SYSTEM (American Electric Power)										
Bus code: 0 = load bus; 1 = slack bus; 2 = generator bus										
Bus	Bus	Voltage	Angle	---Load----		----------Generator----------				Injected
No	code	Mag.	Degree	MW	MVAr	MW	MVAr	Qmin	Qmax	MVAr
1	1	1.06	0.0	0.0	0.0	0.0	0	0	0	0
2	2	1.043	0.0	21.70	12.7	40	0	-40	50	0
3	0	1.0	0.0	2.4	1.2	0	0	0	0	0
4	0	1.06	0.0	7.6	1.6	0	0	0	0	0
5	2	1.01	0.0	94.2	19.0	0	0	-40	40	0
6	0	1.0	0.0	0.0	0.0	0	0	0	0	0
7	0	1.0	0.0	22.8	10.9	0	0	0	0	0
8	2	1.01	0.0	30.0	30.0	0	0	-10	60	0
9	0	1.0	0.0	0.0	0.0	0	0	0	0	0
10	0	1.0	0.0	5.8	2.0	0	0	-6	24	19
11	2	1.082	0.0	0.0	0.0	0	0	0	0	0
12	0	1.0	0	11.2	7.5	0	0	0	0	0
13	2	1.071	0	0	0.0	0	0	-6	24	0
14	0	1	0	6.2	1.6	0	0	0	0	0
15	0	1	0	8.2	2.5	0	0	0	0	0
16	0	1	0	3.5	1.8	0	0	0	0	0
17	0	1	0	9.0	5.8	0	0	0	0	0
18	0	1	0	3.2	0.9	0	0	0	0	0
19	0	1	0	9.5	3.4	0	0	0	0	0
20	0	1	0	2.2	0.7	0	0	0	0	0
21	0	1	0	17.5	11.2	0	0	0	0	0
22	0	1	0	0	0.0	0	0	0	0	0
23	0	1	0	3.2	1.6	0	0	0	0	0
24	0	1	0	8.7	6.7	0	0	0	0	4.3
25	0	1	0	0	0.0	0	0	0	0	0
26	0	1	0	3.5	2.3	0	0	0	0	0
27	0	1	0	0	0.0	0	0	0	0	0
28	0	1	0	0	0.0	0	0	0	0	0
29	0	1	0	2.4	0.9	0	0	0	0	0
30	0	1	0	10.6	1.9	0	0	0	0	0

APPENDIX 2

Linedata and Busdata of IEEE 57-Bus RTS

Busdata:

Bus No	Bus Code	Voltage Mag. (p.u.)	Angle (°)	Load MW	Load Mvar	Gen MW	Gen Mvar	Qmin	Qmax	Injected Mvar
1	1	1.04	0	55	17	128.9	-16.1	-200	300	0
2	2	1.01	0	3	88	0	-0.8	-17	50	0
3	2	0.985	0	41	21	40	-1	-10	60	0
4	0	0.981	0	0	0	0	0	0	0	0
5	0	0.976	0	13	4	0	0	0	0	0
6	2	0.98	0	75	2	0	0.8	-8	25	0
7	0	0.984	0	0	0	0	0	0	0	0
8	2	1	0	150	22	450	62.1	-140	200	0
9	2	1	0	121	26	0	2.2	-3	9	0
10	0	1	0	5	5	0	0	0	0	0
11	0	0.974	0	0	0	0	0	0	0	0
12	2	1.015	0	377	24	310	128.5	-150	155	0
13	0	0.979	0	18	2.3	0	0	0	0	0
14	0	0.97	0	10.5	5.3	0	0	0	0	0
15	0	0.988	0	22	5	0	0	0	0	0
16	0	1.013	0	43	3	0	0	0	0	0
17	0	1.017	0	42	8	0	0	0	0	0
18	0	1.001	0	27.2	9.8	0	0	0	0	10
19	0	0.97	0	3.3	0.6	0	0	0	0	0
20	0	0.964	0	2.3	1	0	0	0	0	0
21	0	1.008	0	0	0	0	0	0	0	0
22	0	1.01	0	0	0	0	0	0	0	0
23	0	1.008	0	6.3	2.1	0	0	0	0	0
24	0	0.999	0	0	0	0	0	0	0	0
25	0	0.982	0	6.3	3.2	0	0	0	0	5.9
26	0	0.959	0	0	0	0	0	0	0	0
27	0	0.982	0	9.3	0.5	0	0	0	0	0
28	0	0.997	0	4.6	2.3	0	0	0	0	0
29	0	1.01	0	17	2.6	0	0	0	0	0
30	0	0.962	0	3.6	1.8	0	0	0	0	0
31	0	0.936	0	5.8	2.9	0	0	0	0	0
32	0	0.949	0	1.6	0.8	0	0	0	0	0
33	0	0.947	0	3.8	1.9	0	0	0	0	0
34	0	0.959	0	0	0	0	0	0	0	0
35	0	0.966	0	6	3	0	0	0	0	0
36	0	0.976	0	0	0	0	0	0	0	0
37	0	0.985	0	0	0	0	0	0	0	0
38	0	1.013	0	14	7	0	0	0	0	0
39	0	0.983	0	0	0	0	0	0	0	0
40	0	0.973	0	0	0	0	0	0	0	0
41	0	0.996	0	6.3	3	0	0	0	0	0
42	0	0.966	0	7.1	4.4	0	0	0	0	0
43	0	1.01	0	2	1	0	0	0	0	0
44	0	1.017	0	12	1.8	0	0	0	0	0
45	0	1.036	0	0	0	0	0	0	0	0
46	0	1.05	0	0	0	0	0	0	0	0
47	0	1.033	0	29.7	11.6	0	0	0	0	0
48	0	1.027	0	0	0	0	0	0	0	0
49	0	1.036	0	18	8.5	0	0	0	0	0
50	0	1.023	0	21	10.5	0	0	0	0	0
51	0	1.052	0	18	5.3	0	0	0	0	0
52	0	0.98	0	4.9	2.2	0	0	0	0	0
53	0	0.971	0	20	10	0	0	0	0	6.3
54	0	0.996	0	4.1	1.4	0	0	0	0	0
55	0	1.031	0	6.8	3.4	0	0	0	0	0
56	0	0.968	0	7.6	2.2	0	0	0	0	0
57	0	0.965	0	6.7	2	0	0	0	0	0

Linedata:

From Bus	To Bus	R (p.u.)	X (p.u.)	1/2 B (p.u.)	Tap Ratio
1	2	0.0083	0.028	0.0645	1
2	3	0.0298	0.085	0.0409	1
3	4	0.0112	0.0366	0.019	1
4	5	0.0625	0.132	0.0129	1
4	6	0.043	0.148	0.0174	1
6	7	0.02	0.102	0.0138	1
6	8	0.0339	0.173	0.0235	1
8	9	0.0099	0.0505	0.0274	1
9	10	0.0369	0.1679	0.022	1
9	11	0.0258	0.0848	0.0109	1
9	12	0.0648	0.295	0.0386	1
9	13	0.0481	0.158	0.0203	1
13	14	0.0132	0.0434	0.0055	1
13	15	0.0269	0.0869	0.0115	1
1	15	0.0178	0.091	0.0494	1
1	16	0.0454	0.206	0.0273	1
1	17	0.0238	0.108	0.0143	1
3	15	0.0162	0.053	0.0272	1
4	18	0	0.555	0	0.97
4	18	0	0.43	0	0.978
5	6	0.0302	0.0641	0.0062	1
7	8	0.0139	0.0712	0.0097	1
10	12	0.0277	0.1262	0.0164	1
11	13	0.0223	0.0732	0.0094	1
12	13	0.0178	0.058	0.0302	1
12	16	0.018	0.0813	0.0108	1
12	17	0.0397	0.179	0.0238	1
14	15	0.0171	0.0547	0.0074	1
18	19	0.461	0.685	0	1
19	20	0.283	0.434	0	1
21	20	0	0.7767	0	1.043
21	22	0.0736	0.117	0	1
22	23	0.0099	0.0152	0	1
23	24	0.166	0.256	0.0042	1
24	25	0	1.182	0	1
24	25	0	1.23	0	1
24	26	0	0.0473	0	1.043
26	27	0.165	0.254	0	1
27	28	0.0618	0.0954	0	1
28	29	0.0418	0.0587	0	1
7	29	0	0.0648	0	0.967
25	30	0.135	0.202	0	1
30	31	0.326	0.497	0	1
31	32	0.507	0.755	0	1
32	33	0.0392	0.036	0	1
34	32	0	0.953	0	0.975
34	35	0.052	0.078	0.0016	1
35	36	0.043	0.0537	0.0008	1
36	37	0.029	0.0366	0	1
37	38	0.0651	0.1009	0.001	1
37	39	0.0239	0.0379	0	1
36	40	0.03	0.0466	0	1
22	38	0.0192	0.0295	0	1
11	41	0	0.749	0	0.955
41	42	0.207	0.352	0	1
41	43	0	0.412	0	1
38	44	0.0289	0.0585	0.001	1
15	45	0	0.1042	0	0.955
14	46	0	0.0735	0	0.9
46	47	0.023	0.068	0.0016	1
47	48	0.0182	0.0233	0	1
48	49	0.0834	0.129	0.0024	1
49	50	0.0801	0.128	0	1
50	51	0.1386	0.22	0	1
10	51	0	0.0712	0	0.93
13	49	0	0.191	0	0.895
29	52	0.1442	0.187	0	1
52	53	0.0762	0.0984	0	1
53	54	0.1878	0.232	0	1
54	55	0.1732	0.2265	0	1
11	43	0	0.153	0	0.958
44	45	0.0624	0.1242	0.002	1
40	56	0	1.195	0	0.958
56	41	0.553	0.549	0	1
56	42	0.2125	0.354	0	1
39	57	0	1.355	0	0.98
57	56	0.174	0.26	0	1
38	49	0.115	0.177	0.003	1
38	48	0.0312	0.0482	0	1
9	55	0	0.1205	0	0.94

AUTHOR'S PROFILE



Fathiah Zakaria received her Bachelor's degree (Hons) in Electrical & Electronics Engineering from Universiti Teknologi Petronas (UTP) in 2008 and her MSc in Electrical Engineering from Universiti Teknologi MARA (UiTM) in 2014. She is currently pursuing a PhD in Electrical Engineering, specializing in power system, at UiTM Shah Alam, Malaysia. Since 2014, she has been a lecturer at UiTM. Her research interests include artificial intelligence, optimisation, and power system.

LIST OF PUBLICATIONS:

[1] **F. B. Zakaria**, I. B. Musirin, N. B. Aminudin, D. B. Johari, S. A. Shaaya and N. F. B. Ibrahim, "Comparative Analysis in DG Installation Scheme for Resilience Enhancement," *2024 IEEE 4th International Conference in Power Engineering Applications (ICPEA)*, Pulau Pinang, Malaysia, 2024, pp. 311-316, doi: 10.1109/ICPEA60617.2024.10498681.

[2] **Fathiah Zakaria**, Ismail Musirin, Norziana Aminudin, Dalina Johari, Sharifah Azwa Shaaya, Rahmatul Hidayah Salimin, A. V. Senthil Kumar, Nor Azwan Mohamed Kamari, Nur Farahiah Ibrahim; Load shedding technique for voltage security and resilience improvement in power system. *AIP Conf. Proc.* 23 July 2025; 3320 (1): 050010. https://doi.org/10.1063/5.0286270

[3] **Zakaria, F.** *et al.* (2024). Enhancing Power System Resilience Through Evolutionary Programming for High Impact Low Probability Events. Proceedings of the 7th International Conference on Electrical, Control and

Computer Engineering-Volume 2. InECCE 2023. Lecture Notes in Electrical Engineering, vol 1213. Springer, Singapore. https://doi.org/10.1007/978-981-97-3851-9_19

[4] **Zakaria, F.**, I. Musirin, N. Aminudin, D. Johari, S. A. Shaaya, N. L. Ismail, and A. S. Kumar. "Enhancing Power System Resilience Through Optimized Load shedding Strategies." *Semarak International Journal of Electronic System Engineering* 4, no. 1 (2024): 1-9.

[5] N. F. Ibrahim, I. Musirin, N. Z. Mohamad, N. A. M. Kamari, M. N. Abdullah and **F. B. Zakaria**, "Integrated Immune Chaotic Evolutionary Programming (IICEP) for Integrating Battery Energy Storage System in Transmission Network," *2024 IEEE 4th International Conference in Power Engineering Applications (ICPEA)*, Pulau Pinang, Malaysia, 2024, pp. 182-186, doi: 10.1109/ICPEA60617.2024.10498731.

[6] R. H. Salimin, I. Musirin, Z. A. Hamid, N. Aminuddin, **F. Zakaria** and A. V. Senthil Kumar, "Comparative Analysis of Multi Optimization Techniques under Load Variations in Optimal Reactive Power Dispatch," *2024 IEEE 4th International Conference in Power Engineering Applications (ICPEA)*, Pulau Pinang, Malaysia, 2024, pp. 327-331, doi: 10.1109/ICPEA60617.2024.10498487.

[7] N. F. Ibrahim, I. Musirin, N. A. Mohamed Kamari, N. Z. Mohamad, F. A. Bakri and **F. B. Zakaria**, "Scalable Optimization of BESS Integration in Transmission Networks using IICSEP: A Case Study on Large-Scale Systems," *2025 IEEE Industrial Electronics and Applications Conference (IEACon)*, Kota Kinabalu Sabah, Malaysia, 2025, pp. 153-158, doi: 10.1109/IEACon64690.2025.11253600.

[8] Nur Farahiah Ibrahim, Ismail Musirin, **Fathiah Zakaria**, Nor Zulaily Mohamad, Nor Azwan Mohamed Kamari, Mohd Noor Abdullah; Effect on multi-BESS installation using IICEP technique for minimizing loss in transmission networks. *AIP Conf. Proc.* 23 July 2025; 3320 (1): 050009. https://doi.org/10.1063/5.0286267

[9] I. Musirin *et al*., "Integrated Optimization Technique for Renewable Energy Distributed Generation and Battery Energy Storage in Loss and Voltage Stability Control," *2025 IEEE 5th International Conference in Power*

Engineering Applications (ICPEA), Bandar Baru Bangi, Malaysia, 2025, pp. 130-135, doi: 10.1109/ICPEA65539.2025.11198498.

[10] I. Musirin *et al*., "A Computational Intelligence-Based Self-Healing Strategy for Enhancing Power System Survivability," *2025 IEEE 5th International Conference in Power Engineering Applications (ICPEA)*, Bandar Baru Bangi, Malaysia, 2025, pp. 242-247, doi: 10.1109/ICPEA65539.2025.11198323.

[11] F. D. Rokip *et al*., "Mixed-Mode Energy Management in Power Systems Using Embedded Tree-Evolutionary Programming Technique," *2025 IEEE 5th International Conference in Power Engineering Applications (ICPEA)*, Bandar Baru Bangi, Malaysia, 2025, pp. 236-241, doi: 10.1109/ICPEA65539.2025.11198394.

[12] I. Musirin *et al*., "Multi-Optimization Techniques for Voltage Control Study Under Generator Outage in Power Transmission System," *2025 IEEE 5th International Conference in Power Engineering Applications (ICPEA)*, Bandar Baru Bangi, Malaysia, 2025, pp. 136-141, doi: 10.1109/ICPEA65539.2025.11198454.

[13] R. H. Salimin, I. Musirin, Nor Azwan Mohamed Kamari, Z. A. Hamid, M. H. Hussain, **F. Zakaria,** "Effect Of Generator Participation in Optimal Reactive Power Dispatch for Multi-objective Optimization", *PaperASIA,* https://doi.org/10.59953/paperasia

[14] N. E. S. A. Nasrudin, R. H. Salimin, I. Musirin, M. H. Hussain, **F. Zakaria**, N. F. Ibrahim, "Optimal Electric Vehicle Charging System and Wind Turbine Placement for Loss Control Using Integrated Optimization Technique in Distribution System", *2026 IEEE 6th International Conference in Power Engineering Applications (ICPEA)*, Langkawi, Malaysia, 2026

LIST OF ACHIEVEMENTS:

[1] Gold Award, International Tinker Innovation & Entrepreneurship Challenge (2nd). Universiti Teknologi MARA Cawangan Johor Kampus Pasir Gudang, Johor, Innovative Power Grid Solutions: Strengthening Resilience Against Disruption.

[2] Best Commercialization Award, International Tinker Innovation & Entrepreneurship Challenge (2nd). Universiti Teknologi MARA Cawangan Johor Kampus Pasir Gudang, Johor, Innovative Power Grid Solutions: Strengthening Resilience Against Disruption.

[3] Silver Award, International Tinker Innovation & Entrepreneurship Challenge (2nd). Universiti Teknologi MARA Cawangan Johor Kampus Pasir Gudang, Johor, Revolutionizing power resilience: innovative optimization for distributed generation integration.

[4] Gold Award, Semarak International Research Article Competition III 2024 (SIRAC III 2024), Enhancing Power System Resilience through Optimized Load shedding Strategies.

LIST OF COPYRIGHT:

[1] Evolutionary Choatic Cloning-Squirrel Algorithm (ECCSA), CRDV2024W08794, 19 Decemeber 2024